Systems analysis of nucleic acids to model outcome and biological characteristics of neuroblastoma

Charlotte Mary Haunch-Smith

Submitted in accordance with the requirements for the degree of

Doctor of Philosophy

The University of Leeds

Leeds Institute of Cancer and Pathology

School of Medicine

September, 2018

The candidate confirms that the work submitted is her own and that appropriate credit has been given where reference has been made to the work of others.

This copy has been supplied on the understanding that it is copyright material and that no quotation from the thesis may be published without proper acknowledgement.

The right of Charlotte Mary Haunch-Smith to be identified as Author of this work has been asserted by her in accordance with the Copyright, Designs and Patents Act 1988.

Acknowledgements

Abstract

Neuroblastoma (NB) cells in the bone marrow (BM) at diagnosis are powerful indicators of poor outcome, the BM being a frequent reservoir for drug refractory disease. Improved outcome for some children will only be realised when treatments to eradicate BM disease have been developed. I have therefore isolated NB cells from BM aspirates of children with high-risk disease and investigated the self-renewal, migratory capacity and clinical significance of this disease. I have optimised methods for analysis and reporting of miRNA expression profiles using TaqMan® miRNA arrays to identify miRNAs or miRNA regulated pathways that are drivers of BM disease and investigated the potential of miRNAs as biomarkers of risk in liquid biopsies including BM aspirates and blood.

The median infiltration of BM with NB cells was 17% (range 0-94%); a high infiltration of BM with NB cells was predictive of a worse EFS (p=0.0012). Heterogeneous self-renewing capacity was observed in both colony and spheroid formation assays. Colony formation predicted EFS (p=0.012). Migratory cells were identified in all NB cultures; the migration index was highly heterogeneous (median 127±23, n=93, range 7.5-427.5) and did not predict EFS.

Hierarchical clustering of NB miRNA profiles revealed that NB cells from BM are heterogeneous. Pathway analysis revealed enrichment of the PI3K pathway in propagated NB cells. Treatment of cells with PI3K inhibitors reduced the viable NB cell number, validating the approach taken. Furthermore miR-618, reported to modulate growth via the PI3K pathway, was significantly associated with both self-renewal and survival. Circulating miRNAs in BM and PB predicted EFS.

In conclusion, NB cells from the BM of children with high-risk disease are highly heterogeneous. miRNAs are suitable candidates as circulating biomarkers of risk for more personalised treatment, although further investigations are needed to functionally validate their specific roles and design miRNA-mediated therapies.

Table of Contents

List of Tables

List of Figures

Abbreviations

°C	degrees Celsius
µg	microgram
µl	microliter
µM	micromolar
µm	micron
Ago	argonaute
ALK	Anaplastic lymphoma kinase
amp	ampicillin
ANOVA	analysis of variance
A-o-D	Assay-on-Demand™
APC	allophycocyanin
APITID1	apoptosis inducing TAF9 like domain 1
ARID	AT-rich interactive domain-containing protein
ATP	adenosine triphosphate
ATRX	α-thalassaemia/mental retardation syndrome X linked
ATTC	American Tissue Type Collection
BAF	BRG1/BRM associated factor
BCR-ABL	breakpoint cluster region protein- Abelson murine leukaemia viral oncogene homolog 1 fusion
BDNF	brain derived neurotrophic factor
BEACON	bevacizumab added to temozolomide ± irinotecan for children with refractory/relapsed neuroblastoma
BIRC5	baculoviral IAP repeat containing 5
BM	bone marrow
bp	base pair
BRCA	breast cancer susceptibility
BSA	bovine serum albumin
BuMel	bulsulfan/melphalan
CADM1	cell adhesion molecule 1
CAMTA1	calmodulin binding transcription activator 1

CAZ1	castor zinc finger 1
CCIA	Children's Cancer Institute Australia
CCLG	Children's Cancer and Leukaemia Group
CCRG	Children's Cancer Research Group
CDC42	cell division control protein 42 homolog
CDK2	*cyclin-dependent kinase 2*
cDNA	complementary DNA
CEM	carboplatin/etoposide/melphalan
CF	colony formation
CHD5	chromatin-helicase-DNA binding gene 5
CLL	chronic lymphocytic leukaemia
CNOT1	CCR4-NOT transcription complex subunit 1
CO_2	carbon dioxide
CRISPR	clustered regularly interspaced short palindromic repeats
Ct	cycle threshold
CXCR4	C-X-C chemokine receptor type 4
DAB	3'diaminobenzidine
DCX	doublecortin
ddH_2O	double distilled water
DGCR8	DiGeorge syndrome critical region in gene 8
dH_2O	distilled water
DMEM	Dulbecco's Modified Eagle Media
DMSO	dimethyl sulfoxide
DNA	deoxyribonucleic acid
DNase	deoxyribonuclease
dNTP	deoxyribonucleotide triphosphate
DTT	dithiothreitol
ECells	exosome producing cells
EDTA	ethylenediaminetetacetic acid
EEA1	early endosome antigen 1
EFS	event free survival

eIF4F	eukaryotic initiation factor 4F
ELIZA	enzyme-linked immunosorbent assay
EMEM	Minimum Essential Eagle's Media
EPHA2	ephrin type-A receptor 2
ERK	extracellular signal-regulated kinase
ErbB	epidermal growth factor receptor
EXP5	exportin 5
FCS	foetal calf serum
FIFO	first-in-first-out
FITC	fluorescein isothiocyanate
FSC	forward scatter
g	gram
GAPDH	glyceraldehyde 3-phosphate dehydrogenase
GD$_2$	disialoganglioside II3(NeuAc)2GgOse3Cer
GFP	green fluorescent protein
Grp75	stress-70 protein
GTP	guanosine triphosphate
h	hour(s)
H&E	haematoxylin and eosin
H2AFX	H2A histone family member X
HER2	human epidermal growth factor receptor 2
HIF	hypoxia-inducible factor
HIV	human immunodeficiency virus
HMGA	high mobility group A
HR	high-risk
Hsp	heat shock protein
HVA	homovanillic acid
I-131 MIBG	idoine-131-meta-iodobenzylguanidine
IFN	interferon
IL-2	interleukin-2
IL-6	interleukin-6
INRG	International Neuroblastoma Risk Group

INS	International Neuroblastoma Stage
kb	kilobase
KCl	potassium chloride
kDa	kilodalton
KEGG	Kyoto Encyclopaedia of Genes and Genomes
KIF1Bβ	kinesin family member 1Bβ
L	litre
LA	low adherence
LAMP-1	lysosomal-associated membrane protein 1
LB	Lysogeny broth
let-7	lethal-7
LIN28B	lin-28 Homolog B
lin-4	lineage-4
LINES	Low and Intermediate Risk Neuroblastoma European Study
M	molar
MACS	magnetic activated cell sorting
MAPK	mitogen-activated protein kinase
MAT	myeloablative therapy
MAX	myc-associated factor X
MCM	minichromosome maintenance complex component
MDM2	Mdm2-p53 binding protein homolog
mg	milligram
MgCl2	magnesium chloride
MgSO$_4$	magnesium sulphate
MIBG	meta-iodobenzylguanidine
MIEKK3	mitogen-activated protein kinase kinase kinase 3
min	minute(s)
miRISC	miRNA RNA silencing induced complex
miRNA	microRNA
MKI	mitosis-karyorrhexis index
ml	millilitre

mM	millimolar
MMP-9	matrix metallopeptidase 9
MNST	malignant nerve sheath tumour
MRD	minimal residual disease
MREC	Medical Research and Ethics Committee
mRNA	messenger RNA
MRP1	multidrug resistance-associated protein 1
MRP4	multidrug resistance protein 4
MSC	mesenchymal stem cell
mTOR	mammalian target of rapamycin
MW	molecular weight
NaCl	sodium chloride
NB	neuroblastoma
NB84	neuroblastoma 84
NCAM	neuronal cell adhesion molecule
NEAA	non-essential amino-acids
NEB	New England Biolabs
NET	norepinephrine transporters
ng	nanogram
NGF	nerve growth factor
NHR	not high-risk
nM	nanomolar
nm	nanometre
NME1	nucleoside diphosphate kinase A
NT3	neurotrophin 3
o/n	overnight
OC	other cancer
OCD1	ornithine decarboxylase
oncomiR	oncogenic miRNA
OS	overall survival
PB	peripheral blood
PBS	phosphate buffered saline

PBST	PBS containing 0.1% tween
PC	principle components
PCA	principal component analysis
PCR	polymerase chain reaction
PE	R-phrcoerythrin
PFA	paraformaldehyde
pg	picogram
PHOX2B	paired-like homeobox 2B
PI3K	phosphatidylinositol-4,5-bisphosphate 3-kinase
PLC	phospholipase C
PMSF	phenymethylsulfonyl
pre-miRNA	precursor miRNA
pri-miRNA	primary miRNA
RANKL	receptor activator of nuclear factor kappa-B ligand
Ras	Rat sarcoma
RCells	routinely cultured cells
RIN	RNA integrity number
RIPA	radio immunoprecipitation assay
RNA	ribonucleic acid
RNA Pol II	RNA polymerase II
RNase	ribonuclease
ROX	6-carboxy-X-rhodamine
rpm	revolutions per min
RT	reverse transcriptase
RTqPCR	reverse transcriptase quantitative PCR
s	second(s)
SD	standard deviation
SDS	sodium dodecyl sulphate
SEM	standard error of the mean
SIOPEN	International Society of Paediatric Oncology European Neuroblastoma Research Network
siRNA	small interfering RNA

SMAD3	mothers against decapentaplegic homolog 3
snoRNA	small nucleolar RNA
SOC	Super Optimal broth with Catabolite repression
SSC	side scatter
STAT	signal transducer and activator of transcription
SVD	singular value decomposition
SWI/SNF	switch/sucrose non-fermentable
T25	$25cm^2$ tissue culture
T75	$75cm^2$ tissue culture
TATA TBP	TATA-box-binding protein
TBST	tris buffered saline containing 0.1% tween
TGF-β	transforming growth factor beta
TH	tyrosine hydroxylase
TLDA	TaqMan® Low Density Array
TNF-α	tumour necrosis factor alpha
TRBP	trans activating response protein
TRK	tropomyosin receptor kinase
TSG-101	tumour susceptibility gene 101
TVD	topotecan-vincristine-doxorubicin
U	units
UFE4B	ubiquitination factor E4b
UK	United Kingdom
UoL	University of Leeds
UoN	University of Newcastle
UTR	untranslated region
UV	ultraviolet
v/v	volume/volume
VMA	vanillylmandelic acid
w/v	weight/volume
wcc	white cell count
XLMR	X-linked mental retardation

Chapter 1 Introduction

1.1 Neuroblastoma (NB)

Neuroblastoma (NB) is a rare childhood cancer that accounts for 8-10% of childhood cancer cases and 15% of childhood cancer deaths (Park *et al.*, 2010). The cancer arises in differentiated and/or differentiating cells of the embryonic neuronal crest, developing from the sympathetic nervous system (Thorner, 2014). NB is an extremely heterogeneous disease, some tumours will regress spontaneously, some remain localised whilst some continue to grow and spread (Schoot *et al.*, 2013). NB cells are usually highly malignant, so called high-risk (HR) although cases of spontaneous regression and differentiation occur in 3.3-10.7% of patients (Lehara *et al.*, 2012). The median age at diagnosis is 18 months; some rare cases are detected before birth via ultrasound (Kesrouani, 1999). Around 60-70% of children survive to 5 years (Monclair *et al.*, 2009), if diagnosed under 1 year then the outlook is better than for older children; those diagnosed before the age of one have a five year survival of 83% compared to 43%. Children with HR NB have a 20% chance of surviving; however this is increased to 30% with targeted immunotherapy. There are approximately 100 new cases each year within the United Kingdom (UK).

1.1.1 Diagnosis and symptoms

NB most frequently, in 65% of cases, arises in the adrenal medulla or lumbar sympathetic ganglia (Cheung and Dyer, 2013). Children present with a variety of symptoms that may be caused by the primary tumour, metastases or systemic effects in response to hormones released by the tumour cells. The primary tumour frequently grows within the abdomen and in these cases children frequently present with a large distended abdomen or a large lump or swelling within the abdomen. The tumour may press against blood vessels to cause swelling, or against the bladder prompting difficulties urinating. Metastases to lymph nodes or bone can cause pain which causes the child to limp, or in extreme cases results in an inability to walk. The bone marrow (BM) metastases cause decreased blood components; platelets, red

blood cells and white blood cells, leading to tiredness, irritability, weakness, bruising and frequent infections. The tumour secretes hormones into its microenvironment; these spread around the body causing paraneoplastic syndrome including diarrhoea, reddening of the skin, sweating, fever, increased heart rate and blood pressure.

The diagnosis of NB is made using the following criteria: age of a patient at diagnosis, histology of the tumour, *MYCN* amplification, elevated urinary catecholamine levels, site of tumour and metastases. The age of a patient at diagnosis is indicative as neuroblastoma normally presents in children under the age of five (Eklöf and Gooding, 1967).

The histology is assessed firstly to determine if the cells are cancerous; then used to inform a diagnosis. If NB is confirmed, histological characteristics of the tumour are used to determine NB differentiation status. NB tumours consist of small round cells which are a common histology seen in other tumours such as Ewing's sarcoma or rhabdomyosarcoma, so further observations are needed (Cullinane *et al.*, 2003). NB frequently contains nests of cells within a neurofibrillary structure, these rosettes are known as Homer-Wright rosettes. These are not unique to NB and their presence is not essential for a diagnosis. Immunohistochemistry is also used to identify NB cells; antibodies for neuron-specific markers such as neuroblastoma 84 (NB84) are commonly used (Shimada *et al.*, 1999, Cullinane *et al.*, 2003). Unlike Ewing's sarcoma and acute lymphoblastic lymphoma, enbloc or punctuate Periodic acid-Schiff staining is not seen in NB histology (Cullinane *et al.*, 2003). Tumours are varied in their histology and can be fully undifferentiated comprising of small round cells or have signs of differentiation with well-defined nuclei and large cytoplasm. The Shimada scale (The International Neuroblastoma Pathology Classification) is used to assess the clinical and biological characteristics of the NB. The tumours are first classified as stroma poor or stroma rich, examples of each are illustrated in Figure 1.1. Nodular, stroma rich tumours have an unfavourable outcome but intermixed differentiation states in stroma rich tumours have a favourable outcome (Shimada *et al.*, 1984). The stroma poor group is further divided into favourable and unfavourable using age at diagnosis, differentiation state of the cells, degree of maturation and mitosis-karyorrhexis index (MKI). MKI is an expression of apoptosis

in a cell; karyorrhectic cells have condensed and fragmented nuclei these cells are counted by a pathologist to give the MKI. A high MKI value suggests rapid turnover in NB. There are three grades of MKI; low ≤2% is the most favourable group; intermediate 2-4% and high ≤4% (Shimada *et al.*, 1999).
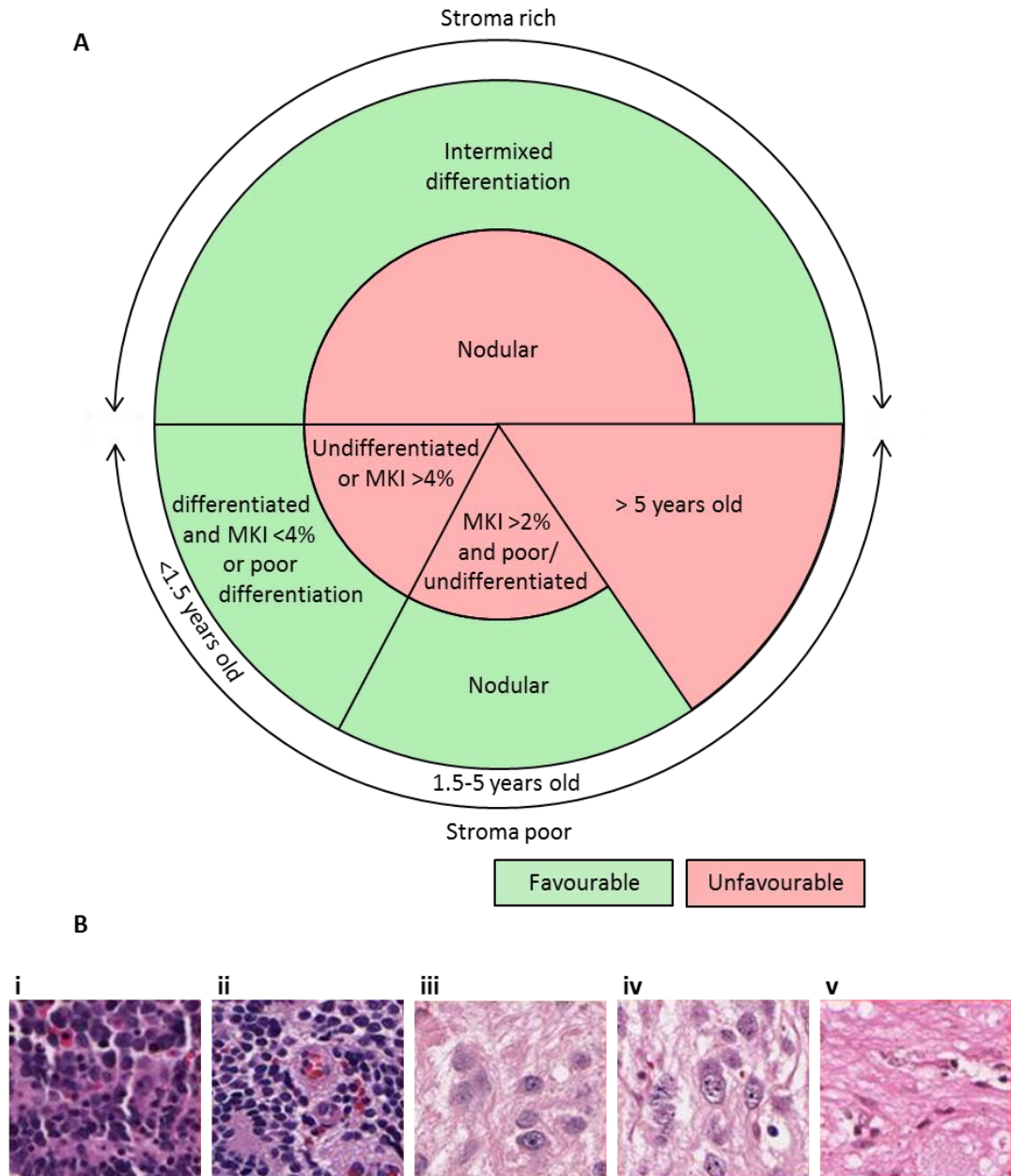
Figure 1.1 Unfavourable and favourable prognostic groups of NB.

A, Schema to show impact of age of patient at diagnosis, differentiation status, stroma status and MKI index on patient prognosis. B, Immunohistochemistry on NB i-iii show the differentiation grade used in Shimada classification; i is undifferentiated, ii poorly differentiated, iii is differentiating. iv and v show stromal development; iv is stroma poor and v is stroma rich.

The primary site of the tumour informs diagnosis. There are several ways to identify the site of the tumour. An ultrasound may be used to detect tumours in the abdomen and also show swollen kidneys which can occur due to the decreased urine outflow caused by the enlarged lymph nodes. The ultrasound is quick, easy and does not expose the patient to high levels of radiation, but is limited as it cannot detect metastases beyond the abdomen. Meta-iodobenzylguanidine (MIBG) scans are a key tool in diagnosing NB. The scan uses the radioisotope iodine-131-meta-iodobenzylguanidine (I-131 MIBG) as a tracer to detect tumour cells which appear 'bright' on the scan, identifying the tumour. The I-131 MIBG is taken up into the NB via norepinephrine transporters (NET) as it is an analogue of noradrenaline (Streby *et al.*, 2014). The specificity is due to the increased expression of NET on 90% NBs; however, there are 1 in 10 false negatives with MIBG scans as 10% of tumours do not have increased NET expression. Images are taken up to 72 hours (h) after the tracer has been injected. The bladder appears as a 'hot spot' in MIBG scans; this is because of the renal excretion of the I-131 MIBG, this can be reduced through good hydration (Matthay *et al.*, 2010). MIBG scans identify the abdominal tumours and some metastases as well but it can be hard to identify bone metastases using this method (Lessig, 2009, Schmidt *et al.*, 2013). MIBG scans are used to assess response to treatment as well as aiding diagnosis, Figure 1.2.

Most NBs produce and secrete catecholamines, a hormone normally produced by differentiated sympathetic nerve cells. Catecholamines are then broken down into metabolites; the presence of metabolites can be screened for in the urine, elevated levels are indicative of NB. Catecholamine tests are done to screen levels of the metabolites Homovanillic acid (HVA), Vanillylmandelic acid (VMA) (Pritchard *et al.*, 1989). Elevated levels of HVA or VMA are detected in urine using high performance liquid chromatography with electrochemical detection (Barco *et al.*, 2014). Normal levels of VMA and HVA are dependent on age. VMA in patients under 1 year old should be <27 microgram/milligram (μg/mg) and over a year <18 μg/mg; HVA less than a year <35 μg/mg and over a year 23 μg/mg. Elevated levels are classified as 2 times the normal level and above (Smith *et al.*, 2010).

The presence of bone metastases is another factor used in diagnosing NB as metastases to BM is present in 50% of NB patients (Chu *et al.*, 2011) and has prognostic implications. It is therefore important to have a quantitative and reliable method to detect metastases in the bone. This is done by supplementing the MIBG scan with bilateral BM biopsies. Ideally BM metastasis is evaluated in in 2 BM aspirates and 2 BM trephines (Burchill *et al.*, 2017). Cancerous cells within the BM are detected by examining these BM samples; both trephines and aspirates can be analysed for the presence of NB cells. Clinical practice is lacking in consistency of standardised BM evaluations, some hospitals and centres use only trephines or aspirates and some use both. Once a patient is diagnosed with NB the cancer is then staged to decide which course of treatment should be used.
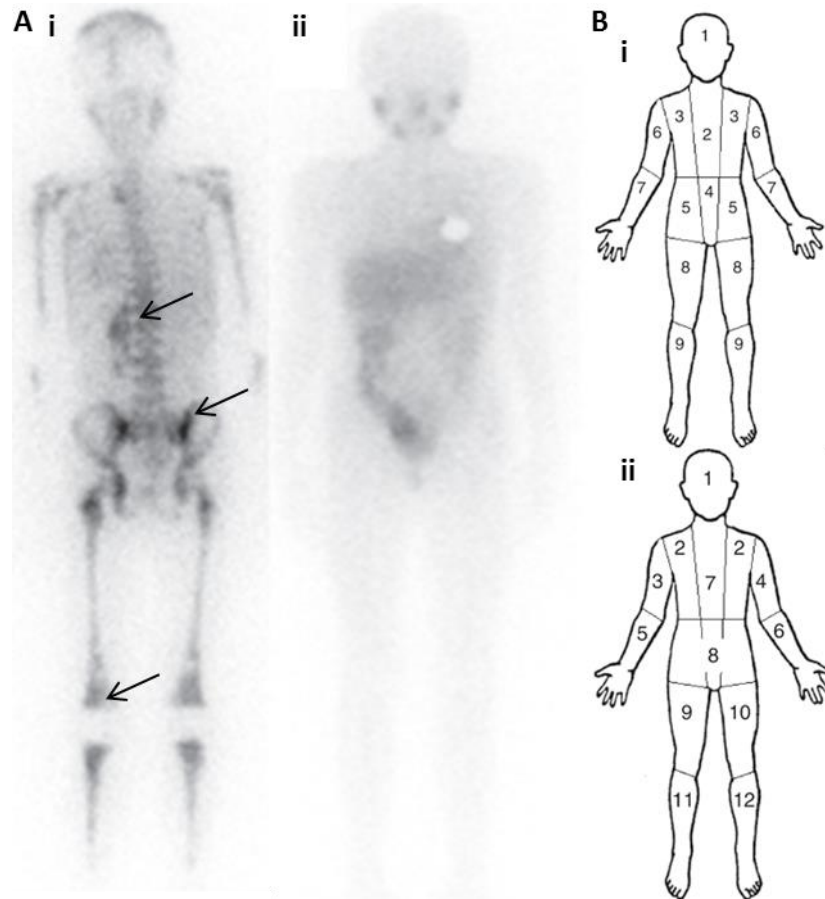
Figure 1.2 MIBG scan on an 8 ½ year old female.

A, MIBG scan on an 8 ½ year old female with widespread skeletal involvement of stage 4 NB. A i, is taken at diagnosis where metastatic 'bright' spots can be seen (highlighted by arrows) and A ii, shows end of therapy scan where no metastases are detected. B,. Summary of the Curie MIBG scoring system where the skeleton is divided into 9 segments and a tenth section is used to count soft tissue involvement, each segment is given a score; 0, no sites per segment; 1, 1 site per segment; 2, more than 1 site per segment; 3, diffuse involvement (>50% of the segment). B ii, demonstrates the International Society of Paediatric Oncology European Neuroblastoma Research Network's (SIOPEN) MIBG scoring system which divides the skeleton into 12 anatomic segments. Each segment is then graded as; 0, no sites per segment; 1, 1 discrete site per segment; 2, 2 discrete lesions; 3, 3 discrete lesions; 4, >3 discrete foci or single diffuse lesions involving <50% of a bone; 5, diffuse involvement of >50-95% whole bone; 6, diffuse involvement of the entire bone. Adapted from (Matthay *et al.*, 2010).

1.1.2 Staging

There are currently two different staging classifications for NB, the International Neuroblastoma Risk Group (INRG) and the International Neuroblastoma Stage (INS; Table 1.1). Staging systems are used to establish a consistent approach to treatment and risk stratification. The stages are based on clinical criteria and respective risk factors. INRG revised the staging criteria and risk classification of NB in 2009 in order to allow direct comparison of international risk-based clinical trials to evaluate the effectiveness of therapies (Monclair *et al.*, 2009).

Table 1.1 The INS and INRG stages systems of NB.

Adapted from (Monclair *et al.* 2009) and (Brodeur *et al.*, 1993) respectively. ^ipsilateral – on the same side of the body as the primary tumour, *contralateral – on the opposite side of the body as the primary tumour.

International Neuroblastoma Stage	Description	International Neuroblastoma Risk Group Stage	Description
1	Localized tumour with complete gross excision, with or without microscopic residual disease; ipsilateral^ lymph node negative for tumour	L1	Localized tumour not involving vital structures as defined by the list of image-defined risk factors and confined to one body compartment
2A	Localized tumour with incomplete gross excision; ipsilateral^ lymph nodes negative for tumour microscopically	L2	Loco regional tumour with presence of one or more image-defined risk factors
2B	Localized tumour with or without complete gross excision, with same side non adherent lymph nodes positive for tumour. Enlarged contralateral* lymph	M	Distant metastatic disease (except stage MS)

	nodes must be negative microscopically.		
3	Unresectable unilateral tumour infiltrating across the midline (vertebral column), with or without regional lymph node involvement; or localized unilateral tumour with contralateral regional lymph node involvement; or midline tumour with bilateral extension by infiltration or by lymph node involvement.	MS	Metastatic disease in children younger than 18 months with cancer confined to skin, liver, and/or BM.
4	Any primary tumour with metastases to distant lymph nodes, bone, BM, liver, skin and/or other organs (except as defined for 4S)		
4S	Localized primary tumour with metastases limited to skin, liver and/or BM, with BM involvement fewer than 10% total malignant nucleated cells. The MIBG scan would be negative for BM. When patient is under 1 year of age		

1.1.3 Prognosis

Several clinical prognostic factors are taken into account when assigning children with NB to a risk group: age, grade of tumour, MYCN amplification and metastases. The age at diagnosis is considered as a patient under 18 months has a better

prognosis than one older than 18 months (Cheung and Dyer, 2013). The grade of the tumour takes into account the amount of 'normal' looking cells; the higher the proportion of normal looking cells the better the prognostic outlook (Shimada *et al.*, 1999). Presence of metastases predicts a poor outcome, BM involvement portends for an especially poor outcome. The level of metastases is assessed using MIBG scans using the Curie scoring system or the International Society of Paediatric Oncology European Neuroblastoma Research Network's (SIOPEN) scoring system (Figure 1.2) and evaluation of metastasis in the BM using histology and cytology of trephines and aspirates respectively.

These prognostic risk factors are used in addition to stage to inform the patient risk category; low, intermediate or high. A low-risk patient is one with stage 1, 2A, 2B, 3 and 4S all with no *MYCN* amplification as *MYCN* amplification is an indication of poor prognosis (Wang *et al.*, 2013). HR patients are those with stage 4 NB with or without *MYCN* amplification or stage 2A, 2B, 3 and 4S with *MYCN* amplification. *MYCN* is not prognostic in children with stage 4 disease. The staging and risk group of NB patients is important as each group follows a different treatment course.

1.1.4 Treatment and outcome

The treatment of NB patients is dependent upon the risk category of the patient. Low-risk patients are mostly treated with surgery alone to remove the tumour and in some stage 4S cases no surgery is needed, and with close observation and supportive care some tumours regress spontaneously (Lehara *et al.*, 2012). Regressive tumours are mostly small localised tumours; however large tumours in stage 4S patients can also spontaneously regress. Overall survival (OS) for patients with low-risk NB under the age of 12 months is 91% and under the age of 21 years 95% (Cheung and Dyer, 2013). Intermediate-risk patients have a lowered survival rate of 89.2% and are generally treated with surgery and moderate intensity chemotherapy (Cheung and Dyer, 2013).

Low and Intermediate Risk Neuroblastoma European Study (LINES; NCT01728155) combines non-HR patients into a single protocol, with the aim of improving survival using prognostic classifications to inform treatment. LINES stratifies patients based on risk, in low-risk cases LINES aims to reduce the treatment given to children who

have good prognosis, whilst selecting those with poor prognosis for chemotherapy using the genomic profile of the tumour. Similarly, intermediate-risk patients with good prognosis receive reduced chemotherapy, this minimises adverse side effects. Children with predicted poor prognosis from histology results identifying poor differentiation receive increased radiotherapy and retinoic acid treatment. Adjuvant treatment is introduced to intermediate-risk children whose prognosis is poor identified by *MYCN* amplification. Stage 4 children receive the same moderate treatment that yielded good results in the SIOPEN studies.

The LINES protocol also addresses NB identified *in utero*, there is currently no clear optimal management choice for these children. The aim for these children is to maintain high survival using a non-operative therapeutic approach involving monitoring and if warranted, surgery.

HR NBs are harder to treat as they have either extensively metastasized or are *MYCN* amplified and therefore highly aggressive tumours. They have a lower survival rate of 31.1% (Cheung and Dyer, 2013). There is no standard of care available for HR patients, instead they are treated within clinical trials. Typically, treatment within a clinical trial for the HR patients follows 3 stages; induction therapy, consolidation and treatment to eradicate minimal disease. Most clinical trials involve dose-intensive chemotherapy, followed by surgical resection of the tumour if an adequate response is seen. Then the patient undergoes myeloablative therapy (MAT) and radiotherapy followed by autologous stem cell rescue. In the European HR study (HR-NBL1.5/SIOPEN) each patient was then given anti-GD_2 (disialoganglioside II3(NeuAc)2GgOse3Cer) immunotherapy and 13-cis-retanoic acid with or without interleukin-2 (IL-2).

There are many clinical trials available worldwide; for the purpose of this thesis I will explore the SIOPEN HR NB studies (HR-NBL-1.0/SIOPEN, HR-NBL-1.5/SIOPEN or HR-NBL-1.7/SIOPEN; recruitment from 11.10.2012-30.06.2017); ethical approval number 01/04/087 and clinical trial number NCT01704716) to illustrate the format of a clinical trial to treat HR NB. Clinical samples were received for laboratory work from children registered on these trials.

The SIOPEN HR NB studies are randomised interventional clinical trials open for patients with HR NB. As depicted in Figure 1.3, the patients first undergo induction therapy, and are assessed for adequate response, which is classed as less than three hot spots on the MIBG scan (Ladenstein *et al.*, 2010). Patients that do not respond to the induction therapy are taken off the trial to have topotecan-vincristine-doxorubicin (TVD), if after a maximum of 3 rounds of TVD the patient has responded they are re-entered onto the trial. Patients that have responded to induction therapy undergo a stem cell harvest before MAT. After MAT the patient receives radiotherapy then minimal residual disease (MRD) therapy to remove any remaining NB cells.
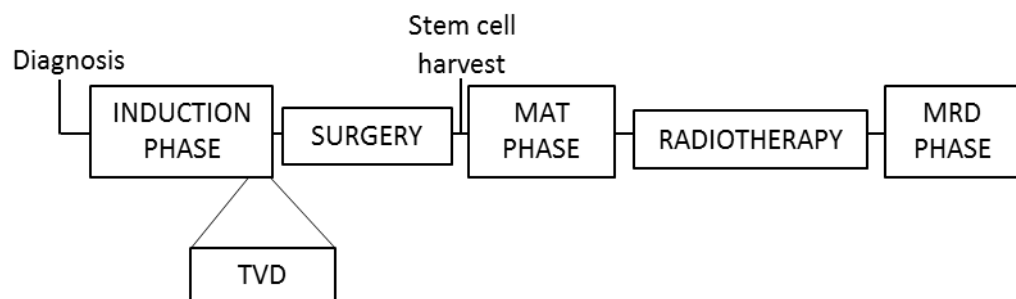
Figure 1.3 Therapy schematic for SIOPEN HR NB trials.

> MAT represents myeloablative therapy. MRD represents minimal residual disease therapy. The patient first undergoes induction therapy then if adequate response is seen undergoes MAT. This is followed by radiotherapy and finally MRD treatment. If an inadequate response is not seen after induction the patient receives TVD, if an adequate response is then met the patients follows the rest of the treatment. If after TVD an adequate response is not met the patient is removed from the trial.

The stem cell harvest is needed as MAT causes BM ablation which leads to the loss of haematopoietic stem cells due to the high-dose radiation or chemotherapy. Bulsulfan/melphalan (BuMel) proved to be much more effective and less toxic than carboplatin/etoposide/melphalan (CEM) (Burchill, personal communication) and so the trial was adapted to remove the BuMel/CEM randomisation; to only give children BuMel during MAT and focused on the benefits of administering cis retinoic acid and anti-GD$_2$ post radiotherapy with or without IL-2. After BuMel, patients have their stem cells reintroduced and are then put onto a course of radiotherapy. The updated trial then uses another randomisation, one arm is anti-GD$_2$ antibodies with IL-2 and the other is anti-GD$_2$ antibodies without IL-2. The anti-GD$_2$ antibody therapy is used

to minimise any residual disease or any disease reintroduced via stem cell harvest (Matthay *et al.*, 1993). The anti-GD$_2$ antibodies target remaining NB cells and target them for destruction by the host's immune cells, killing the NB cells.

If children do not respond to the induction therapy or TVD then they are offered alternative treatment, most likely entering a randomised phase IIb trial of bevacizumab added to temozolomide ± irinotecan for children with refractory/relapsed NB (BEACON) in which children are treated with bevacizumab and other chemotherapeutics. BEACON is designed for patients with NB which does not respond to HR treatment, or those who have relapsed.

The next great challenge is to identify the non-responders and develop novel ways to target these especially aggressive NBs. Improved outcomes for NB might best be achieved by developing a more personalised therapeutic approach to treatment. *MYCN* is currently used to decide the stage of disease, and therefore it is being used to select children for treatment at diagnosis; this is the basis of personalised treatment. As more biomarkers and complementary therapies are identified, the therapy plan becomes more specific.

1.1.5 Biology

There are many biological factors reported to affect the progression and characteristics of NB. Amplification of *MYCN* is the only genetic abnormality that is in current clinical use as a staging tool (see Section 1.1.2), however this may soon change with further understanding of the biological relevance and clinical utility of each factor. It is anticipated that the identification and understanding of new prognostic and predictive biomarkers will inform better patient staging and more effective, less toxic, therapeutics.

1.1.5.1 Genetic factors

The transcription factor *MYCN*, mapping to 2p24.1, was first identified as a key oncogenic driver of NB in the 1980s. Amplification of the gene is reported in 22% of cases (Domingo-Fernandez *et al.*, 2013, Brodeur *et al.*, 2014). Many studies have shown that amplification of *MYCN* leads to increased proliferation, migration and invasion and not surprisingly *MYCN* amplification is linked to unfavourable

characteristics and poor prognosis. Amplification of *MYCN* in stage 1, 2 or 3 tumours results in the patient being upgraded to HR because of this strong link to poor outcome. *MYCN* protein binds with myc-associated factor X (MAX) to form a heterodimer that binds to E boxes in promoters within the genome, either activating or repressing transcription of the gene. The exact molecular mechanisms through which *MYCN* drives oncogenesis remain elusive although it is known to regulate thousands of target genes that are likely to have roles in proliferation and aggressive phenotype. Anaplastic lymphoma kinase (ALK), minichromosome maintenance complex component (MCM) 7, high mobility group A (HMGA), Mdm2-p53 binding protein homolog (MDM2), multidrug resistance-associated protein 1 (MRP1) and ornithine decarboxylase (ODC1) are all identified *MYCN* target genes and their co-amplification is observed often (Hogarty *et al.*, 2008, Gamble *et al.*, 2012, Domingo-Fernandez *et al.*, 2013). High levels of MYCN protein expression have been reported in the absence of a *MYCN* amplification, this could be due to increased levels of ALK and extracellular signal-regulated kinase (ERK) 5 - these pathways are discussed later (Domingo-Fernandez *et al.*, 2013).

ODC1 encodes the rate-limiting enzyme for polyamine synthesis. Polyamines are organic cations that enhance translation, transcription and replication. Levels of OCD1 are elevated in rapidly proliferating tissues as aberrant levels of ODC1 cause accumulation of polyamines leading to the increased proliferation (Hogarty *et al.*, 2008). Polyamine pathway homeostasis is controlled by *MYCN* (Gamble *et al.*, 2012), co-amplification of *OCD1* and *MYCN*, often being reported as indicating poor prognosis. *OCD1* over expression has been reported in NB cells without *MYCN* amplification from children with HR disease, where it indicates poor prognosis independent of *MYCN* amplification (Gamble *et al.*, 2012). Inhibition of ODC1 has an anti-tumour effect in tumours, suggesting that polyamine sufficiency is necessary for tumorigenesis.

Wild type *ALK* codes for a receptor tyrosine kinase that mediates proliferation, migration and invasion, and is expressed in the developing sympathoadrenal lineage of the neuronal crest, the cells in which NB are known to arise (Louis and Shohet, 2014). The full molecular pathways of ALK are not fully understood (Hasan *et al.*,

2013) but it is known to activate phospholipase C (PLC), Rat sarcoma (Ras), signal transducer and activator of transcription (STAT) 3/5 and phosphatidylinositol-4,5-bisphosphate 3-kinase (PI3K) leading to cell proliferation, cell renewal and cell survival (Brodeur and Bagatell, 2014, Louis and Shohet, 2014). *ALK* was first identified as a gene of interest in NB as mutated *ALK* is present in 75% of hereditary cases (Moreno *et al.*, 2013, Brodeur and Bagatell, 2014). Hereditary NB is rare and accounts for just 1-2% of incidence, most NB are sporadic. Both mutations of the gene and increased expression of ALK have been linked to poor prognosis in NB, occurring in 9% and 3% of sporadic NB respectively (Pugh *et al.*, 2013). The involvement of ALK in tumour development has been confirmed using ribonucleic acid (RNA) and chemical inhibitors of ALK, both of which cause decreased proliferation and increased apoptosis of NB cells (Hasan *et al.*, 2013). Amplification of *ALK* is almost always seen alongside *MYCN* amplification as they share a regulatory feedback pathway. ALK induces *MYCN* transcription through the ERK pathway and stabilisation of *MYCN* protein is a induced through the PI3K pathway. In turn MYCN increases *ALK* transcription (Linder *et al.*, 2014).

ALK inhibitors have been developed, one example being crizotinib which showed promise in clinical trials for anaplastic large cell lymphoma *ALK* translocated tumours, with 100% of treated patients achieving clinical benefit (Moreno *et al.*, 2013). Unfortunately only 1 in 11 of NB patients with mutations in *ALK* were reported to show any response to crizotinib in a small pilot study (Mosse *et al.*, 2013). This lack of activity may reflect a common mutation in the ALK gene, F1174L, which is reported in 34.7% of mutated *ALK* NB (De Brouwer *et al.*, 2010b). F1174L is thought to cause the receptor tyrosine kinase to become resistant to the inhibitor (Linder *et al.*, 2014). Targeting the F1174L mutated ALK may provide a more effective inhibitor.

ERK5 is a member of the mitogen activated protein kinase family and indirectly activated by ALK through mitogen-activated protein kinase kinase kinase 3 (MEKK3). ERK5 increases expression of MYCN at the transcriptional level, the exact mechanism is not yet known but could prove helpful in identifying a druggable target to prevent increased levels of *MYCN* transcription. ERK5 may also prove helpful to overcome ALK inhibitor resistance, since initial studies have shown synergy between inhibitors

of ALK and ERK5 (Umapathy *et al.*, 2014). The anti-tumour effect of these inhibitors in combination was active in tumours with the F1174L *ALK* mutation that are resistant to crizotinib, which is an encouraging observation that may in the future prove to be of benefit for patients with both *ALK* and *MYCN* amplified NB. Inhibitors of ERK5 need to be designed with acceptable toxicity. More insight into the mechanism of ERK5 regulation of *MYCN* is needed to develop such inhibitors.

Paired-like homeobox 2B (*PHOX2B*) is another factor that has been strongly implicated in hereditary cases of NB. Hereditary NB is rare, 1-2% of all cases (Moreno *et al.*, 2013) as described above, 75% are caused by *ALK* activating mutations a further 5% contain *PHOX2B* inactivating mutations (Brodeur and Bagatell, 2014). Consistent with a role of *PHOX2B* in predisposing children to NB, there is a 20% incidence of NB in patients with Ondine's curse where inactivating mutations of *PHOX2B* are present (Trochet *et al.*, 2005, Brodeur and Bagatell, 2014). *PHOX2B* mutations are present in 4% of patients with sporadic NB (Louis and Shohet, 2014). *PHOX2B* encodes a homeodomain transcription factor that promotes cell cycle exit and drives the differentiation of neural crest precursors to sympathetic neurons along with *PHOX2A* (Cheung and Dyer, 2013). When *PHOX2B* loss of function mutations arise the regulation of calcium in the differentiating cells is lost, preventing them from further differentiation (Louis and Shohet, 2014). Patients with less differentiated tumours have a poorer prognosis. Furthermore PHOX2B can inhibit ALK; therefore loss of function of PHOX2B contributes to the pathogenesis of NB through deregulation of ALK.

Neurotrophin receptors tropomyosin receptor kinase (TRK) A, TRKB and TRKC and their cognate ligands nerve growth factor (NGF) brain derived neurotrophic factor (BDNF) and neurotrophin 3 (NT-3) respectively each play roles in NB. TRK neurotrophin receptors have roles in development and maintenance of the central and peripheral nervous system (Brodeur *et al.*, 2014). TRKA and TRKC are involved in development of sensory and sympathetic nerves (Brodeur *et al.*, 2014). The TRKA and NGF pathway has a role in spontaneous regression that is observed in many stage 4S patients. It is thought that other factors also play a role in this regression such as cellular and humoral immune responses, telomere shortening and epigenetic

changes. Increased *TRKA* expression is linked to favourable features of NB such as younger age at diagnosis and no *MYCN* amplification; high TRKA levels are reported in low stage tumours (Brodeur and Bagatell, 2014). The regression is also dependant on expression of the ligand NGF in the microenvironment; when NB cells with high expression of *TRKA* were exposed to high NGF *in vitro* the cells differentiated and survived for a long time (Brodeur and Bagatell, 2014). This evidence suggests *TRKA* has a role as a tumour suppressor gene (TSG) in NB but there have been no links to inactivation of *TRKA* in unfavourable NB cases.

TRKB expression is a predictor of unfavourable NB. Overexpression of *TRKB* and *BDNF* is reported in 36% of children and is indicative of aggressive NB especially when accompanied with *MYCN* amplification (Brodeur and Bagatell, 2014). TRKB is involved in motor neuron development and when activated by BDNF the pathway causes invasion, metastasis, angiogenesis and drug resistance whilst preventing differentiation of cells (Matsumoto *et al.*, 1995, Ho *et al.*, 2002, Brodeur *et al.*, 2014). Mutations in *TRKB* have not been identified in NB but increased expression is thought to be linked to *MYCN* amplification as 50-60% of HR NB show *TRKB* over expression, perhaps due to indirect activation by *MYCN* (Brodeur *et al.*, 2014). Studies have shown that inhibition of *TRKB* increases apoptosis and therefore potentially sensitises cells to chemotherapeutics. Lestaurtinib, a TRKB inhibitor is currently in clinical trials for patients with refractory NB, the phase I study showed some stabilisation of disease (9/46) and partial response (2/46) however there has been no further evaluation to date (Minturn *et al.*, 2011).

There are many genetic profiling studies in NB but like many other paediatric cancers the mutational profile is relatively silent, with few informative mutations. Therefore, studies have turned to focus on epigenetic events that may drive malignant transformation leading to NB. These changes may be useful prognostic, predictive biomarkers and potential targets for therapy.

1.1.5.2 Epigenetic factors

Tumour cell ploidy is also a prognostic indicator in NB, less aggressive tumours with localised disease in younger patients tending to have hyperploidy and less chromosomal aberrations (Domingo-Fernandez *et al.*, 2013). Patients with tumours

that are hyperploid have a more favourable outcome with 90% long-term survival (Kaneko and Knudson, 2000) whereas HR tumours are associated with high levels of chromosomal aberrations (Cheung and Dyer, 2013). With an increase in age at diagnosis come an increased likelihood of chromosomal aberrations increases and the ploidy of the tumour is no longer prognostic; in children over the age of 2 years at diagnosis the prognostic significance of ploidy is lost, limiting its clinical utility (Domingo-Fernandez *et al.*, 2013).

Loss of 1p and 11q are reported to predict poor outcome in NB (Domingo-Fernandez *et al.*, 2013), as are gains of 17q (Cheung and Dyer, 2013). Losses of 3p, 4p, 9p and 14q and the gain of 1q, 2p, 7q and 11p have also been described in children with poor outcome but these are less well established (Cheung and Dyer, 2013).

Deletion of chromosome 1p is reported in 20-35% of all NBs and 70% of HR NBs (Domingo-Fernandez *et al.*, 2013, Brodeur and Bagatell, 2014) and strongly correlates with *MYCN* amplification and poor outcome. The predictive value of 1p deletions reflects the loss of several TSG in this region including: calmodulin binding transcription activator 1 (*CAMTA1*), miR-34a, kinesin family member 1Bβ (*KIF1Bβ*), castor zinc finger 1 (*CASZ1*) and genes involved in chromatin remodelling (Domingo-Fernandez *et al.*, 2013, Brodeur and Bagatell, 2014). Low levels of these TSGs are linked to an unfavourable prognosis. Decreased expression of *CASZ1*, a zinc finger transcription finger important in neural development and differentiation, is linked to increased age at diagnosis and is under expressed in 77% of NBs from patients over the age of 18 months (Liu *et al.*, 2011, Brodeur and Bagatell, 2014). *CAMTA1* is another TSG coding for a transcription factor involved in neural differentiation and inhibition of proliferation, low levels are reported to be an indicator of poor outcome independent of *MYCN* status (Domingo-Fernandez *et al.*, 2013). miR34a causes activation of caspase 3/7 apoptosis pathway, causing cell death, miR34a also targets *E2F* which in turn has anti-proliferative effects (Welch *et al.*, 2007b). Interestingly miR34b/c are coded by chromosome 11q which is frequently lost in NB, although the role of these micro RNAs (miRNAs) is currently unclear. There are other genes that are still being explored as TSG lost on chromosome 1p important in NB such as

ubiquitination factor E4b (*UFE4B*) and apoptosis inducing TAF9 like domain 1 (*APITD1*) (Domingo-Fernandez *et al.*, 2013).

Loss or deletions of chromosome 11q occur in 25% of NB and are predictive of poor outcome (Brodeur and Bagatell, 2014). As in chromosome 1p there are TSGs that regulate chromatin remodelling including the H2A histone family member X (*H2AFX*) that are lost when 11q is deleted, as well as the cell adhesion molecule 1 (*CADM1*). CADM1 is an immunoglobulin cell adhesion molecule that mediates cell to cell interactions and is involved in neuronal cell development (Cheung and Dyer, 2013, Brodeur and Bagatell, 2014). Decreased expression of *CADM1* also causes increased proliferation (Domingo-Fernandez *et al.*, 2013). H2AFX is needed for genomic stability; decreased levels of H2AFX lead to increased genetic aberrations and greater cancer susceptibility. Decreased levels of CADM1 and H2AFX are linked to aggressive clinical behaviour of NB cells (Domingo-Fernandez *et al.*, 2013). Unlike chromosome 1p deletions, chromosome 11q deletions are usually inversely related to *MYCN* amplification, although there is a rare sub-set of tumours which contain both. These observations suggest there are genes key to the pathogenesis and character of NB on chromosome 11q, which support the introduction of chromosome 11q deletion as a prognostic factor in clinical practice to help decide the optimal treatment course for individual children (Louis and Shohet, 2014).

The most common genetic aberration in NB, the unbalanced gain of chromosome 17q, is reported in 90% of HR NB patients and is linked to the loss of chromosome 1p and *MYCN* amplification (Kaneko and Knudson, 2000, Domingo-Fernandez *et al.*, 2013). It is seen as a controversial NB prognostic factor as there is conflicting literature as to its independence without other factors (Domingo-Fernandez *et al.*, 2013). The region of gain on chromosome 17q is variable but mostly involves 17q21-15 (Brodeur *et al.*, 2014). There is not much known about the mechanisms in which the chromosome gain causes unfavourable outcome but increased surviving/baculoviral IAP repeat containing 5 (BIRC5) and Nm23/nucleoside diphosphate kinase A (NME1) occur when there is chromosome gain (Brodeur *et al.*, 2014). BIRC5 is an anti-apoptotic and pro-survival factor, and associated with poor outcome. NME1 is a nucleoside diphosphate kinase that is responsible for the

synthesis of many cellular nucleoside triphosphates which affects cell proliferation and differentiation. In many cancers, high levels of NME1 are a positive prognostic factor as it is viewed as a TSG gene, however increased levels of NME1 in NB is prognostic of aggressive unfavourable phenotype (Brodeur *et al.*, 2014).

There are several genes involved in chromatin remodelling that have been linked to NB. Most well-understood are chromatin-helicase-DNA binding gene 5 (*CHD5*), α-thalassaemia/mental retardation syndrome X linked (*ATRX*) and AT-rich interactive domain-containing proteins 1A and 1B (*ARID1A ARID1B*) (Brodeur *et al.*, 2014).

ATRX is part of a complex which regulates adenosine triphosphate (ATP)-dependant chromatin remodelling nucleosome assembly and regulates telomere length (Brodeur *et al.*, 2014). Mutations in *ATRX* are thought to result in loss of function and have an overall prevalence of 2-3% (Brodeur *et al.*, 2014). ATRX is associated with X-linked mental retardation (XLMR) but children with XLMR do not have an increased incidence of NB, suggesting that ATRX alone is not enough to initiate NB. There is a strong association between *ATRX* mutations and the age at diagnosis in stage 4S, around 17% in children between 18 month and 12 year olds and 44% in over 12 year olds with no mutations seen in children under 18 months suggesting *ATRX* has links to stage 4S NB (Cheung *et al.*, 2012). *ATRX* mutations also correlate to the length of telomeres (Louis and Shohet, 2014). Cancer cells need to maintain telomeres to survive, 30% of NB show increased telomerase activity, however this does not directly result in longer telomeres, and it is thought that *ATRX* mutations activate alternative lengthening of telomeres and this could cause the survival of NB cells (Cheung and Dyer, 2013).

ARID1A/B are essential components of the switch/sucrose non-fermentable (SWI/SNF) neural progenitor-specific chromatin-remodelling BRG1/BRM associated factor (BAF) complex which is important in self-renewal of multipotent neural stem cells (Brodeur *et al.*, 2014). ARID1B is also thought to have a role in chromatin structure. Mutations in the ARID1 proteins are observed in 11% of NB and have been associated with early treatment failure and decreased survival (Sausen *et al.*, 2013). Increases in the BAF complex specific to neural progenitor is observed in HR NB, however neuron specific BAF complex is increased in low-risk cases. Neural

progenitor BAF signalling disruption keeps the cells in an undifferentiated state, this aberrant signalling is linked to *ARID1* mutations and could explain the link between mutations in *ARID1* and poor outcome in NB patients (Sausen *et al.*, 2013).

CHD5 is a TSG that is preferentially expressed in the nervous system and testis (Brodeur *et al.*, 2014). CHD5 is involved in forming nucleosome remodelling complexes that are transcriptionally repressive by facilitating deoxyribonucleic acid (DNA) methylation causing changes in gene expression. Located to chromosome 1, it is lacking a copy in chromosome 1 deletion NBs. The loss of the other allele is due to epigenetic silencing (Brodeur *et al.*, 2014). The epigenetic silencing is thought be through hyper methylation of the promoter, induced by *MYCN* amplification (Domingo-Fernandez *et al.*, 2013), explaining the correlation between low expression of *CHD5* and *MYCN* amplification. A correlation between low *CHD5* and advanced stage, older age and unfavourable outcome is also reported (Domingo-Fernandez *et al.*, 2013, Brodeur *et al.*, 2014). Children with high levels of CHD5 have a favourable outcome, supporting experiments that have shown inducing expression of *CHD5 in vitro* decreases tumorigenicity of the NB cells (Fujita *et al.*, 2008).

Lin-28 homolog B (LIN28B) is part of a family of RNA binding proteins that regulate the transcription of the miRNAs of the lethal-7 (let-7) family (Brodeur *et al.*, 2014). LIN28B inhibits the processing of let-7 miRNAs by preventing Drosha from preparing the primary miRNA for export (Domingo-Fernandez *et al.*, 2013). High levels of LIN28B are reported during development as it plays a significant role in determining cell fate and the stem cell like factors of the cells (Zhu *et al.*, 2010). LIN28B overexpression is associated with HR NB, poor survival and adverse risk factors; LIN28N is also over expressed in other cancers such as hepatocellular carcinoma. It is thought that over expression of LIN28B could be linked to a single nucleotide polymorphism within the LIN28B gene (Domingo-Fernandez *et al.*, 2013). The over expression of LIN28B is an independent prognostic factor for poor survival.

Genetic profiling is becoming more appealing in NB as heterogeneity can be seen within the stages, including variety of response and characteristics of the tumour. It is hoped that through genome analysis subgroups can be identified to help risk stratification and guide novel therapeutics. In addition to MYCN status, currently

only chromosome 11p has been included in clinical practice for assessing prognosis and outcome in NB patients. Messenger RNA (mRNA) signatures could be used in clinics to further group NB patients, as has been done with other cancers (van 't Veer *et al.*, 2002). There is a plethora of prognostic biomarkers described in NB, but validation and comparisons using multivariate analyses are needed to establish which, if any, can benefit children with NB if they were to be adopted in clinic.

One study suggests 3 genomic subtypes of NB, type 1, type 2A and type 2B (Abel *et al.*, 2011). Type 1 tumours are low-risk, triploid, have high TRKA and are most likely to spontaneously regress. Type 2 tumours follow a more aggressive clinical course: type 2A tumours are of intermediate-risk and have high levels of lost chromosome 11q and high levels of gain of chromosome 17q; type 2B tumours are HR with high levels of *MYCN* amplification high gain of chromosome 17q and loss of 1p (Fischer *et al.*, 2010, Abel *et al.*, 2011). Analysis of 3 published microarray NB datasets identified four significant clusters using 74 discriminative genes on a population of 148 NBs. From these genes 6 could be used to discriminate between the 4 clusters identified, these genes were *ALK, BIRC5, CCND1, MYCN, NTRK1* and *PHOX2B.* Clusters 1, 2 and 3 fitted well with types 1, 2A and 2B already identified. The fourth cluster tended to have a high tumour stage, poor outcome, loss of chromosome 11q, low levels of ALK/BIRC5/PHOX2B and have no *MYCN* amplification (Abel *et al.*, 2011). There are additional signatures that have potentially equal importance, however not all signatures agree with each other, most likely due to difference in approaches to profiling and analysis.

Combining both epigenetics with the genetic consequences, studies have also looked at expression differences between specific epigenetic subsets of NB such as within NB with loss of chromosome 11q, which appears in around 30% of all NB (Fischer *et al.*, 2010, Brodeur and Bagatell, 2014). These studies identified a gene expression classification that identified 2 prognostically distinct subgroups of NB patients with 11q loss. Similar results are reported when analysing gene expression in NBs with no *MYCN* amplification; within HR patients, prognostic subgroups were identified (Asgharzadeh *et al.*, 2006). Theses subgroups had clinically indistinguishable metastatic disease but using gene expression signatures were segregated into those

with a progression-free survival of 16% or 69%. Further development of the HR subgroups could improve development of clinical trials aimed at improving NB outcome. The difference in specific mRNA profiles could indicate novel biomarkers or targets for therapy, this could allow better prognosis and treatment outcome.

1.2 BM disease in NB

As previously described, the presence of NB cells in the BM is a predictor of poor outcome (Monclair *et al.*, 2009, Viprey *et al.*, 2014) and one of the major challenges for cure. Over 70% of metastatic disease presents in the BM (DuBois *et al.*, 1999), where it is thought to contribute to disease progression and relapse. The elimination of these cells is one of the greatest challenges for cure of some children.

1.2.1 Detection

BM samples are taken to determine the extent of NB; trephines and aspirates are analysed for the presence of NB cells. For a BM aspiration a thin hollow needle is used to remove a sample of liquid BM which is smeared onto slides for analysis. A BM trephine involves removing a small piece of bone and BM using a needle, retaining the structure of the BM inside. The INRG recommends evaluation in 2 aspirates and trephines from bilateral sides. Evaluation using cytology of aspirates and histology of trephines remains gold standard in clinical practice but offers limited sensitivity when NB infiltration is below 10% (Cheung *et al.*, 1997).

High sensitivity for NB cell detection within the BM is important for tumour staging and for monitoring the therapeutic response of a patient, therefore a highly reliable detection method is needed. Low sensitivity may lead to underestimation of BM involvement. Both immunocytology and reverse transcriptase quantitative polymerase chain reaction (RTqPCR) offer improvements of both sensitivity and specificity in detecting NB cells within BM aspirates allowing detection of a single NB cell in 1 million normal cells (Beiske *et al.*, 2009). Results from both methodologies are predictive of outcome, encouraging their implementation within clinical practice (Moss *et al.*, 1991, Seeger *et al.*, 2000, Viprey *et al.*, 2014).

For detection of NB cells using immunocytology it is recommended to stain for GD_2. Although rare, some NB cells do not express GD_2 (Schumacher-Kuckelkorn *et al.*, 2017) so a secondary stain for other NB markers such as neuronal cell adhesion molecule (NCAM) or PHOX2B are advised (Komada *et al.*, 1998, Mehes *et al.*, 2001). The expression of PHOX2B in NB can also be exploited to detect NB cells within the BM using RTqPCR (Viprey *et al.*, 2014). In addition to PHOX2B, the expression of tyrosine hydroxylase (TH) may be quantified, these 2 NB markers are analysed against the reference gene β2-microglobulin (β2M) (Viprey *et al.*, 2007, Stutterheim *et al.*, 2008, Viprey *et al.*, 2014). There are additional methods that allow detection of NB cells within the BM including flow cytometry, but the need for high cell number makes implementation in clinic difficult (Komada *et al.*, 1998, Swerts *et al.*, 2004).

1.2.2 Biology

In order to eradicate NB from the BM the biology of these interactions must be understood. BM metastasis nearly always confers a poor prognosis in cancer (Weilbaecher *et al.*, 2011) and it is clear the interactions between tumour cells and the BM microenvironment play a role in the survival of these cells.

The mechanisms of metastasis to the BM are yet to be completely understood, however specific pathways thought to be involved have been identified. NB cells use blood vessels to access circulation, and can be detected in peripheral blood (PB) (Burchill *et al.*, 1994). The high incidence of BM metastasis is thought to be a result of its 'fertile' environment; including the high levels of growth factors beneficial to tumour cells. The homing of NB cells to the BM may be assisted by expression of C-X-C chemokine receptor type 4 (CXCR4), through complex interactions with stromal-derived factor-1 (SDF-1) (Geminder *et al.*, 2001, Sohara *et al.*, 2005). The invasion of NB cells into the BM is through an osteoclastic process (HaDuong *et al.*, 2015). The bone is a dynamic tissue, constantly remodelling to maintain integrity; haematopoietic derived osteoclasts reabsorb bone whilst mesenchymal derived osteoblasts replace bone. Osteolytic processes are activated by production of receptor activator of nuclear factor kappa-B ligand (RANKL) by both NB cells and activated osteoclasts and further fuelled by increased interleukin-6 (IL-6) release by mesenchymal stem cells (MSC) in response to NB cell presence (Ara *et al.*, 2009,

Rastogi *et al.*, 2015). This causes bone degradation allowing invasion of NB cells and releases growth factors to stimulate tumour proliferation (Ara *et al.*, 2009). Additional to increased proliferation within the BM, the NB cells continue to utilise the microenvironment to thrive, regulating other processing including angiogenesis. Matrix metallopeptidase 9 (MMP-9) expression recruits BM cells to the tumour where they contribute to angiogenesis (Jodele *et al.*, 2005).

The changes to the BM manifest clinically causing leukopenia and bi-cytopenia, as the normal haematopoiesis is suppressed by NB cells (Rastogi *et al.*, 2015). Net bone loss is also observed as the NB cells activate resident osteoclasts (Sohara *et al.*, 2005).

Although the presence of NB cells in the BM is statistically significant there is little information about the genotype of disseminated NB cells. Gaining knowledge on these cells is hindered by the varying infiltration levels which is usually below 30% at diagnosis (Abbasi *et al.*, 2015). There are currently few studies in which the genotype of NB cells isolated from the BM has been investigated (Morandi *et al.*, 2012, Scaruffi *et al.*, 2012, Vandewoestyne *et al.*, 2012, Abbasi *et al.*, 2015). However from current observations genetic aberrations present in the primary tumour have been detected (Vandewoestyne *et al.*, 2012); good genomic resolution has allowed detection of minor deletions (Abbasi *et al.*, 2015); and gene profiling has informed upregulated pathways (Morandi *et al.*, 2012, Scaruffi *et al.*, 2012). From comparisons between primary tumour and BM derived cells, upregulation of genes involved immune response including interferon (IFN) and histocompatibility antigen have been detected (Morandi *et al.*, 2012, Scaruffi *et al.*, 2012). These results give insight into how the NB cells evade the host immune response and highlight potential pathways to treat either to return normal physiological BM environment, preventing NB support, or to directly target NB cells.

1.3   Circulating biomarkers

Biomarkers are ways of quantifying biological processes, pathogenesis, responses to therapy and characteristics that inform biological processes. There are a large variety of biomarkers including biological material such as circulating tumour cells, miRNA and enzymes that can be detected and measured in the circulation, blood,

excretions, urine, saliva and tissue samples such as BM or tumour biopsies. Measurements gained from imaging are also a type of biomarker such as images from MIBG scans used in NB (Lessig, 2009). A biomarker may be a collection of changes to form a signature such as gene expression, translocations or proteomics. The large range of biomarkers means analysis is varied and must be adapted to suit the type of biomarker.

Biomarkers are screened for in two different ways: through knowledge-based experiments which use current knowledge of the biology of the disease to identify candidates or through unbiased experiments, using high throughput screening to find potential biomarkers (Henry and Hayes, 2012). Knowledge-based approaches, such as systems biology, use experiments that integrate information such as molecular pathways (Page *et al.*, 2013). Unbiased experiments test thousands of targets in high throughput data analysis to identify potential biomarkers and signatures to be evaluated.

1.3.1 Clinical applications

Biomarkers have been used in a clinical setting to inform areas such as risk of disease, diagnosis, prognosis, prediction, and in monitoring both toxicity and response to therapy. Biomarkers to inform risk of disease are usually genetic mutations that are passed through the germline to the patient and can be identified by methods such as genetic profiling. The breast cancer susceptibility genes 1 (BRCA1) and 2 (BRCA2) genes increase a person's chance of breast and ovarian cancer by as much as 80% (Hernandez *et al.*, 2014). BRCA1 and BRCA2 are TSG involved in maintaining genomic integrity (Welcsh and King, 2001). Mutations in BRCA mean the DNA is not repaired and mutations accumulate leading to cancer development. The BRCA genes are identified by genetic testing of a blood sample. The risk assessment biomarkers allow patients to make informed decisions about preventative measures such as having a mastectomy and oophorectomy if they are BRCA positive. A subset of these biomarkers are screening biomarkers which are used for early detection which means lower morbidity.

Diagnostic biomarkers are used to determine whether the patient has a disease, as the levels of a diagnostic biomarker will be different to that of a healthy individual.

The increased levels of urinary catecholamines in suspected NB patients are used to diagnose the disease.

Prognostic and predictive biomarkers provide information on patient outcome. Prognostic biomarkers give information on the likely course of the disease regardless of treatment, whereas predictive biomarkers indicate the chance of response or resistance to a specific therapy, allowing the best therapies to be selected. The presence of metastatic disease for example is a prognostic biomarker for many cancers as the spreading of cancer around the body usually means outcome is poor, localised disease indicates a better prognosis. The presence of the translocation found in the Philadelphia chromosome forming breakpoint cluster region protein-Abelson murine leukaemia viral oncogene homolog 1 fusion (*BCR-ABL*) is used as a predictive biomarker in chronic myeloid leukaemia for treatment with imatinib (Yeung and Hughes, 2012). Imatinib is a tyrosine kinase inhibitor and *BCR-ABL* gives a constitutively active tyrosine kinase and therefore presence of *BCR-ABL* predicts a good response to imatinib. Another example of a predictive biomarker would be the presence of human epidermal growth factor receptor 2 (HER2) on breast cancer cells to inform their response to trastuzumab, a HER2 specific antibody (Gajria and Chandarlapaty, 2011).

Biomarkers used for monitoring disease response are measured regularly to assess either toxicity levels in response to a drug or therapy to ensure the patient is not in danger of a serious adverse response or to assess the effect of the drug on the disease, to determine how effective the treatment is. Prostate specific antigens levels can be used to indicate response to therapy as they reflect the level of disease in patients with prostate cancer (Makarov *et al.*, 2009).

Biomarkers can also be used as surrogate end points. End points are used to characterise how the patient (in a clinical trial) feels or survives (Strimbu and Tavel, 2010) the goal being to detect improved survival. Biomarkers offer an indication of the treatment effectiveness and safety earlier than the end point of event free survival (EFS) and hence the term, surrogate end point. Using biomarkers in this way may allow for quicker drug approval, lowering costs of trials and lend to making decisions about new therapies earlier (Alan D. Smith, 2014, Smith *et al.*, 2014).

1.3.2   Therapeutic exploitation

Biomarkers can provide information on pathogenesis of disease and this can be used to create new targeted therapies. These may be therapies targeting the biomarker themselves or against a target identified as a result of pathway knowledge gained from biomarker discovery. Biomarkers that can be targeted directly by a therapy are known as druggable biomarkers (Saletta *et al.*, 2014).

Targeting biomarkers can be difficult as they are often present around the whole body and on normal cells and fluids, therefore specific targeting could expose the patient to high levels of toxicity. This can occur in NB as GD2, a biomarker for NB cells, is also present on peripheral nerve cells (Brodeur *et al.*, 2014). This is why disease-specific biomarkers are very appealing as therapeutic targets. Prostate specific antigens can be classed as both monitoring and druggable biomarkers and are also an example of disease-specific biomarkers. Cancer vaccines and monoclonal antibodies have been developed to target the prostate cancer cells by targeting PSA (Makarov *et al.*, 2009). The vaccines prime the host's immune cells to target and kill the prostate cancer cells, eradicating the disease.

1.3.3   Personalised medicine

Personalised medicine uses biomarkers to identify the best treatment for a patient's specific disease. For example a patient with NB that presents with *MYCN* amplification and *ALK* amplification could be given a course of chemotherapy including a panel of drugs tailored to each of these biomarkers. This is possible due to an understanding of the treatment's effect mechanism and how the biomarker contributes to the disease progression. The most applicable biomarkers for personalised (stratified) medicine are predictive and therapeutic biomarkers. Predictive biomarkers allow identification of therapies the patient will respond well to. Together with therapeutic biomarkers these can be used to optimise drug efficiency and reduce toxicity.

1.4 microRNA

microRNA (miRNA) are single stranded RNAs, 21-25 nucleotides long that originate from hairpin shaped precursors (Ambros *et al.*, 2009). Their role within the cell is to regulate levels and translation of mRNAs, with over 60% of human protein coding genes being controlled by miRNAs (Esteller, 2011). Lineage-4 (lin-4) was the first miRNA to be described; after genetic screening in nematodes it was shown to have a regulatory role in early development (Lee *et al.*, 1993, Wahid *et al.*, 2010). In 2000 let-7 was the second miRNA to be described and was observed to regulate late development process in *Caenorhabditis elegans* (Reinhart *et al.*, 2000). Advances in high-throughput technologies and bioinformatics processing has enhanced miRNA research, currently there are 4719 human miRNAs described on miRBase (www.mirbase.org). There is much interest in miRNAs in the field of oncology as they have shown promise as good prognostic and predictive biomarkers as well as therapeutic targets (Di Leva *et al.*, 2014).

Nomenclature of miRNAs is important as miRNAs synthesised from the same transcript can have different downstream targets and the same miRNA sequence can occur at multiple loci within the genome (Ambros *et al.*, 2009). Recommendations guide the naming of miRNAs, except for historical miRNAs lin-4 and let-7 (Ambros *et al.*, 2003). The first three letters of the miRNA identify the species, hsa for *Homo sapiens* and mus for *Mus musculus* Many miRNAs are evolutionarily conserved (Lagos-Quintana *et al.*, 2001), making it useful to give orthologs the same reference number and to ensure unrelated sequences do not have the same number. The number of the miRNA is given consecutively unless the sequence is similar to or identical to a previously identified miRNA. In the case of a similar miRNA sequence differing by 1 or 2 nucleotides, the same number is given but followed by a, b … n. When a miRNA is discovered with the same sequence it is given the same number followed by -1, -2 … -n as shown in Figure 1.4, C. Each hairpin precursor gives rise to two miRNAs: one of which is degraded (the passenger strand) and the other binds to an argonaute protein (Ago) to become a functioning miRNA. In rare cases both strands are loaded to Ago and become functioning miRNAs (Khvorova *et al.*, 2003). The less abundant or passenger miRNA was initially given a * to denote this (Figure

1.4, B). However this proves difficult when searching for miRNAs in databases as * is not a recognised search term. To overcome this the different miRNAs are referred to as -3p and -5p dependant on which arm of the hairpin precursor they derive from as illustrated in Figure 1.4, A.
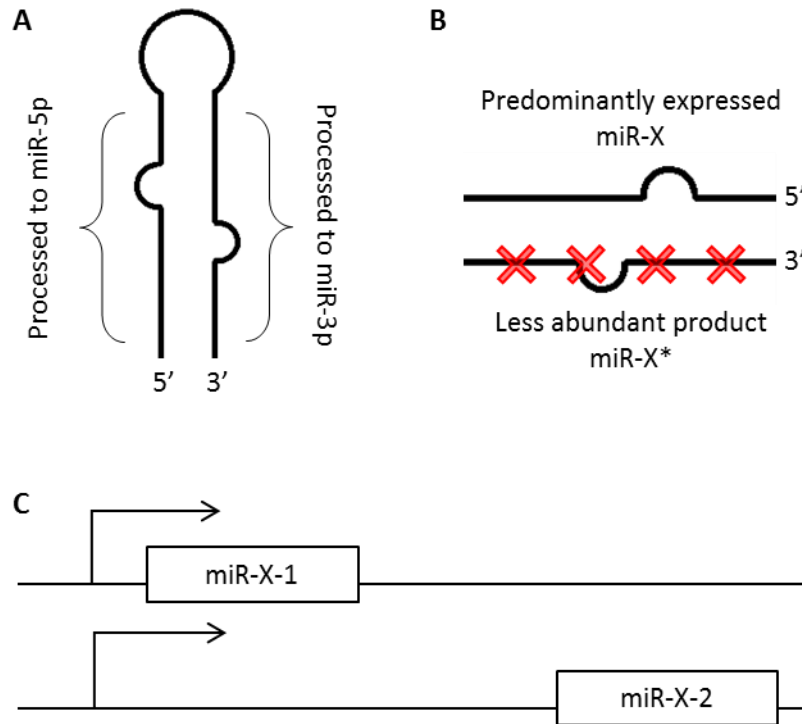
Figure 1.4 Nomenclature of miRNAs.

> A, Mature miRNA can be processed from both arms of the pre-miRNA, the arm the miRNA has been processed from is identified by either -3p if from the 3' arm or -5p if from the 5' arm. B, There is usually one arm of the pre-miRNA that is predominantly expressed as the mature miRNA. The most abundant form has no asterix, the least abundant form is followed by an asterix*. However this nomenclature can be unhelpful as searching for * in databases such as miRBase is not possible so a preference for -3p or -5p denotation is emerging. C, Mature miRNAs with the same sequence but differing gene loci are followed with -1, -2, -3 etc.

1.4.1 Synthesis

miRNAs are transcribed within the nucleus, modified in the cytoplasm, and can then act within the cell or if packaged in vesicles and exported affecting distal sites (Wahid *et al.*, 2010). miRNA coding regions can be positioned at different places within the genome, either intergenic, intronic or exonic (Figure 1.5). The majority of miRNAs are intergenic and are positioned in non-coding regions of the genome, approximately 50% are clustered and processed as a poly-cistronic primary transcript

(Wahid *et al.*, 2010). miRNAs positioned within coding regions are intronic or exonic, positioned within introns or exons respectively (Figure 1.5).
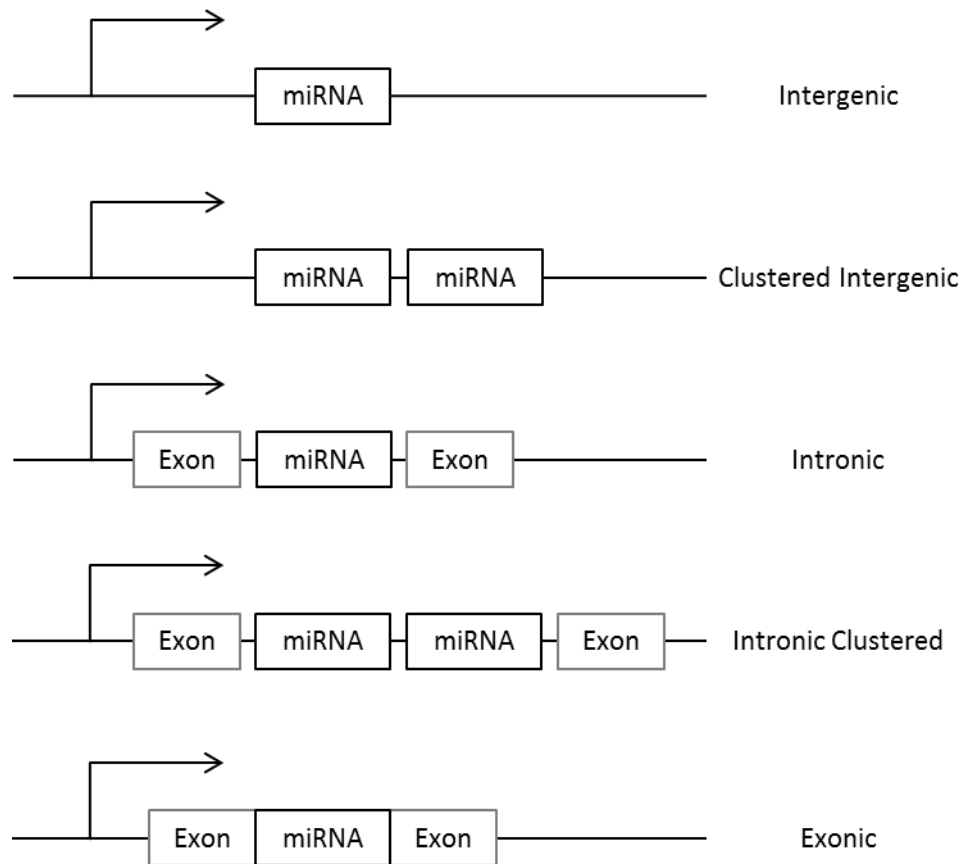
Figure 1.5 The positioning of miRNA transcripts on the genome.

    miRNA genes can be intergenic, positioned in non-coding regions of the genome. Intergenic miRNAs are most commonly clustered and therefore expressed as poly-cistronic primary transcripts. Some miRNA are alone and transcribed as mono-cistronic primary transcript. miRNAs can be mono or clustered within coding and non-coding transcription units also. They can exonic, fall in an exon of a gene or intronic, coded in the intron of a gene. Exonic intragenic miRNAs are also referred to as mirtronic.

Intronic miRNAs are thought to be processed alongside their host intron and therefore share common expression patterns (Ramalingam *et al.*, 2014), however it has been demonstrated that intronic miRNA expression can occur independently of the host gene promoter (Monteys *et al.*, 2010). There is little know about exonic miRNA processing, for the purpose of this review the synthesis of miRNA, Figure 1.4, will be explained using an intergenic single miRNA transcript.

Most miRNAs are transcribed by RNA polymerase II (RNA Pol II); a small population possessing Alu repeats are able to be transcribed by RNA polymerase III (RNA Pol III).

The transcript is processed into a 33nt hairpin precursor with a 5' cap and a poly A tail known as the primary miRNA (pri-miRNA). Drosha, a class 2 ribonuclease (RNase) III enzyme, and its co-enzyme DiGeorge syndrome critical region in gene 8 (DGCR8) are together known as the microprocessor complex, cleaving the pri-miRNA. DGCR8 binds to the single stranded RNA flanking segment of the pri-miRNA, guiding Drosha to cleave approximately 11 base pairs (bp) from the stem loop joint releasing the 5' cap and the poly A tail leaving a 2nt 3' overhang of the precursor miRNA (pre-miRNA) (Wahid *et al.*, 2010). The 60-70 nt hairpin pre-miRNA can be recognised by exportin 5 (EXP5), a Ran guanosine triphosphate (GTP)-dependant nuclear transport receptor (Lund *et al.*, 2004). EXP5 in the presence of Ran guanosine triphosphate exports the pre-miRNA from the nucleus into the cytoplasm of the cell through nuclear pore complexes. It is hypothesised that the EXP5 identifies 3' over hanged produced after Drosha cleavage and binds. The pre-miRNA is released into the cytoplasm as the GTP cofactor is hydrolysed (Lund *et al.*, 2004). Pre-miRNA is then cleaved in the cytoplasm at the terminal loop by dicer and trans activating response protein (TRBP) to give the 5' and 3' miRNA strands. dicer is an RNase III enzyme that is extremely specific cutting 22nt from the terminus of the pre-miRNA. The cofactor protein kinase interferon-inducible double stranded RNA-dependant activator and Ago have been shown to be needed for dicer function in cells (Koscianska *et al.*, 2011). Either the 5' or 3' strand can bind to Ago, forming the miRNA RNA silencing induced complex (miRISC) this is determined by the thermo dynamic stability of the ends of each miRNA (Khvorova *et al.*, 2003). The strand with the less stably paired 5' end is likely to be bound to Ago. The other strand, known as the passenger strand, is released from the Ago, dicer, and TRBP complex and degraded. This process is illustrated in Figure 1.6.
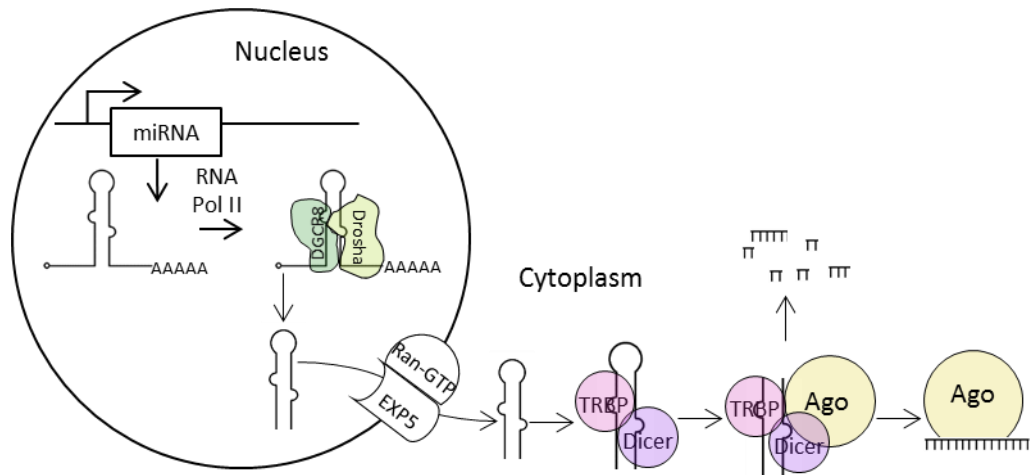
Figure 1.6 miRNA synthesis schematic.

> The miRNA is transcribed by RNA polymerase II (RNA Pol II). The capped and polyadenylated hairpin structure produced is the pri-miRNA and is several kilobases long, characterised by a stem loop structure. The pri-miRNA is cleaved by nuclear Drosha/DGCR8 (DiGeorge critical region 8) heterodimer at the stem releasing the pre-miRNA. Exportin 5 (EXP5) in the presence of cofactor Ran-GTP exports pre-miRNA into the cytoplasm. Dicer and TRBP bind to the pre-miRNA and cleave at the terminal loop releasing the miRNA duplexes. The passenger strand of miRNA is degraded and the guide strand remains bound to Ago as mature miRNA.

In 2009 it was shown that the miRNA maturation mechanism (Figure 1.4) thought to be universal to all miRNAs includes specific maturation steps that occur in individual miRNAs (Winter *et al.*, 2009). There are also alternative synthesis pathways for miRNAs such as the mirtron pathway which is not dependant on Drosha and the miR-451 pathway which is dicer independent (Zhi *et al.*, 2014). It is also known that biogenesis of specific miRNAs can be regulated such as lin-28 and let-7. Lin-28 is a stem cell specific regulator of let-7 and blocks the microprocessor cleavage of let-7 pri-miRNA (Winter *et al.*, 2009, Molenaar *et al.*, 2012).

1.4.2   Function

For the miRNA to be functional it needs to form the miRISC. After binding to Ago during the dicer cleaving, the miRNA is stabilised. For most miRNAs the Ago protein it binds to is Ago2 (Winter *et al.*, 2009), this complex forms the core of the miRISC. The full composition of miRISC is not known but other members of the Ago family are thought to bind along with other cofactors to create active miRISC. The miRNAs then guide the miRISC complex to the target mRNA and down regulate the gene

expression. miRNAs control a huge range of processes including cell proliferation, cell death, metabolism and differentiation through post transcriptional control of gene expression. One miRNA can have many target mRNAs and one mRNA can be targeted by several different miRNAs forming a complex miRNA-mRNA interaction network. miRNAs inhibit expression of targeting specific mRNAs in two ways, through translational repression or mRNA degradation initiation. The mechanism is determined by the complementarity of the miRNA to the target mRNA.

Most miRNAs possess binding sites in the 3' untranslated region (UTR), some pair with mismatches to the mRNA, and others bind with full complementarity (Wahid *et al.*, 2010). When the miRNA binds with high complementary to the mRNA degradation is initiated. The evidence for mRNA degradation by miRNA is the decrease in levels of target mRNA as the levels of miRNA increases (Huntzinger and Izaurralde, 2011). There are different models for how this degradation of mRNA occurs, one prominent hypothesis states that deadenylation of the mRNA is important to initiate the 5' to 3' mRNA decay pathway (Eulalio *et al.*, 2009). If there is some mismatch in the pairing of the miRNA to the target mRNA then translational repression occurs. Similarly to mRNA degradation there are several models for translational repression. Normally the eukaryotic initiation factor 4F (eIF4F) complex recognised the 5' cap of the mRNA and assembles the 40S ribosomal subunit to form the pre-initiation complex, elongation then occurs after the joining of 60S ribosomal subunit (Cooper, 2000). Both the initiation and elongation steps of translation are thought to be repressed by the presence of miRISC (Wahid *et al.*, 2010). The miRISC competes with the eIF4F for the 5' cap binding site it also prevents 60S assembly with the pre initiation complex, both lead to repression of initiation. Early ribosomal dissociation is a proposed model that leads to prevention of elongation (Petersen *et al.*, 2006). It is unclear as to which pathway is dominant and there is still much debate. The disruption of miRNA regulation through depleted or increased levels of miRNA has been shown to contribute to disease.

miRNAs have more recently been shown to have upregulatory effects on their targets through relief of repression (Vasudevan *et al.*, 2007), further adding to the complexity of the miRNA regulatory network. miRNA 369-3 is an example of miRNA

upregulatory effects. The seed sequence of miR-369-3 lies within the tumour necrosis factor alpha (TNF-α) AU-rich elements, which are areas that regulate mRNA stability, through binding here TNF-α expression is activated. These effects were only seen *in vivo* under serum starved conditions to slow proliferation of cells. It is thought that miRNAs oscillate between repression and activation dependant on stimuli and cell cycle.

1.4.3 Role within cancer

Some miRNAs are oncogenic (oncomiR) enhancing cancer phenotypes such as increased proliferative and drug resistance (Haug *et al.*, 2015). Conversely, miRNAs with tumour suppressing properties have also been described with the ability to decrease pro-tumour mechanisms such as migration and angiogenesis (Althoff *et al.*, 2015). These oncomiRs and tumour suppressive miRNAs provide further information and understanding to changes occurring within cancer.

Regulation of miRNA expression is not fully described, miRNA expression can be controlled by transcription factors and other miRNAs in response to stimuli (MacFarlane and Murphy, 2010), 10% of regulation is thought to be a result of DNA methylation (Han *et al.*, 2007). Aberrant expression of genes in cancer can lead to changes in levels of downstream targeted miRNAs, such as the upregulation of *MYCN*. In NB *MYCN* is upregulated in 22% of cases and has been linked to the upregulation of 7 miRNAs (Schulte *et al.*, 2008, Domingo-Fernandez *et al.*, 2013). Of these miRNAs, miR-221 expression was induced my *MYCN in vitro* and overexpression is linked to other cancers.

1.5 miRNA in NB

miRNAs are extremely important in development and therefore miRNAs are likely to play a role in NB. One of the first miRNA profiling studies in NB identified a signature of 32 differentially expressed miRNAs, including miR-184 (Chen and Stallings, 2007b). miR-184 overexpression is shown to induce the apoptosis of NB cells (Chen and Stallings, 2007). miR-184 is a repressed downstream target of MYCN overexpression *in vitro* has been shown to inhibit the growth and induce apoptosis of NB cells through decreasing levels of AKT2 (Foley *et al.*, 2010). The study also identified a

substantial difference of miRNA expression in *MYCN* amplified NB patients that are at a higher risk with a poorer prognosis - these miRNAs are important as they can identify altered pathways that could be increasing the aggressive phenotype. Several other studies have also observed this change in miRNA expression between *MYCN* amplified and non-amplified samples (Schulte *et al.*, 2008, Schulte *et al.*, 2010). Within these signatures there are miRNAs that are targets of *MYCN*, but more interestingly there are miRNAs that are linked with increased *MYCN* signalling but not direct downstream targets of the gene (Zhi *et al.*, 2014). Alongside the obvious therapeutic benefit of HR NB specific miRNAs, groups have also identified miRNA signatures that are highly expressed in low-risk NBs, creating the potential for prognostic and predictive applications allowing for better treatment selection for patients (De Preter *et al.*, 2011). Currently there are low survival rates for children with NB that have *MYCN* amplification, these miRNAs can provide therapeutic options for non-responsive *MYCN* NB.

1.5.1 Therapeutic exploitation of miRNA in NB

Research into miRNAs has grown rapidly since 1993 and it is clear that miRNAs are differentially expressed between normal and NB (Tsang *et al.*, 2003, Murray *et al.*, 2015) but there are currently no miRNA treatments or stratifications approved for routine clinical use. It is well characterised that miRNAs can serve as biomarkers in cancer, aiding diagnosis, staging, and predicting response to treatment, particularly enhanced by tissue-specific signatures of miRNAs. Tumour biopsy samples or more excitingly circulating cells or cell-free miRNAs can be profiled with potential for a range of clinical applications. Currently most biomarker studies have been retrospective and not further validated within independent cohorts; prospective studies are needed to evaluate miRNA biomarker signatures' worth in a clinical setting. Exploiting miRNAs for therapeutic strategies is a large research area, using mimetics to reinstate tumour suppressing miRNAs and the associated pathways, or knockdown strategies to target oncomiRs both offer therapeutic benefits. It has been shown in several *in vivo* studies that miRNA mimetics can alter the characteristics of cancer cell lines, similarly inhibitors of oncomiRs reduces

aggressive phenotypes such as migration and proliferation (Hsu *et al.*, 2014, Althoff *et al.*, 2015).

Within the field of NB miRNAs can serve as good biomarkers both for diagnosis and staging of NB (Bienertova-Vasku *et al.*, 2013). As mentioned above, many studies have identified miRNA panels that are differentially expressed in different subtypes, such as *MYCN* amplified and between risk groups (Chen and Stallings, 2007c, Bray *et al.*, 2009, Bienertova-Vasku *et al.*, 2013). miRNAs have the advantage over mRNAs of being much more stable biomarkers. Packaging into exosomes, high-density lipoproteins, or association with Ago proteins, protects miRNAs against processing by ribonucleases. After extraction it has been shown that miRNAs remain stable for up to 12 months when stored at -70 degrees Celsius (°C) (Sourvinou *et al.*, 2013). The heterogeneity within NB is a major obstacle for biomarker discover, a biomarker must overcome this heterogeneity within samples and be specific, sensitive and preferable non-invasive.

Further application of miRNA biomarkers within NB could be to assess response and predict or detect relapse by detecting circulating tumour cells. BM metastasis are present in 50% of children with NB and these cells are more aggressive and drug resistant (Meads *et al.*, 2008). These infiltrating cells could be detected in BM aspirates using a NB panel of miRNAs, however BM aspirates are a very invasive procedure (Chu *et al.*, 2011). A solution to this could be to use secreted signatures specific to aggressive BM metastatic cells, detectable from a blood sample, a much less invasive procedure. This strategy would exploit the ability of NB cells to secrete miRNAs into the microenvironment in vesicles such as exosomes. There is only one published study investigating the BM infiltrating NB cell miRNA profile, the results suggest differential expression of 160 miRNAs in the metastatic cells compared with tumour (Stigliani *et al.*, 2015).

As discussed above, the miRNA profile of NB infiltrating cells could be used to detect relapse or even metastasis that is not detected through cytology or MIBG scans. Further knowledge can be gained about the differences in metastatic BM cells from tumour by profiling the miRNA of these BM infiltrating NB cells. Through this, identification of miRNAs dysregulated in aggressive NB is possible and will inform the

mechanisms propagating the metastasis and support of BM infiltrate NB cells. Of the 160 miRNAs differentially expressed further analysis and criteria were applied to identify miR-659-3p as a key biological miRNA (Stigliani *et al.*, 2015).

Exploitation of miRNAs to treat NB can be achieved by one of two strategies; miRNAs can be targeted for degradation to prevent them from aiding the cancer growth, or mimetics can be administered to return depleted miRNA levels to normal for a therapeutic benefit. A combination of miRNA and small interfering (si)RNA therapy has been used *in vivo* to treat ovarian cancer cell lines. Reduction in tumour growth was seen after siRNA-mediated silencing of the oncogene ephrin type-A receptor 2 (EPHA2), this was enhanced when an miRNA targeting EPHA2 was also administered (Nishimura *et al.*, 2013). This study shows the benefit of miRNA therapy for inclusion in a multi model strategy, by boosting existing drugs' anti-tumour effects.

Currently there is just one miRNA drug to have reached clinical trial, MRX34, a mimic of the tumour suppressor miR-34 which affects multiple oncogenic pathways (Bader, 2012). MRX34 is produced by Mirna, the mimic is encapsulated in a liposomal nanoparticle delivered through injection. The drug was entered into in a phase I (NCT01829971) clinical trial recruiting patients with melanoma, lymphoma, multiple myeloma, liver and lung cancer who have end stage disease. In September 2016, this trial was halted due to multiple immune-related serious adverse events, three of these resulting in death (Beg *et al.*, 2017). In the report for the phase I study preliminary results show partial response in patients with renal cell carcinoma, melanoma and hepatocellular carcinoma. If adverse side effects can be corrected then miRNA therapies are achievable and have a benefit for patients with cancer. Within NB miR-34 has been identified as a potent tumour suppressor, with upregulation decreasing tumour growth (Welch *et al.*, 2007b, Tivnan *et al.*, 2011, De Antonellis *et al.*, 2014). Mirna also have mimetics for miR-215, miR-101, miR-16 and let-7 in the pipeline. To get a functioning miRNA mimetic into cancer cells requires several challenges to be overcome. Although there are many obstacles to overcome for miRNAs to become routinely used as biomarkers and therapeutic strategies within clinics, miRNAs show huge potential and with further screening and validation could have a great impact on patient survival.

1.6   Hypothesis and aims

The hypothesis of my thesis is that miRNAs are drivers of the self-renewing metastatic disease of BM in children with HR NB, and may be useful biomarkers to improve stratification of children for more personalised adaptive treatment exploiting miRNAs or the pathways that they regulate as targets for the development of more effective kinder treatment to improve outcomes.

To test my hypothesis I have:

1. Isolated and characterised NB cells from BM aspirates of children with HR disease (Chapter 2).

2. Examined the miRNA expression profile of NB cells isolated from the BM to investigate their heterogeneity and identify candidate driver pathways of self-renewal, migration and survival (Chapter 3).

3. Examined the expression of miRNAs in BM aspirates, blood and exosomes to reveal candidate miRNAs that may be used as minimally invasive tools to predict patient response and outcome (Chapter 4).

Chapter 2 Isolation and characterisation of NB cells from BM aspirates

2.1 Introduction

NB cells metastasise to the BM in 50% of patients with HR disease. Those with the highest levels of infiltration have reduced survival (Viprey *et al.*, 2014, Corrias *et al.*, 2018). These BM infiltrating cells are hard to treat as they present with aggressive phenotypes and efficient delivery of chemotherapeutics into the BM is difficult, the BM is also a common site of relapse (Matthay *et al.*, 1993, Seeger *et al.*, 2000). Isolating and characterising these cells is therefore critical to identify the drivers of this drug-resistant metastatic disease so that targets for the development of more effective treatment can be identified to eliminate BM disease, with the goal of improving survival for children with HR NB.

The NB cells were first isolated from the normal BM cells of the microenvironment and propagated to allow larger cell numbers for multiple methods of characterisation, including studying the phenotype of these cells. Magnetic activated cell sorting (MACS™) technology has been used by many groups to enrich or deplete cell populations for specific cell types by positive or negative selection of cells exploiting cell-surface antigens. Using this approach for positive selection of cells, a magnetic field is used to bind antigen expressing cells allowing separation from negative cells which can be washed from the column (as depicted in Figure 2.2). A stable cell-surface antigen is the most useful marker to enrich for specific cell populations as this allows for isolation of NB cells GD_2 expression was used in this study.

Whilst GD_2 is a cell surface disialoganglioside expressed in tumours of neuroectodermal origin such as NB and melanoma (Mujoo *et al.*, 1987, Tsuchida *et al.*, 1987), it is also expressed by some normal cells including neurons, skin melanocytes, and peripheral pain fibres (Lammie *et al.*, 1993). Importantly, expression of GD_2 has also been reported MSCs that reside within the BM (Martinez *et al.*, 2007, De Giorgi *et al.*, 2011).

In these studies the culture conditions have been optimised to propagate NB cells, however it was important to characterise the GD_2 positive cells to confirm they were indeed NB. Using immunocytology, cells were examined to confirm expression of GD_2 and for expression of additional NB markers TH, PHOX2B and nestin (Burchill *et al.*, 1994, Thomas *et al.*, 2004).TH is the rate limiting enzyme for catecholamine biosynthesis (Daubner *et al.*, 2011), a feature of NB cells which is exploited for diagnosis by the detection of catecholamine metabolites in urine (Laug *et al.*, 1978) PHOX2B encodes a homeodomain transcription factor that promotes cell cycle exit and drives the differentiation of neural crest precursors to sympathetic neurons along with PHOX2A (Cheung and Dyer, 2013). Both TH and PHOX2B mRNAs have been used to quantify infiltration of NB cells in the BM (Burchill *et al.*, 1994, Trager *et al.*, 2003). Nestin is an intermediate filament protein expressed by neural progenitor cells and several malignancies (Neradil and Veselska, 2015). In NB nestin expression is thought to be a marker of stem-like cancer cells, correlating to high MYCN expression and playing a role in tumorigenesis (Thomas *et al.*, 2004, Ma *et al.*, 2014).

Where it was possible to propagate NB cells, their migration and self-renewal from a single cell was examined. These are putative phenotypes of aggressive cancer cells which describe the self-renewing drug resistant cells disseminated within the BM. Self-renewal from a single cell was assessed both in suspension in media and within semi-solid agar.

The aims in this chapter were:

1. To isolate and propagate NB cells from BM aspirates of children with HR NB
2. To characterise the GD_2 positive fraction of BM cells
3. To assess migration and self-renewal properties of NB cells

2.2 Materials and methods

2.2.1 Cell line culture

Cell lines were routinely maintained in culture by Ms Louise Jeffers or Ms Kimberley Cass, when 80% confluency was reached cells were trypsinised and split at a ratio of 1:5 as described in 2.2.5.1. The cell lines listed in Table 2.1 were used throughout this thesis as controls or references.

Table 2.1 Positive cell lines used for studies.

Characteristics of control cell lines used. Details of the source, origin, cell type and media for each. McCoy's 5A, Roswell Park Memorial Institute (RPMI) 1640, Dulbecco's Modified Eagle's (DMEM) and Minimum Essential Eagle's (EMEM) media and glutamine were sourced from Sigma (Missouri, USA). Non-essential amino-acids (NEAA) and sodium pyruvate were sourced from Thermo Fisher (Paisley, UK). All cell lines are of human origin. Cells sourced from the Children's Cancer Institute Australia (CCIA) were kindly donated by Professor Michelle Haber. Cells sourced from the University of Newcastle (UoN) were kindly donated by Dr Chris Redfern. Cells sourced from the University of Leeds (UoL), Lab 1 were kindly donated by Professor Maggie Knowles. ATTC denotes American Type Tissue Collection. FCS represents foetal calf serum. mM denotes millimolar and nM denotes nanomolar

Cell Line	Source	Origin	Cell Type	Media
BE(2)C	CCIA	2 year old, male	NB, *MYCN* amplified	DMEM + 10% FCS+ 2mM glutamine
HEK-293FT	UoL, Lab 5	unknown	Sub-line HEK-293; Human embryonic kidney cells with adenovirus type 5 DNA	D-MEM (high glucose), 10% FCS, 0.1% nM NEAA, 6mM glutamine, 1mM MEM sodium pyruvate
IMR-32	ATTC	13 month old, male	NB,*MYCN* amplified	50% DMEM, 50% RPMI 1640 + 10% FCS + 2mM glutamine

Jurkat	UoL, Lab 5	14 year old, male	Acute T Cell Leukaemia	RPMI 1640 + 10% FCS+ 2mM glutamine
Kelly	CCIA	1 year old, female	NB, *MYCN* amplified	RPMI 1640 + 10% FCS+ 2mM glutamine
SH-SY5Y	UoN	4 year old, female	NB, thrice-cloned sub-line of SK-N-SH	DMEM + 10% FCS+ 2mM glutamine
SK-N-MC	ATTC	14 year old, female	Ewing's sarcoma, EWS-FLI-1 Type 1 translocation	DMEM F12 + 10% FCS+ 2mM glutamine
SK-N-SH	ATTC	4 year old, female	NB, Non-*MYCN* amplified	50% DMEM, 50% EMEM + 10%FCS + 2mM glutamine
U-2 OS	ATTC	15 year old, female	Osteosarcoma	McCoy's 5A + 10% FCS + 2mM glutamine

2.2.2   Clinical samples

Upon suspected diagnosis of NB, BM aspirates (1 millilitre (ml)) were taken from children in the UK and Ireland. Aspirates were transported from UK centres, for the isolation of NB cells, at room temperature in 12ml of Leeds Antibiotic Media (LAM; RPMI 1640 media with 2mM glutamine, 100 units (U) penicillin (Sigma), 0.1mg/ml streptomycin (Sigma) and 10% foetal calf serum (FCS, Labtech International Ltd, East Sussex, UK). All children with HR disease were treated in HR-NBL-1.0/SIOPEN, HR-NBL-1.5/SIOPEN or HR-NBL-1.7/SIOPEN (recruitment from 11.10.2012-30.06.2017); ethical approval number 01/04/087 and clinical trial number NCT01704716. After confirmation of NB diagnosis samples were propagated where informed consent had been given; for HR patients this was consent through the trial ethics and for other NB patients consent was given through the Children's Cancer and Leukaemia Group (CCLG) tissue bank, with Medical Research and Ethics Committee (MREC) approval.

Once received in the laboratory all samples were recorded and tracked using the sample management software Achiever (Achiever Laboratory Management Software, Interactive Software Ltd, Birmingham, UK).

Within the duration of the trial BM aspirates were taken at additional time points throughout the trial as shown in Figure 2.1, upon receipt of BM aspirate samples, GD$_2$ positive cells were isolated and propagated.
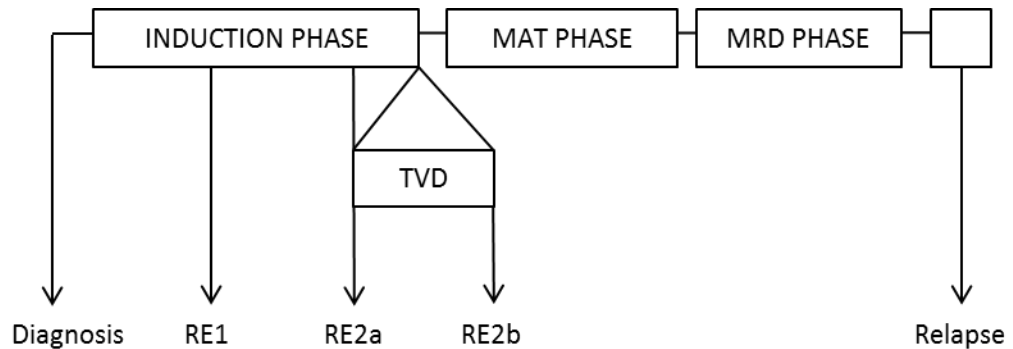
Figure 2.1 Time points at which BM aspirates were taken from children entered into HR-NBL-1.0/1.5/1.7.

MAT represents myeloablative therapy. MRD represents minimal residual disease therapy. Diagnostic samples were taken before administration of any drugs. RE1 samples were taken mid-induction, at day 40 of treatment. RE2a samples were taken at the end of the induction phase, day 80 of treatment. Re2b samples were taken from patients that required extra chemotherapeutics (TVD cycles) before moving onto MAT phase, samples were taken at the end of the TVD treatment. The time points across all trials remained the same but the therapies used within each stage of treatments changed across trials.

2.2.3   Isolation of GD$_2$ positive cells from BM

On arrival, each sample was processed using the MACS™ system (Miltenyi Biotech, Bisley, Surrey, UK) as summarised in Figure 2.2. Briefly, BM aspirate was centrifuged at 405g for 5 minutes (min) to separate the cellular fraction and red cells were lysis was performed; BM was incubated in 10ml erythrocyte lysis buffer (Buffer EL, Qiagen, Manchester, UK) at 4°C for 10 min. The white cells were pelleted by centrifugation at 405g for 5 min. The white cell count (wcc) was determined by counting the viable white cell number using the trypan blue exclusion assay and a Neubauer haemocytometer. To label GD$_2$ positive cells 60 microliters (μl) MACS buffer (bovine serum albumin, BSA, 0.5%; (weight/volume, w/v) Sigma and ethylenediaminetetacetic acid (EDTA; 2mM) in 1X phosphate buffered saline (PBS;

(w/v), Oxoid Limited, Basingstoke, UK), 20µl FcR blocking reagent (Miltenyi Biotech) and 10µl anti-GD$_2$ (14.G2a, 0.5mg/ml, BD Biosciences, Oxford, UK) was added per 1x10^7 cells and incubated at 4°C for 30 min. After washing by adding 2ml of MACS buffer, cells were pelleted by centrifugation at 405g for 5 min. Cells were then incubated for 15 min at 4°C in 80µl MACS buffer and 20µl rat anti-mouse IgG2a+b microbeads (Miltenyi Biotech) per 1x10^7 cells to label GD$_2$ positive with the magnetic microbeads. After washing by addition of 2ml MACS buffer, cells were pelleted by centrifugation at 405g for 5 min and resuspended in 500µl of MACS buffer. An LS column (Miltenyi Biotech) was placed into the QuadroMACS™ separator (Miltenyi Biotech) and primed with 3ml MACS buffer. The cells were placed into the primed LS column, the column was washed 3 times with 3ml MACS buffer and the cells not magnetically labelled, therefore not held within the magnetic field of the column, and were collected into a falcon tube. The LS column was then removed from the magnetic field of the QuadroMACS™ separator and 5ml of MACS buffer was flushed through using the plunger, eluting the positive cells into a new falcon tube. Both fractions were centrifuged at 405g for 5 min and the viability of recovered cells, resuspended in LAM, was counted using the trypan blue exclusion assay and a Neubauer haemocytometer. GD$_2$ negative cells were seeded into a 25cm^2 tissue culture flask (T25, Corning, Falcon) in LAM as this is optimum for NB cell growth, ensuring any non-GD$_2$ positive cells could propagate. The low adherence (LA) plate assay, as described in Section 2.2.6.1, was set up using GD$_2$ positive cells and remaining cells were seeded into a T25 flask in LAM. Both fractions were incubated in a humidified chamber at 37°C, 5% carbon dioxide (CO$_2$) in air. If after 4 weeks there were no viable cells in the positive flask, both fractions were discarded. Positive cells were maintained in culture until each investigation summarised in Figure 2.3 had been completed; cells were then resuspended in dimethyl sulfoxide (DMSO, 10% in LAM; (volume/volume, v/v), Sigma) and placed into cryovials and frozen gradually to -80°C to minimise the number cell passages.
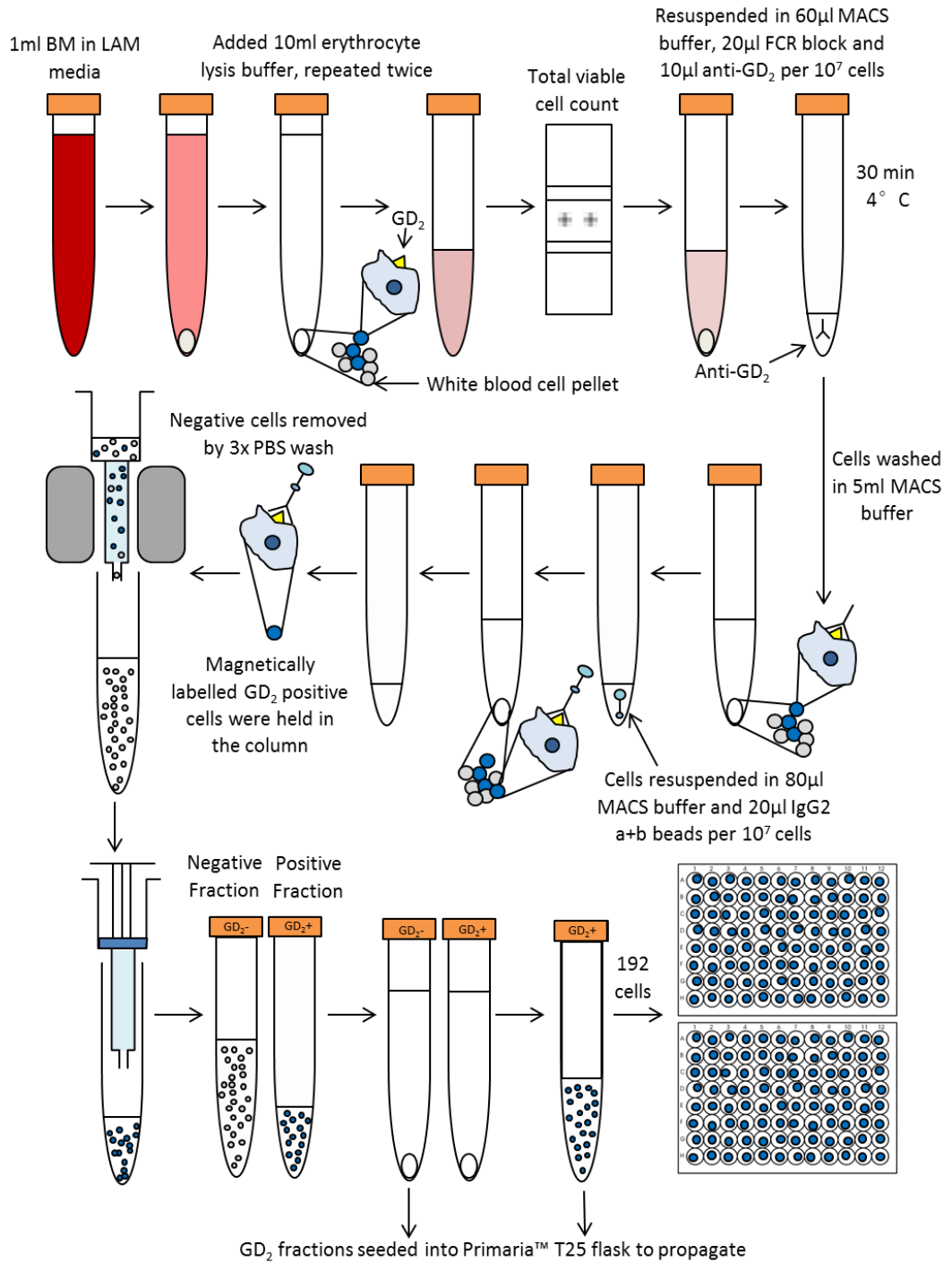
Figure 2.2   Isolation of GD₂ positive cells from BM aspirates.

Cells were isolated using MACS™ cell sorting technology. MACS buffer contained BSA (0.5%; w/v) and 2mM EDTA in PBS. GD₂ antibody (clone 14.G2a) was sourced from BD Biosciences.
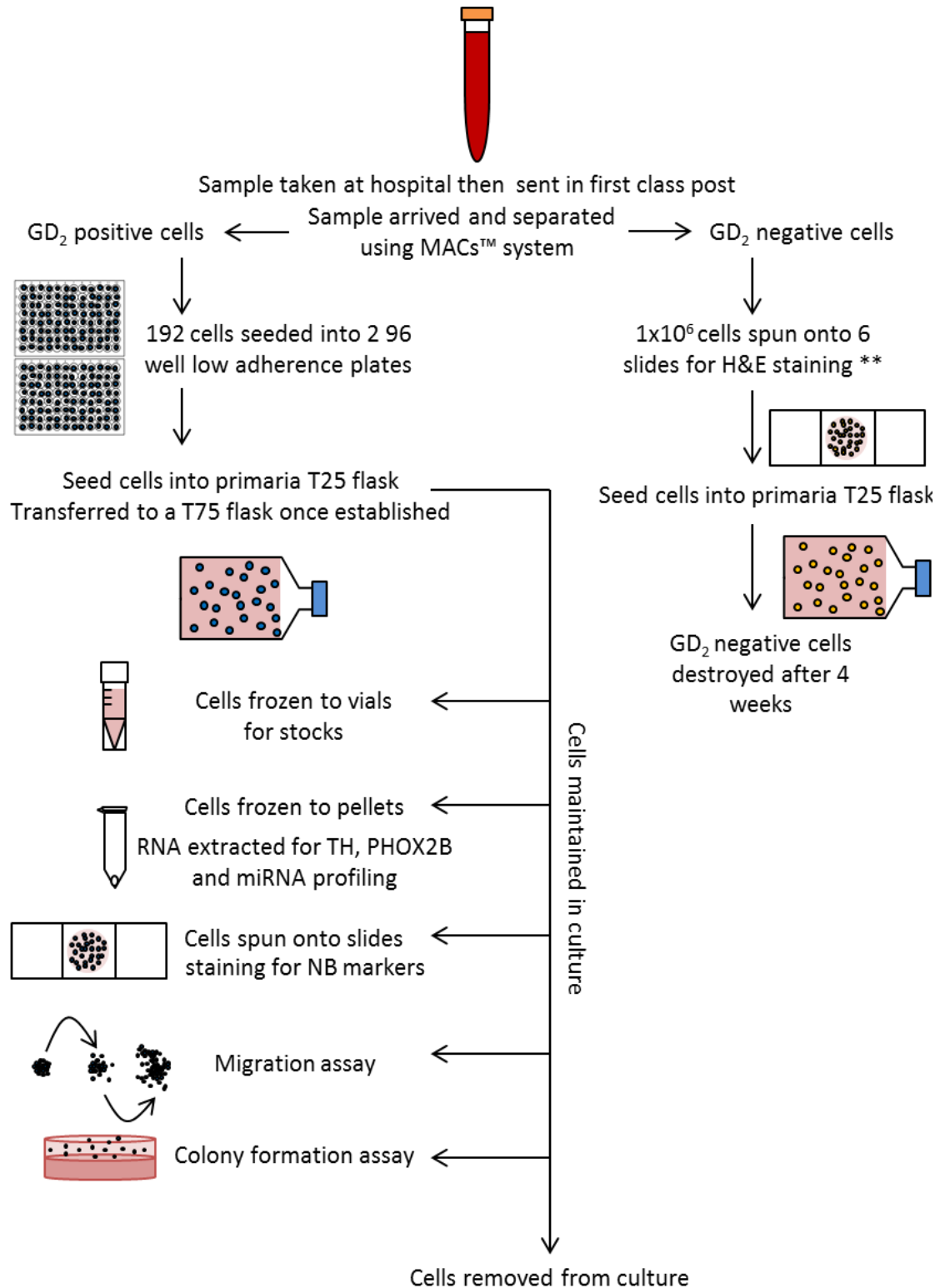
Figure 2.3 Schema of characterisation of GD₂ positive and negative cells whilst maintained in culture.

The LA assay was not set up for all samples, those with insufficient number of positive cells were instead seeded into a flask. **negative cells were not spun onto slides for haematoxylin and eosin (H&E) staining for every samples processed.

2.2.4   Characterisation of GD$_2$ negative cell population from BM

2.2.4.1   Culture of GD$_2$ negative cells

The GD$_2$ negative cells were maintained in culture to establish if the BM aspirates contained GD$_2$ negative NB cells that could be propagated. Flasks were discarded after 4 weeks or when propagation of GD$_2$ positive cells growth was seen, after adding distel (10% in water; (v/v), Snailwell, Cambridgeshire, UK) disinfectant for 30 min the flasks were sent for sterilisation via autoclaving then for incineration.

2.2.4.2   Cytospins of GD$_2$ negative cells for haematoxylin and eosin staining

After separation the number of GD$_2$ negative cells was counted using the trypan blue exclusion assay and a Neubauer haemocytometer, 6×10^5 cells were resuspended in 3ml of PBS from which 6 cytospins of 0.5ml each were prepared. Cytospins were prepared on superfrost® microscope slides (Thermo Fisher) by centrifugation at 1,000g x 3 min of 0.5ml per slide using a Hettich cyto-system (Hettich rotor-fix 32A, Manchester, UK). Excess PBS was aspirated before removing the fastening ring and chamber. Slides were dried by centrifugation at 3,000g for 1 min and leaving overnight at room temperature. Cytospins were wrapped in foil and stored at -20°C until used for characterisation studies.

Once dry, to allow identification of cell morphology the slides were stained with haematoxylin (identify nucleic acid) and eosin (non-specific protein stain) as described in Table 2.2. After dehydration in xylene cover slips were fixed over the cells using a drop (approximately 10µl) of DPX mountant (Sigma). Slides were examined by light microscopy (Olympus CKX41 microscope; Olympus, Southend-on-Sea, Essex, UK) and imaged using Cell B software (Olympus).

Table 2.2 Protocol for haematoxylin and eosin (H&E) staining.

The procedure was performed in a fume hood. Mayer's haematoxylin (2.3%; v/v 80ml haematoxylin (0.5M in absolute ethanol, Sigma) 97.7%; v/v 3400ml sodium iodate solution (2mM in dH_2O; Sigma), citric acid (6mM in dH_2O; Acros Organics, Thermo Fisher), chloral hydrate (0.35M in dH_2O; Sigma), aluminium potassium sulphate (0.34 molar (M) in dH_2O; Sigma)) was passed through filter paper before use.

Solution	Incubation Time
Mayer's haematoxylin (2.3%; v/v)	30s
Running tap water	5 min
Scott's solution (2% magnesium sulphate (Sigma); 0.35% sodium bicarbonate (Sigma))	1 min
Running tap water	5 min
Eosin (0.5% w/v, Sigma)	2 min
Running tap water	5 min
70% Ethanol	1 min
90% Ethanol	1 min
100% Ethanol	2 min
100% Ethanol	2 min
Xylene	2 min
Xylene	2 min

2.2.5 Characterisation of GD_2 positive NB cells from BM aspirates

2.2.5.1 Culture of GD_2 positive cells

GD_2 positive cells were propagated in culture in Tissue Culture Zero (an isolated culture facility for primary cells until mycoplasma negativity is confirmed); when they reached 80% confluency (assessed by examination of flasks at 10X magnification using a light microscope) cells were transferred from a T25 flask into a $75cm^2$ tissue culture flask (T75, Primaria™, Falcon) and maintained in culture on Primaria™ plastic (Falcon, BD Biosciences) in LAM. Cells were passaged whenever they reached 70-80% confluency, media was aspirated then cells were washed with PBS, incubated for 2 min in EDTA (0.1% in PBS; (w/v), Invitrogen, Thermo Fisher) followed by incubating in 5ml trypsin (0.25% in PBS; (v/v), Sigma) for 2 min or until cells had detached as determined by light microscopy (Nikon TMS, Nikon, Kingston upon

Thames, Surrey, UK) at 10X magnification. Flasks were tapped gently to remove cells from the plastic surface. LAM (5ml) was added to the flask and the cells were collected by centrifugation at 405g for 5 min, cells were resuspended in 6ml fresh media and split between flasks at a ratio of 1:3. Cells were cultured in a humidified chamber (Sanyo CO_2 Incubator, MCO-2OAIC, Sanyo Gallenkamp Plc., Loughborough, UK) in 5% CO_2 in air at 37°C. All cultures were mycoplasma negative; cultures were tested within a month after isolation for mycoplasma using the EZ-PCR mycoplasma test (Geneflow Ltd, Fradley, Staffordshire, UK) by Mrs Andrea Berry or Ms Kimberley Cass.

2.2.5.2 Immunocytology for NB markers

A 70% confluent flask of cells was trypsinised (Section 2.2.5.1), pelleted by centrifugation at 405g for 5 min and resuspended in PBS (500ul per cytospin; Section 2.2.4.2). Immunocytology staining for NB markers on cytospins prepared from primary cells was carried out by Mrs Andrea Berry. NB primaries were analysed for expression of each protein using optimised conditions as described in Table 2.3. For each antibody and sample a matching isotype control was included, and in each batch of analyses a cytospin of a positive NB cell line was included. After NB marker immunocytology, all cytospins were counterstained with haematoxylin, dehydrated and then mounted as described in Section 2.2.4.2.

2.2.5.2.1 Immunocytology using EnVision™ detection systems

All reagents were used as provided in the EnVision™ kit (Dako, Agilent, California, USA), incubations were carried out at room temperature, unless otherwise stated using the Shandon™ Sequenza™ staining rack (Thermo Fisher). Cytospins were fixed and permeabilised using conditions stated in Table 2.3, any endogenous peroxidase activity was quenched by incubating the cytospins for 5 min in peroxidase block. Residual block was removed by incubating cytospins for 2 min in ddH_2O then 2 min in tris buffered saline with tween (TBST; 33mM Tris HCl, 75mM NaCl, 0.1% tween (v/v), Sigma, in double distilled water (ddH_2O); pH 7.4). Primary antibody was diluted to the predetermined concentration (see Table 2.3) in antibody diluent then applied to cytospins and incubated for 30 min, unless otherwise stated. To remove primary antibody, cytospins were washed twice for 2 min TBST. Labelled polymer-HRP was

applied to cytospins and incubated for 30 min. The cytospins were then washed twice for 2 min in TBST. Positive staining was visualised by incubating cytospins with 3'diaminobenzidine (DAB) substrate for 15 min. This resulted in the production of a brown precipitate that could be identified on examination under light microscopy. Cytospins were then rinsed in running tap water for 1 min, counterstained and mounted.

2.2.5.2.2 Immunocytology using 3-stage peroxidase

Incubations were carried out at room temperature, unless otherwise stated using the Shandon™ Sequenza™ staining rack. Cytospins were fixed using conditions stated in Table 2.3, then incubated in peroxidase block (EnVision™ kit reagent) for 5 min to quench any endogenous peroxidase activity present within the tissue; this was followed by 2 washes in TBST to remove residual hydrogen peroxide. The Avidin/Biotin blocking kit (ab64269, Abcam, Cambridge, UK) was used to block endogenous biotin or biotin-binding proteins present within the tissue. The Avidin/Biotin blocking kit contains pre-diluted reagents that were used as supplied, the contents of kit components are company proprietary. Cytospins were incubated with Avidin D solution for 10 min then washed twice for 2 min in TBST, then incubated with Biotin solution for 10 min then washed twice for 2 min in TBST. Primary antibody diluted in antibody diluent (EnVision™ kit reagent) to the predetermined concentration (see Table 2.3) was applied to the cytospins and incubated for time specified in Table 2.3. Cytospins were then rinsed twice for 2 min in TBST, secondary antibody (Goat anti-Rat IgG-Fc Fragment cross-adsorbed Antibody Biotinylated (A110-236B); Cambridge Bioscience, Cambridge, UK) diluted 1:100 in antibody diluent was applied and cytospins incubated for 30 min. The cytospins were rinsed twice for 2 min with TBST then incubated with streptABcomplex for 30 min then rinsed twice for 2 min with TBST. Cytospins were then incubated with DAB substrate for 15 min, rinsed in running tap water for 1 min, counterstained and mounted.

Table 2.3 Optimised antibody information and conditions for labelling of NB cytospins.

All incubations were at room temperature unless otherwise stated. EnVision™ detection kits were supplied by Dako, Agilent. o/n denotes overnight. All markers were detected using the EnVision™ unless marker with * which indicates 3-stage-peroxidase detection was used. MRP4 represents multidrug resistance protein 4. PFA represents paraformaldehyde.

Target	Antibody	Dilution	Positive control	Fixation	Permeabilisation and block
CD45	Rabbit ab40763 (Abcam)	1:100	Jurkat	4% PFA in PBS 10 min	
CD57	Mouse ab187274 (Abcam)	1:100	U-2 OS	4% PFA in PBS 10 min	0.1% triton-x in PBS 10 min
GD$_2$	Mouse 554272 (BD Biosciences)	1:100	IMR-32	4% PFA in PBS 10 min	
MRP1	Mouse ab24102 (Abcam)	1:50 o/n 4°C	BE(2)C	100% methanol 5 min -20°C	10% BSA, 0.1% tween in PBS 1h
MRP4*	Rat ab15602 (Abcam)	1:20 o/n 4°C	BE(2)C	100% acetone 2 min -20°C	
NCAM	Mouse MA1-06801 (Thermo Fisher)	1:200	Kelly	4% PFA in PBS 10 min	
Nestin	Rabbit ab105389 (Abcam)	1:50 o/n 4°C	IMR-32	4% PFA in PBS 10 min	0.1% triton-x in PBS 10 min
PHOX2B	Mouse SC-376997 (Santa Cruz, Texas, USA)	1:40	IMR-32	4% PFA in PBS 10 min	0.1% triton-x in PBS 10 min
TH	Mouse MA1-26654 (Thermo Fisher)	1:40 o/n 4°C	IMR-32	4% PFA in PBS 10 min	0.1% triton-x in PBS 10 min

2.2.5.3 RTqPCR for NB gene expression

Assessment of NB gene expression, TH and PHOX2B mRNA RTqPCR was carried out by Ms Laura Sethi and Dr Virginie Viprey. RNA was extracted and quantified as described in Section 3.2.1.1.1 and stored in single use aliquots at -80°C. For each

target 100 nanograms (ng) of total RNA was added to the reverse transcriptase (RT) reaction. RNA was heated in a heating block at 95°C for 5 min then cooled on ice prior to addition of 10µl of RT mix (Table 2.4). The RT reaction (20µl) was incubated in a heating block at 37°C for 1h. Negative controls of each primary RNA sample with no RT enzyme and RNA from a positive control cell line for each marker were included in each assay. Each RNA sample was also amplified for the house keeping gene β2M.

Table 2.4 RT mix for analysis of NB genes TH and PHOX2B and positive control gene β2M.

MgCl$_2$ represents magnesium chloride. dNTP denotes deoxyribonucleotide triphosphate.

Reagent	Volume (µl)	Concentration in the reaction tube	Supplier
TaqMan™ Universal PCR Master Mix	2	1x	Thermo Fisher
dNTPs (10mM)	2	1mM	GE Healthcare (Buckinghamshire, UK)
MgCl$_2$ (100mM)	1.6	8mM	Sigma
Random hexamer primers (0.6µg/µl)	1	1.8µg	Thermo Fisher
RNasin Plus RNase Inhibitor	0.4	48U	Promega (Southampton, UK)
Superscript III RT	0.2	120U	Thermo Fisher
RNase-free H$_2$0	2.8	-	-

Amplification of TH, PHOX2B and the housekeeping gene β2M mRNA used the TaqMan assay (all reagents supplied by Thermo Fisher). Polymerase chain reaction (PCR) was performed for TH and PHOX2B in a 64 µl reaction containing 16µl of complementary DNA (cDNA) and for β2M, 4µl cDNA was added to a total reaction volume of 21µl. For all targets cDNA was added to PCR mix containing 1x TaqMan Universal PCR Master Mix, 100nM forward primer, 100nM reverse primer and 100nM probe, primer and probe sequences are listed in Table 2.5. Samples were analysed for target in triplicate in a 96 well Thermo-fast PCR plate, sealed with

MicroAmp Optical Adhesive Film on a 7900HT Fast Real Time System (Thermo Fisher) for 40 cycles of PCR; 50°C for 2 min, 95°C for 10 min followed by 40 cycles of 95°C for 15s and 60°C for 1 min.

Table 2.5 Primer and probe sequences for TH, PHOX2B and β2M PCR reactions.

Primer/probe	Sequence
TH forward primer	5'-ATTGCTGAGATCGCCTTCCA-3'
TH reverse primer	5'-AATCTCCTCGGCGGTGTACTC-3'
PHOX2B forward primer	5'-CAGGGACCACCAGAGCAGT-3'
PHOX2B reverse primer	5'-CTGCTTGCGCTTCTCGTTGA-3'
β2M forward primer	5'-GAGTATGCCTGCCGTGTG-3'
β2M reverse primer	5'-AATCCAAATGCGGCATCT-3'
TH probe	5'-ACAGGCACGGCGACCCGATTC-3'
PHOX2B probe	5'-TACGCCGCAGTTCCTTACAAACTCTTCAC-3
β2M probe	5'-CCTCCATGATGCTGCTTACATGTCTC-3'

2.2.6 Self-renewal assays

To assess the self-renewal abilities of the isolated NB cells two assays were performed, the LA and the soft agar colony formation (CF) self-renewal assays. Both assays assess the ability for a single cell to divide, the LA assay looks at self-renewal in a suspended state and the CF assay, self-renewal in a semi-solid state.

2.2.6.1 Low adherence self-renewal assay

After separation, GD$_2$ positive cells were resuspended by gently pipetting to produce a single cell suspension of 5 cells per ml in LAM. A single cell in 200μl of media was then pipetted into each well of two 96 well ultra-low adherence plates (Corning, SLS, Nottingham, UK). The plates were incubated in a humidified chamber in 5% CO$_2$ in air at 37°C. After 20 days the plates were visualised using light microscopy (CKX41 microscope; Olympus) at 10X magnification and the number of wells containing spheres counted for each plate. A sphere was defined as a clump of more than 5 cells. The self-renewal efficiency was calculated using the formula:

Self-renewal efficiency (%) = (number of wells containing a sphere/number of single cells seeded (192)) x 100

The probability of seeding 1 cell per well was assessed by Ms Mariona Chicón Bosch. Using the cell line SK-N-MC, two 96 well Primaria™ adherence plates were seeded with a single cell per well, as described above and incubated in a humidified chamber at 37°C, 5% CO_2 in air for 24h. Each well was then washed in 200µl PBS, fixed with 100µl PFA 4% in PBS at room temperature for 15 min, then washed with PBS again. The cells were incubated with 0.2µg/ml 4', 6-diamindino-2-phentlindole (DAPI, Sigma) in 50µl PBS in the dark for 30 min at room temperature to stain the nuclei. After replacing DAPI solution with PBS cell number was assessed by light microscopy (CKX41 at 4X and 10X magnification), the number of cells detected in each well was recorded.

2.2.6.2 Colony formation self-renewal assay

Solutions of 3% and 5% agar (w/v; Sigma) in distilled water (dH_2O) were prepared and sterilised in the autoclave by exposure to high pressurised steam at 121°C for 15 min. These were then stored at room temperature until required. The 5% agar solution was heated in a microwave until fully liquid, then 0.5ml was added to 4.5ml LAM warmed to 37°C in a water bath. This was mixed thoroughly to give a 0.5% agar solution which was poured carefully into a 60x15mm petri dish (Falcon) avoiding the introduction of bubbles and left to solidify. A single cell suspension containing 1.8×10^5 cells was prepared in 4.5ml of LAM and 0.5ml of 3% agar at 37°C. The suspension was poured on top of the solidified 0.5% agar layer and allowed to solidify.

For each sample the assay was set up in triplicate; the NB cell line IMR-32 cells was included as a positive control. The agar plates were placed in 120x120mm square dishes containing a 35x10mm open petri dish (Falcon) with 2ml dH_2O to prevent the agar from drying out and incubated in a humidified chamber in 5% CO_2 in air at 37°C for 20 days.

Plates were examined for colonies at days 10 and 20. The number of colonies formed was scored in 16 randomly selected independent fields of view across the plates. Each field of view was scored through the whole depth of the 0.3% cell containing layer of agar using light microscopy (Nikon Eclipse TS100, Nikon) at 10X magnification. A colony was scored if more than 5 cells were present.

Colony forming efficiency (%) = (number of colonies formed in field of view/number of cells seeded in field of view) x 100

Number of cells in field of view = (volume of agar scored ($\pi r^2 d$)/volume of agar in the whole plate ($\pi r^2 d$)) x number of cells seeded

2.2.7 Migration assay

At the start of the experiment (day 1) $1x10^3$ cells (in 200µl of LAM) were added to 8 wells of a 96 well ultra-low adherence plate and incubated in a humidified chamber in 5% CO_2 in air at 37°C for 5 days to induce spheroid formation. On day 5, 8 wells of a 24 well plate were coated with 300µl of gelatin (0.1% in sterile dH_2O; (w/v) Sigma) and incubated for 1h at 37°C to allow the gelatin to solidify at optimal temperature for cell growth. Any gelatin that did not set was gently aspirated from the well and 900µl of LAM was added to each well. The spheroids were then transferred into the wells; 100µl of excess media was carefully removed from the spheroid containing well, discarded and the remaining 100µl containing a single spheroid was transferred using a P1000 pipette (Gilson, Wisconsin, USA) and gently placed in the centre of each coated well. A P1000 pipette tip, the largest was used to give least chance of disrupting the spheroid, transference of the spheroid could be confirmed by visual inspection. The plate was then incubated in a humidified chamber at 5% CO_2 in air at 37°C for 1h to allow the spheroid to adhere. SK-N-SH spheroids were used as a positive control.

Each well was imaged using an Olympus CKX41 microscope using x4 objective and Cell B software at 0, 24, 48 and 72h post transfer of the spheroids to the 24 well plate. The images were analysed using Volocity®. The freehand tool was used to outline the spheroid core and migration zone for each image, as illustrated in Figure 2.4. The pixel count for both zones at each time point was noted. The migration value was then determined. For each sample, of the 8 wells set up 3 were selected at day 0 of analysis, these same wells were imaged every 24h.

Migration for time point = (migration zone for time point-core at time point)/core at 0h

ID	Item Name	Name	Population	Color	Type	Pixel Count
1	SKNSH P4...	ROIs 1	ROIs	(blue)	Object	20687
2	SKNSH P4...	ROIs 2	ROIs	(green)	Object	222102
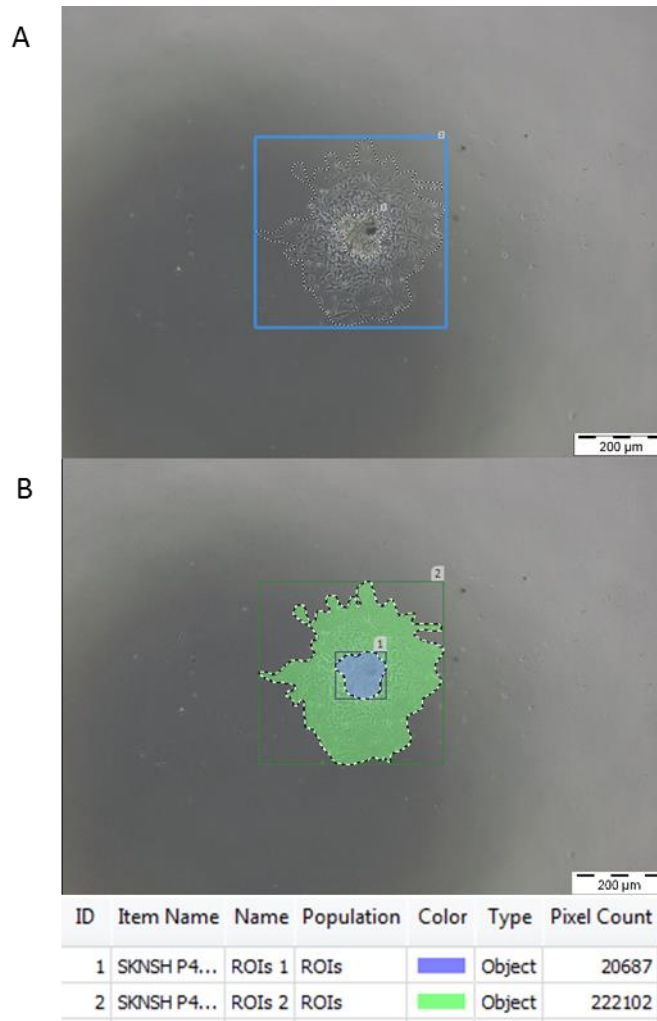
Figure 2.4 Volocity® software analysis of migration assay.

> Figure shows SK-N-SH (P49) control cell line at 72h. A, image panel in Volocity®, 1 denotes area around core and 2 denotes the area the cells have migrated. B, measurement panel; the blue highlights the core and the green shows migration area of cells. Pixel counts were noted for calculating the migration index.

2.2.8   Statistical methods

2.2.8.1   Goodness of fit test to determine probability of seeding a single cell into each well

The mean and median number of cells per well was first calculated. The ability to manually seed 1 cell per well was determined using a chi-square goodness of fit test. The test determined the best fitting λ under Poisson distribution with λ representing the most likely number of cells in each well. A result of 1 or under would give confidence that seeing a colony in a well is not due to seeding more than 1 cell per

well. The probability of seeding 2 or more cells ($\lambda \geq 2$) was also calculated using a chi-square goodness of fit test.

2.2.8.2   Comparison of colony size between cell line control and primary cultures

Colony size was quantified using Volocity®. Pixel counts for the area of each colony were recorded for 4 primary cultures and 5 repeats of the control cell line IMR-32. Mean colony size was compared using an unpaired t-test.

2.2.8.3   Comparisons between diagnostic cohorts and time points

BM aspirate and phenotype data were assessed for significance between different diagnostic cohorts and between time points within the HR NB cohort. Differences were analysed using a one-way analysis of variance (ANOVA) with a Tukey post-hoc test to compare across more than 2 groups. A threshold of 0.05 was used for significance.

2.2.8.4   HR NB survival analyses

The prognostic value of propagation success, GD_2 % infiltration, wcc and phenotype assay results were evaluated using log rank (Mantel-Cox) test and visualised as Kaplan-Meier plots using the computer programme SPSS (IBM Ltd, Hampshire, UK). EFS was defined as the time from diagnosis to the time of first event; first event could be relapse or death, with censoring at date last seen for surviving patients. OS was calculated as the time from diagnosis to death, regardless of the number of events that may have occurred, with censoring at the date last seen. Patients without EFS or OS follow up data were excluded from the analysis. Where the data was not binary, optimum cut offs were determined by analysing each possible threshold using the log-rank test, the cut off with the best long-rank chi-square being used.

2.3 Results

2.3.1 GD$_2$ negative cells shared morphology with normal BM cells and did not propagate

There was a difference in morphology between GD$_2$ positive and negative cells whilst in culture on plastic, illustrated in Figure 2.5. The negative populations did not propagate and H&E stained cytospins were indicative of white blood cells.
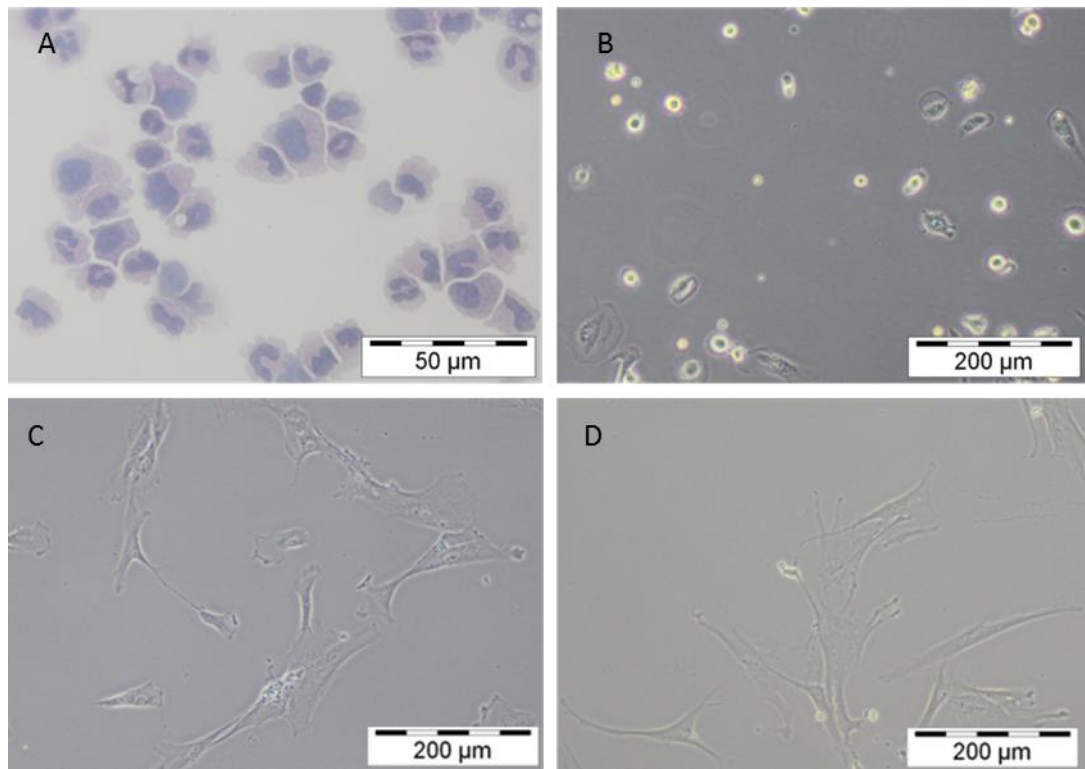
Figure 2.5 Morphology of GD$_2$ negative and positive cells.

A and B both show GD$_2$ negative fractions; A depicts H&E staining and B shows cell morphology when cultured on plastic. C and D show GD$_2$ positive cells in culture on plastic.

2.3.2 BM aspirates received during trial recruitment

Throughout the recruitment period of the SIOPEN HR NB trials (1.0, 1.5 and 1.7) samples were collected between 11.10.2012 and 30.06.2017, 331 BM aspirates have been received and processed to isolate NB GD$_2$ positive cells. As depicted in Figure 2.7, 12% (n=40) of these samples were destroyed as patients were not consented. The rate of non-consent may be explained as the samples are acquired prior to diagnosis, with informed consent being taken post-diagnosis; many of these non-

consented patients were non-NB or low/intermediate-risk NB. A diagnosis of HR NB was confirmed in 75% (217/291) of samples and these will subsequently will be referred to as HR NB. Of these 217 samples 164 were taken at diagnosis, these children were recruited onto a version of the HR NB trial that was recruiting at the time, this breakdown is depicted in Figure 2.6, A.

BM aspirates were taken at different time points throughout the trial as described in Section 2.2.2, 8% (18/217) at RE1, 10% (21/217) at RE2a, 6% (13/217) at RE2b and 1% (1/217) at relapse, summarised in Figure 2.7. The mean number of BM aspirates received per year was 31 (range 13-51), calculated including aspirates received at all time points, Figure 2.6, B. Different time point samples were only received in 2016 and 2017, therefore most were from patients recruited onto the later trials.
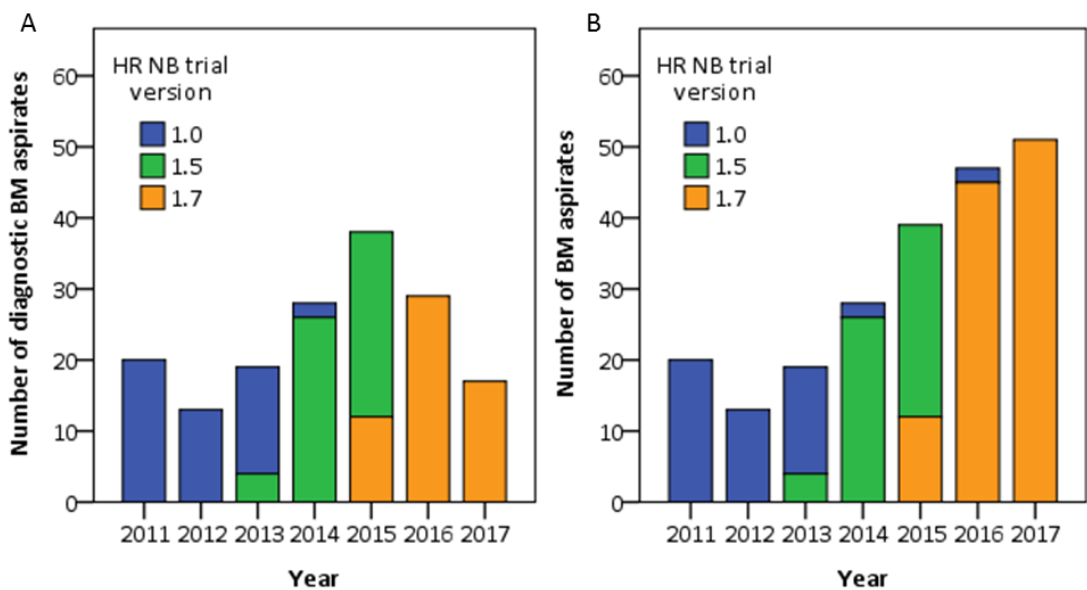
Figure 2.6 Histogram of number of BM aspirates received throughout the duration of SIOPEN HR NB trials.

The SIOPEN HR NB trials recruited from 11.10.2012 to 30.06.2017. A, shows diagnostic BM aspirates received, indicative of new patients, n=164. B, shows BM aspirates from all time points, n=217. Blue indicates SIOPEN HR-NBL-1.0; green SIOPEN HR NBL-1.5; orange SIOPEN HR-NBL-1.7.

Samples that were not HR (NHR) NB (n=73) were retained after parents of children had given CCLG consent for the use of material in research (Section 2.2.2), upon which cells were propagated and stocks frozen. Of these patients a diagnosis of intermediate and low-risk NB accounted for 79% (58/73), subsequently referred to

as NHR NB. The remaining 21% (16/73) were diagnosed with other cancers (subsequently referred to as OC), including ganglioneuroblastoma (n=5), ganglioneuroma (n=4), and one each of desmoplastic small round cell tumour, Ewing's-like CD99 positive tumour, hepatoblastoma, malignant nerve sheath tumour (MNST), paraganglioma, pheochromocytoma and rhabdomyosarcoma (Table 2.6); diagnoses were confirmed by histology, immunohistochemistry, age at diagnosis and genetics as appropriate in the referring centre). Ganglioneuroblastoma was not included within the NB groups as they are composed of ganglion cells with differentiating neuroblasts and have a more favourable outcome (Katz and Krishnamurthy, 2008).
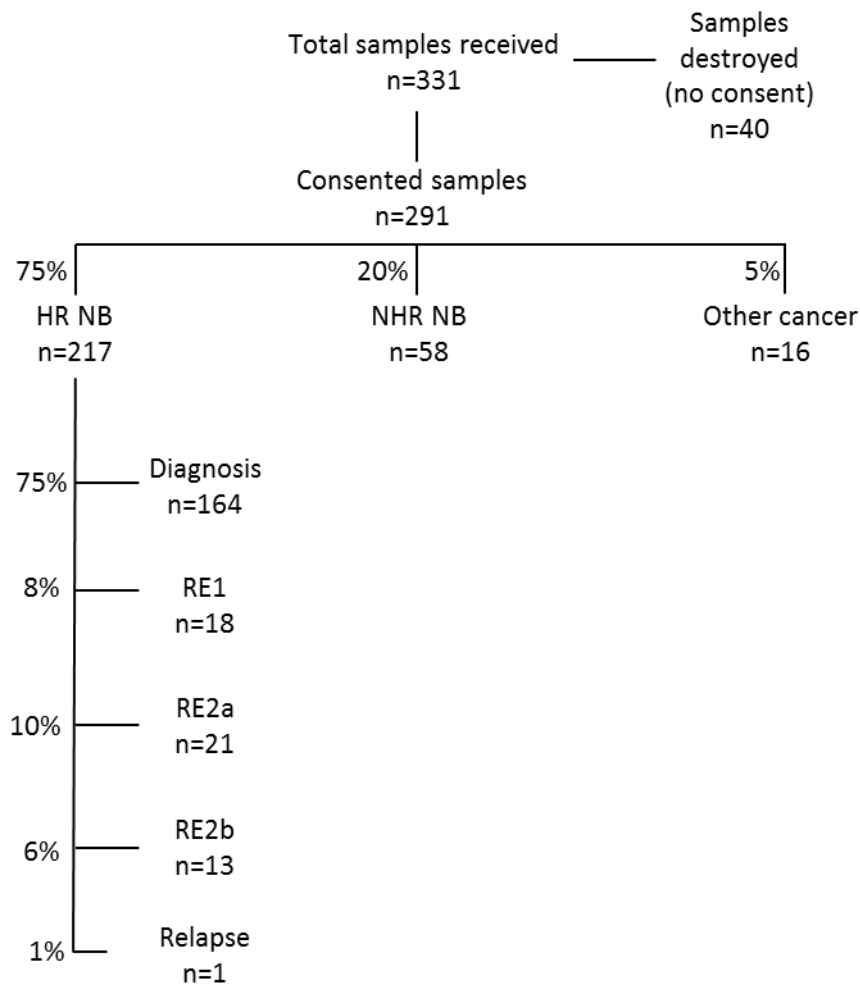
Figure 2.7 Summary of BM aspirates received, n=331.

> BM aspirates were received between 11.10.2012 and 30.06.2017. HR NB denotes BM aspirates received from patients on a SIOPEN HR NB trial; NRH NB denote those from patients diagnoses with low or intermediate NB. BM aspirates from patients with non-NB diagnoses are referred to as other cancer.

Table 2.6 Summary of the patients with non-NB diagnoses.

GD$_2$ infiltration of the BM aspirates is calculated as a percentage of the total wcc.

Diagnosis of patients with other cancers	Cases	Description	GD$_2$ positivity (%)
Ganglioneuroblastoma	5	Derived from neural crest cells, but unlike NB contains both mature and immature cells. Confirmed by histology (Lonergan *et al.*, 2002).	10 (range 0.3-47)
Ganglioneuroma	4	Highly differentiated tumour of mature ganglion cells derived from neural crest cells (benign). Confirmed by histology (Lonergan *et al.*, 2002).	3 (range 1-7)
Desmoplastic small round cell tumour	1	Rare aggressive cancer that presents as masses in abdomen. Confirmed by presence of *EWSR1-WT1* genes (Gerald and Haber, 2005).	0.3
Ewing's like CD99 positive tumour	1	Small round cell bone/soft tissue cancer. Confirmed by presence of CD99 (Burchill, 2003).	4
Hepatoblastoma	1	Rare cancer of the liver, predominantly in infants. Confirmed by histology (Hiyama, 2014).	1

Malignant nerve sheath tumour (MNST)	1	Originated from peripheral nerves or nerve sheath cells, most cases in adults. Confirmed by histology (Farid *et al.*, 2014).	5
Paraganglioma	1	Extra-adrenal neuroendocrine neoplasm, closely related to pheochromocytomas. Confirmed by biochemical testing and imaging (Martucci and Pacak, 2014).	2
Pheochromocytoma	1	Adrenal neuroendocrine tumour, origin in chromaffin cells secreting high catecholamines. Confirmed by biochemical testing and imaging (Martucci and Pacak, 2014).	10
Rhabdomyosarcoma	1	Soft tissue tumour common in children. Confirmed by histology (Panda *et al.*, 2017).	6

2.3.3 Isolation and propagation GD$_2$ positive cells isolated from BM aspirates

2.3.3.1 GD$_2$ positive cells were successfully propagated from BM aspirates

Cells were successfully propagated in 47% (144/291) of cultures. There was no significant difference in propagation success of GD$_2$ positive cells from HR NB samples (46% (99/217) and other sample types. It is worth noting, the initial 33 HR samples were separated, frozen and subsequently analysed, the propagation success of these samples was 18% (6/33) compared to 51% (93/184) in cells that were propagated immediately after separation, this suggests through freeze thawing cells the self-renewing properties of these cells are diminished.

The success of propagation shows no change across HR NB, NHR NB or OC, with NHR NB samples successfully propagating in 33% (19/48, 9 are unknown as have been frozen straight from separation and propagation ability not yet tested) OC had a success rate of 56% (9/15, 1 unknown as was frozen straight from separation and propagation ability not yet tested).

2.3.3.2   Samples taken at different time points within the trial show no trend in propagation

There is no trend in propagation as samples are received throughout the trial. As reported above diagnostic samples had a culture success of 44%, no statistical difference was seen between any of the other time points; RE1 67%, RE2a 33%, RE2b 46%. Statistical analysis was not possible with samples taken at relapse as n=1 and this sample was successfully propagated.

2.3.3.3   GD$_2$ positive cells were successfully isolated across diagnosis cohorts

There were data on GD$_2$ cell infiltration of BM aspirates available for 90% (262/291) of cases, of the unavailable data 21 of these samples were HR NB, 7 NHR NB and 1 OC. The mean percentage of GD$_2$ positive cell population across all samples was 14% (range 0-94%, n=262) reported as the percentage GD$_2$ positive cells infiltration of the wcc. HR NB samples had a mean GD$_2$ infiltration of 17% (range 0-94%, n=196), significantly greater than the NHR NB (mean=4%, 0-55%, unpaired t-test p=1x10^{-9}) and OC (6%, 0-47%, n=15, unpaired t-test p=0.002). This result is concordant with there being a high infiltration of NB cells in the BM in patients with HR NB.

Total wcc did not correlate to the GD$_2$ infiltration (R^2=0.04); the mean wcc of 262 analysed samples was 2x10^7 cells (range 3x10^4-4x10^8). There was no significance in wcc between diagnostic cohorts, HR NB samples had a mean wcc of 2x10^7 cells (n=51, range 9x10^4-4x10^8), the NHR NB 2x10^7 cells (n=15, range 26x10^4-1x10^8) and OC 3x10^7 cells (range 2x10^6-2x10^8).

When comparing these data to the success of propagation, in HR NB samples successful (mean=15%, range 0-92%, n=98) or unsuccessful culture (mean=19%, range 0-94%, n=99; unpaired t-test p=0.23) there was no correlation between GD$_2$ infiltration and the success of propagation. Successfully cultured had a mean of 12%

whilst those unsuccessful was 16%. However, when compared propagation success to either the number of GD_2 positive or white blood cells significance was seen. Samples that went on to propagate had a mean wcc of $3x10^7$ whereas unsuccessful samples the mean value was significantly lower ($p=1.8x10^{-7}$) at $9x10^6$. The GD_2 positive counts were also significantly higher ($p=0.005$) in the samples that showed successful propagation (mean=$9x10^5$) than those that did not (mean=$4x10^5$).

2.3.3.4   Survival analysis using BM aspirate data

It may be hypothesised that cells that propagate in culture are more self-renewing and therefore the corresponding patients would have a worse outcome. There was no significant difference in survival when using success of propagation to analyse the HR NB data; OS p=0.5, EFS p=0.68, n=163 (1/164 no survival data available) as shown in Figure 2.8. This may be as culturing cells on plastic is not truly representative of growth within the BM microenvironment. The level of NB disease in the BM is reported to predict for outcome in HR NB (Moss *et al.*, 1991, Komada *et al.*, 1998, Seeger *et al.*, 2000, Merugu and Tweddle, 2017, Corrias *et al.*, 2018). The percentage of GD_2 infiltration had prognostic significance for both OS (p=0.0067, Figure 2.9, A) and EFS (p=0.0012, Figure 2.9, B). This adds to the evidence that children with a higher NB burden in their BM will have a poorer outcome.
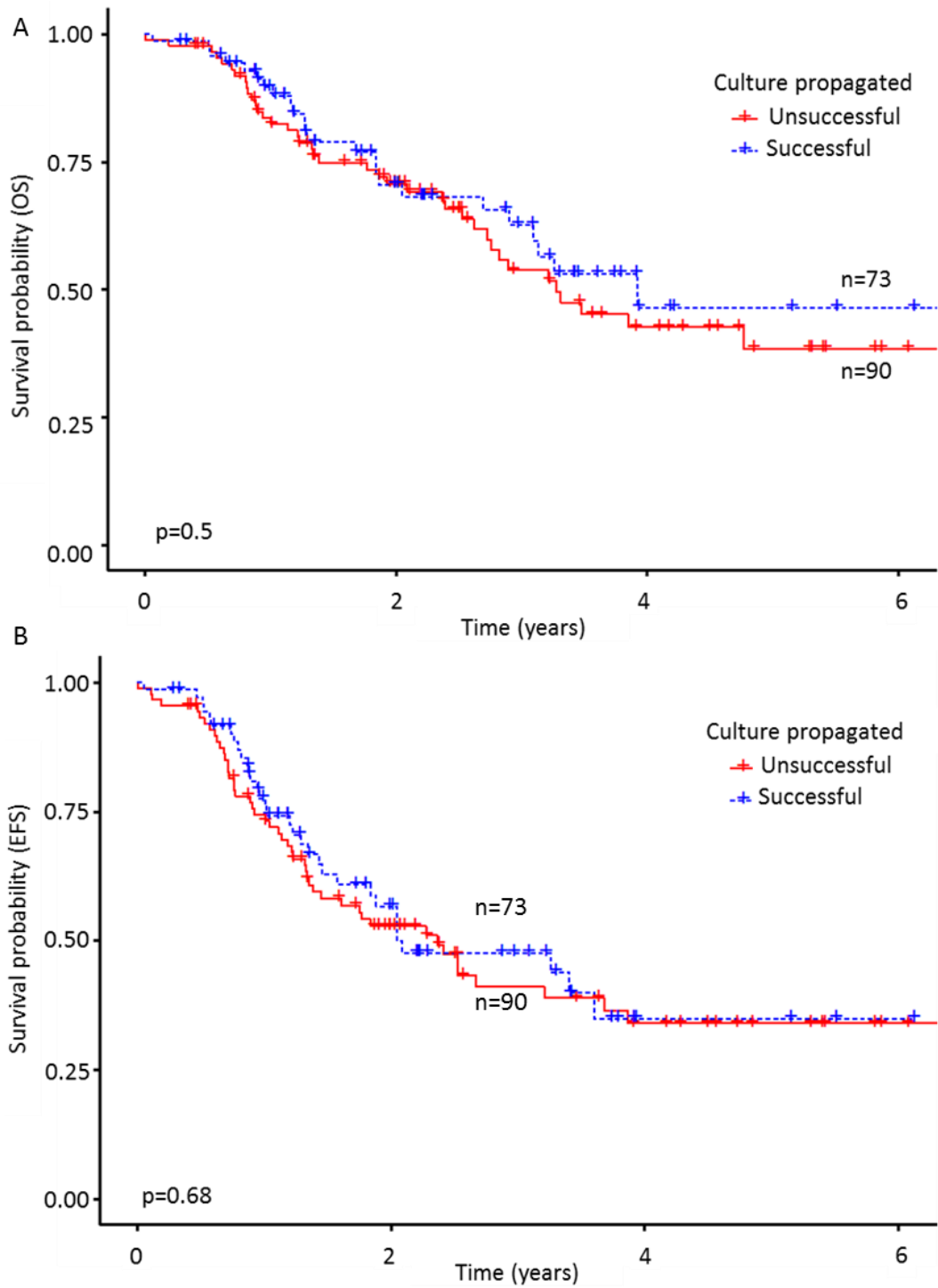
Figure 2.8 Survival vs propagation success.

Kaplan-Meier survival curves of A, OS and B, EFS in relation to the success of culture. Red line = unsuccessful propagation, blue line = successful propagation, n = number of samples analysed.
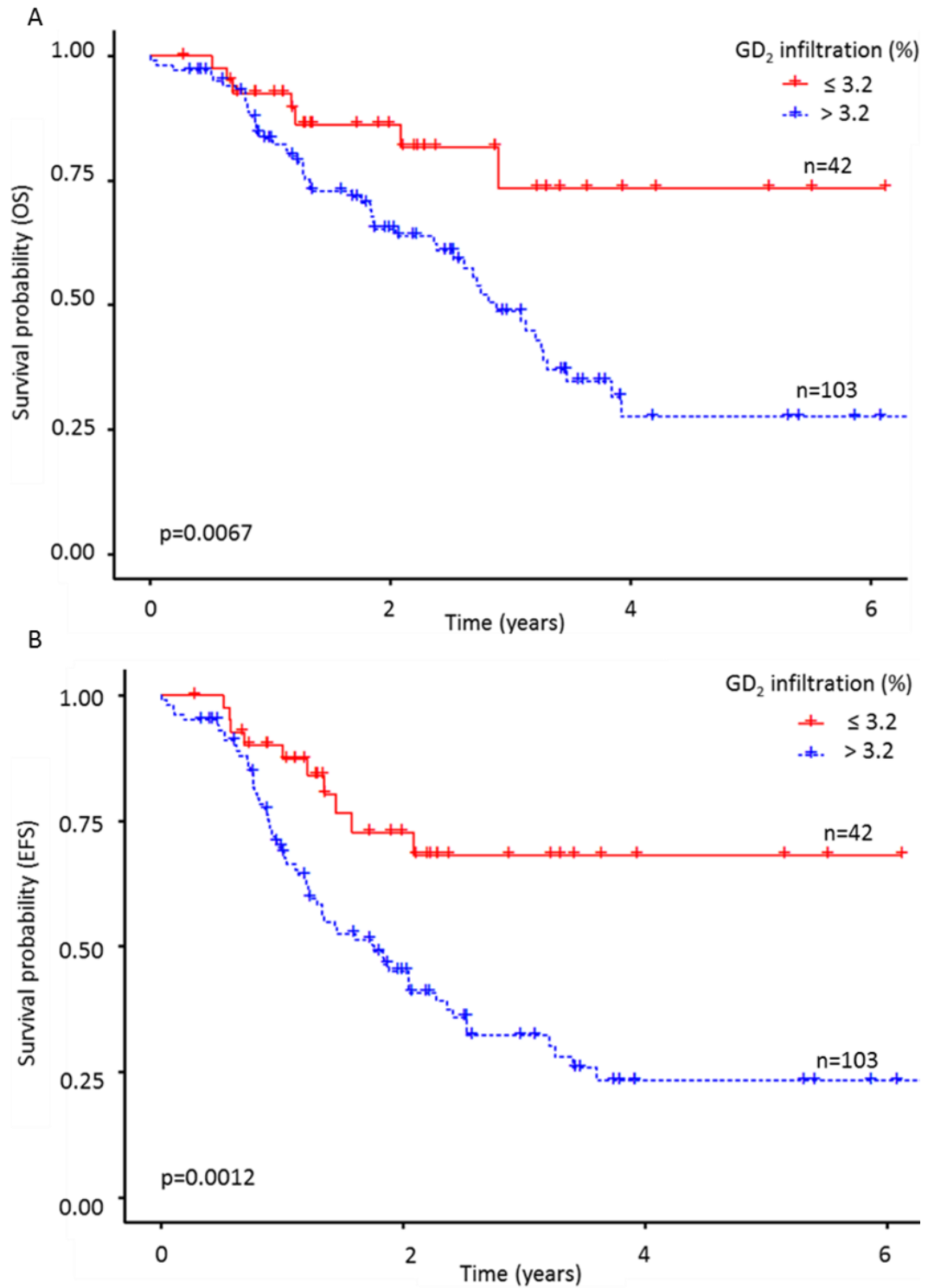
Figure 2.9 Survival vs GD₂ infiltration.

Kaplan-Meier survival curves of A, OS and B, EFS in relation to the percentage of GD₂ cells in the BM aspirate at diagnosis. Red line = infiltration equal to or less than 3.2%, blue line = infiltration greater than 3.2%, n = number of samples analysed.

2.3.4 Primary HR NB cultures heterogeneously express markers

All samples analysed were negative for expression of the haematopoietic marker CD45 (0/62), this confirmed there was no co-propagation of BM leukocytes. GD_2 was detected in 96% (64/67) samples analysed, lack of expression in 3 samples is surprising as GD_2 was the marker used to isolate cells. It may be that culturing conditions have caused reduction in expression for these samples. None of the samples expressed TH (0/43). However, 61% (38/62) expressed the NB marker PHOX2B. MRP1 (66/66) and MRP4 (61/61) were detected in 100% of samples analysed, with a range of intensity and frequency across samples. CD57 was expressed by 23% (15/55), in positive cytospins the staining was occasional highlighting cells with an aggressive phenotype. Nestin expression was detected in 75% (50/67) of samples with varying intensity. NCAM was expressed by 54% (34/63) of samples. Representative images of immunocytology for each marker are shown in Figure 2.10. Matching isotype control cytospins for each analysis showed no positive staining (data not shown). These results indicate NB cells were isolated and propagated from the BM aspirates with a heterogeneous genotype.
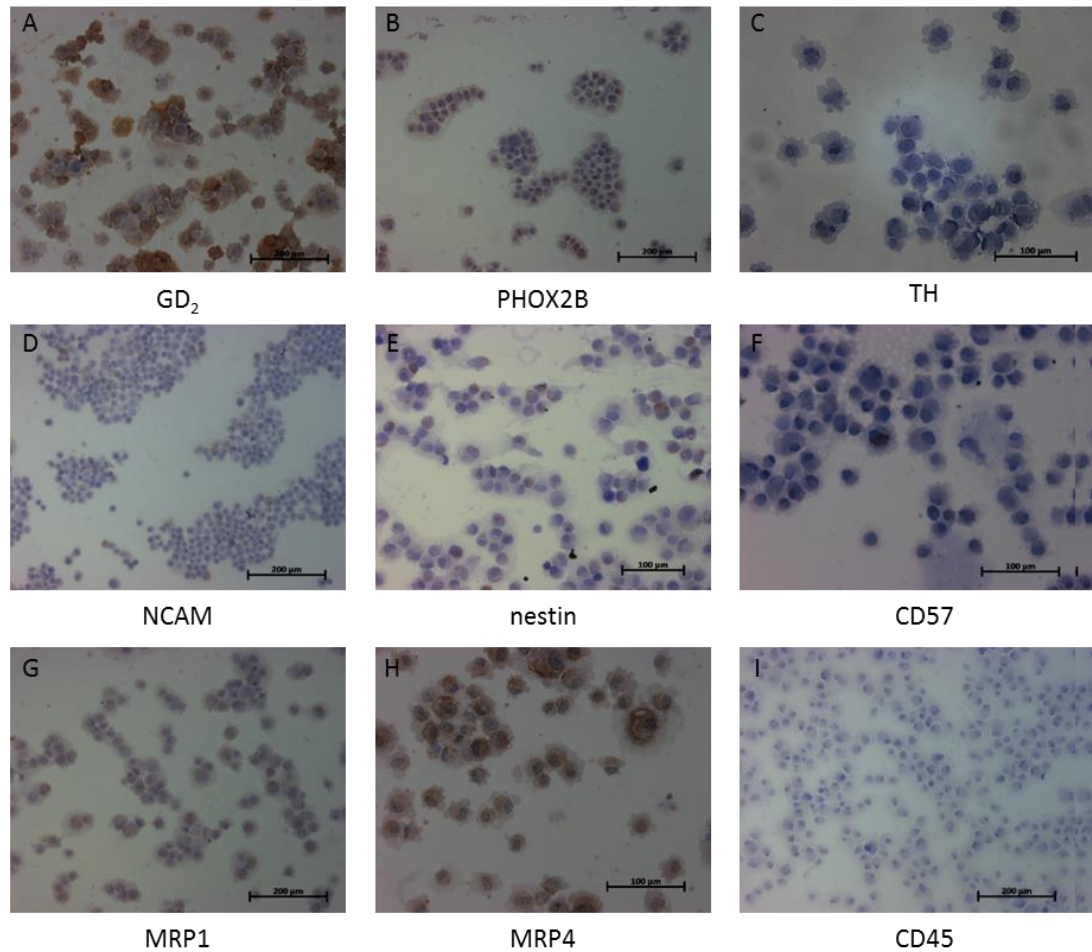
Figure 2.10 Immunohistochemistry of HR NB primary cells.

TH (C) and CD45 (I) were negative on all samples. MRP1 (G) and MRP4 (H) were detected on all samples. Positive expression of GD_2 (A), PHOX2B (B), NCAM (D), nestin (E) and CD57 (F) was detected heterogeneously. Haematoxylin was used as a counterstain to identify cell nuclei.

2.3.5   RTqPCR confirms TH is expressed in HR NB primary cultures

TH was detected by RTqPCR in 100% (27/27) of samples, however this expression was not seen by immunocytology as described in Section 2.3.4. PHOX2B was only detected in 1/27 (4%) sample but was detected by immunocytology.

2.3.6   Self-renewal ability of primary NB cells from children with HR disease

2.3.6.1   Best fitting Poisson distribution for seeding cells into a single well

Analysis of cells seeded showed the mean number of cells per well as 1.6 and the median result was 1. Upon analysis using chi-square goodness of fit test, the Poisson

distribution showed the best fit using λ=1, with the probability of having 1 cell per well of 0.9. The probability of having 2 or more cells in any well was 0.09. These results showed high confidence that results of self-renewal are not due to incidence of seeding more than 1 cell per well.

2.3.6.2   Low adherence spheroid formation.

In diagnostic HR NB LA data was available for 130/164 samples, of these 95% showed spheroid forming ability with a mean of 6% (n=123, range 0-31%, Figure 2.11).
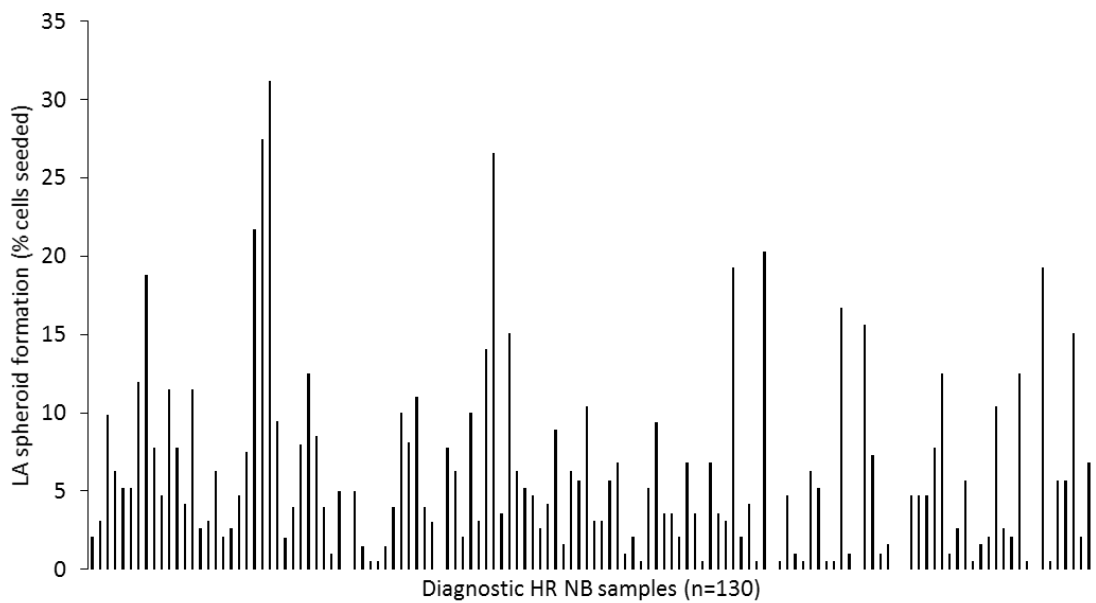
Figure 2.11 Low adherence spheroid formation of diagnostic HR NB cells at 20 days.

Results are the number of single cells that formed a spheroid, calculated as a percentage of total cells seeded.

There was no significant effect of LA spheroid formation on either OS (p=0.06, Figure 2.12, A) or EFS (p=0.15, Figure 2.12, B). Similar to the propagation success this may be due to the differences in environment from the BM to suspension in a well.
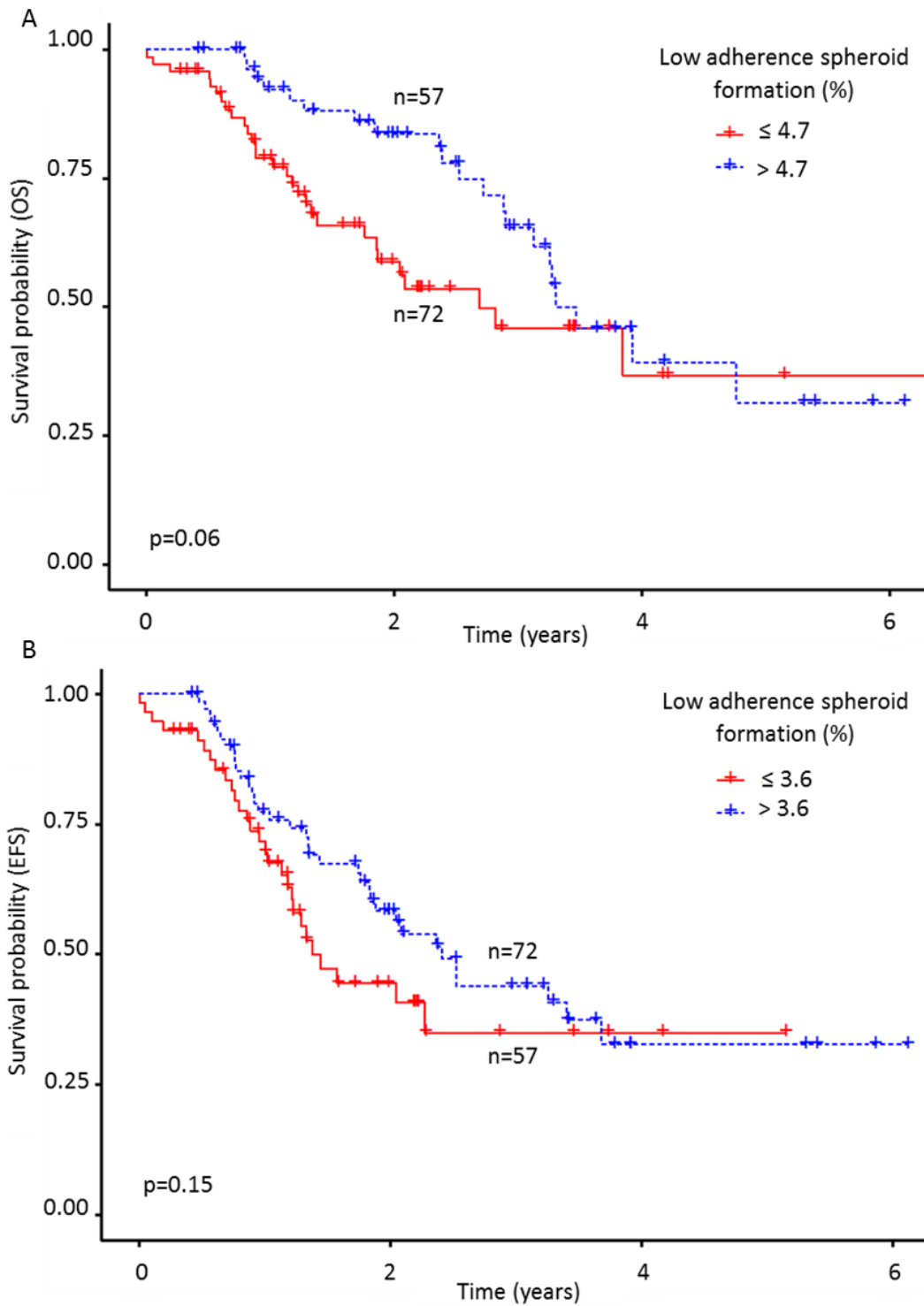
Figure 2.12 Survival vs LA spheroid formation.

> Kaplan-Meier survival curves of A, OS and B, EFS in relation to the low adherence spheroid formation efficiency (%) at day 20. Different optimum cut points were determined for the OS (4.7%) and the EFS (3.6%) for this data. Red line = spheroid formation efficiency equal to or less than optimal cut point, blue line = spheroid formation efficiency greater than optimal cut point, n = number of samples analysed.

The spheroid formation assay was the only feature of samples not diagnosed as HR NB that was characterised as the assay is performed upon separation of cells. There was no change in spheroid formation across diagnosis groups (one-way ANOVA p=0.3); NHR NB mean percentage 5% (n=41, range 0-31); OC mean percentage 4% (n=9, range 0-24), as shown in Figure 2.13.
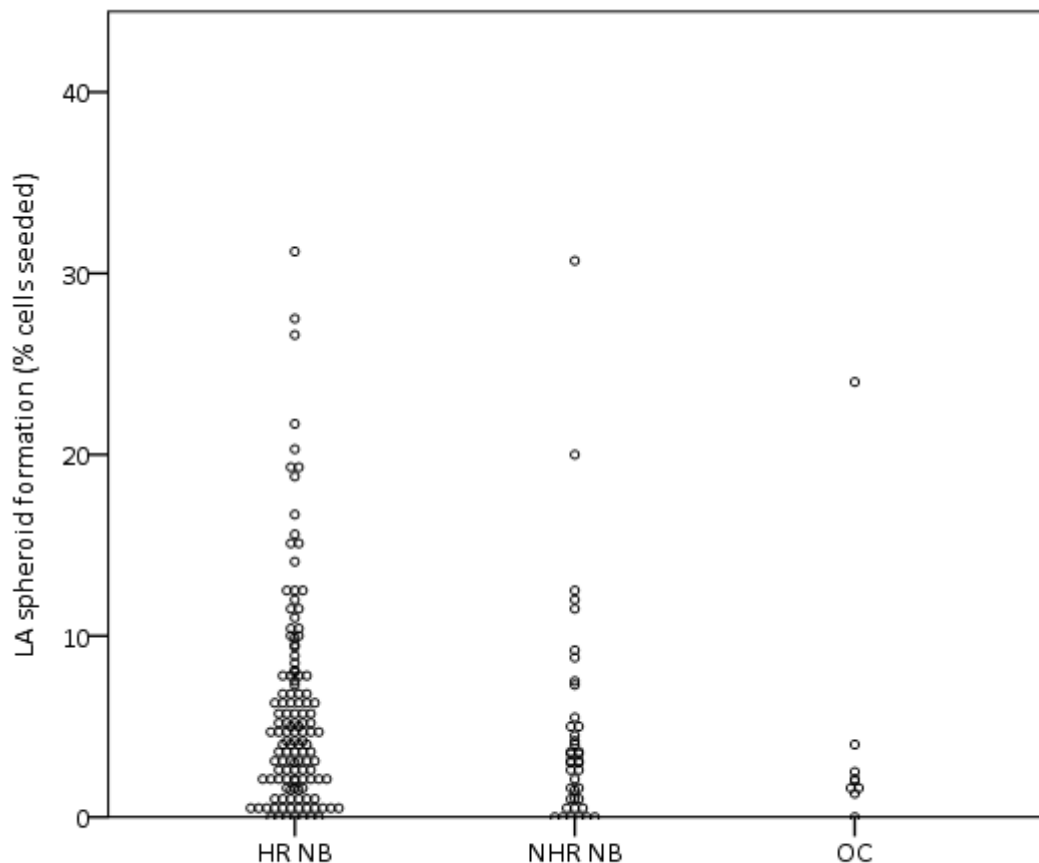
Figure 2.13 Low adherence spheroid formation in HR NB, NHR NB and OC.

There was no statistical difference between the different diagnostic sub-groups.

2.3.6.3   Colony forming efficiency across HR NB samples

Colony forming efficiency was heterogeneous across the diagnostic primary HR NB cultures examined; mean colony forming efficiency at day 20 was 1.5% (range 0-9, n=72, Figure 2.14). The IMR-32 colonies were significantly larger at day 20 (unpaired t-test p=0.0002) than those produced by NB primary cultures as depicted in Figure 2.15 with images of colonies. IMR-32 independent repeats (n=33) also showed a significantly higher colony forming efficiency both at day 10 with a mean efficiency

of 5.8% (unpaired t-test p=9x10^{-14}, range 1.6-11.6) and at day 20 with mean efficiency of 9.2% (unpaired t-test p=3x10^{-19}, range 3.3-13.3) when compared to primary cultures.

The mean colony forming efficiency was significantly higher at day 20 compared to day 10 (0.8%, range 0-3, n=72; p=0.0001). Most samples produced visible colonies within 10 days (93%; 67/72), in four cases, colonies were only visible after 20 days, and in 1 case no colonies were present at day 10 or 20.
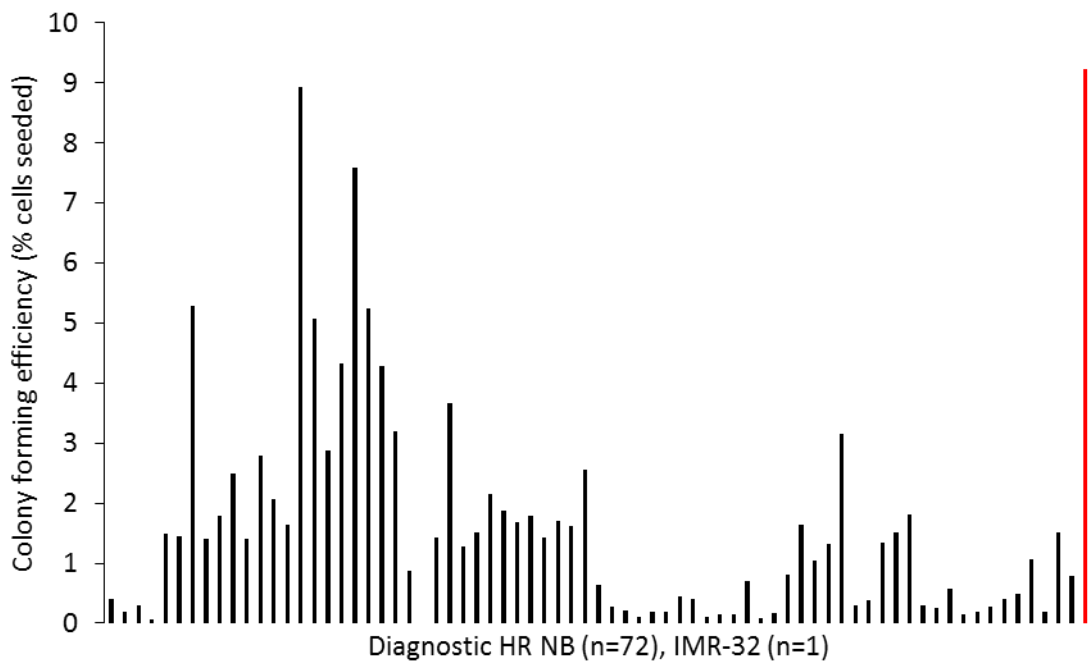
Figure 2.14 Colony forming efficiency at day 20 across HR NB diagnostic cultures.
Black bar = HR NB cultures, n=72. Red bar = IMR-32 positive control cell line.
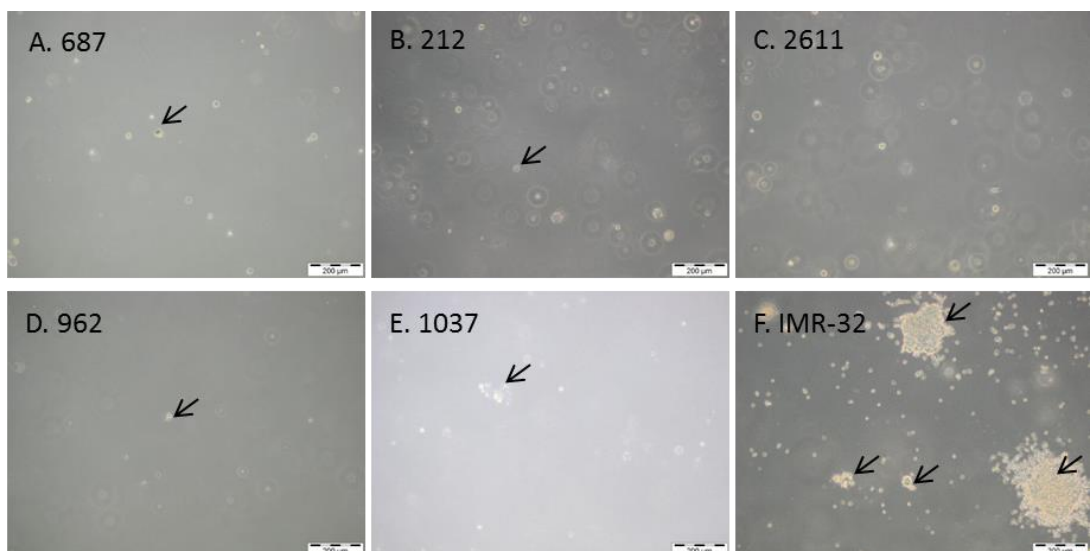
Figure 2.15 Images of colony formation at day 20.

A-E shows 5 HR NB diagnostic samples, F shows IMR-32 positive control cell line. Colonies are highlighted using arrows, the mean pixel count of IMR-32 colonies was 16855 and HR NB was 2835.

Colony formation efficiency showed significance when compared to OS (p=0.0016, Figure 2.16, A) and EFS (p=0.012, Figure 2.16, B), with a higher efficiency predictive of increased survival. These may seem counter intuitive as children whose cells have a greater self-renewing phenotype may be identified as those with more aggressive cells and in turn have a worse outcome. However, an increased CF is indicative of increased cell turnover, a process necessary for chemotherapeutic effect. As a result patients whose cells are self-renewing will have a better response to cell cycle drugs and therefore an improved outcome.
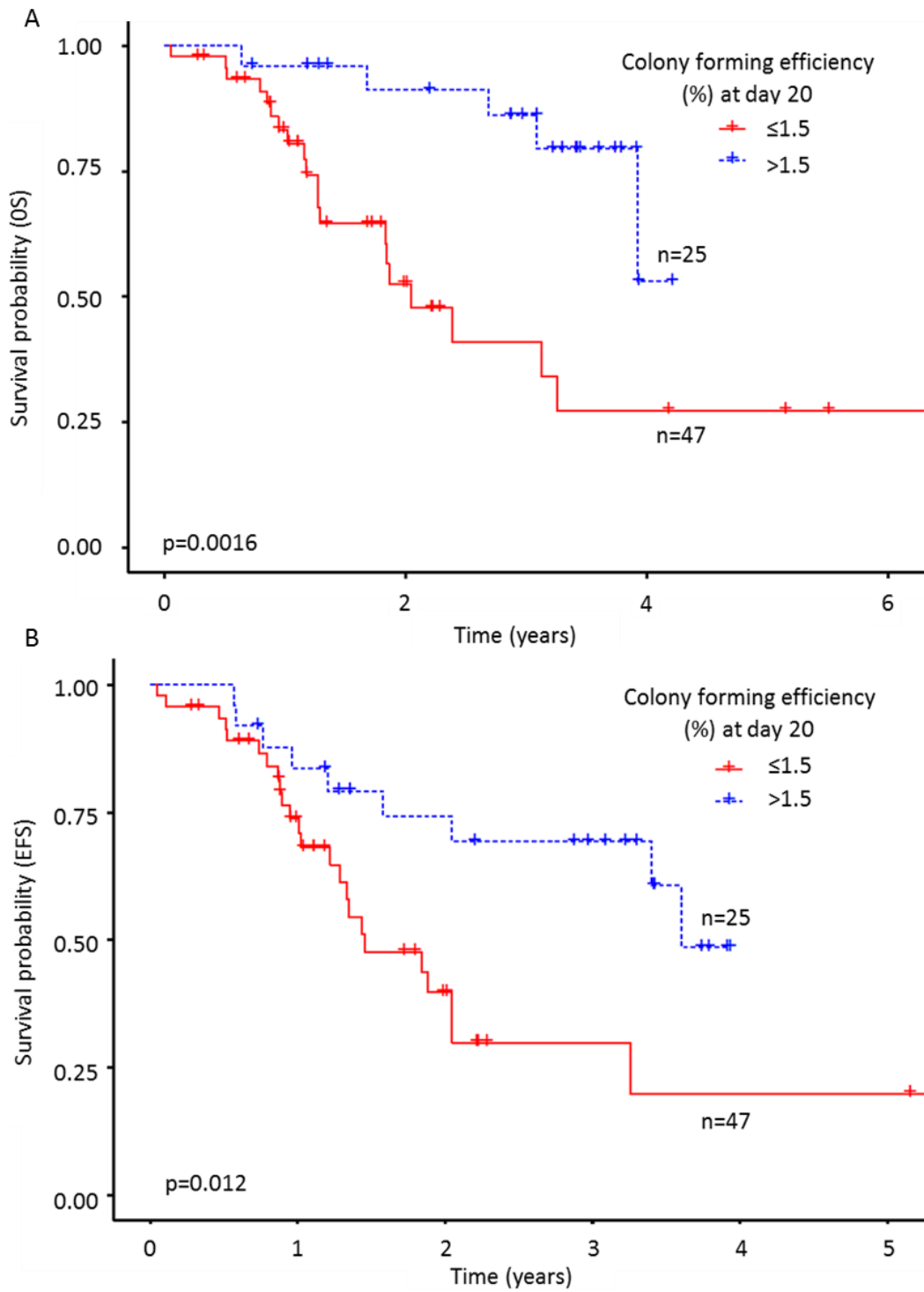
Figure 2.16 Survival vs colony forming efficiency.

Kaplan-Meier survival curves of A, OS and B, EFS in relation to the colony formation efficiency (%) at day 20 using optimum cut point. Red line = spheroid formation efficiency equal to or less than 1.5%, blue line = spheroid formation efficiency greater than 1.5%, n = number of samples analysed.

2.3.7 Migration ability in primary cultures

73 diagnostic HR NB cultures have migration data, of the investigated NB cells, all were able to migrate. Migration index increased with time from 24h to 72h, in all diagnostic HR NB primaries except one (Figure 2.17). The migration values were heterogeneous with a mean value at 72h of 122 (n=73, range 7.5-427.5). The heterogeneity of migration phenotype is visible in Figure 2.18 and Figure 2.19. These images also highlight the differences in the population of cells within the core that throughout the assay may increase in number (B ii), disperse (B iv) or remain constant (B i) emphasising the need to normalise the migration values against size of core from the same time point. Migration index of SK-N-SH cells was 26 (n=34, range 4.6-75.8) at 72h, 5 primaries had a migration index less than this, meaning 95% (89/93) had a higher migration index than the SK-N-SH cell line.
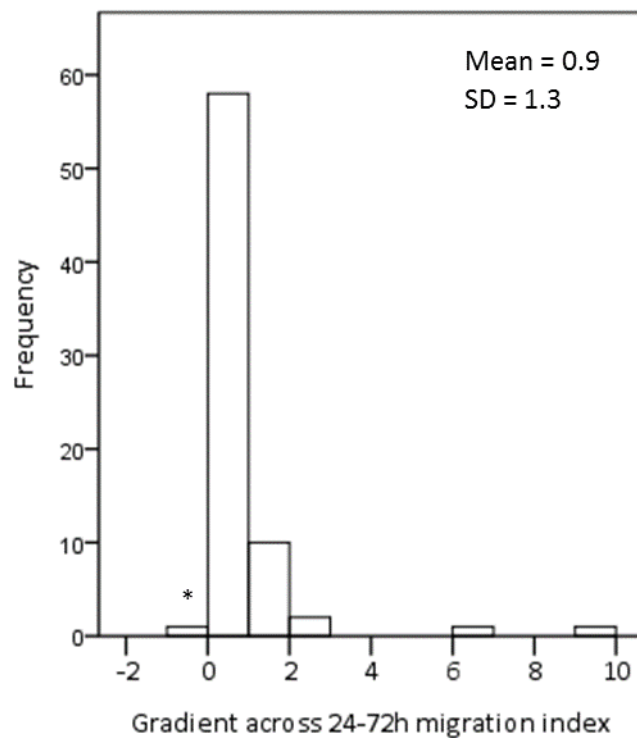
Figure 2.17 Histogram of migration index gradients across diagnostic HR NB samples.

One sample (highlighted with *) had a negative gradient of -0.2, indicative of no increase in migration across the 72h.
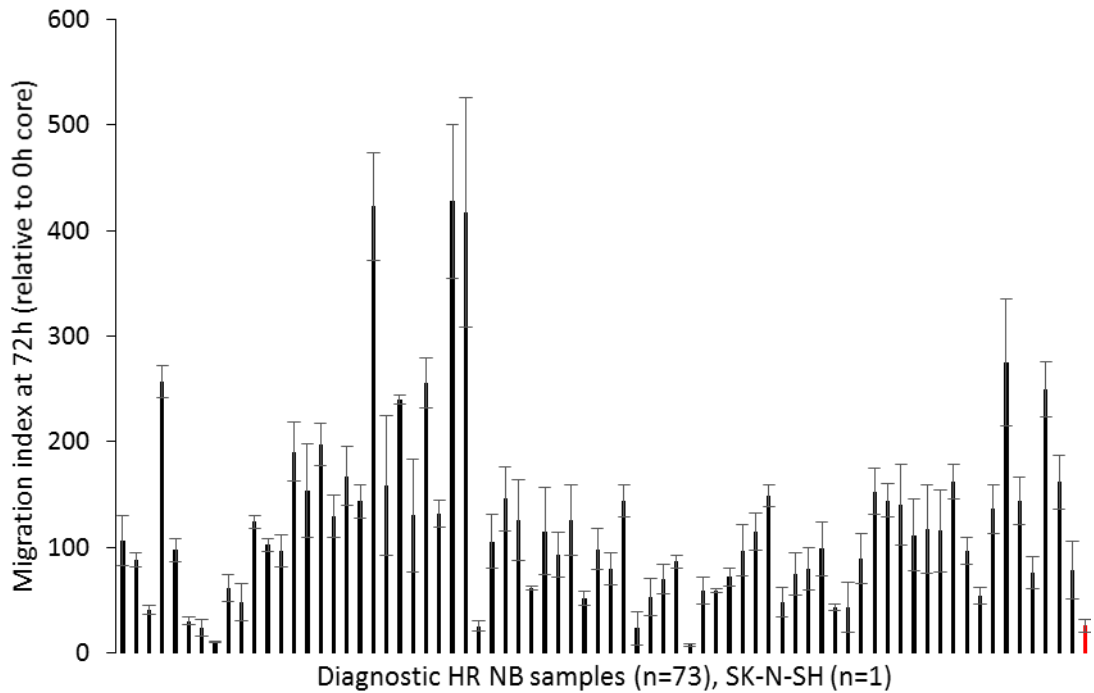
Figure 2.18 Migration index at 72h for HR NB diagnostic samples and SK-N-SH.

SK-N-SH is the positive control cell line used = Red bar. Results are shown as mean ± standard error of the mean of one experiment (n=3).

There was no significant effect of migration on OS (p=0.21, Figure 2.20, A) or EFS (p=0.3, Figure 2.20, B). This may suggest migration does not impact outcome, or it may show the migration assay is not representative of migration within the BM.
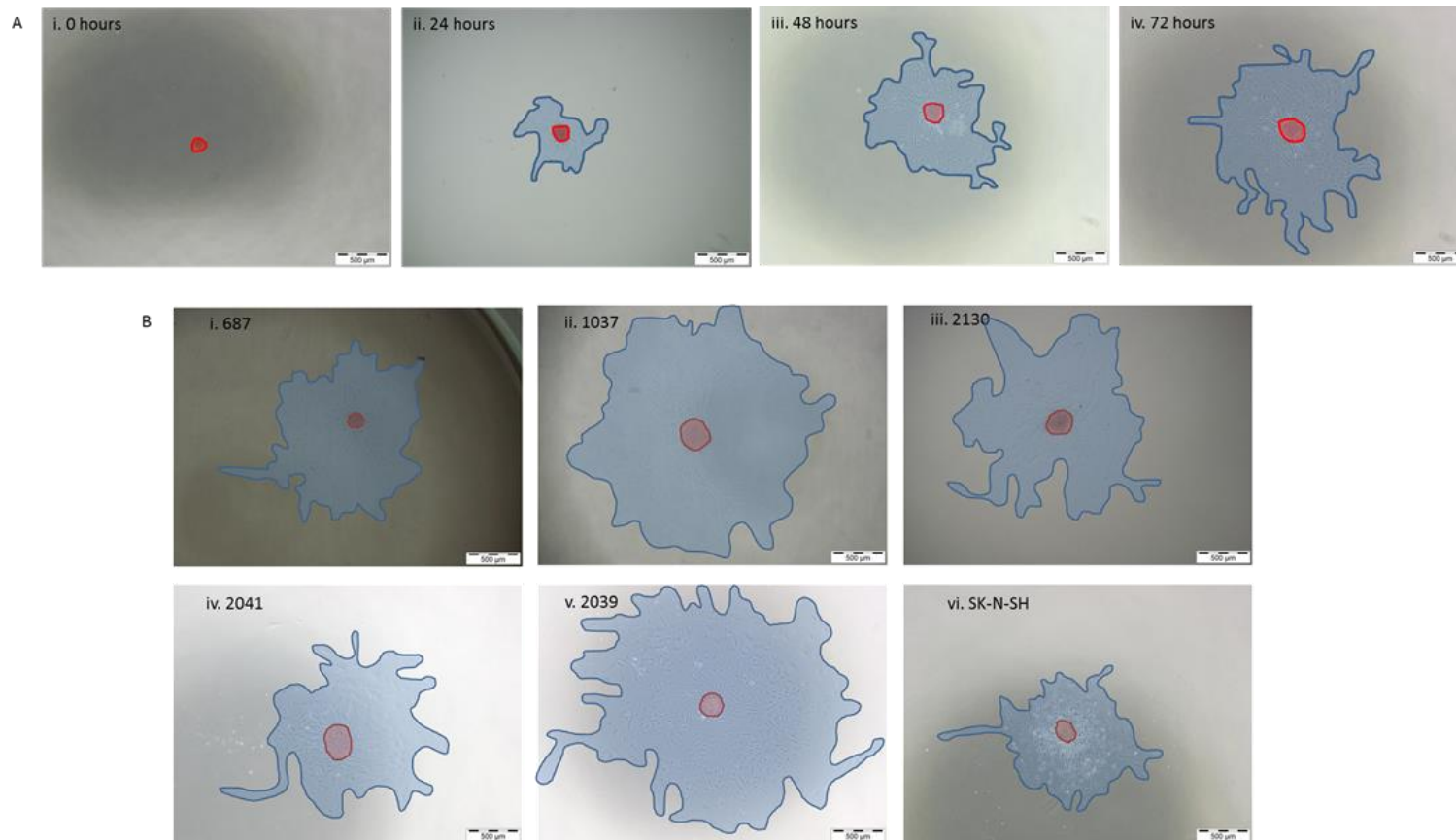
Figure 2.19 Images of migration across time points and in different samples.

A, Images of spheroid migration taken throughout the assay at i 0h ii 24h iii 48h iv 72 show increased migration with time. Red area highlights the spheroid core and blue shows the migration area. B, Images at 72h demonstrate the heterogeneity of migration across HR NB diagnostic samples i-v and SK-N-SH positive control vi.
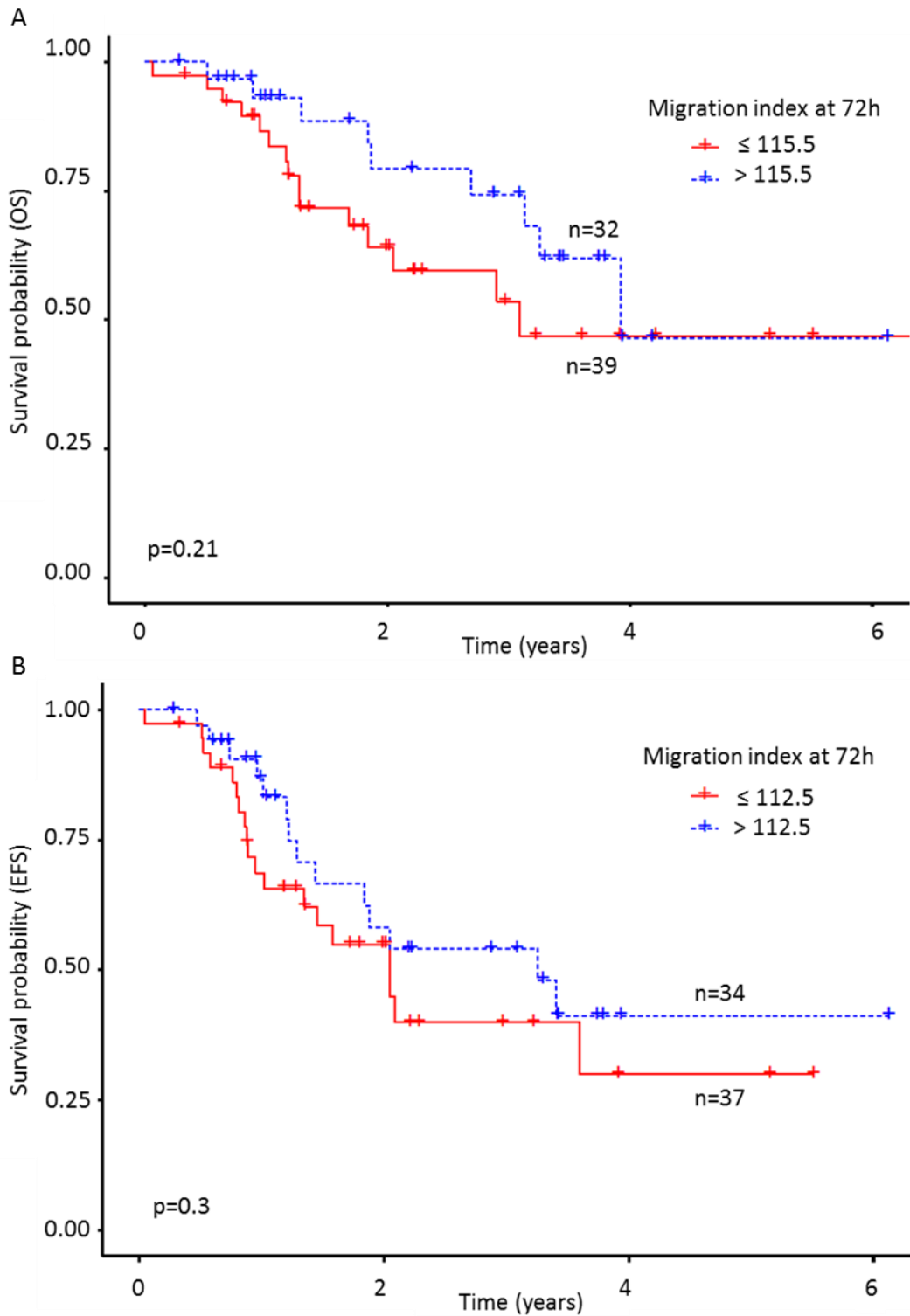
Figure 2.20 Survival vs migration.

Kaplan-Meier survival curves of A, OS and B, EFS in relation to the migration index of cells at 72h. Different optimum cut points were determined for the OS (115.5) and the EFS (112.5) for this data. Red line = migration index equal to or less than optimal cut point, blue line = migration index greater than optimal cut point, n = number of samples analysed.

2.3.8 No relationship between phenotype of NB primaries and the infiltration of NB cells within the BM

No correlations were revealed between the self-renewal assays (LA and CF) or migration when compared to the % of GD_2 positive cells in the BM (Figure 2.21). The lack of correlation between the results of self-renewal assays and infiltration was interesting as it could be hypothesised that cells with a greater self-renewing phenotype would lead to larger disease burden within the BM. Similarly cells with a greater migration capacity may lead to increased NB cells within the BM, but this correlation was not seen.

A

$y = 0.3381x + 17.826$
$R^2 = 0.0038$

B

$y = -0.0462x + 24.387$
$R^2 = 0.0265$

C

$y = -1.5385x + 20.803$
$R^2 = 0.0121$
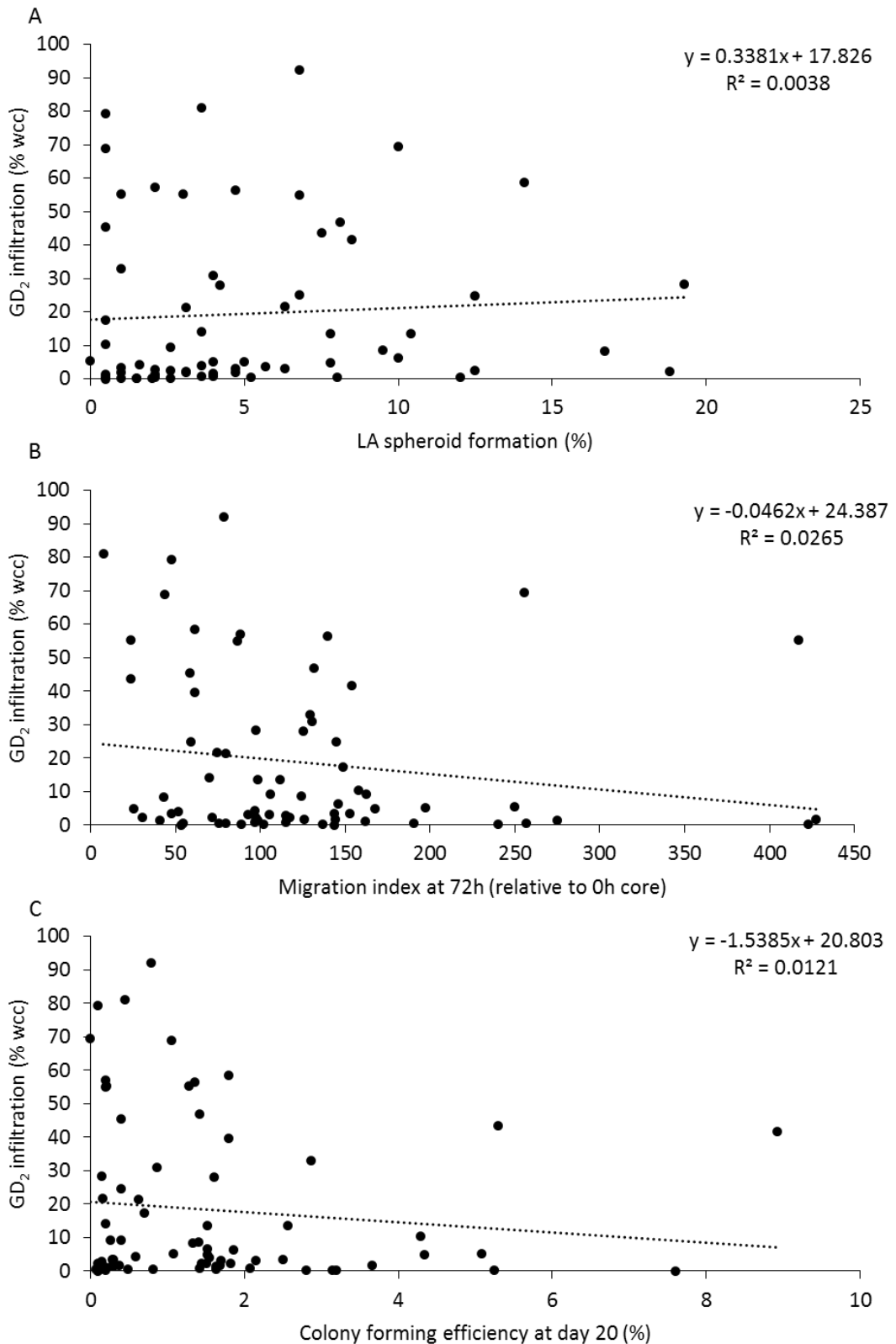
Figure 2.21 Relationship between GD_2 infiltration and cell phenotype.

Scatter plots illustrating the relationship between GD_2 infiltration against A, LA spheroid formation, B, migration, C, colony forming efficiency in HR NB diagnostic samples.

2.3.9 No relationship between self-renewal and migration of NB primaries

No correlations were revealed between the different self-renewal assays (LA and CF) and migration (Figure 2.22). The lack of correlation between the results of LA and CF assays was unexpected since both are assessing the ability of a single cell to self-renew. Intuitively one expects this reflects experimental differences in the assays, one examining self-renewal of cells in semi-solid agar (CF) and the other in liquid media (LA). A further explanation could be the effect of propagating the primary cells on plastic since the LA assay is set up from GD_2 positive cells immediately after isolation from the BM aspirates whereas the CF assays (which require higher cell number) are set up from cells propagated on plastic through several passages. Correlation between migration and either self-renewing phenotype may be hypothesised in either direction. Firstly, if a cancer cell is adaptive it would respond equally well to either a self-renewing or migratory environment, giving a positive correlation between the phenotypes. Conversely it may be argued that a cell able to migrate would not be able to self-renew, dependent on the cell cycle.
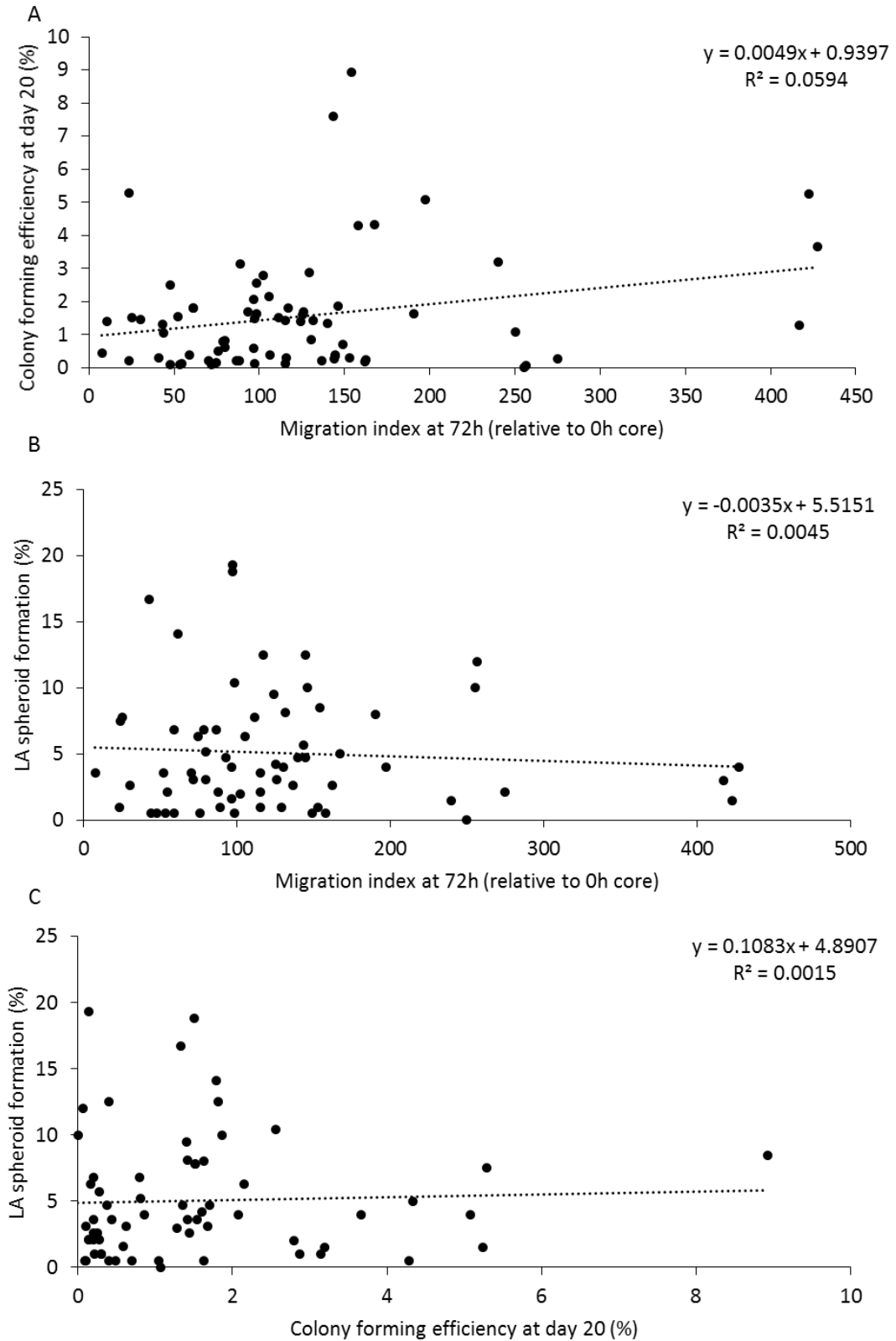
Figure 2.22 Relationship between cell phenotypes.

Scatter plots illustrating the relationship between A, colony forming efficiency and migration, B, LA spheroid formation and migration, C, colony forming efficiency and LA spheroid formation in HR NB diagnostic samples.

2.3.10 Evaluation of self-renewal and migration in NB cells isolated from children at different time points in trial

There was no significant change in self-renewal measured using the self-renewal (CF or LA) or migration assay in HR NB cells isolated from BM aspirates taken from children at diagnosis, mid-induction (RE1), end of induction (RE2a, RE2b) or relapse (Figure 2.23). Interestingly there no general trend in any of the phenotypes measured in NB samples taken from BM aspirates collected from children post treatment. This could reflect different responses to treatment or disease course across the different patient populations.

Tukey post-hoc adjusted p-value				
Time point		LA	CF	Migration
Dx	RE1	0.6	0.8	0.3
	RE2a	0.1	0.9	1
	Re2b	0.9	0.6	0.9
RE1	Dx	0.6	0.8	0.3
	RE2a	0.9	0.9	0.7
	Re2b	0.9	0.9	0.6
RE2a	Dx	0.1	0.9	1
	RE1	0.9	0.9	0.7
	Re2b	0.7	0.9	1
RE2b	Dx	0.9	0.6	0.9
	RE1	0.9	0.9	0.6
	RE2a	0.7	0.9	1
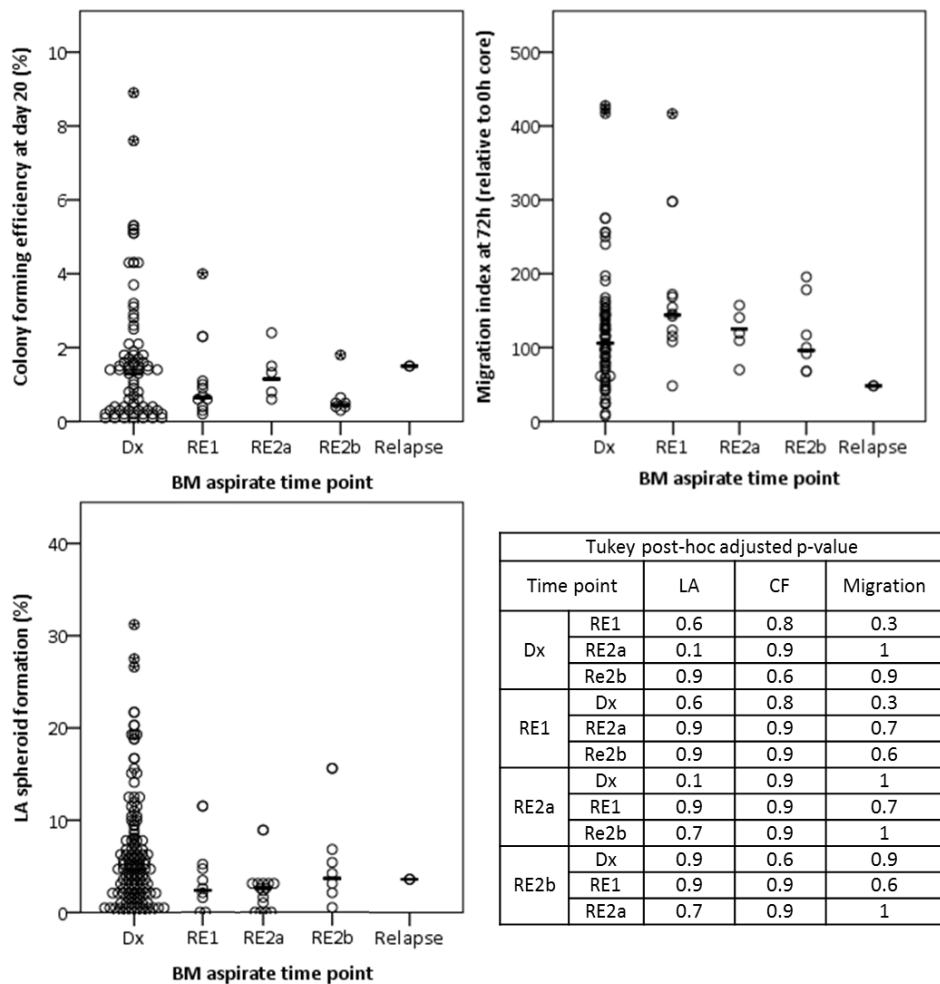
Figure 2.23 Dot plot and ANOVA summary of phenotype across trial time points.

Phenotype differences across time points were compared using ANOVA with Tukey post-hoc corrections. Dot plots show all data points for each phenotype across all time points, mean values for each group are indicated by the bar. Dx represents diagnosis.

2.3.10.1 Evaluation of self-renewal and migration across samples from the same patient

The 53 samples taken at later time points were from 35 different patients. Of these 26 had paired diagnostic samples. For each of these patients it is possible to compare the LA spheroid formation as this assay does not require successful propagation. There was LA data available to compare across 17 patients. There are no obvious commonalities of trend patterns when individual patient data is interrogated (Figure 2.24, A).
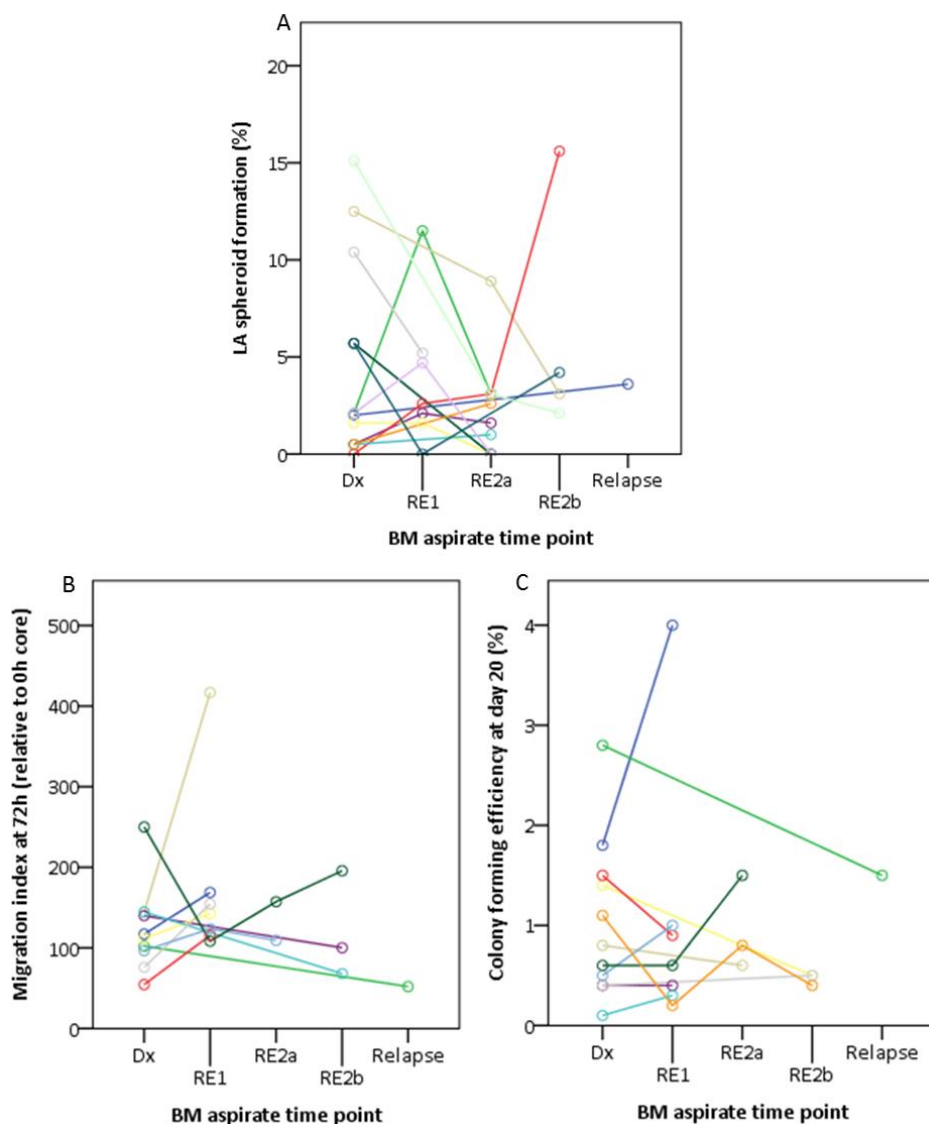
Figure 2.24 Phenotype data across time points for patients with matched samples.

Line graphs illustrating changes of phenotype in patients with matched samples; each colour denotes an individual patient. A, LA spheroid formation, B, colony forming efficiency and C, migration index.

When unsuccessful propagation samples were removed 25 samples from 11 patients remained. Of these 9 had 1 additional sample (5 with RE1, 1 with RE2a, 2 with RE2b, 1 with relapse); 1 had 2 additional samples (RE1 and RE2a); 1 had 3 additional samples (with RE1, RE2a and RE2b). For these samples comparisons for CF and migration could be made. CF data was available for all samples (Figure 2.24, C) and migration data was available for 24/25 samples (Figure 2.24, B), allowing comparison across 10 patients. Similar to the LA data, there were no obvious trends for the colony forming efficiency or the migration index.

2.4   Discussion

A total of 99 HR NB cultures were successfully enriched, propagated and characterised from BM aspirates. These cultures showed heterogeneous expression of NB markers both at a protein and RNA level. *In vitro* cultures exhibited the ability to self-renew and migrate, again heterogeneously. These primary cultures are a useful tool in characterising metastatic NB cells, more informative than cell lines that have been in culture for decades, becoming well adapted to culture and as a result may differ genetically and phenotypically from the origin (Pan *et al.*, 2009).

GD$_2$ was selected as a marker to isolate NB cells for several reasons. Practically, the cell surface expression of GD$_2$ on NB cells (Wu *et al.*, 1986) allowed for direct binding of antibody to cells without the need for permeabilisation of cells and importantly no loss of cell viability, which means it was possible to propagate cells downstream. Secondly, GD$_2$ is a disialoganglioside present on the membrane of both primary NB and metastatic circulating NB cells (Swerts *et al.*, 2004), with restricted expression on normal tissue (Wu *et al.*, 1986). GD$_2$ has been exploited in treatment for MRD (Navid *et al.*, 2010) and in other studies to isolate or identify NB metastasis in the BM (Swerts *et al.*, 2005, Abbasi *et al.*, 2015, Merugu and Tweddle, 2017). Heterogeneity seen across the infiltration of GD$_2$ positive cells (%) was consistent when comparing these infiltration data to other groups with reported infiltration rates 0.05-50% across 69 BM samples (Abbasi *et al.*, 2015).

However, GD$_2$ is reported to be expressed on other cells that may be present in the BM, such as MSCs and natural killer cells (Martinez *et al.*, 2007). Furthermore, studies have shown that in rare cases some BM NB cells do not express GD$_2$ [28,29].To prevent the loss of GD$_2$ negative NB cells, in my studies I retained the GD$_2$ negative cell fraction and tried to propagate tumour cells from this fraction. It is important to note that GD$_2$ presenting cells such as MSCs in the BM have a different morphology and growth conditions differing from those used to culture NB cells. H&E staining of GD$_2$ negative cells revealed multi and bi-lobed nuclei, indicative of neutrophils, eosinophils and basophils, although no cells were successfully propagated in the culture conditions adopted.

Predictive value of NB cells in BM was assessed by several metrics. There was no predictive significance when utilising propagation data, but the GD_2 infiltration percentage significantly predicted outcome when assessing EFS. Patients whose infiltration of GD_2 positive cells was above 6.5% had a poorer outcome (p=0.01), although not significant when using OS data (p=0.07) the same separation trend was seen. Quantification of NB cells in the BM is reported in other studies to predict outcome, patients with a larger tumour cell burden within the BM predicted to do worse (Seeger *et al.*, 2000, Corrias *et al.*, 2008).

The isolation of NB cells from BM has been explored by other groups, some groups rely on removal of normal BM cells or the increased self-renewal ability of NB cells with no selection (Hansford *et al.*, 2007b). A consistency across many studies is to first remove the red blood cells, here we use erythrocyte lysis buffer, many other studies utilise lymphoprep, a density gradient technique to give a fraction of white blood cells, including NB cells, to be pipetted from the tube (Abbasi *et al.*, 2015). Several other studies also exploit GD_2 as a marker of NB within the BM (Swerts *et al.*, 2005, Scaruffi *et al.*, 2012, Abbasi *et al.*, 2015, Merugu and Tweddle, 2017). In addition to the use of GD_2 several groups exploit NCAM as an alternative or additional marker (Vandewoestyne *et al.*, 2012, Abbasi *et al.*, 2015, Merugu and Tweddle, 2017). NCAM expression was recorded in 37/66 cultures, however, as a marker of differentiation NCAM expressing cells will be more differentiated and in turn less aggressive cells (Winter *et al.*, 2008).

Many of the aforementioned studies isolating NB cells from BM used cells at separation for analysis, there are fewer publications reporting on the isolation and propagation of BM NB cells (Hansford *et al.*, 2007b, Nakanishi *et al.*, 2007, Scaruffi *et al.*, 2012, Bate-Eya *et al.*, 2014). There are also a selection of studies of propagation of NB cells from primary NB tissue. Magnetic bead isolation was used in this study as it allows separation under sterile conditions, reducing the risk of infection in downstream culture, also advantageous is the high cells viability after separation. In primary NB cells isolated from tumour tissue the same approach was used, conversely to remove lymphocytes, the resultant NB cells were reported to have a non-adherent culture phenotype (Nakanishi *et al.*, 2007). Non-adherent

culture was not established in any of the primary cultures, in samples where floating groups of cells were seen viability was assessed using trypan blue and a Neubauer haemocytometer, and no viable spheroids were seen in culture flasks.

Further to the NCAM staining described above, GD_2 positive cells were also characterised to give additional confidence in NB isolation. Immunocytological assessment of additional markers TH, PHOX2B, nestin, MRP1, MRP4 and CD57 showed heterogeneous staining. CD45 was utilised to ascertain no infiltration of BM leukocytes, this marker has been implemented in other studies as a negative selection (Komada *et al.*, 1998, Hansford *et al.*, 2007, Merugu and Tweddle, 2017). Nestin was not expressed in all cultures as reported in some studies (Hansford *et al.*, 2007) this may be as some cultures are more differentiated and therefore express less of the neural stemness marker. Fewer samples expressed CD57, indicative of increase aggressive phenotype including invasiveness. This occasional detection of CD57 is reported in other studies analysing expression of NB cell within the BM (Esser *et al.*, 2011). The multidrug resistance proteins MRP1 and MRP4, associated with poor outcome in NB were detected in all samples analysed. Although documented as a NB marker it is worth noting NB84 was not used in this panel as a preliminary selection of samples showed no positivity in accordance with literature (Bomken *et al.*, 2006), suggesting that NB84 is an unsuitable marker for BM NB cells.

TH is the rate limiting enzyme for catecholamine biosynthesis, a feature of NB, and the presence of TH mRNA confirms infiltration of NB cells in the blood and BM (Burchill *et al.*, 1994, Trager *et al.*, 2003). TH mRNA was detected in all cultured NB samples, however there was no detection of TH protein when cytospins were analysed using immunocytology. PHOX2B is a gene involved in early development of nerve cells and is a putative NB marker (Pattyn *et al.*, 1999), protein was detected by immunocytology in 41/65 cultures but no mRNA was detected by RTqPCR.

Consistent with the potential of NB cells in the BM to metastasise and produce tumours, all samples had the capacity to migrate and were capable of self-renewal assessed using *in vitro* models. It may be hypothesised that those patients whose cultures show the greatest migratory or self-renewing phenotype will give poorest clinical outcome. Upon assessment of survival and response data with phenotype

characteristics, the migration index was not predictive of survival. A high self-renewing phenotype, when assessed using the CF assay, is predictive of increased survival, contrary to the hypothesis. This correlation may be due to cells with greater turn over, or high self-renewal are patients that will show greater cell death due to the activity of chemotherapeutics used to treat patients within the HR trials.

All the HR NB cultures were able to migrate and 95% (68/73 of diagnostic cultures; 20/20 later time points) were more migratory than the SK-N-SH (control). SK-N-SH cells were derived from a NB metastasis to the BM, as were the samples. Perhaps continued culture reduces the migratory phenotype within the cells, as the SK-N-SH cells were derived in 1970 and during these studies have been passaged upwards of 30 times compared with 3-8 for the primary NB cells. One study looking at migration of NB cell lines used a chemotaxis chamber also assessing the invasiveness of cells, which is not directly comparable to the 24 well plate assay used in this study (Lynch *et al.*, 2012). A wound healing assay assesses the ability of cells to migrate across a scratch made in a confluent well. This assay was used to assess the migratory ability of NB cell lines, it was shown that *MYCN* amplified cells had larger migration ability (Gangoda *et al.*, 2015), SK-N-SH cells are non-*MYCN* amplified and *MYCN* amplification is not present for all HR NB patients; perhaps this explains the heterogeneity seen across migration index. The 5 samples that did not have a larger migration value than the control cell line were all derived from patients with a *MYCN* amplified tumour so it may be other genetic factors responsible.

The heterogeneity of results from the CF assay fits with the clinical presentation of BM disease in NB, which is hugely variable (Ora and Eggert, 2011), even within children that have HR disease (Viprey *et al.*, 2014). Both self-renewal assays are limited by the challenge to replicate the BM microenvironment, a more informative assessment of self-renewal would be to test the ability of isolated cells to produce tumours and metastasise using *in vivo* subcutaneous and colonisation mouse models. Interestingly, one study reports higher self-renewal ability of HR sample to low-risk; self-renewal capacity of tumour cells was assessed through the limit of their sphere formation in liquid culture recorded in number of passages (Hansford *et al.*, 2007b). The HR NB samples were reported to undergo a median of 6 passages, with

the maximum 15. These data are similar to culturing tendencies of the BM NB cells in this study, where most cultures would begin to senesce before reaching passage 20 (data not shown). Although there are several NHR NB cultures that propagated, these were not assessed for colony forming efficiency, however this provides an interesting possibility for future investigations.

The NHR samples were assessed for self-renewal using LA spheroid formation. Analysis between HR and NHR NB showed no difference in the ability between the groups to produce spheroids. This finding perhaps reflects the similarities of cells residing within the BM, that they are a similar sub section of cells from the NB primary tumour exhibiting similar phenotype. The presence of NB cells within BM is contradictory to a diagnosis of NHR NB as the INRG task force states patients with widely disseminated disease to the BM should be staged as M (Monclair *et al.*, 2009). Within the M stage, unless under 18 months, patients are categorised as HR. Patients that are under 18 months at the time of diagnosis with BM metastasis are designated a unique risk stratification, 4S, of the diagnoses in the NHR NB group 5 were classified as 4S. Perhaps these findings illuminate pitfalls within the current strategies to determine metastasis to BM in children with NB.

Proposed further studies would have included expanded characterisation of isolated BM NB cells to explore other phenotypes including the sensitivity to therapies. Response to common chemotherapeutics such as vincristine and doxorubicin, as used in the HR NB trials may have highlighted cultures with a higher drug refractory phenotype. Patients with low drug refractory phenotypes may be hypothesised to show the best response in clinic. As described above the potential to better characterise the migratory and self-renewing phenotypes may be considered in future studies.

As discussed above, different confirmation of NB status of cells has been used by other groups. These additional characterisations may have been added at either the initial separation stage, perhaps to assess the purity of isolated positive cells, or throughout passage to ensure cultivation was of NB cells. Perhaps a small amount of isolated cells when in surplus may have been used for flow cytometry analysis of further expression markers, or including GD_2 to assess purity of isolated positive

cells. BM was analysed using the Imagestream imaging flow cytometer for the presence of disseminated tumour cells using markers GD_2 and NCAM (Merugu and Tweddle, 2017). This characterisation does not allow further cultured as the methodology requires fixation, and therefore a surplus population of cells would be necessary. Unfortunately interrogation of cell counts eluded the higher the number of cells the more likely the success of propagation, therefore removing cells from the culture flask may result in decreased propagation success. Thus hindering the aims of this study, namely to isolate and characterise NB cells from the BM.

There are not many genetic changes present in NB, therefore further characterisation of epigenetic regulators was explored, focusing on miRNA expression. This choice was informed by the wide reaching effects of miRNAs. To profile each culture for miRNAs would allow interrogation of the driving factors behind the aggressive phenotypes, illuminating key pathways or targets for novel treatments.

Chapter 3 miRNA profiling of NB cells isolated from BM aspirates

3.1 Introduction

miRNAs regulate multiple cellular processes to drive the development of cancer, including NB (Guo *et al.*, 2010, Tivnan *et al.*, 2012, Stigliani *et al.*, 2015, Zhao *et al.*, 2015). The ability of a single miRNA to modulate expression of several target genes might be exploited in the clinic to develop more personalised therapeutics, selecting patients' for treatment based on expression of driver miRNAs and treating them with agents targeting those oncogenic miRNAs. Such an approach might be more specific leading to reduced toxicity in patients. By interrogating miRNA profiles of NB cells isolated from the BM of children with HR NB I have hypothesised that oncogenic miRNAs driving aggressive phenotypes may be identified. In turn these could benefit patients' by improving clinical stratification and novel therapeutic development to eradicate BM disease.

There is great potential within NB for both single and multiple miRNA signatures to inform diagnosis, stratification or to monitor progression of patients' cancer. Stratification of patients using miRNA profiles has been explored within NB, with signatures significantly linked to each stage or risk category, and within stages to further identify poor survival patients, unlikely to respond to treatment. Within HR patients several miRNAs have been identified that are down regulated in patients with increased survival (Scaruffi *et al.*, 2009). These miRNAs target genes implicated in neuronal differentiation, with reduction in these miRNAs leading to increasing differentiation in the cancer and therefore increased survival; more highly differentiated cells is indicative of a good prognosis.

The miRNA profile of tissues and tumour cells can be evaluated using different detection platforms including RTqPCR, NanoString technology, hybridisation-base arrays and miRNA sequencing (Git *et al.*, 2010, Foye *et al.*, 2017). The most frequently adopted approach is using RTqPCR, which is user-friendly, requires small amounts of good quality RNA, and has a high dynamic range and a reasonably high throughput. The TaqMan® Low Density Array (TLDA; Thermo Fisher) uses a 384 well format to assess expression by RTqPCR of 377 annotated miRNA targets, 3 small

nucleolar RNAs (snoRNA; one in triplicate) and 1 *Arabidopsis thaliana* miRNA (as a negative control well) as shown in Appendix A. These miRNA TLDAs were chosen for this study for several reasons (above) and importantly because they measure expression of annotated miRNAs, to allow unambiguous interpretation of results and the design of downstream validation of targets. Downstream analysis can be used to inform inhibitor experiments, and biological validation can confirm mechanisms of pathogenesis. Furthermore, this platform has been utilised within the SIOPEN clinical trial, analysing PB and BM aspirates of children on the HR NB trial, it was therefore beneficial to keep the platform standardised to allow analysis across different samples types (Chapter 4). However the normalisation of miRNA expression presents a problem in analyses of this kind, since there is not a universally accepted reference miRNA. Examples of RNAs that have been used to normalise results include mir-16, mir-26a, and snoRNAs such as U6 and U48. Different criteria for normalisation and interpretation of data can affect reproducibility and clinical evaluation of miRNAs. It was therefore essential that I design and validate a work pipeline to quantify miRNAs in NB cells and establish the best normalisation method to ensure the quality of data used in statistical analyses.

In the previous chapter I have characterised the phenotype of NB cells isolated from BM aspirates at diagnosis. These cells are highly migratory and self-renewing. Within this chapter my goal was to profile the miRNAs of these cells to investigate their biological heterogeneity and the functional significance of expressed miRNAs.

The aims of this chapter were therefore:

1. To investigate the expression of 377 annotated miRNAs in a panel of 50 NB primary cultures derived from BM aspirates
2. To develop standardised pipelines for optimal analysis and interpretation of results
3. To identify miRNAs driving migration and self-renewal in NB cells
4. To functionally validate the miRNAs identified as significantly linked to migration and self-renewal

3.2   Materials and methods

3.2.1   Profiling miRNA expression in primary NB cultures using TLDAs

Primary BM derived NB cells (n=60) from a 70% confluent T75 flask were pelleted after trypinisation (Section 2.2.5.1) and stored at -80°C until used for RNA extraction.

3.2.1.1   RNA extraction, quantification and quality assessment

RNA was extracted from NB BM cell pellets using the miRNeasy mini kit (Qiagen) and assessed for quality using the Agilent RNA 6000 Pico kit (Agilent). For analysis using the miRNA TLDA, the RNA concentration needed to be equal to or greater than 125ng/µl so that 400ng of RNA could be analysed on each plate. After spectrophotometric measurement of nucleic acid quantity samples that were not at a high enough concentration were further concentrated using the RNeasy MinElute Cleanup Kit (Qiagen).The small RNA content of the extracted total RNA was assessed using the Agilent small RNA kit (Agilent).

3.2.1.1.1.   Extraction of total RNA from cell pellets

RNA was extracted from cell pellets using the miRNeasy mini kit; all buffers are company proprietary. As depicted in Figure 3.1, A, the cell pellet was resuspended in 700µl QIAzol (Qiagen) and vortexed to ensure complete lysis then incubated at room temperature for 5 min. The lysate was passed through a QIAshredder (Qiagen) spin column, centrifuged at 13,000g for 2 min, to ensure complete homogenisation. Chloroform (140µl) was added to the lysate and mixed well by shaking vigorously by hand for 15s. The sample was then centrifuged at 12,000g for 15 min at 4°C. The supernatant was carefully aspirated from the cell pellet and added to an equal volume of 100% ethanol and mixed by pipetting, it was then added to a miRNeasy spin column and centrifuged for 15s at 8,000g. The flow through (FT) was discarded and the column washed by adding 350µl of buffer RWT and centrifuged at 8,000g for 15s. To eliminate any contaminating genomic DNA, 80µl buffer RDD containing 10µl deoxyribonuclease (DNase) I (Qiagen) was added to the column membrane and incubated for 15 min at room temperature. The column was further washed by adding buffer RWT (350µl) and centrifuged at 8,000g for 15s, the FT was discarded. Buffer RPE (500µl) was added to the column and centrifuged at 8,000g for 15s, the

FT was discarded and the same volume of RPE buffer was added to the column and centrifuged at 8,000g for 2 min. The column was placed into a fresh collection tube and centrifuged at 13,000g for 1 min to remove residual buffers. RNase free water (30µl; Qiagen) was added directly to the membrane and centrifuged for 1 min at 8,000g to elute the RNA. To increase the yield of RNA, eluted water was pipetted back onto the membrane and the column was re-centrifuged at 8,000g for 1 min. The concentration of RNA was measured as described in Section 3.2.1.1.2, aliquoted in single use aliquots to avoid freeze thaw and stored at -80°C.

When the RNA concentration was less than 125ng/µl it was concentrated using the RNeasy MinElute Cleanup Kit RNA (Figure 3.1, B). RNA (28µl) was added to 70µl of RNase free water, 350µl of buffer RLT and 700µl of 100% ethanol and mixed well by pipetting. Up to 700µl of the sample was added to an RNeasy MinElute spin column in a 2ml collection tube and centrifuged for 15s at 8,000g, the FT was discarded. This step was repeated until the entire sample had passed through the spin column. The column was then placed in a new 2ml collection tube and 500µl of buffer RPE was added to the top of the column which was then centrifuged at 8,000g for 15s. The FT was discarded and 500µl of 80% ethanol was added to the top of the column which was then centrifuged for 2 min at 8,000g. The spin column was placed in a new 2ml collection tube and centrifuged at 13,000g for 5 min to remove excess buffer from the column. The column was placed in a new 1.5ml collection tube and 14µl of RNase free water was carefully pipetted into the centre of the spin column membrane. The column was centrifuged for 1 min at 13,000g. The eluate was collected and the RNA concentration determined as described in Section 3.2.1.1.2. If the RNA concentration was still insufficient (<125ng/µl) after concentration RNA was extracted from a second cell pellet.

3.2.1.1.2. Assessment of nucleic acid quantity and quality

The concentration and purity of RNA was measured using the Nanodrop (Labtech International Ltd). The Nanodrop anvil surface was cleaned with RNase free water and the machine was corrected to zero using RNase free water. The Nanodrop was then loaded with 1µl of RNA solution and the concentration of RNA (ng/µl) was recorded. The absorbance of nucleic acids at 260nm and 280nm are used to calculate

the 260/280 ratio for each sample, if this value was between 1.8-2.1 this indicated the sample was free from contaminants. The quantity of RNA was determined assuming an absorbance of 1 at 260nm was equivalent to an RNA concentration of 40µg/ml (calculated using Beer's law (Rodger, 2013)).
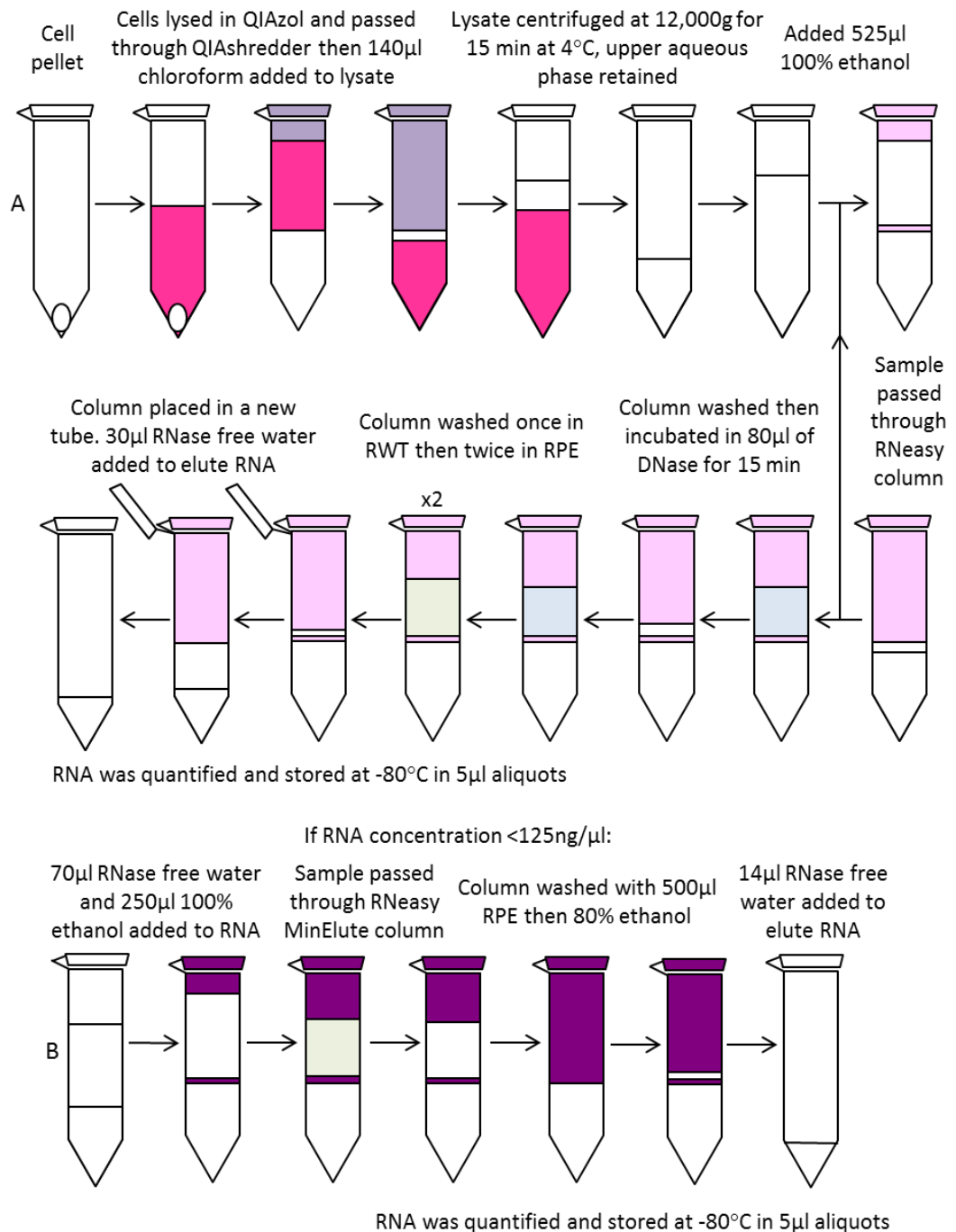
Figure 3.1 RNA extraction and concentration.

A, extraction of RNA using miRNeasy mini kit; B, concentration of RNA using MinElute kit. All buffers are company proprietary.

The Agilent RNA 6000 Pico kit was used to assess the quality of total RNA in all samples by measuring the RNA integrity number (RIN) which is measured on a scale of 1 (represents degraded RNA) to 10 (represents good quality RNA). The RIN was developed using adaptive learning tools and uses several factors including signal areas, intensities and the ratio of 18S and 28S bands from the electropherogram (Schroeder *et al.*, 2006). RNA was diluted in RNase free water to a concentration of 5ng/µl and heated at 70°C for 2 min prior to analysis. The RNA dye concentrate was warmed to room temperature for 30 min before use. RNA dye concentrate (1µl) was added to an aliquot of prepared gel and vortexed well. The gel dye mix was centrifuged at 13,000g for 10 min. A new chip was docked onto the chip priming station and 9µl of gel-dye mix was added to the G* port. The chip priming station was then closed and the syringe sealed and compressed to distribute the gel; this was released after 1 min. Another 9µl of gel-dye mix was added to both G ports and 9µl of conditioning solution was added to the CS port. Five µl of RNA marker was added to ports 1-11, and then 1µl of a sample was loaded into each sample port and 1µl of ladder to the L port. A further 1µl of RNA marker was added to any ports that did not contain sample. The chip was then vortexed for 1 min at 2,400 revolutions per min (rpm) on the IKA vortexer (IKA, catalogue number 3617036, Oxford, UK) and loaded onto the Agilent Bioanalyser 2100 (Agilent). The chip was analysed using the 2100 expert software (version B.02.08.SI648 (SR3), Agilent) using the eukaryote total RNA pico assay settings.

The small RNA kit (Agilent) was used to quantify the miRNA concentration and percentage of miRNA in the small RNA of each sample. RNA was diluted in RNase free water to a concentration of 5ng/µl and heated at 70°C for 2 min prior to analysis on the Agilent Bioanalyser 2100. All reagents were warmed to room temperature 30 min before use. Filtered gel (40µl) was added to 2µl of dye concentrate and mixed thoroughly by pipetting. The tube was then centrifuged at 13,000g for 10 min. The small RNA chip was then loaded in the same way as the Agilent RNA 6000 Pico kit described above. The chip was analysed using the 2100 expert software using small RNA v1.2 assay settings.

3.2.1.2   Conversion of RNA to cDNA using RT and MegaPlex™ primers

Total RNA was diluted in RNase free water so that each sample contained 400ng in a volume of 3.2µl. To each sample reagents from the TaqMan® MicroRNA Reverse Transcription Kit (Thermo Fisher) and MegaPlex Primers Pool A v2.1 (Thermo Fisher) were added as listed in Table 3.1.

Table 3.1 Components in the MegaPlex™ RT reaction.

All reagents were sourced from Thermo Fisher. The MegaPlex™ primers Pool A v.2.1 contains predefined primers to be used with the miRNA TLDA human A card, enabling simultaneous synthesis of cDNA for 377 mature miRNAs, 3 snoRNAs and the negative control *Arabidopsis thaliana* miRNA.

Reagent	Volume per sample (µl)	Concentration in the reaction tube
MegaPlex™ RT Primers Pool A v2.1 (10x)	0.8	1.06x
dNTPs with dTTP (100mM)	0.2	2.6mM
MultiScribe RT (50U/µl)	1.5	75U
10X RT Buffer	0.8	1.06x
MgCl$_2$ (25mM)	0.9	3mM
RNase Inhibitor (20U/µl)	0.1	2U
400ng total RNA in RNase free water	3.2	-
Total volume	7.5	-

The contents of each tube were mixed by pipetting and pulse centrifuged to bring the tube contents into the bottom of the tube. All samples were then chilled on ice for 5 min. The samples were then placed in the thermal cycler TC500 (Techne, Bibby Scientific Ltd, Staffordshire, UK) and run through 40 cycles of 16°C (anneal) x 2 min, 42°C (RT) x 1 min, 50°C (denature) x 1s; the sample was then held for 5 min at 85°C (terminate reaction) and finally at 4°C. The cDNA was stored at -80°C until used.

3.2.1.3 RTqPCR using miRNA TLDA human A card to assess expression of 377 miRNAs

The miRNA TLDA was used to profile 377 annotated miRNAs, 3 snoRNAs (U44, U48 and U6) and 1 *Arabidopsis thaliana* miRNA in 54 (6/60 insufficient RNA) BM NB primary cell cultures.

The miRNA TLDAs were allowed to equilibrate to room temperature for 30 min before use. Then, 6µl of cDNA was added to 444µl RNase free water and 450µl TaqMan® Universal PCR Master Mix no AmpErase UNG (Thermo Fisher) and mixed gently. Next 100µl of this mix was added to each of the 8 ports of the miRNA TLDA card. The array card was then centrifuged at 2,000g for 1 min. The centrifugation step was repeated. The array card was then sealed and the ports were removed and the miRNA TLDA was run on the 7900 HT Fast Real-Time PCR System (Thermo Fisher) using the SDS 2.4 platform (Thermo Fisher) or using the QuantStudio™ 12K Flex Real-Time PCR System (Thermo Fisher). Prior to PCR the miRNA TLDA was heated to 95°C for 10 min to activate the AmpliTaq Gold® DNA polymerase then the sample was amplified for 40 cycles of 95°C (denature) for 15s and 60°C (anneal and extend) for 1 min.

The data were exported to and opened in RQ Manager 1.2.1 (Thermo Fisher) if analysed using the 7900 HT Fast Real-Time PCR System or QuantStudio™ 12K Software v1.2.2 (Thermo Fisher), if the QuantStudio™ 12K Flex Real-Time PCR System was used.

3.2.2 Analysis of raw miRNA profile data

Within the analysis software the amplification curves were visually inspected to ensure good S shaped curves with clear initiation, exponential and plateau phases. Quality control flags were checked for each well, and particular attention was paid to BADROX (indicates bad passive reference signal, when the 6-carboxy-X-rhodamine (ROX) reference signal is abnormal) and PRFDROP (indicated when passive reference signal changes significantly near the cycle threshold (Ct)) flags, the amplification curves and multicomponent plots of any highlighted wells were visually inspected to evaluate if the data were to be included in downstream analysis. If the amplification curve for that well was not of good quality it was omitted from analysis.

It was also omitted from analysis if the multicomponent plots did not show stable fluorescence of ROX, the reference fluorescence as this value is used to determine the ΔRn value which in turn determines the Ct.

The Ct values were derived using an automatic baseline and a manual threshold set to 0.2 ΔRn, this threshold was chosen as all amplification curves crossed this point in exponential phase. Amplification data were exported and saved as .txt files for downstream analysis. Data was stored in two places, in a secure folder on the University N drive server and in the Cloud server provided by Thermo Fisher; data is backed up in both sites. Data were checked against the criteria depicted in Figure 3.2 to identify failed miRNA TLDAs which were excluded from downstream analyses; miRNAs with a Ct value >35 were denoted as not expressed since when Ct values reach 35-40 the results are not reproducibly detected (Thermo Fisher recommendation (Guthrie *et al.*, 2008, Chen *et al.*, 2009, Viprey *et al.*, 2012, Jorge *et al.*, 2017)).
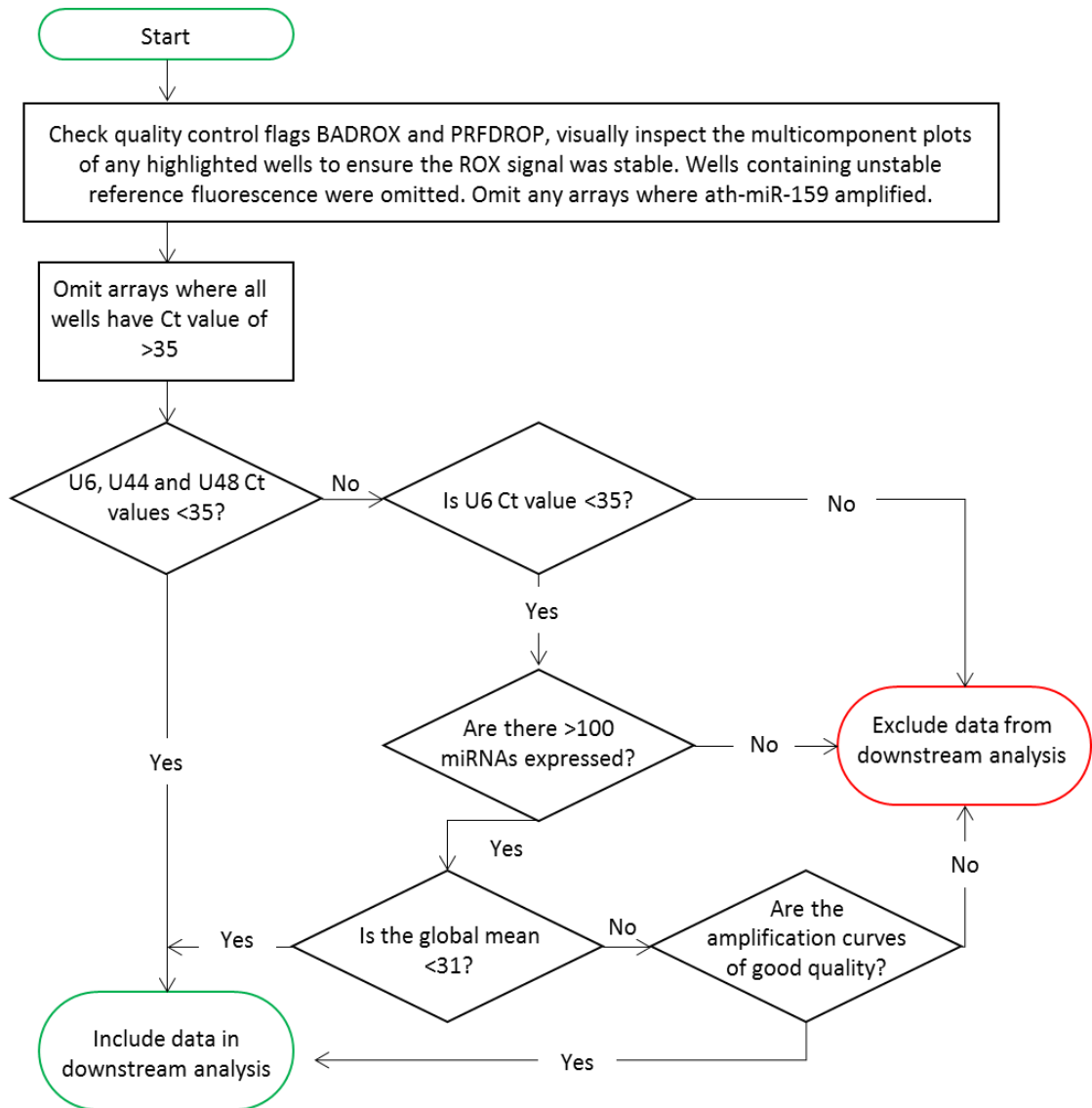
Figure 3.2 Quality control workflow for miRNA TLDA data.

BADROX indicated a bad passive reference signal. PRFDROP indicated a significant change in the passive reference signal near the cycle at which the Ct values was determined. U6, U44, U48 are the snoRNAs. This workflow ensured only experimentally sound data was taken forward into the statistical analysis.

3.2.2.1 Optimisation of the best normalisation method

A miRNA was accepted as expressed if the Ct value was less than 35. Ct values were analysed using the open source programming software, R (Bioconductor software, R Core Team, Vienna, Austria). To determine the best normalisation method I created an R script to normalise Ct values using the global mean (the average of all expressed miRNAs within each miRNA TLDA) and each reference on the miRNA TLDA (U6, U44, U48) to produce delta Ct values (ΔCt, calculated as shown below). ΔCt values are equal to the difference in threshold cycles for the target miRNA and reference, in

this case global mean. These values were used to generate box plots, allowing visualisation of data and calculation of the standard deviation across the median Ct values for each set of normalised data.

$$\Delta Ct = Ct \ (of \ miRNA) - Ct \ (reference)$$

Normalisation was also evaluated in data kindly provided by Dr Maria Corrias from the Giannina Gaslini Institute, which included miRNA profiles from the miRNA TLDA human A and B cards. Both NB primary tumour (n=12) and BM NB cell profiles (n=12) were provided. This additional data allowed validation in both an independent cohort and different miRNA expression panel.

3.2.2.2 Bioinformatics to visualise miRNA expression profile patterns

The ΔCt values were used to generate heat maps using the online tool ClustVis (Metsalu and Vilo, 2015). The data were clustered hierarchically for both miRNAs and miRNA TLDAs (DH'haeseleer, 2005). Similarity metrics used were Euclidean distance for miRNAs and correlation for miRNA TLDAs, all data were clustered with complete linkage.

Principal components analysis was performed using ΔCt values with no scaling using singular value decomposition (SVD) imputation performed by the online tool ClustVis (Metsalu and Vilo, 2015). PCA helps to summarise data with minimum characteristics by identifying measurements that are related and therefore redundant. Plots were generating using principal component (PC) 1 and PC2 as the axis to visualise subgroups within the data set. These two methods were combined to identify significant clusters or groups that were isolated in both analyses

3.2.3 Identification of enriched pathways in primary NB cells using miRNA expression

Analysis of miRNA profiles was used to identify enriched regulatory pathways in NB cells. The functional value of this approach was evaluated by examining the effect of inhibitors to one enriched pathway on NB viable cell number. Expression of 103 miRNAs in 50 NB BM cell samples were included in the pathway analysis, snoRNAs U44, U48 and U6 were removed. The average ΔCt (normalised to the global mean) and standard deviation across the 103 expressed miRNAs were calculated. The

miRNAs were then ranked first from highest to lowest expression and then by variation using smallest to highest standard deviation. After ranking, the top 10% of the list were used in pathway analysis.

3.2.3.1 Identification of enriched pathways using miRPath

The top 10% of ranked miRNAs were used to identify potential downstream targets by revealing the biological pathways that had enriched p-values using the DIANA-miRPath pathway analysis web-server (Vlachos *et al.*, 2015) and Kyoto Encyclopaedia of Genes and Genomes (KEGG, Kanehisa Laboratories, Japan). Within miRPath the data was analysed using pathways union which takes all significantly targeted pathways from the miRNA list given and performs an enrichment analysis for each pathway to miRNA, generating an enrichment p-value. Merged p-values are calculated for each pathway using Fisher's Exact meta-analysis, p-values represent 1-chance of pathway being enriched in by at least 1 miRNA derived using an A Posteriori analysis method. Analysis was performed using validated gene targets derived from Tarbase. Results, including KEGG pathway name, enrichment p-value, number of miRNAs and the number of gene targets involved in each pathway, were exported as .csv files for further evaluation.

3.2.3.2 Targeting PI3K pathway in primary NB cells

The PI3K pathway was identified as significantly enriched in BM NB cells using the approach described above. To assess the ability of the miRNA TLDA and miRPath analysis method to identify functionally relevant pathways the effect of two PI3 kinase inhibitors on cell viability was evaluated, alone and in combination with the doxorubicin.

Two PI3K inhibitors were selected; PI103 (SYN-1065, Cambridge Bioscience) and LY294002 (9901, New England Biolabs (NEB, Hertfordshire, UK), (Vlahos *et al.*, 1994)). Both inhibitors have been utilised in studies using NB cell lines (Johnsen *et al.*, 2007, Segerström *et al.*, 2011), additionally LY294002 was used in a phase I study for children with relapsed or refractory NB (NCT02337309). Stock solutions of each inhibitor were prepared at a concentration of 10mM in DMSO. Doxorubicin (Sigma) was prepared as a 3.4mM stock solution in deionised distilled water and stored at -20°C.

SH-SY5Y (control NB cell line) and 3302 (BM NB primary culture) were harvested (Chapter 2, Section 2.2.5.1), seeded in a 6-well Primaria™ plate at a density of 5×10^4 and 2×10^4 cells per well respectively and incubated overnight to allow cells to adhere. Cells were then treated with inhibitors PI103, 0.125-2 micromolar (µM) or LY294002, 1-16µM alone or in combination with doxorubicin (7.5-120nM). All treatments were performed in triplicate. Cells were also treated with the DMSO vehicle (controls) and experiments were carried out on three independent occasions.

3.2.3.3   Measuring viable cell number: Automated Vi-cell

Viable cell number at 72h was determined using the trypan blue exclusion assay on the automated Vi-cell. Cells were harvested, as previously described in Section 2.2.5.1 and resuspended in 0.5ml fresh media. An equal volume of trypan blue was added to the cell suspension which was then analysed on the Vi-cell. Viable cells are identified by clear cytoplasm and cell size; the size of cells was set to detect NB primaries and the SH-SY5Y control NB cell line. Viable cell number is calculated as number of viable cells $x10^6$/ml.

3.2.4   Statistical analysis to identify miRNAs predicting phenotype

The miRNA expression profiles of 50 BM NB cell cultures were analysed to identify any relationship between miRNAs and migration or self-renewal as measured using the CF assay (Section 2.2.6.2) or LA assay (Section 2.2.6.1).

Logistic regression was used to analyse the data using a binary format for miRNA expression. Migration and self-renewal of the same 50 BM NB cells was used to check for any associations between high/low migration or self-renewal with presence/absence of the 377 annotated miRNAs. Samples with a value over the median were denoted as 1 for the phenotype, those with a value under as 0. As previously described a miRNA was accepted as expressed if the Ct value was less than 35, miRNA expressed were denoted as 1 and those not expressed (Ct value >35) denoted as 0. Logistic regression was performed by Professor Walter Gregory using Stata (StataCorp. 2017. *Stata Statistical Software: Release 15*. College Station, TX: StataCorp LLC), Benjamini-Hochberg multiple testing correction was used. A significant adjusted p-value threshold of 0.05 was used.

Linear regression was also used to analyse the data using a continuous variable format. Expression levels of 377 miRNAs from the profiles of 50 BM NB cells were tested for correlation with migration and both low adherence and colony forming self-renewal ability. Once again Benjamini-Hochberg multiple testing correction was used to correct for the false discovery rate. A significant p-value threshold of 0.05 was used.

3.2.5 Validation of differentially expressed miRNA using Assay-on-Demand™ RTqPCR

Assay-on-Demand™ (A-o-D; Thermo Fisher) use the same primer and probe sets utilised in the miRNA TLDA but are used for single assay RTqPCR. Experimental validation was essential to ensure the results from the miRNA TLDA were reproducible, as the assay on demand have a higher sensitivity, therefore low level expression that may have given a negative result in the miRNA TLDA analysis suggesting the miRNA is not present in the sample may be detectable in the validation RTqPCR. miRNAs that fall under this would perhaps not validate as the false negative would influence the logistic regression result with more samples in the not expressed binary group than are actually the case.

3.2.5.1 Identification of a reference miRNA for A-o-D RTqPCR

To identify the most robust single control miRNA from the TLDA platform, R script from the normalisation analysis in Section 3.2.2.1 was adapted to normalise data to any miRNA expressed in all 50 samples (n=103). The ΔCt values generated were used to calculate standard deviations across the median values across the 50 BM NB cell profiles. Normfinder, was used to independently generate a list of candidate housekeeping miRNAs, using expression stability within the sample set to rank candidate miRNAs (Andersen *et al.*, 2004). The output contained the list of ranked genes from most suitable reference to least. Standard deviations from both approaches were combined to determine the best overall reference gene.

3.2.5.2 Conversion of RNA to cDNA using RT for analysis with A-o-D primers

miRNAs identified as significantly related to phenotype (migration or self-renewal) were validated using single tube RTqPCR assays. The primer and probe mixes

(Assays-on-Demand™, Thermo Fisher) were the same as those used in the miRNA TLDA. The same RNA extract was used for both the miRNA TLDAs and RTqPCR reactions. miR-30b-5p (assay ID 000602, from Section 3.2.5.1) was used as a reference miRNA and the NB cell line BE(2)C was chosen as a positive reference as reproducible Ct values (standard deviation <0.05 Ct) were produced for each miRNA using 20ng RNA. RTqPCR results were reported as ΔΔCt, calculated in the below equation.

$$\Delta\Delta Ct = \Delta Ct\ sample - \Delta Ct\ positive\ control\ (BE(2)C)$$

miRNAs 618 (assay ID 001593), 186-5p (assay ID 002285), 744-5p (assay ID 002324), let-7c-5p (assay ID 000379), 487a-3p (assay ID 001279), 331-5p (assay ID 002233) and 885-5p (assay ID 002296) were analysed. RT reactions contained 20ng of total RNA (diluted in RNase free water to 5µl), RT mix (components listed in Table 3.2) and 3µl of TaqMan® assay specific RT primer. Each sample was mixed well by pipetting then pulse centrifuged to bring the contents to the bottom of the tube. All samples were then placed on ice for 2 min and transferred to the thermal cycler TC500 and amplified for 1 cycle of 16°C for 30min, 42°C for 30min, 85°C for 5min with final hold at 4°C.

Table 3.2 Components for miRNA A-o-D RT reaction.

All reagents were sourced from Thermo Fisher. Total volume 7.5µl.

Reagent	Volume (µl)	Concentration in tube
MegaPlex RT Primers (10x)	0.8	1.06x
dNTPs with dTTP (100mM)	0.2	2.6mM
MultiScribe RT (50U/µl)	1.5	75U
10X RT Buffer	0.8	1.06x
MgCl$_2$ (25mM)	0.9	3mM
RNase Inhibitor (20U/µl)	0.1	2U
20ng total RNA in RNase free water	3.2	-

3.2.5.3   RTqPCR for expression of miRNAs significantly linked to phenotype

The cDNA (4.8µl) was added to 67.21µl PCR mix; 3.6µl TaqMan® small RNA assay (20X), 36µl TaqMan® universal PCR master mix II (no UNG) and 27.61µl RNase free water. Samples (20µl) were set up in triplicate, transferred to a MicroAmp® fast

optical 96 well reaction plate (Thermo Fisher) and the plate sealed using a MicroAmp® optical adhesive film (Thermo Fisher). The plate was placed on the QuantStudio™ 12K flex real-time PCR system (Thermo Fisher) and the reaction was activated by incubation at 95°C for 10 min then 40 PCR cycles of 15s at 95°C and 60s at 60°C. Results were analysed with a threshold of 0.1 and an automatic baseline using QuantStudio™ 12K software.

3.2.5.4   Optimisation of miRNA single assay RTqPCR

The efficiencies of each of the assay on demand were assessed using serial dilutions of 20, 10, 5 and 1ng of BE(2)C RNA in the RT reaction (Section 3.2.5.2). The results were plotted on a scatter graph, the R square and slope were exported to calculate the efficiency using the below equation. Amplification efficiency percentages over 90% and under 105% were accepted as good.

$$Efficiency\ (\%) = (10^{(-1/slope)})\ x\ 100$$

3.2.5.5   Correlation of miRNA TLDA and A-o-D miRNA expression

Expression of miRNAs from both the miRNA TLDA and A-o-D experiments were both normalised to miR-30b-5p to allow the best comparison of the data. These ΔCt values were plotted against each other using a scatter plot and a line of best fit was generated, the slope and R square for each of these was noted.

3.2.6 HR NB miRNA survival analyses

The expression of miRNAs identified as significantly linked to phenotype as measured by miRNA TLDA and A-o-D were analysed for significance with survival data. miRNA ΔCt values were evaluated using log rank (Mantel-Cox) test and visualised as Kaplan-Meier plots using SPSS. EFS was defined as the time from diagnosis to the time of first event; first event could be relapse or death, with censoring at date last seen for surviving patients. OS was calculated as the time from diagnosis to death, regardless of the number of events that may have occurred, with censoring at date last seen. Patients without EFS or OS follow up data were excluded from the analysis. Where the data was not binary cut offs were determined by analysing each possible threshold; the cut off with the best log-rank chi-square being used. In the case where the miRNA were not expressed (Ct value >35), the ΔCt was

set to 10. This value is representative of a ΔCt that would be generated from a Ct of 35.

3.2.7 Knockdown of miR-618 in NB cell lines

3.2.7.1 Cell lines and tissue culture

NB cell lines were cultured as previously described (Section 2.2.5.1). HEK-293FT cells were kindly donated by Professor Maggie Knowles and maintained in optimum media (Table 2.1). This cell line was chosen as it is fast growing, highly transfectable and produces high viral titres.

3.2.7.2 Production of vector DNA

Plasmids MZIP000-PA-1 (pGreenPuro Scramble Hairpin control) and MZIP618-PA-1 (custom anti-miR sequence targeting hsa-miR-618 cloned into CMV-GFP-T2A-puro-H1-amiR, SI505A-1 vector) were purchased from Cambridge Bioscience Ltd; the plasmids were provided as 1µg plasmid DNA and as transformed bacteria in a stab culture.

3.2.7.2.1 Transformation and expansion of bacteria in packaging and envelope vectors

Packaging and envelope vectors for generation of lentiviral particles, (psPAX2 and pCMV-VSV-G) were kindly donated by Professor Maggie Knowles, Lab 5, UoL, both original sourced from Addgene (Cambridge, Massachusetts, USA). XL-1 blue competent cells (Stratgene, supplied by Thermo Fisher) were thawed slowly on ice, then 50µl was added to a round-bottomed polypropylene tube and 50ng of each vector DNA was added then inverted to mix. The cells were incubated on ice for 20 min then placed in a water bath at 42°C for 45s then back onto ice for 2 min to allow the DNA to enter the bacteria. Each vector mix was added to 150µl Super Optimal broth with Catabolite repression (SOC) media (20g/litre (L) tryptone, 5g/L yeast extract, 4.8g/L magnesium sulphate (MgSO$_4$), 3.6g/L dextrose, 0.5g/L sodium chloride (NaCl), 0.19g/L potassium chloride (KCl), Sigma) then incubated at 37°C with vigorous shaking for 10 min, allowing expression of antibiotic resistance before adding to plate. Transformed bacteria were streaked onto Lysogeny broth (LB) agar plates containing 100µg/ml ampicillin (amp, Sigma) using a sterile inoculation loop.

Plates were inverted and incubated for 16h at 37°C in a dry chamber (Sanyo CO_2 Incubator). For packaging and envelope vectors, 1 stab culture was chosen. The chosen culture for each vector was then added to a further 200ml LB media containing 100µg/ml amp and further incubated with vigorous shaking at 37°C for 16h. The bacteria were harvested by centrifugation at 6,000g for 15 min (Avanti® J-26 XP Centrifuge, Beckman Coulter, Buckinghamshire, UK) and the supernatant removed to obtain bacterial pellets. For both MZIP000-PA-1 and MZIP618-PA-1 vectors 6 single colonies were picked from bacterial streaks (Cambridge Bioscience) using a pipette tip and placed in 5ml LB media containing 100µg/ml amp. Each culture was incubated overnight at 37°C with vigorous shaking (approximately 300rpm, Innova® 4200, New Brunswick Scientific, supplied by Eppendorf UK, Stevenage, UK). Minipreparation (Section 3.2.7.2.2) of each culture was performed to obtain vector for restriction digest to confirm the identity of the vector.

3.2.7.2.2   Minipreparation of DNA

The vector DNA was extracted using the GenElute™ Plasmid Miniprep Kit (Sigma); all buffers are company proprietary. Briefly, the pellet was resuspended in 200µl resuspension buffer and vortexed to mix thoroughly. The solution was then lysed using 200µl of lysis solution, inverted 8 times and incubated for 5 min at room temperature. This reaction was neutralised by adding 350µl of neutralising solution and inverted 6 times, debris was pelleted by centrifugation at 12,000g for 10 min. The clear lysate was then added to a primed GenElute Miniprep binding column, centrifuged at 12,000g for 1 min and the FT discarded. The column was washed by passing 750µl of washing solution through the column by centrifugation at 12,000g for 1 min; the FT was discarded and the column dried by centrifugation at 13,000g for 2 min. The GenElute Miniprep column was transferred to a clean collection tube and DNA was eluted in 100µl RNase free water by centrifugation at 12,000g for 1 min. DNA was quantified using the nanodrop (Section 3.2.1.1.2) and stored in single use aliquots at -80°C until required.

3.2.7.2.3   Restriction digest of DNA vectors

To confirm that the clones contained the correct vector a sample of each vector was digested using restriction enzymes MluI (NEB) and BamHI (NEB) or ClaI (NEB) and

ScaI HF (NEB). DNA was defrosted and 1µg was digested with either; 10U MluI, 20U BamHI in 1X 3.1 buffer (NEB) or 10U ClaI, 20U ScaI HF in 1X cut smart buffer (NEB) in nuclease-free H_2O and incubated for 2h at 37°C. Samples were analysed by agarose gel electrophoresis. Agarose (1% (w/v) Invitrogen) was dissolved in 150ml 1X Tris-Borate EDTA (TBE) buffer (90mM orthoboric acid (Sigma) and 2mM EDTA at pH 8) by heating gently in a microwave. After cooling 30µl of DNA stain Nancy-520 (Sigma) was added to the sample, to stain double stranded DNA, which was mixed and then poured gently into a Horizon™ agarose gel tray (Invitrogen), a comb was inserted to produce sample loading wells. After the gel had solidified samples were loaded, diluted 1:6 in gel loading buffer (0.4mM Ficoll (Type 400; Sigma), 17.3mM SDS, 0.4mM bromophenol blue (Sigma) and 5.6mM orange G (Sigma). A 1 kilobase (kb) DNA ladder (10µl containing bromophenol blue; NEB) was also added to estimate the size of DNA fragments. The gel was electrophoresed at 80V for 90 min. Products were visualised under ultraviolet (UV) light using a trans-illuminator (Bio-Rad Laboratories, Hertfordshire, UK). Using the vector map, the predicted size of fragments following digest with MluI and BamHI was 4618kb and 3307kb for MZIP-618-PA-1 containing the MluI cut site and a linearised band at 7841kb for MZIP-000-PA-1. The digest containing ClaI and ScaI HF should produce bands at ~5100kb and ~2800kb for both vectors. Clones with these fragments were selected for expansion (Section 3.2.7.2.1).

3.2.7.2.4 Maxipreparation of DNA

After confirmation that plasmids contained the correct DNA, they were purified from bacterial pellets using the Plasmid Maxi kit (Qiagen); all buffers are company propriety. The pellet was resuspended in 10ml buffer P1 then 10ml buffer P2 was added to lyse the bacteria. The lysis was stopped after incubation at room temperature for 5 min by adding 10ml of buffer P3 and incubated on ice for 10 min. The sample was centrifuged at 20,000g for 30 min and the supernatant collected; this step was performed twice. The pooled supernatants were added to a primed QIAGEN-tip 500 and allowed to enter the resin by gravity. The QIAGEN-tip was washed twice with 30ml buffer QC. The QIAGEN-tip was placed into a new collection column and the DNA was eluted into 15ml buffer QF. The DNA was then precipitated

by adding 10.5ml isopropanol, mixed thoroughly and centrifuged at 15,000g for 30 min at 4°C. The supernatant was discarded and the pellet was washed in 5ml of 70% ethanol then centrifuged again at 15,000g for 10 min. The supernatant was carefully aspirated and discarded. The pellet was left to air dry for 10 min and DNA dissolved in 100µl RNase free water. The yield of DNA was determined using the nanodrop as described in Section 3.2.1.1.2.

3.2.7.2.5   Generation of lentiviral vectors in HEK293FT cells

Work with lentiviral vectors was conducted in a Class II tissue culture facility designated for virus work. All waste liquids and plastics were decontaminated for 30 min using 10% Virusolve® (Amity International, Barnsley, UK). After lentiviral vector work all gloves, tissues and used plastics were left in the hood for at least 30 min to eliminate any aerosols generated, they were then decontaminated and disposed by autoclaving. To produce lentiviral particles, 1µg of either MZIP-000-PA-1 or MZIP-618-PA-1 vector DNA along with 1µg psPAX2, 200ng pCMV-VSV-G were added to 750µl Opti-MEM™ reduced serum media (Thermo Fisher) and mixed gently by pipetting in a polypropylene tube. To each mix 8µl of transfection reagent TransIT-293 (Mirus Bio, Wisconsin, USA) was added and mixed gently by pipetting then incubated at room temperature for 30 min. The mix was added dropwise to a T25 flask of HEK-293FT cells, at 50% confluency, and the flask rocked gently to evenly distribute the mix across the cells. Cells were incubated at 37°C in a virus designated humidified chamber with 5% CO_2 in air. After 16h virus containing media was aspirated from cells and replaced with 5ml fresh media and incubated for a further 24h. Media was collected and replaced, incubated for a further 24h and collected again and pooled, at 48h the virus titre is highest. Pooled media was passed through a 0.45 micron (µm) filter to remove any dead cells or large vesicles, aliquoted and stored at -80°C.

3.2.7.2.6   Infecting target cell lines with lentiviral vectors

Cells were seeded into T25 flask to be at 50% confluency the following day, 3 flasks (control, MZIP-000 and MZIP-618) for each cell line (BE(2)C, SK-N-SH and Kelly) were seeded. The following day media was replaced with 2ml viral supernatant diluted in 2ml growth media containing 1µg/ml hexadimethrine bromide (Polybrene®, Sigma)

to enhance transduction (Davis *et al.*, 2002). Cells were incubated at 37°C in a virus designated humidified chamber with 5% CO_2 in air for 6h then virus mix was removed and replaced with 5ml media. After 48h cells containing the vector were selected by replacing media with media containing puromycin (0.8µg/ml BE(2)C and SK-N-SH, 0.25µg/ml Kelly). Cells containing the vector would be resistant to puromycin as the resistance gene is present in the construct. Infected cells were maintained in puromycin containing media until the no virus control cells had all died. Cells were maintained in Class II conditions for 2 passages or 10 days after infection, after this time no lentiviral particles were present as confirmed by enzyme-linked immunosorbent assay (ELIZA) for human immunodeficiency virus (HIV) retroviral RT activity in the cell media (Roche, Sigma). The absorbance of samples is directly correlated to the level of RT present, the absorbance of samples was not above that of the negative control.

3.2.7.2.7 Measuring GFP expression in cells by flow cytometry

After puromycin selection cells were trypsinised (Section 2.2.5.1) centrifuged at 405g for 5 min, resuspended in 1X PBS then pelleted again by centrifugation at 405g for 5 min and finally resuspended in 1ml flow cytometry buffer (0.5% BSA, 2mM EDTA in PBS). Green fluorescent protein (GFP) expression was analysed by flow cytometry (Attune®, Thermo Fisher) using an excitation laser of 480 nanometre (nm). A total of 10,000 events were measured for each sample. The GFP expression was compared to control cells which had not been infected with a lentiviral GFP plasmid, median GFP fluorescence and percentage of cells expressing GFP were determined using Attune® cytometric software 1.2 (Thermo Fisher).

3.3   Results

3.3.1   Quality assessment and quantification of total and small RNA

RNA was extracted from 60 pellets of NB BM cells. From these 52 samples yielded sufficient RNA for miRNA profiling by miRNA TLDA. In the remaining 8 cases RNA was concentrated; 2/8 were suitable for miRNA TLDA. Additional samples were available for 2 of the remaining 6 samples, although on re-extraction the concentration of RNA remained insufficient. In total 54 samples were suitable for analysis on the miRNA TLDA. The concentration of total RNA from NB BM cells that were analysed by miRNA TLDA were all greater than 125 ng/µl (range 125-763 ng/µl). Variations in RNA reflect different cell number in the pellet and differing RNA content of cells.

All total RNA extracted from NB BM cells had a RIN greater than 9 (range 9-10) indicative of good quality RNA with little degradation. To avoid further degradation RNA was kept on ice and stored frozen at -80˚C in single use aliquots to prevent degradation through multiple freeze thaw cycles. Small RNA was quantified for miRNA content, total RNA extracts had concentrations of small RNA ranging from 6.6-4592.7 picogram (pg)/µl with the percentage of miRNA (of small RNAs) ranging from 5-32%.

3.3.2   50 HR NB miRNA TLDA profiles showed good data

Fifty of the miRNA profiles generated BM NB cells passed quality control (Figure 3.2). From the 54 profiles 2 failed, no amplification curves seen, and were not included in the subsequent analyses.

3.3.3   Optimal normalisation method for miRNA TLDA data is the global mean

Normalisation is crucial to reduce experimental variation allowing the differentiation of true biological changes. In these data we used an automatic baseline which is calculated across the cycles where only noise is detected, normally cycles 3-15. A manually set threshold of 0.2, was chosen for its position as all curves were in exponential phase and parallel to one another.

The optimal method of normalisation was reporting data using the global mean which had a standard deviation of 0.15. In addition to this evidence the global mean is reported to be powerful and robust (insensitive to outliers), leading to improved identification of differentially expressed genes (Mestdagh *et al.*, 2009).

A low standard deviation across normalised miRNA profile median ΔCt values is indicative of low dispersion. It must be noted that the standard deviation can be affected by outliers and therefore visualisation of the data as box plots to complement the evaluation of a normalisation method was used.

The 50 HR NB samples were analysed for best normalisation method. When normalised to U6, a snoRNA against which miRNAs are commonly reported in literature, the variation of the data was increased (standard deviation = 1.08), this can be visualised in Figure 3.3. Again, an increase in variation across samples was seen, to a lesser degree, when snoRNAs U44 and U48 were used for normalisation; standard deviation of 0.41 and 0.67 respectively. Another justification for not using U6, U44 or U48 is there is no correlation between miRNA concentration and mRNA concentration. The global mean was again the most suitable reference gene when either independent NB or other cancer profiles were studied.

The normalisation methods were validated in 4 independent data sets received from the Giannina Gaslini Institute, using 12 BM NB cells and 12 NB tumour samples, both analysed using miRNA TLDA card A and miRNA TLDA card B. In these studies the global mean was again determined as optimal in BM NB samples (standard deviation = 0.18 (card A) and 0.3 (card B)) and when evaluated in 12 tumour profiles (standard deviation = 0.2 (card A) and 0.23 (card B), data not shown). U6 produced a smaller standard deviation in the cohort of tumour profiles, with the standard deviation across ΔCt medians at 0.6 for card A and 0.54 for card B; this shows that U6 is a suitable reference in some cases, perhaps more suited to specific sample sets. The proposed miRNA set from Mestdagh *et al.*, 2009 was tested; when miR-191 and miR-103 were averaged and used to normalise the standard deviation was 0.67, less optimal than the global mean. However the global mean remains superior when using the miRNA TLDA across all sample sets.
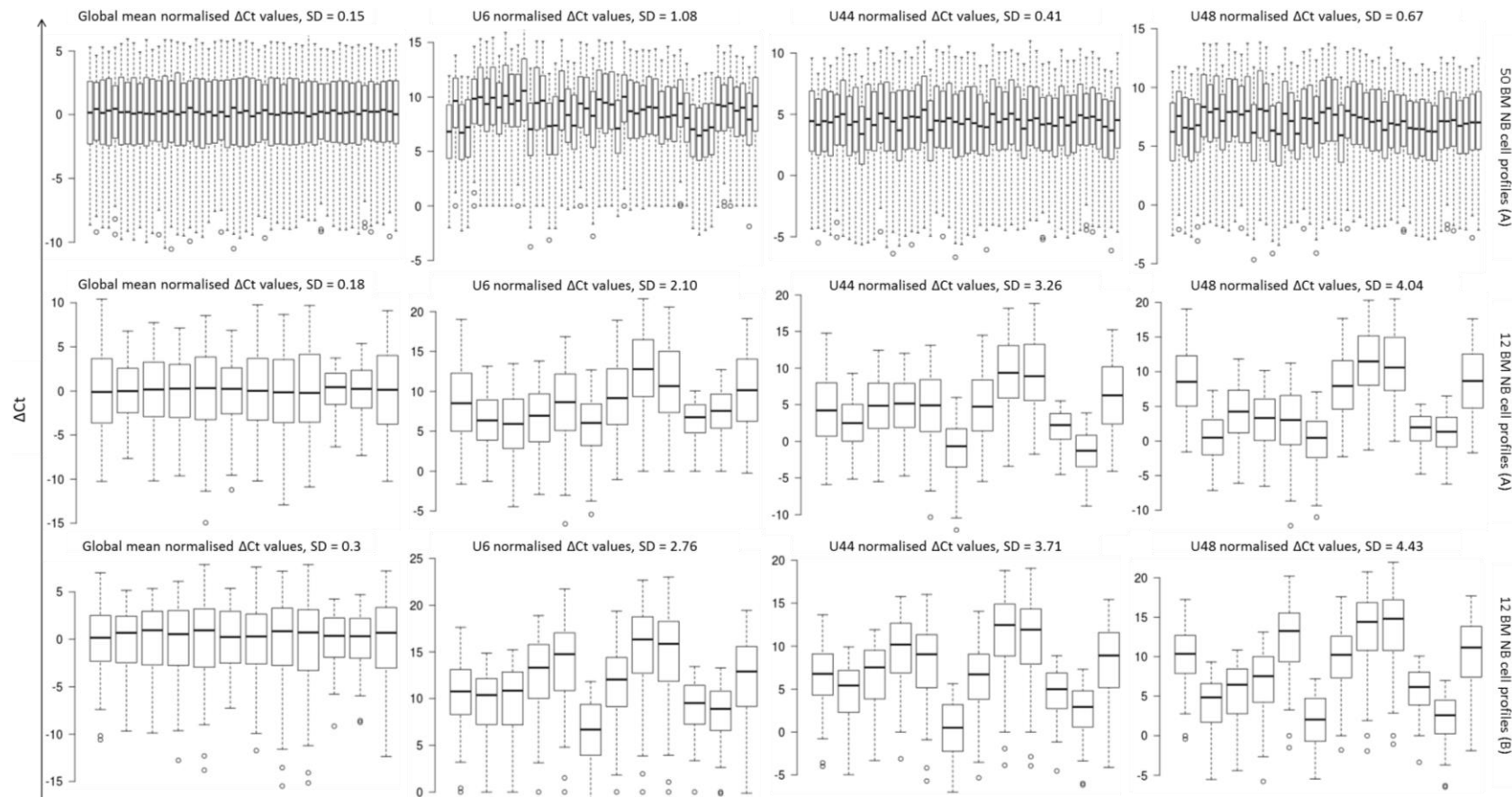
Figure 3.3 Data visualisation for optimising normalisation using 50 HR NB cell miRNA profiles. SD = standard deviation across median ΔCt values in the samples. Centre lines show the medians; box limits indicate the 25th and 75th percentiles; whiskers extend 1.5 times the interquartile range from the 25th and 75th percentiles, outliers are represented by dots. ΔCt for 50 BM NB and validation miRNA profiles after normalisation using U6, U44, U48 or the global mean. (B) denotes the data which was generated by analysis using miRNA TLDA card B.

3.3.4 miR-30b-5p was the optimal miRNA to be used as a reference gene

miRNAs expressed (Ct values <35) in all 50 samples n=106 were evaluated using both Normfinder and my R code to evaluate potential reference miRNAs. The standard deviations from both analyses were combined and ranked on stability (lowest to highest combined standard deviation). The top 4 results from both analyses are shown in Table 3.3. miR-30b-5p had the lowest overall standard deviation and was used as the reference gene for the A-o-D RTqPCR for validation.

Table 3.3 Results from R code and Normfinder to assess best reference miRNA.

Standard deviation (SD) represents the variance across miRNA TLDA profiles after normalisation to the reference miRNA. Normfinder is a publicly available code to determine the best reference gene.

miRNA	R code SD	Normfinder SD	combined SD
hsa-miR-374a-5p	0.39	0.40	0.395
hsa-miR-30c-5p	0.40	0.39	0.395
hsa-miR-30b-5p	0.42	0.29	0.355
hsa-miR-134-5p	0.47	0.51	0.490

3.3.5 miRNA expression profiles of BM NB cells show clustering into distinct groups both in heatmap and PCA

The NB cell profiles had an average expression of 164/377 miRNAs (range 134-187). Differential clustering of BM NB samples showed specific cluster groups (Figure 3.4), highlighting the heterogeneity of miRNA profiles within the population. PCA analysis again showed the distinct clusters within profiles. The most noticeable cluster that is separated in both visualisations is the group of 4 samples, in the heatmap the first cluster on the left, and on the PCA plot the bottom right cluster, these are the same 4 samples, further clinical investigation may explain the isolation of these, but from these analysis they are not clustering on the tumour stage or MYCN status.
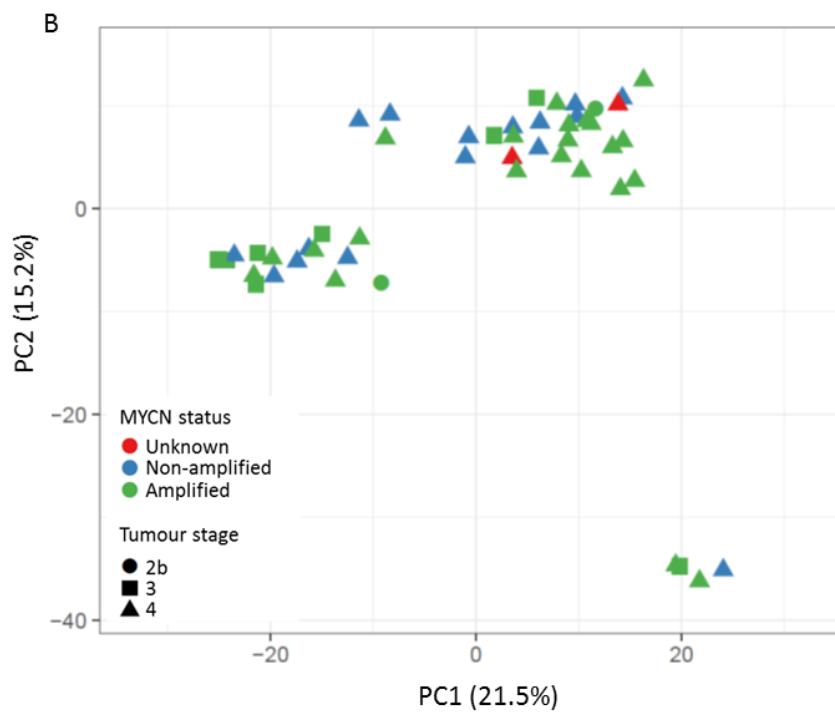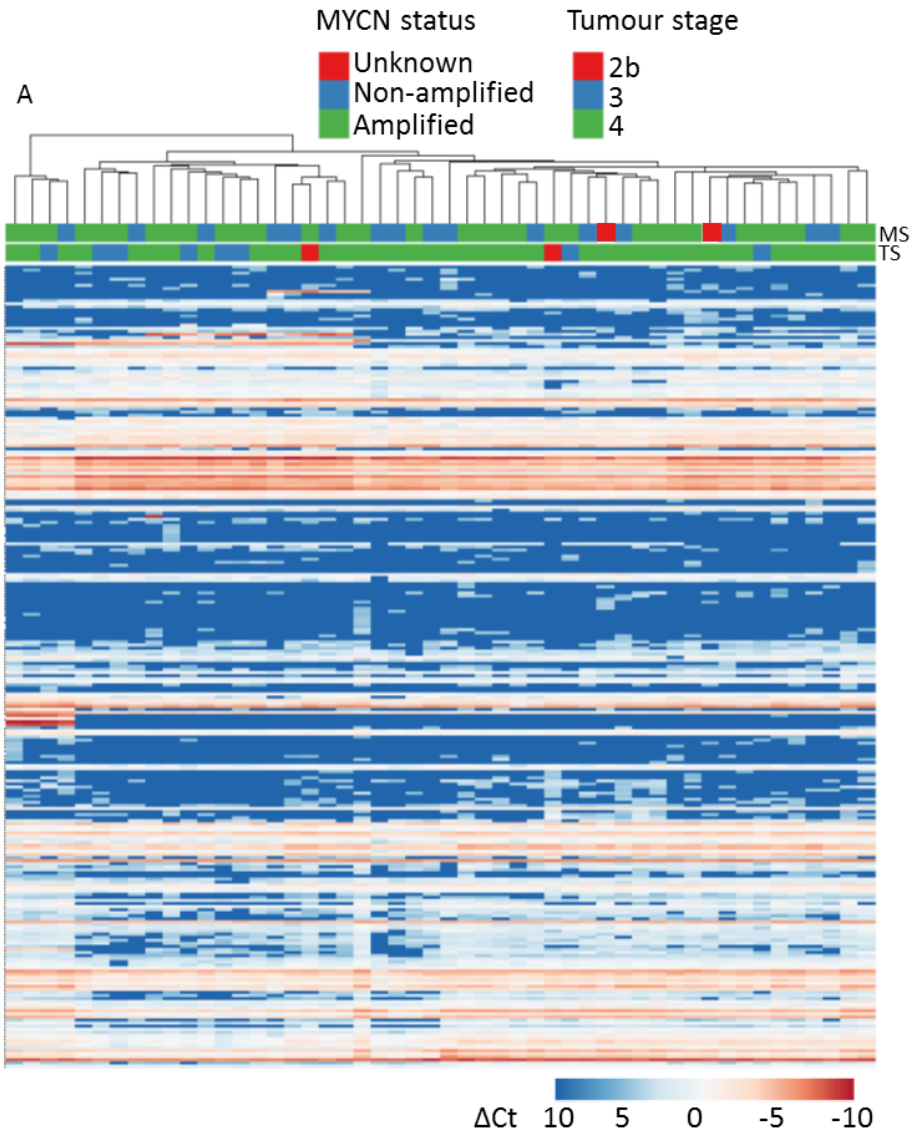
Figure 3.4 Data visualisation of 50 HR NB cell miRNA profiles.

The heatmap and PCA plots were generated using ΔCt values normalised to the global mean in ClustVis. For both the MYCN status (MS) is shown; red = unknown, blue = non-amplified, green = amplified. A, blue shows low expression of miRNA and red shows high expression. Samples are on the horizontal axis and miRNAs on the vertical. Both rows and columns were clustered hierarchically. Similarity metrics used were Euclidean distance for miRNAs and correlation for samples, all clustered with complete linkage. The heatmap depicts the tumour stage (TS) as red = stage 2b, blue = stage 3 and green = stage 4. B, PC1 explains 21.5% of the variance and PC2 15.2%. Each point on the PCA plot represents a HR NB cell sample. Tumour stage on the PCA plot is represented by shape; circle = stage 2b, square = stage 3, triangle = stage 4.

3.3.5.1   Identification of the most highly and consistently expressed miRNAs

After removal of snoRNAs (U6, U44 and U48) 103 miRNAs were expressed in every sample. The ΔCt values of these miRNAs were ranked to assess expression levels; the average and standard deviation of ΔCt values for each of these miRNA was calculated and these values were ranked, with the smallest ΔCt (highest expression) and standard deviation (low variance) prioritised, yielding the most highly consistently expressed miRNAs at the top. Pathway analysis then took the top 10% (n=10) of these miRNAs. Average ΔCt and standard deviation of these miRNAs are listed in Table 3.4.

Table 3.4 Top 10% miRNAs most consistently and highly expressed in NB BM cells.

ΔCt values are reported to the global mean.

miRNA	Average ΔCt	ΔCt SD
miR-222-3p	-8.04	0.82
miR-24-3p	-7.23	0.68
miR-29a-3p	-6.53	0.52
miR-31-5p	-6.27	0.58
miR-145-5p	-5.99	0.84
miR-16-5p	-5.86	0.79
miR-100-5p	-5.51	0.67
miR-138-5p	-5.27	0.94
miR-574-3p	-5.14	0.58
miR-99a-5p	-4.99	0.56

3.3.5.2 Pathways identified by most highly consistently expressed miRNA lists

In total 71 pathways were enriched with a Benjamini-Hochberg adjusted p-value less than 0.05. Exported results gave the number of miRNAs involved in each pathway and the number of downstream target genes these miRNAs regulated involved in each pathway, alongside the enrichment p-value. Pathways were ranked with the highest number of genes at the top, Table 3.5 lists the top 10 pathways ranked on gene involvement.

Table 3.5 Top 10 enriched pathways in NB BM cells.

> The pathways were ranked on gene involvement; p-values are Bonferroni adjusted. MAPK represents mitogen-activated protein kinase.

KEGG pathway	p-value	Number of genes involved	Number of miRNAs involved
Pathways in cancer	2.7×10^{-9}	249	10
PI3K signalling pathway	0.0001	194	10
Proteoglycans in cancer	1×10^{-19}	145	10
MAPK signalling pathway	0.04	142	10
Viral carcinogenesis	3×10^{-7}	140	10
Focal adhesion	7×10^{-5}	134	10
Endocytosis	0.002	133	10
miRNAs in cancer	2×10^{-8}	131	10
Epstein-Barr virus infection	0.004	124	10
Protein processing in endoplasmic reticulum	4×10^{-10}	124	10

The most significant pathway was pathways in cancer which involves multiple cellular pathways including the PI3K pathway which was also enriched; with the second highest gene number involvement. The PI3K was chosen to take forward for downstream inhibitor studies to provide a proof of principle of this approach to

identifying biologically relevant pathways. The PI3K pathway was chosen as it was the highest singular pathway but also due to prior knowledge of its described importance in NB. A further advantage of using the PI3K in further studies was the putative inhibitors available commercially.

3.3.6 Proof of principle; PI3K pathway is enriched in BM NB cells and therefore important to cell survival

The PI3K pathway is aberrant in many cancers and inhibition of the pathway is currently under test in a clinical trial (NCT02337309) for refractory NB. The trial includes treatment with the inhibitor LY294002. Doxorubicin is a cytotoxic drug that is used in the treatment of many cancers. Treatment of BM NB cells with PI3K inhibitors alone (Figure 3.5) or in combination with doxorubicin (Figure 3.6) reduced cell viability. In all treatments the primary cultures showed less cell death than the cell line SH-SY5Y, with no additive killing effect seen in combination therapies. Concentrations of both inhibitors used were within the clinical range, under the concentration known to elicit off target effects.
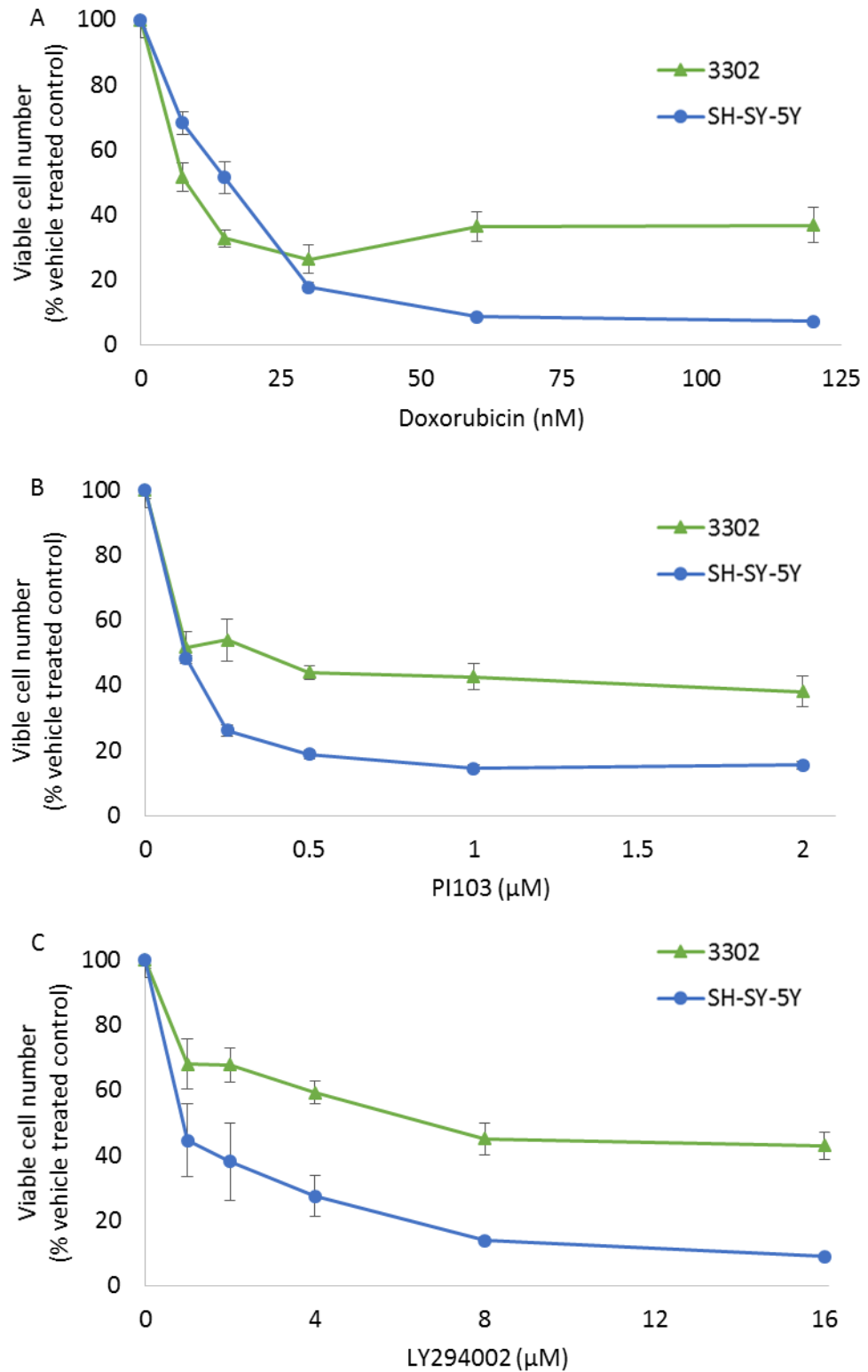
Figure 3.5 Effect of PI3K inhibition on NB viable cell number.

NB cells were treated with increasing concentrations of A, cytotoxic drug doxorubicin or PI3K inhibitor B, PI103 or C, LY294002. Viable cell number determined by trypan blue exclusion assay using automated vi-cell, expressed as a mean percentage of vehicle treated control (±SEM, n=9). 3302 is a primary HR NB culture and SH-SY5Y a NB cell line.
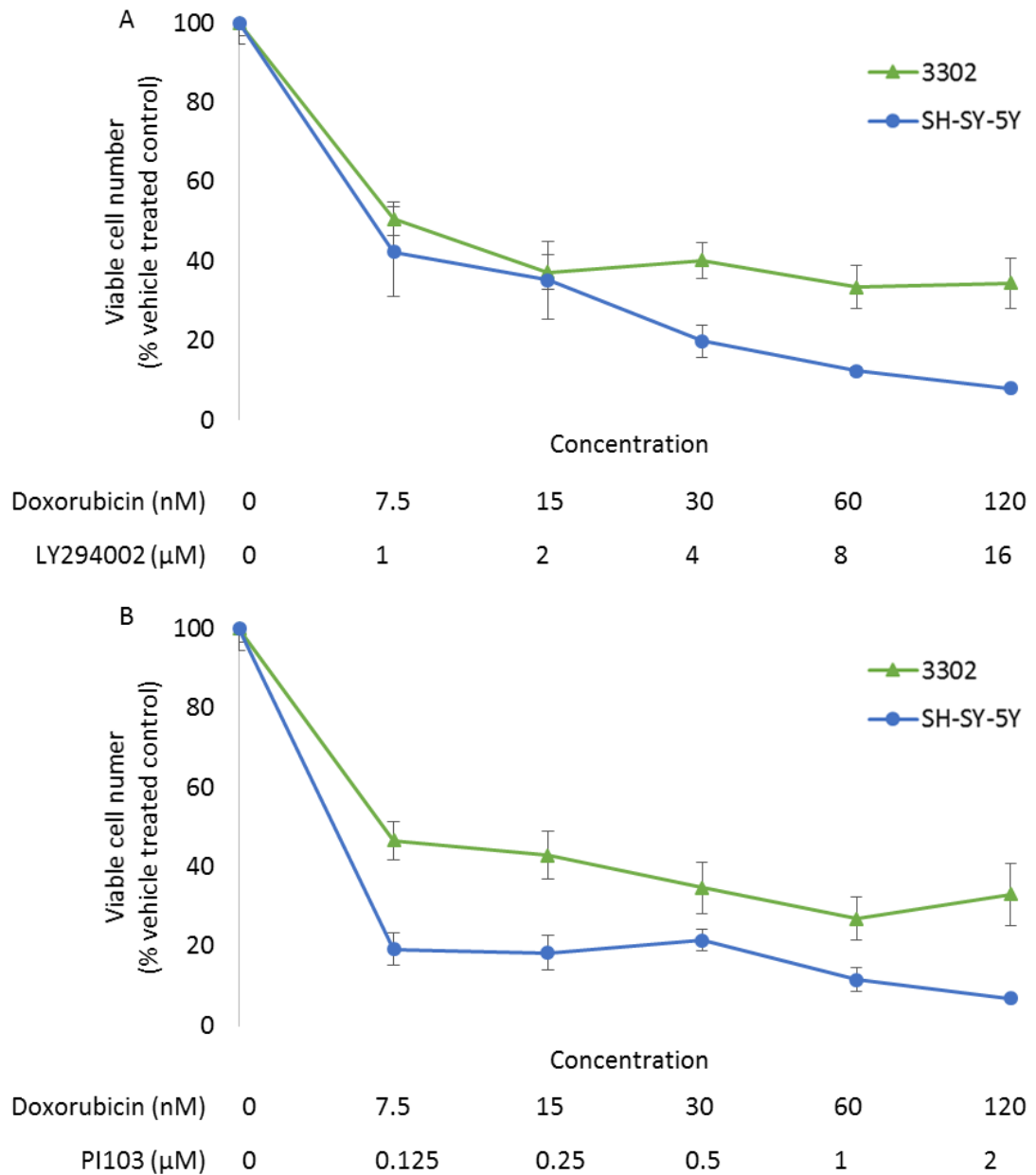
Figure 3.6 Effect of PI3K in combination with doxorubicin on NB viable cell number.

NB cells were treated with increasing concentrations of doxorubicin and PI3K inhibitor A LY294002 or B, PI103. Viable cell number determined by trypan blue exclusion assay using automated vi-cell, expressed as a mean percentage of vehicle treated control (±SEM, n=9). 3302 is a primary HR NB culture and SH-SY5Y a NB cell line4.

3.3.7 Correlation of miRNAs with migration and self-renewing ability

Logistic regression identified expression of 1 miRNA related to colony formation. Linear regression identified significant correlations between migration and 3 miRNAs; colony formation and 5 miRNAs; low adherence and 1 miRNA, listed in Table 3.6.

Table 3.6 Nine statistically significant miRNAs related to NB cell phenotype.
Phenotypes analysed were migration or self-renewal, either colony formation (CF) or low adherence (LA). * denotes the only miRNA identified as significant using logistic regression. Adjusted p-value threshold of 0.05. Global mean was used for normalisation of miRNA expression.

miRNA	Phenotype	Adjusted p-value	Number of samples in which miRNA expressed	Correlation of high miRNA expression with low or high phenotype
miR-885-5p	Self-renewal (LA)	0.05	11	High
miR-618	Self-renewal (CF)	0.0001	31	High
miR-186-5p	Self-renewal (CF)	0.002	50	High
miR-744-5p	Self-renewal (CF)	0.002	50	Low
let-7c-5p	Self-renewal (CF)	0.01	48	Low
*miR-331-5p	Self-renewal (CF)	0.02	21	High
miR-523-3p	Migration	0.005	4	High
miR-487a-3p	Migration	0.02	14	High
miR-518f-3p	Migration	0.05	5	High

To ensure miRNAs that were verging on significance with multiple phenotypes were not missed these 9 miRNAs were combined with any miRNAs present in the top 10 (when ranked on significance) of multiple analyses regardless of p-value. Additional

miRNAs identified by this analysis were miR-500a-5p, miR-888-5p, miR-139-5p and miR-518b. In total this gave 14 candidate miRNAs that were then assessed to create a more robust list of miRNAs for downstream validation. Firstly miRNAs that were not expressed in 10% of the HR NB samples were removed. The resulting 10 miRNAs were then plotted to visualise correlation against significant phenotype and ΔCt distribution was visualised as histograms (data not shown). After these steps 7 miRNAs; miR-618, miR-186-5p, miR-744-5p, let-7c-5p, miR-487a-3p, miR-331-5p and miR-888-5p were taken forward for statistical and biological validation.

3.3.7.1   RTqPCR did not validate miRNA TLDA expression

All A-o-D primer and probe sets optimised well with efficiencies within the accepted range of 90-105% (Table 3.7).

Table 3.7 Efficiency of A-o-D primer and probe sets.

Efficiencies of each A-o-D primer and probe set were evaluated. Good % efficiencies are between 90-105%

miRNA	R square	Slope	Efficiency	% Efficiency
miR-331-5p	0.75	-3.2	2.0	105
miR-885-5p	0.95	-3.5	1.9	91
let-7c-5p	0.97	-3.1	2.0	105
miR-186-5p	0.97	-3.5	1.9	92
miR-618	0.99	-3.5	1.9	94
miR-487a-3p	0.97	-3.4	2.0	95
miR-744-5p	0.98	-3.3	2.0	101
miR-30b-5p	0.96	-3.4	2.0	98

The ΔCt values normalised to miR-30b-5p for both miRNA TLDA and A-o-D RTqPCR were correlated, R square values were all under 0.4 representing no correlation. For some of these miRNAs this may be reasoned as the expression range was low (miR-331; Ct range 2.4, miR-744; Ct range 2.1) or due to a low level of samples expressing the miRNA (miR-487a; n=14 and miR-885; n=5) or due to the low level of expression (miR-885; minimum Ct 32.8 and let-7c; minimum Ct 30.2). However, miR-618 and miR-186 were not explained by this reasoning.

3.3.7.2   Correlation of miRNA expression measured using A-o-D RTqPCR with phenotype and survival

A significant correlation was validated between miR-618 and colony forming efficiency (p=0.009) when expression was assessed using A-o-D RTqPCR. The correlation was contradictory to that seen when analysing the miRNA TLDA expression. For A-o-D data, the lower the expression of miR-618 the greater the colony forming efficiency of the cells.

miR-618 expression was predictive of EFS (p=0.03, Figure 3.7). None of the other miRNAs assessed using A-o-D were predictive. Results from Section 3.2.4 showed colony forming efficiency to also predict EFS, of the 50 patients whose samples were analysed by miRNA TLDA 20 of these had a colony forming efficiency of >1.5 (predictive of survival); of these 95% (19/20) were also classified in the low miR-618 expressing group (predictive of survival). By reducing the levels of miR-618 within NB cells it may be hypothesised this would lead to increased survival and increased colony forming efficiency.
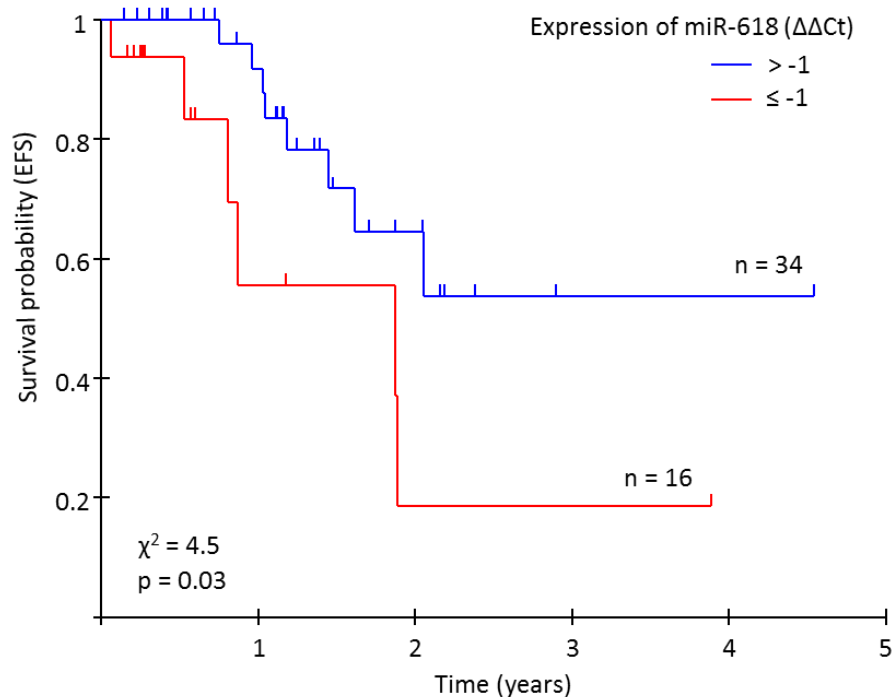
Figure 3.7 Survival vs miR-618 expression in BM NB cells.

Kaplan-Meier survival curve of EFS in relation to the expression of miR-618 in BM NB cells. Red line = $\Delta\Delta$Ct of miR-618 equal to or less than -1, blue line = $\Delta\Delta$Ct of miR-618 greater than -1, n = number of samples analysed.

3.3.7.3 Infection of NB cell lines with lentiviral miR-618 inhibitor plasmid

The lentiviral plasmid containing the miR-618 inhibitor and scramble inhibitor was used to create cell lines with lower miR-618 expression. Unfortunately there was low level increase in GFP positivity when compared with the no virus control, Table 3.8.

Table 3.8 GFP positivity of NB cell lines after infection with GFP lentiviral vector.

The type of vector used for infection is denoted by either -618 for the MZIP-618-PA-1 vector and -000 to denote the MZIP-000-PA-1 vector. No virus control results are also noted.

Cell line	GFP positive (%)	Median BLA-1 of GFP positive cells
Kelly no virus control	3	2173
Kelly-618	3.5	2128
Kelly-000	17	2644
SK-N-SH no virus control	1.5	2757
SK-N-SH-618	21	4112
SK-N-SH-000	10	5381
BE(2)C no virus control	2.6	2765
BE(2)C-618	7.8	4038
BE(2)C-000	3	2819

Due to low infection rates the cells were not representative of a true miR-618 knockdown and therefore no further downstream studies were done.

3.4 Discussion

From the analyses performed in this chapter miR-618 was identified as a miRNA of interest and PI3K a pathway of interest for NB cells isolated from the BM. miR-618 was correlated to self-renewing phenotype. The approach to identify key miRNAs was reasonable and justified by functional validation as PI3K inhibitors caused cell death in NB cells. The investigations identifying miR-618 highlight the importance of experimental validation of findings.

The PI3K pathway has been explored as a therapeutic target in NB and has been targeted in NB cells in other studies (Fulda, 2009). Cell death was seen when NB cells were treated with PI3K inhibitors *in vivo* agreeing with results seen in these studies (Opel *et al.*, 2007, Segerström *et al.*, 2011). The PI3K is activated by ALK mutations; of this gene and increased expression have been linked to poor prognosis in NB, occurring in 9% and 3% of sporadic NB respectively (Pugh *et al.*, 2013). Unfortunately, ALK status of the patients was not available so this could not be interrogated further.

In the literature miR-618 is reported to inhibit anaplastic thyroid cancer (Cheng *et al.*, 2014); genetic variants increase risk of chronic lymphocytic leukaemia (CLL) (Martín-Guerrero *et al.*, 2016); has been implicated in lymphomagenesis (Fu *et al.*, 2014); inhibits migration and invasion in prostate cancer (Song *et al.*, 2017); increases proliferation in HeLa cells (Whitfill, 2014); and modulates growth via PI3K pathway (Yi and Yuan, 2015). The last observation is interesting as this links both miR-618 and the PI3K pathway, 2 targets identified in these studies through different statistical approaches.

In the literature there are many papers which have investigated a similar hypothesis to determine miRNAs that are integral in the self-renewing phenotype of cancer cells. Self-renewal is a key aggressive phenotype of NB but at present there are no direct investigations between NB self-renewal and miRNA. Over 476 papers have been published linking miRNA to self-renewal in humans. In bladder cancer miR-139-5p can inhibit proliferation (Luo *et al.*, 2017), in hepatocellular carcinoma let-7 down

regulates self-renewal (Jin *et al.*, 2016) and in glioblastoma miR-101 can inhibit proliferation as well as migration and invasion (Liu *et al.*, 2017).

There have been several studies into the role miRNAs play in NB cell migration, although none in NB or using the same migration assay as utilised in this chapter. miR-15a is reported to have oncogenic properties in upregulating migration through enhanced metalloprotease expression, whereas several other papers identified miRNAs that dampen the migratory ability of NB cells (Lynch *et al.*, 2012, Xin *et al.*, 2013, Wu *et al.*, 2015). Whilst miR-15a is on the miRNA TLDA and expression was detected in BM NB cells it was not identified as significantly correlating to a phenotype.

In addition to miR-618 several other miRNAs were identified, namely; miR-186-5p, miR-744-5p, let-7c-5p, miR-487a-3p miR-331-5p and miR-885-5p. None of these are reported in studies on NB; except miR-744-5p which is mentioned for its presence in NB tumour samples (Megiorni *et al.*, 2017). Furthermore, there were no reports of miR-487a-3p within cancer. miR-186-5p has been studied in other cancers including colorectal, colon and prostate. In both colon and prostate cancer high levels of miR-186-5p has been linked with increased proliferation, validated by knock down studies reducing the phenotype(Islam *et al.*, 2017, Jones *et al.*, 2018). In contrast to these agreeable findings, in colorectal cancer the inverse was seen (Li *et al.*, 2018). miR-744-5p is reported amongst a panel of 6 miRNAs with diagnostic and prognostic significance in prostate cancer (Miyamae *et al.*, 2015), high levels are described in ovarian cancer to predict improved outcome with *in vitro* high levels increasing apoptosis (Kleemann *et al.*, 2018). Interestingly let-7c-5p overexpression in breast cancer cells inhibited cell proliferation, concurring with the relationship seen in these studies (Fu *et al.*, 2017). Within the literature miR-885 has been linked with NB also, concurring the initial results from the miRNA TLDA. miR-331-5p was not reported in relation to self-renewal or migration but correlated inversely to drug resistance in leukaemia, with relapse showing a marked decrease (Feng *et al.*, 2011). The relationship between relapse and diagnostic miRNA profiles was not explored in this chapter, due to low sample number. miR-885 has also been shown to upregulate metastasis in liver cancer with over expression increasing migration invasion and

development *in vivo* and shown potential as a biomarker for liver cancer in serum samples. In NB high expression was linked to reduced proliferation, increasing p53 through reduced *Cyclin-dependent kinase 2* (CDK2) and MCM5, the reverse correlation than observed in these studies. The range of concurring and contradicting correlations of the identified miRNAs and phenotypes may be due to the large range of downstream genes attributed to each miRNA. In one cancer, one microenvironment or even one patient a miRNA may have different biological effects to another. These varied results highlight the need for full functional validation and understanding of any candidate miRNAs.

Other studies have examined the relationship between miRNAs and other NB aggressive phenotypes, including invasion, proliferation and angiogenesis, these phenotypes were not directly studied in this chapter. However, identifying a miRNA through investigations into one phenotype may highlight other, non-hypothesised tumour suppressive benefits.

A similar study analysing miRNA expression in BM disease compared the profiles to that of primary tumour and identified 160 miRNAs that were differentially expressed. Further analysis to infer biological significance highlighted miR-659-3p as a candidate for further studies (Stigliani *et al.*, 2015). This type of comparison was not possible in this chapter as tumour sample was not available for the patients. However it is interesting that the aforementioned study validated the reduced levels of miR-659-3p in metastatic cells and determined they lead to increasing CCR4-NOT transcription complex subunit 1 (*CNOT1)* which decreases expression of genes containing AU rich element sequences. Further experimental validation of the changes in gene expression and pathway analysis highlighted the focal adhesion pathway. These approaches of miRNA screening followed by biological validation can ultimately lead to potential targetable pathways or specific miRNAs to direct development of novel therapeutics, as in the focal adhesion pathway example mimetics of miR-659-3p may lead to reinstated regulation of *CNOT1* or focal adhesion pathway inhibitors could prevent the downstream phenotypic changes. In this chapter pathway analysis was explored to interrogate the interpretation of data from the miRNA TLDAs, ensuring it was biologically relevant. In a clinical setting the

multiple downstream targets of a single miRNA carries the potential of severe adverse side effects. Conversely it may enhance the potency of miRNA drugs, as many downstream targets may reside within the same oncogenic pathway. It could also limit the number of drugs needed as several targets could be effected, with targeting by one drug potentially reducing toxicity.

Analysis of the miRNA TLDA data from the NB BM primary cells showed great heterogeneity, forming several clusters within visual analyses. These were not explained by MYCN status or stage of the tumour but could be by other genetic landscape features of the cancers. Although miRNAs profiles in this study did not correlate to MYCN status dysregulation of miRNAs within NB has been linked to aberrant expression of genes, specifically *MYCN*. Around 22% of NBs have amplified *MYCN* and this has been linked to the upregulation of several oncogenic miRNAs (Schulte *et al.*, 2008, Domingo-Fernandez *et al.*, 2013). Heterogeneity across NB miRNA profiles is not all explained by the *MYCN* status of tumours. Differential expression within HR NB has been used to group patients into relevant prognostic sub populations, unlike above studies, using miRNAs independent of *MYCN* status (De Preter *et al.*, 2010, Bienertova-Vasku *et al.*, 2013).

There are several published papers in which miRNAs are profiled in NB tumour (Bienertova-Vasku *et al.*, 2013, Althoff *et al.*, 2015, Beckers *et al.*, 2015). These profiles show great heterogeneity, as was seen within the tumour and BM NB profiles kindly shared by Maria Corrias (Giannina Gaslini Institute, Italy) and the BM NB samples profiled in this chapter. Cluster analysis including additional BM NB profiles showed the Italian samples grouped into a separate arm of the cluster, upon further investigation experimental differences were established. Once NB cells are isolated from the BM in Leeds these cells are cultured on plastic for several passages, whereas in Italy RNA was extracted from the cells at separation. It is documented that culturing on plastic changes expression profiles of primary cells and could explain the clustering pattern (Januszyk *et al.*, 2015).

The normalisation method was one of several challenges faced when using the miRNA TLDAs to generate miRNA profiles. Across the BM NB and tumour profiles the best normalisation method was the global mean, this finding is reported in several

publications (Mestdagh *et al.*, 2009, Viprey *et al.*, 2012, Bockmeyer *et al.*, 2016). Across published datasets there is no standard to which data is analysed, normalised or reported. Worryingly when U6, a snoRNA, was evaluated as a reference gene a large amount of experimental noise was added to the data. The use of U6 as a reference is common in published data sets as it is a recommended reference gene by Thermo Fisher. Upon further investigation U6 did not perform as badly in the cohort of tumour profiles, with the standard deviation across ΔCt medians at 0.6 compared with the global mean of 0.2, both an improvement on the non-normalised value of 0.86, this shows that perhaps U6 is a suitable reference in some cases, although the global mean is superior when using the miRNA TLDA. These results also highlight how reference genes may be sample specific.

The miRNA TLDA can be performed with starting material of 100ng RNA. Lesser starting amounts require a pre-amp step which adds variables and the potential introduction of amplification bias (Chen *et al.*, 2009). As the platform was already in use on the SIOPEN clinical trial the experimental procedure was standardised to allow analysis between groups. As is most common in current practice, the standard operating procedure for the trial loaded a fixed amount of RNA (400ng) of each sample to assess miRNA expression. As there is no relationship between the concentration of miRNA and RNA it would be hypothesised that loading a set amount of miRNA would be more informative. However, it is important to keep in mind that loading with miRNA presents more challenges, as measuring miRNA concentrations proves difficult and costly, and the use of good normalisation strategies will account for some variation in loading.

There are several ways in which to analyse the expression of miRNAs in samples. These include the miRNA TLDA or A-o-D RTqPCR, microarrays, NanoString technology and sequencing; each having their own pitfalls and benefits. Microarrays allow screening of a large number of miRNAs but lack sensitivity and specificity. Sequencing however is highly sensitive and allows detection of novel miRNAs from little starting material. Unfortunately sequencing is costly and is less user friendly as analysis requires specialist bioinformaticians. The NanoString uses barcode technology to multiplex the measurement of multiple miRNAs. High sensitivity and

the high-throughput abilities are advantages of the NanoString but high expressing gene signals may dwarf lower ones and optimisation is required for each tissue of interest. RTqPCR high-throughput assays are available for screening of miRNA profiles, with 384 assays on one miRNA TLDA, with high sensitivity, specificity and a large dynamic range. The aims of this study were to identify miRNAs that are linked to aggressive oncogenic phenotypes, to allow downstream identification of pathways to which these miRNAs are integral, or inhibitors to target these miRNAs. For this purpose it was beneficial to identify the expression levels of miRNAs with annotated functions and target mRNAs, allowing streamlining of biological analysis and generation of validation experiments.

In summary, the pipeline to identify miRNAs and pathways of interest is solid, however these studies have highlighted the need for good normalisation and experimental validation. Expression of these highlighted miRNAs and other miRNAs in a circulating setting of NB will be explored next.

Chapter 4   Predictive power of miRNAs in the BM and PB

4.1   Introduction

The functional importance of miRNAs has been explored in the previous chapter, through analysis of miRNA profiles in NB cells isolated from the BM and assessing correlations with cell phenotype. miRNAs as biomarkers have been a subject of research in NB to inform risk, diagnosis, prognosis, prediction and to monitor response to therapy (Lin *et al.*, 2010, De Preter *et al.*, 2011, Vinklarek *et al.*, 2014). These are most usually assessed using tests carried out in tumour samples. Analysis of tumour can present some challenges as the location of the primary tumour may not be known, or may be hard to access, the biopsy taken might not contain tumour cells and repeated invasive biopsies may not be practical or parallel the evolving genotype of the cancer. Circulating biomarkers overcome some of these challenges as they can be monitored more readily in real-time samples obtained through less invasive procedures such as collecting blood. The stability of miRNAs owing to packaging into exosomes, high-density lipoproteins or association with Ago proteins, which protect against processing by ribonucleases makes them ideal candidate biomarkers (Etheridge *et al.*, 2011, Zhang *et al.*, 2012, Sohel, 2016).

In addition to diagnostic and prognostic information that impacts on clinical decisions, the discovery of miRNAs as novel biomarkers could lead to development of new therapies. miRNAs have vast biological functions; regulating multiple pathways, informing the pathogenesis of NB more than a single RNA (Dragomir *et al.*, 2018). As such, miRNAs could identify targets that could be used to create new targeted therapies. These may be therapies targeting the miRNA directly or against a target or targets identified as a result of pathway knowledge gained. Biomarkers that can be targeted directly by a therapy are known as druggable biomarkers (Saletta *et al.*, 2014). miRNAs are involved in multiple diseases, changing responses to many pathways, so altering expression for therapy may result in adverse side effects (Dragomir *et al.*, 2018). Conversely, the multiple targets of miRNAs may enhance their therapeutic potency, as many downstream targets may reside within the same oncogenic pathway to produce a multiple hit. This approach might also

limit the number of drugs needed for successful treatment as several targets could be affected by one drug, this could also theoretically reduce toxicity.

To explore the potential of miRNA signatures as circulating biomarkers, I have evaluated whole BM and PB to assess if miRNAs can predict OS or EFS. Furthermore, miRNAs were profiled in exosomes isolated from metastatic NB cells and these profiles were checked in plasma collected from NB patients to derive functional significance.

The aims of this chapter were therefore:

1. To test the hypothesis that miRNAs in BM or PB of children with NB may predict EFS.

2. Establish whether circulating miRNAs reported in the literature to be predictive of EFS in cancer patients are predictive in children with NB.

3. To determine whether miRNAs that drive self-renewal or migration of NB cells identified in Chapter 3 might be circulating biomarkers and predict outcome.

4. To isolate NB derived exosomes, profile the miRNA cargo to establish if miRNAs predictive of survival in PB and BM might have functional significance.

4.2   Materials and methods

4.2.1   Clinical samples

In addition to the BM collected into LAM as described in Section 2.2.2; BM (0.5ml x 2, one from right and one from left) and PB (2ml) samples were also collected at diagnosis from children with HR NB treated throughout the SIOPEN HR NB trials. These samples were taken directly into PAXgene® Blood RNA Tubes (PAX tube; PreAnalytiX, Qiagen) and plasma from 4ml PB collected into an EDTA tube (separated by centrifugation at 1,800g for 10 min) was aliquoted into 1ml cryovials. Samples were frozen and stored at -80°C in the clinical or reference laboratory prior to shipping to Leeds on dry ice. All samples were stored in Leeds at -80°C prior to processing. All samples were taken after informed consent; ethical approval number 01/04/087 and clinical trial number NCT01704716.

4.2.2   Isolation of small RNA from BM, PB and plasma

Samples collected between 11.10.2012 until 01.08.2013 were processed for RNA isolation using the PAXgene® Blood RNA Kit (Qiagen, Section 4.2.2.1). The FT from each step of this kit was collected in a 2ml eppendorf and stored for small RNA isolation using the RNeasy MinElute Cleanup Kit (Qiagen, protocol described in Section 3.2.1.1.1). Small RNAs were extracted from samples received between 02.08.2013 and 30.06.2017 using the PAXgene™ blood miRNA kit (Qiagen, Section 4.2.2.2) where total RNA (including miRNAs) are isolated together in one eluate, eliminating the need to retain the FT for further processing.

4.2.2.1   Small RNA isolation using PAXgene® Blood RNA Kit flow through

All buffers in the PAXgene® Blood RNA Kit are company proprietary. The PAX tubes protect RNA against degradation by RNases and therefore minimise changes in the gene expression (Viprey *et al.*, 2012).

The PAX tubes were incubated at room temperature for a minimum of 2h to fully defrost prior to RNA isolation, then centrifuged at 5,000g for 10 min. The supernatant was removed and the pellet fully resuspended by vortexing in 4ml RNase-free water, the sample was then centrifuged for 10 min at 5,000g, the

supernatant removed and discarded. The washed pellet was then resuspended in 350µl buffer BR1 and vortexed until visibly dissolved. The sample was transferred into a 1.5ml eppendorf with 300µl buffer BR2 and 40µl proteinase K, the mixture was vortexed for 5s then held at 55°C for 10 min using a shaker-incubator at 400rpm (Grant-bio PCMT shaker, SLS). To ensure complete lysis the sample was passed through a PAXgene Shredder spin column placed in a 2ml collection tube and centrifuged for 3 min at 13,000g. The supernatant was added to a fresh 1.5ml eppendorf containing 350µl of 100% ethanol. The sample was then passed through a PAXgene RNA spin column placed in a 2ml collection tube by centrifugation at 8,000g for 1 min. The FT was placed in a fresh 2ml eppendorf for isolation of small RNAs including miRNAs.

The remainder of the method was to extract RNA for other downstream studies. The column was then washed by adding 350µl buffer BR3 and centrifuging for 1 min at 8,000g. The column was then treated with DNase and incubated at room temperature for 15 min. A further 350µl buffer BR3 was passed through the column followed by 2 loads of 500µl buffer BR4, at every stage the FT was added to the 2ml eppendorf for small RNA isolation. The column was then dried by centrifugation for 1 min at 8,000g. RNA was eluted into a fresh 1.5ml collection tube by adding 40µl buffer BR5 to the column and centrifuging for 1 min at 8,000g, the eluate was then reapplied to the column and this final centrifugation repeated to increase the yield. The eluate was incubated for 5 min at 65°C to denature the RNA for downstream applications.

4.2.2.2   Small RNA isolation using PAXgene™ blood miRNA kit

The protocol is the same as that for the PAXgene blood RNA (Section 4.2.2.1) except that 700µl of isopropanol is added to precipitate the RNA instead of 350µl 100% ethanol and buffers BR1-4 are replaced by buffers BM1-4 respectively; all buffers are company proprietary. In addition, the FT is not retained.

4.2.2.3   Isolation of RNA from plasma samples

RNA was isolated from plasma using the miRNeasy Serum/Plasma Kit (Qiagen), all buffers are company proprietary. The plasma (200µl) was incubated in a water bath at 37°C until thawed.1ml of QIAzol Lysis Reagent was added and mixed well by

vortexing. The sample was incubated for 5 min at room temperature then 1ml of chloroform was added before further a 3 min incubation at room temperature. The sample was then centrifuged at 12,000g for 15 min at 4°C. The upper aqueous phase was transferred to a fresh 1.5ml eppendorf with 500µl 100% ethanol. The sample was passed through an RNeasy MinElute spin column in a 2ml collection tube using centrifugation at 8,000g for 15s, FT then discarded. The column was washed by adding 700µl buffer and centrifuged at 8,000g for 15s then 500µl buffer RPE and centrifuging for 15s at 8,000g. Ethanol (80%, 500µl) was added to the column which was then centrifuged for 2 min at 8,000g, FT was discarded. The column was then dried by centrifugation at 13,000g for 5 min before eluting RNA into 14µl RNase free water by centrifugation at 13,000g for 1 min.

4.2.3   Quantification and quality check of isolated RNA

RNA isolated from BM and PB was quantified using the Nanodrop as described in Section 3.2.1.1.2 and the quality of total RNA and the small RNA enrichment assessed using the Agilent Bioanalyser 2100 as described in Section 3.2.1.1.2. The amount of RNA isolated from plasma was not quantified.

4.2.4   miRNA TLDA to profile expression of miRNA in BM, PB and plasma

For BM and PB samples 400ng of total RNA was added to the RT, as described in Section 3.2.1.2. Due to the lower yield of RNA from plasma samples 3.2µl (maximum volume) of the RNA was added to the RT. The RT conditions were the same for all samples and amplified using conditions described in 3.2.1.2. Finally the miRNA TLDA was performed as previously described in 3.2.1.3. As reported in Chapter 3, only profiles that passed the quality control work flow were used in downstream analysis (Figure 3.2).

4.2.5   Cell culture

The NB cell line SH-SY5Y was used to optimise exosome isolation and characterisation. Exosomes were then isolated and characterised from 8 primary NB cultures, maintained as described in Section 2.2.5.1, culture conditions are described in Table 2.1. For isolation of exosomes cells were washed 3 times with PBS then incubated in depleted serum media for h in a humidified chamber in 5% C° in air at

37°C. For all exosome experiments the parent cells were harvested and counted so that exosome number could be reported relative to the number of cells from which the exosomes were derived. Cells were also collected and stored at -80°C to allow paired analysis of exosomes and cells if required.

Table 4.1   Cell line and primary cultures used for exosome isolation and characterisation.

Primary cultures were derived as described in Section 2.2.3 by Children's Cancer Research Group (CCRG), the gender of these patients is unknown.

Cell line/ primary culture	Source	Origin	Cell Type	Media
SH-SY5Y	CCIA	Human, 4 years old, female	Human NB Non-*MYCN* amplified	DMEM + 10% FCS + 2mM glutamine
284	CCRG	Human, 4 years old	Human NB BM derived	LAM
601	CCRG	Human, 3 years old	Human NB BM derived	LAM
1142	CCRG	Human, 1 year old	Human NB BM derived	LAM
2039	CCRG	Human, 2 years old	Human NB BM derived	LAM
2130	CCRG	Human, 3 years old	Human NB BM derived	LAM
4284	CCRG	Human, 4 years old	Human NB BM derived	LAM
23826	CCRG	Human, 8 years old	Human NB BM derived	LAM
24196	CCRG	Human, 2 years old	Human NB BM derived	LAM

4.2.6 Isolation of exosomes from cell culture supernatant using membrane affinity columns

Exosomes were isolated from cell culture supernatant using the exoEasy maxi kit (Qiagen) as summarised in Figure 4.1, all buffers are company proprietary. Media was collected and centrifuged at 3,000g for 15 min and passed through a 0.8μm filter to remove dead cells and large cellular debris. The filtered media was then combined with an equal volume of buffer XBP and mixed by inversion of the tube 5 times. The exoEasy spin column, was placed in a 50ml collection tube, 16ml of sample was loaded on to the column which was centrifuged at 500g for 1 min. The FT was discarded and this was repeated until the total sample mix had passed through the column. The column was then centrifuged at 4,500g for 1 min to remove residual liquid, then 10ml buffer XWP was added to the column and centrifuged at 4,500g for 5 min, the FT and collection tube were discarded. The column was placed into a new collection tube and 400μl of elution buffer (XE) was added to the membrane and incubated at room temperature for 1 min. The tube was then centrifuged at 500g for 5 min , the elute was pipetted back onto the membrane and incubated for a further 1 min at room temperature, the tube was centrifuged at 4,500g for 5 min to elute the exosomes. If RNA was to be extracted from the exosomes, rather than elusion the exosome were eluted by into XE buffer was replaced by adding 700μl of QIAzol, then centrifuged at 4,500g for 5 min to elute exosomes, RNA was extracted using the miRNeasy mini kit (Section 3.2.1.1.1). For all other analyses exosomes were pelleted by transferring the XE eluate to a 1.5ml microcentrifuge polypropylene tube (Beckman Coulter) and centrifugation at 100,000g for 70 min at 4°C (Optima TL ultracentrifuge, rotor TLA-45, Beckman Coulter).
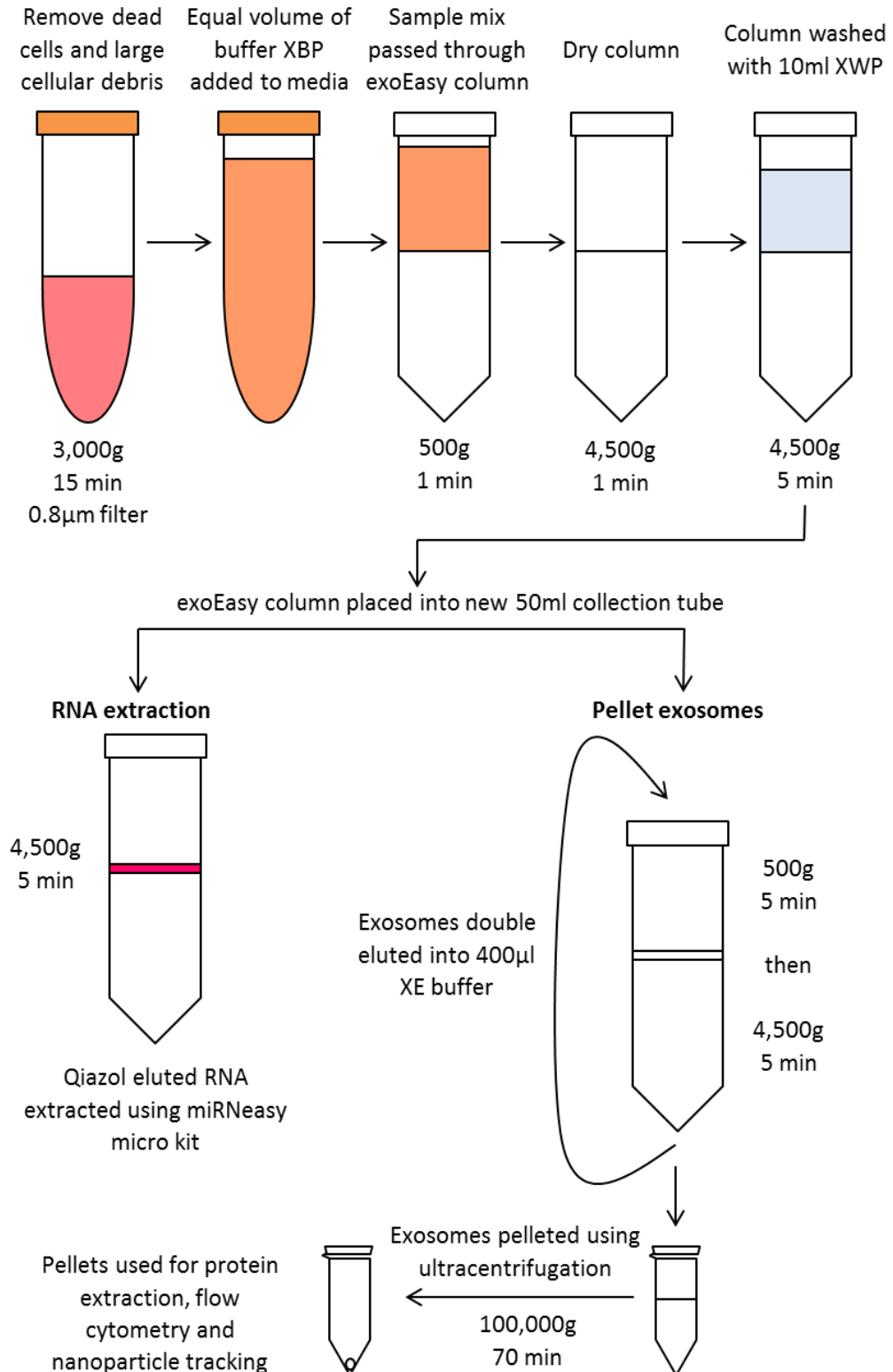
Figure 4.1 Isolation of exosomes from cell culture media using the exoEasy maxi kit.

The kit was supplied by Qiagen, all buffers are company proprietary. The eluent depended upon downstream applications; if RNA was to be extracted, the exosomes were eluted into QIAzol, for all other applications exosomes were eluted into Buffer XE.

4.2.6.1   Optimisation of media for exosome collection

FCS contains bovine exosomes and therefore media containing FCS cannot be used to collect human exosomes derived from human cells. One option to resolve the problem is to remove FCS from media prior to collecting exosomes from cells or remove the exosomes from the FCS by ultracentrifugation. To optimise the best media to replace complete media which contains 10% FCS and glutamine, cells were grown in media containing glutamine and either exosome-depleted serum or no serum to collect exosomes. SH-SY5Y cells were seeded at $2x10^5$ in 6 well Primaria plates. At 24h post seeding the media from each well was aspirated and each well was washed 3 times with 1ml PBS, cells were harvested from a control well to account for any cells removed during washing steps and viable cell number counted after washing 3 times in 5ml 1xPBS. After washing, 3ml of complete media (DMEM + 10% FCS + 2mM glutamine), depleted media (DMEM + 10% FCS ultracentrifuged at 100,000g for 18h + 2mM glutamine) or serum free media (DMEM + 2mM glutamine) was added. Cells were harvested at 24, 48, 72, 96 and 120h post media change and a viable cell count using the trypan blue exclusion assay was performed using the vi-cell. Growth curves were plotted and compared using a 1way ANOVA with Tukey's multiple testing correction using GraphPad Prism (GraphPad Software, California, USA).

4.2.6.2   Optimisation of cell seeding density to reach 90% confluency at 48h

SH-SY5Y cells were seeded into T75 flasks at increasing densities; 0.25, 0.5, 1, 1.5, 2, 2.5, 3 and $4x10^6$ cells, to determine which density at 48h incubation gave 90% confluent flasks. At 24h post seeding media was aspirated and cells washed 3 times with 5ml PBS to ensure all serum-containing media was removed, and then 15ml of depleted media was added to the flask. Cells were incubated for 48h then imaged at 4x and 10x magnification using an Olympus CKX41 microscope and Cell B software. Media was collected and centrifuged for 5min at 405g to pellet any cells, adherent cells were trypsinised and harvested as described in Section 2.2.5.1 and a total viable cell count was performed using the vi-cell. Seeding density experiments were repeated 3 times.

4.2.7 Quantification, sizing and morphology of isolated exosomes

Exosomes are reported to be between 20-150nm and have a concave disc morphology (Lötvall *et al.*, 2014, Vestad *et al.*, 2017), the number secreted by differing cell types can vary (Sohel, 2016). The size and number of isolated exosomes was confirmed using nanoparticle tracking analysis, transmission electron microscopy (TEM) and flow cytometry.

4.2.7.1 Quantification and sizing of isolated vesicles using NTA

The ZetaView® (Particle Metrix, Ammersee, Germany) was used to size and quantify isolated exosomes. For analysis exosome pellets were resuspended in 200µl of 0.1µm filtered PBS and transported to Cell Guidance Systems (Cambridge, UK) on dry ice where they were analysed using the ZetaView®.

At Cell Guidance Systems, exosomes were stored at -80°C and analysed within 10 days. To prime the ZetaView® the measuring platform was rinsed with freshly 0.22µm filtered dH_20 (Merck, Hertfordshire, UK). The quality platform check was performed automatically ensuring the platform had no background reading. The instrument was then calibrated using 100nm latex beads and flushed with PBS to eliminate cross over between beads and sample. Samples were thawed at room temperature then vortexed to ensure homogeneity. Samples were diluted 200 fold in PBS for the first measurement: this dilution was adjusted accordingly so the concentration of particles fell within the recommended range of 10^5-10^{10} particles per cm^3. After analysis the platform was flushed with 0.22µm filtered dH_20 in order to eliminate any residual PBS that may form salt deposits. Finally the platform was filled with air to eliminate stagnant dH_20 between experiments. Data were captured using Software ZetaView 8.03.08.02 with a camera resolution of 0.703µm/pixel taking images at 11 positions over 2 cycles, at a constant temperature of 27°C to allow calculations using Brownian motion laws (Cichocki *et al.*, 2015). Area analysis parameters used were 10-1,000, ensuring the particles measured fall within the limits by defining the number of pixels visible in the window.

4.2.7.2 Sizing and quantification of exosomes using flow cytometry size reference beads

The CytoFLEX flow cytometer (Beckman Coulter) and corresponding CytEXPERT software (Beckman Coulter) were used to visualise fluorescently labelled exosomes, allowing quantification and approximate sizing using gates established against size reference beads.

SH-SH5Y exosome pellets were resuspended in a volume of 0.1μm filtered PBS to give exosomes from $5x10^5$ cells in 1μl, this volume was then pipetted into 0.5ml eppendorfs, in triplicate. To visualise the exosomes 39μl of CellTrace Far Red (CellTrace, Thermo Fisher) was added at a concentration of 1μM. Exosomes were incubated at 37°C for 20 min. A further 960μl of 0.1μm filtered PBS was then added to give a total volume of 1ml. Each sample was analysed at a flow rate of 10μl/min for 2 min.

For all samples the detector gain was set at maximum (3,000) as optimised by Dr Adam Davison (Flow Cytometry Facility, UoL) who determined that these settings achieved the best resolution between signal and noise, as illustrated in Figure 4.2. Increasing the gain maximally allowed for the greatest resolution of all beads sampled from the background noise. There was also minimal contamination from the electronic sampling noise, as the proportions of each sized bead gated events remained constant when compared to the background (data not shown).

After optimisation of the detector gain, a sample of 0.1μm filtered PBS was analysed to optimise the fluorescent thresholds to determine the point at which minimum background was seen for each fluorescent channel. An example of this process using the allophycocyanin (APC) threshold is illustrated in Figure 4.2. This was tested for every channel required; fluorescein isothiocyanate (FITC), APC, R-phrcoerythrin (PE) and V450. The optimal thresholds were 5,000, 7,000, 5,000 and 5,000 respectively.

After these settings were optimised the reference beads Megamix-plus forward scatter (FSC) beads (Biocytex, Marseille, France) were used as size standards on the CytoFLEX flow cytometer. The Megamix-plus FSC beads are a mix of fluorescent beads of diameter 100, 300, 500 and 900nm. The Megamix-plus FSC beads were used to define gates of 100-300nm, 300-500nm and 500-900nm on the dot plots using the

CytEXPERT software, (in Figure 4.2). Megamix plus FSC beads were diluted 1:2 using 0.1µm filtered PBS and analysed using the fluorescent threshold of 5,000 for FITC. Exosomes stained with CellTrace were then analysed using a fluorescent threshold of APC 7,000. DMSO vehicle controls, dye only and unstained exosomes were run in all experiments. All data were analysed using the CytEXPERT software. To analyse this data the CellTrace only sample was first used to define the CellTrace positive gate From this each set of sample data was exported and the event number and median fluorescence of CellTrace positive particles in each of the sizing gates recorded.
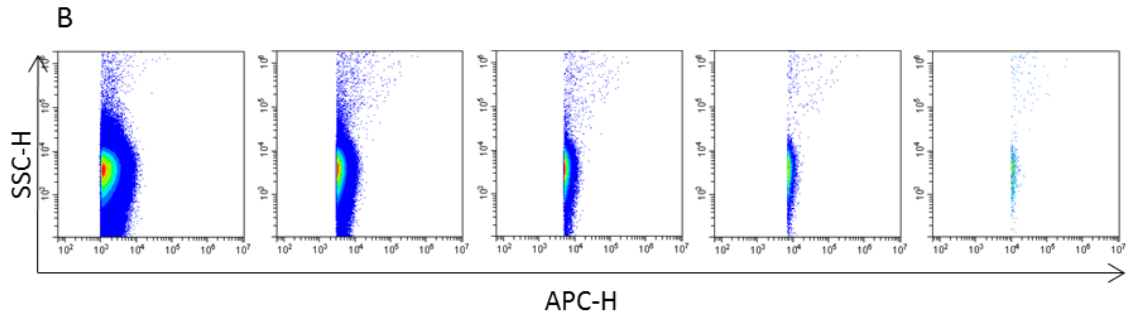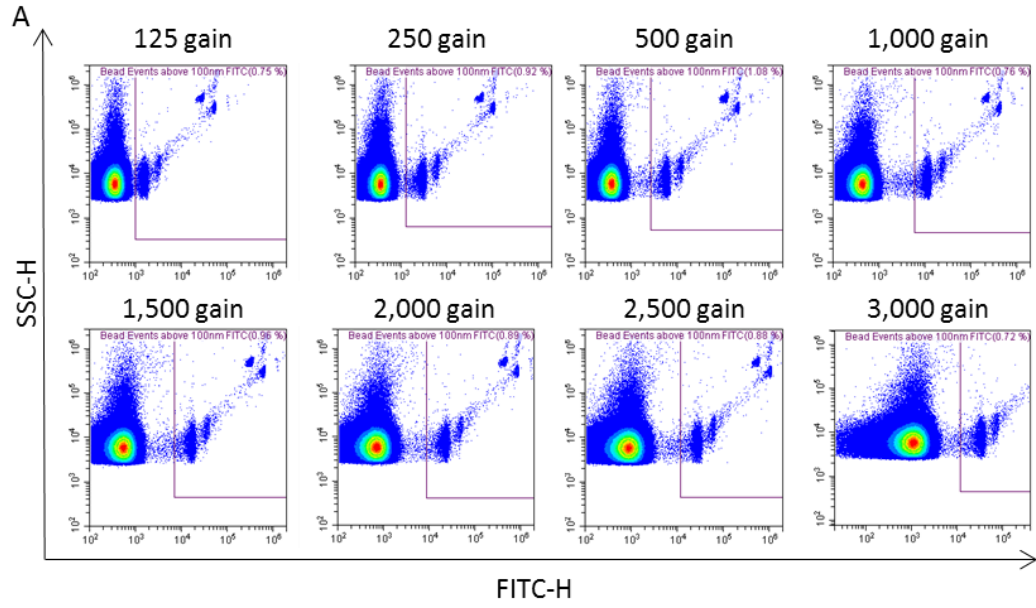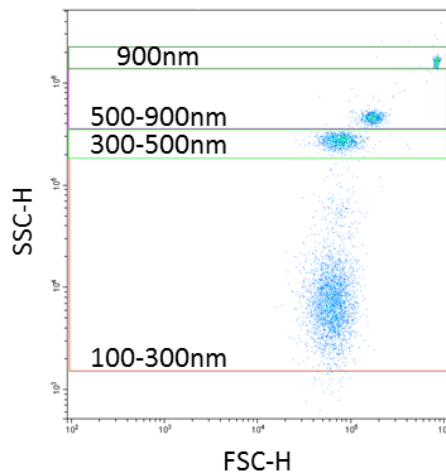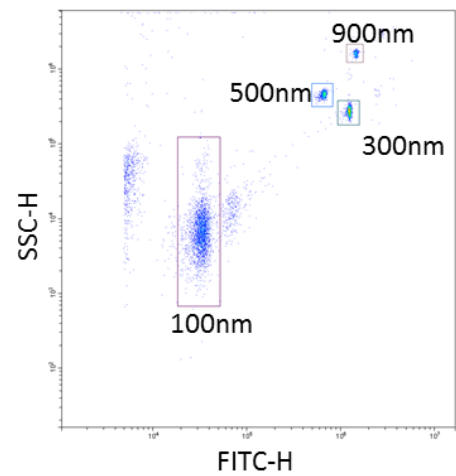
Figure 4.2 Optimisation of flow cytometry to quantify and size exosomes.

> A, The detector gain regulates the sensitivity of the photomultiplier detector, the gain was optimised using a sample of Megamix-plus FSC beads to define the level rendering the best resolution between 100nm beads and the noise. All pseudo colour plots show side scatter height along y-axis and FITC height along x-axis. B, The fluorescent APC threshold was optimised using a sample of 0.1µm filtered PBS. The table denotes the fluorescent threshold set, the number of events detected per µl and the abort percentage of total events, corresponding to the pseudo plots above each column. Abort rate (AR) is the number of events aborted as a percentage of total events. The fluorescent thresholds for FITC, PE and V450 were optimised in the same manner. C i, the size gates are shown around the Megamix-plus FSC beads. Gates on side and forward scatter for 100-300nm, 300-500nm and 500-900nm are shown. C ii, Megamix-plus FSC bead size subsets shown across side scatter and the FITC fluorescence. SSC denotes side scatter; FSC denotes forward scatter.

4.2.7.2.1 Optimisation of CellTrace concentration and cell number for sizing exosomes using flow cytometry

SH-SY5Y exosomes were isolated, resuspended and aliquoted in eppendorfs to contain exosomes derived from 2.5×10^5, 5×10^5, 1×10^6 and 2×10^6 cells. Each quantity of exosomes was stained with 0.25, 0.5, 1 and 2µM of CellTrace. Data were analysed in CytEXPERT first by determining the CellTrace positive gate; this was set at the edge of detected events in the CellTrace only samples. For all samples the abort rate; number of events aborted as a percentage of total events, positive event number; number of events with a fluorescence above the threshold determined by cell trace only and median fluorescence; the median fluorescence of all events denoted positive were exported to assess the optimum staining concentration and exosome producing cell number.

4.2.8 Sizing and quantification of exosomes using TEM

Exosomes were resuspended in 7µl 2% PFA and stored at 4°C until processed by Mr Martin Fuller (Electron Microscopy Faculty, UoL). The sample was pipetted onto Parafilm M (Bemis NA, Sigma Aldrich) and a 3.05mm diameter formvar and carbon coated copper grid (AGAR Scientific, Essex, UK) was inverted into the sample and incubated for 20 min at room temperature. Each grid was then washed 6 times in dH$_2$0 for 3 min. Samples were then stained with 1% uranyl acetate for 10s. After staining grids were left to air dry. Samples were imaged using a JEM 1400

transmission electron microscope (JEOL, Massachusetts, USA) at 100Kv. Images were captured on AMT 1k CCD running on AMT v602 software.

4.2.8.1.1   Optimisation of TEM methodology

The optimal method to process exosomes for TEM was established using exosomes isolated from SH-SY5Y collected every 24h over a 96h period; at each time point isolated pellets were resuspended in 7µl 2% PFA or 0.1µm filtered PBS. There were a total of 20 samples processed; for each time point 4 samples, 2 resuspended in PBS and 2 in 2% PFA. Within each pair one was processed using methyl cellulose and one without as shown in Table 4.2. Methyl-cellulose is reported to improve resolution and enhance membrane contrast (Asadi *et al.*, 2017).

Table 4.2 Optimisation of exosome preparation and processing for TEM.

For each time point (0-96h) 4 samples of exosomes were prepared, two resuspended in PFA and 2 in PBS. Within each of the different resuspensions one sample was processed with methyl cellulose and one without.

Time from isolation to processing (h)	Exosomes resuspended in 2% PFA		Exosomes resuspended in filtered PBS	
0				
24				
48	Methyl cellulose	No methyl cellulose	Methyl cellulose	No methyl cellulose
72				
96				

The samples were all adhered to the grids as described in Section 4.2.8. After washing, samples stained with methyl cellulose were covered by a uranyl acetate. methyl cellulose mix (9:1, 2% methyl cellulose: 4% uranyl acetate) and incubated on ice for 10 min. Non methyl cellulose samples were stained with 1% uranyl acetate, added dropwise and incubated for 10s.

4.2.9 Characterisation of exosomal marker expression by isolated exosomes

Both CD63 and CD81, putative exosomal markers (Willms *et al.*, 2016), were assessed using flow cytometry and immunodetection. Both these markers are tetraspanins reported to be detectable on the external surface of exosomes. Additionally the expression of the NB marker GD_2 was studied using flow cytometry to confirm the NB origin of exosomes detected (Marimpietri *et al.*, 2013). Additional panel of markers was used in immunodetection to provide more evidence of exosomal isolation, these additional markers included tumour susceptibility gene 101 (TSG-101) an additional protein reported to be expressed by exosomes.

4.2.9.1 Analysis of exosomal and NB marker expression using flow cytometry

Isolated exosomes from cells were stained with CellTrace as described in Section 4.2.7.2 before further staining for exosome markers, CD81 and CD63 and the NB marker GD_2. After staining with CellTrace, samples were incubated in antibody (optimised concentrations listed in Table 4.3), diluted in 0.1µm filtered PBS to a staining volume of 100µl, for 30 min at 4°C. Samples were added to 900µl of 0.1µm filtered PBS and analysed on the CytoFLEX using optimised fluorescent thresholds (see Table 4.3). Dual colour staining was performed, in this case both antibodies were added at required concentrations to give 100µl staining volume and incubated for 30 min at 4°C, again this was added to 900µl of 0.1µm filtered PBS and analysed on the CytoFLEX. For dual analysis primary and secondary fluorescent thresholds were used according to the fluorescent channels of the antibodies used.

Table 4.3 Optimised antibody concentrations for flow cytometry analysis.

Concentrations of antibodies for flow cytometry analysis were determined empirically. Each antibody was optimised for staining concentration of exosomes secreted from the equivalent of 5×10^5 SH-SY5Y cells. Firstly each antibody was diluted in 0.1µm filtered PBS to a range of concentrations around the recommended working concentration (deduced using company protocol and literature). These antibody alone dilutions were analysed to assess the concentration at which the abort rate was under 10%. After the maximum concentration was limited by abort rate a dilution curve was performed to find at which point the maximum event number was detected. The antibody concentration and abort rates decreased in a linear fashion (data not shown). Exosome incubations conjugated antibodies were diluted in 0.1µm filtered PBS. Fluorescent thresholds were optimised to give minimum background noise. BD Horizon™ is a subsidiary of BD Bioscience.

Antibody	Conjugated species	Staining concentration	Fluorescent threshold	Supplier (product code)
CD81	FITC Mouse IgG1κ	2.5ng/µl	5,000	BD Horizon™ (551108)
CD63	V450 Mouse IgG1κ	5ng/µl	7,000	BD Horizon™ (561984)
GD$_2$	PE Mouse IgG2a	0.07ng/µl	8,000	BD Horizon™ (562100)

4.2.9.2   Analysis of exosomal and NB marker expression by immunodetection

4.2.9.2.1   Extraction of protein from exosomes

Protein from exosomes and parent cells was done in parallel. To achieve a cell pellet media was aspirated, cells washed once with 5ml ice-cold 1X PBS, scraped into 2ml ice-cold PBS using a cell scraper (Sarstedt Ltd, Nümbrecht, Germany) and centrifuged at 405g for 5min. The supernatant was aspirated. To extract protein the exosome (15µl) or cell pellet (50µl) was resuspended in lysis buffer (1X PBS containing 1% Nonidet P-40, 10mM sodium deoxycholate, 0.1% sodium dodecyl sulphate (SDS)) with protease inhibitor cocktail (0.6mM phenymethylsulfonyl (PMSF), 1mM sodium orthovanadate, 25µM leupeptin, and 30µl/ml aprotinin, all purchased from Sigma). Samples were incubated on ice for 30 min, and cell lysates were centrifuged at 12,470g at 4°C for 10 min. The resulting supernatant was retained as the soluble

protein fraction. Protein concentration was determined using 5µl of the extract, cells diluted 1:10 and exosomes undiluted, the BioRad DC Protein Assay (Bio-Rad Laboratories).

The protein assay is based on the Lowry Assay (Lowry *et al.*, 1951) was used to estimate protein concentration of all samples. All reagents are company proprietary. Briefly, a standard dilution curve was prepared of BSA ranging from 0 to 2mg/ml in 10% radio immunoprecipitation assay (RIPA) lysis buffer. Each sample or standard (5µl) was pipette in triplicate (except exosomes where 1 repeat was used) into wells of a 96 well microtitre place (Nunc-Immuno™, Nalge Nunc Intl., supplied by Thermo Fisher). Working reagent SA was prepared by adding Reagent S (20µl) to Reagent A (1ml) and added to each well (25µl). Reagent B was then added (200µl) to each well and the plate was agitated for 10 seconds (s) followed by 15 min incubation at room temperature. Absorbance of each well was read at 690 nm using a microplate reader (Titertek-Berthold Instruments, supplied by GeneFlow Ltd). Protein concentration in samples was determined from the standard curve generated from the BSA dilutions. For exosome protein the remaining 10µl was divided into 2 aliquots one of which was added to an equal volume of SDS and the other an equal volume of SDS with 20% dithiothreitol (DTT). Protein aliquots were stored at -20°C.

4.2.9.2.2   Immunodetection of exosome specific proteins

Mini-Protean II cell apparatus (Bio-Rad Laboratories) was used throughout. Mini-PROTEAN® TGX™ (4-15%; Bio-Rad Laboratories) precast gel was chosen; the strip and comb were removed. The gel was transferred to the electrophoresis tank containing 2X SDS running buffer (25mM Tris-HCl (MP Biomedicals, Thermo Fisher), 250mM glycine (Sigma), 0.1% SDS). Protein extracts (50µg for cells, 5µl volume for exosomes) in 2X SDS loading buffer were centrifuged briefly at 12,470g to bring down all solution, and loaded into the well alongside 5µl of molecular weight marker (59479; Geneflow Ltd). The gel was electrophorised at a constant voltage of 100 V until the bromophenol blue dye had reached the bottom of the gel.

After completion of electrophoresis the stacking gel was removed and resolving gel placed in transfer buffer (25mM Tris, 192mM glycine, 20% methanol, 0.01% SDS) for 5 min. The Bio-Rad Laboratories transfer kit was assembled using Hybond C-extra

supported nitrocellulose membrane (Amersham Biosciences, Little Chalfont, UK) against the gel, 3mm filter paper (Whatmann, GE Healthcare) and two filter pads (Bio-Rad Laboratories). Proteins were immunoblotted from the gel onto the nitrocellulose membrane at 100V, with constant stirring using a magnetic flea, for 90 min at room temperature.

The membrane was incubated in LI-COR blocking buffer (LI-COR Biosciences, supplied by VWR, Leicestershire, UK) with rapid agitation on an orbital shaker at room temperature for 1h. The membrane was incubated in primary antibody diluted in an incubation solution (50% LI-COR blocking buffer and 50% PBS with 0.1% tween (v/v; PBST) overnight at 4°C with shaking on an orbital shaker. The specificity and concentration of primary antibody (Table 4.4) to minimise background nonspecific binding were optimised using positive control cell extracts. Membranes were washed 3 x 5 min with PBST and subsequently incubated for 1 h in the appropriate secondary antibody at a concentration of 1:5,000, prepared in incubation solution as above. Membranes were washed 3 x 5 min in PBST and 1 x 5 min in PBS to remove tween residue.

Membranes were visualised using the Gel-Doc™ (Bio-Rad Laboratories). To check the efficiency of immunoblotting, membranes were stained using Ponceau S (Sigma) solution for 5 minutes, and rinsed using ddH₂O to reveal the transferred proteins.

Table 4.4 Antibodies and optimised concentrations for western blots.

Concentrations of antibodies for western blots were determined empirically. All incubations with primary antibody were overnight at 4°C, secondary antibody incubations were 2h at room temperature unless otherwise stated. The cellular component each protein is a marker for is listed. CDC42 denotes cell division control protein 42 homolog. Hsp denoted heat shock protein. EEA1 denotes early endosome antigen 1. Grp75 denotes stress-70 protein. TATA TBP denotes TATA-box-binding protein. LAMP-1 denotes lysosomal-associated membrane protein 1. GAPDH denotes glyceraldehyde 3-phosphate dehydrogenase.

Antibody	Cellular location	Species	Optimised concentration	Supplier (product code)
CD63	Exosomal	Mouse monoclonal	1:1,000	Abcam (ab8219)

TSG-101	Exosomal	Mouse monoclonal	1:400	Abcam (ab83)
CD81	Exosomal	Mouse monoclonal	1:200	Santa Cruz (B-11 clone sc166029
CD9	Exosomal	Rabbit monoclonal	1:10,000	Abcam (ab92726)
CDC42	Exosomal	Rabbit monoclonal	1:1,000	Cell Signalling Technology (2466; Massachusetts, USA)
Ago2	miRNA binding	Rabbit monoclonal	1:2,000	Abcam (ab32381)
Hsp70	Mitochondrial	Mouse monoclonal	1:1,000	Abcam (ab47455)
Hsp90	Mitochondrial	Mouse monoclonal	1:1,000	Abcam (ab13492)
EEA1	Endosomal	Rabbit monoclonal	1:10,000	Abcam (ab2900)
Grp75	Mitochondrial	Mouse monoclonal	1:10,000	Abcam (ab2799)
TATA TBP	Nuclear	Mouse monoclonal	1:1,000	Abcam (ab818)
LAMP-1	Lysosomal	Rabbit monoclonal	1:2,000	Abcam (ab24170)
β-Actin	Cytosolic	Rabbit monoclonal	1:10,000	Abcam (ab8226)

GAPDH	Cytosolic	Rabbit monoclonal	1:5000	Cell Signalling Technology (2118)
Pan cadherin	Membrane	Mouse monoclonal	1:800	Abcam (ab22744)
Secondary antibodies; anti-mouse (A21065), anti-rabbit (A21076)	-	-	1:5,000	Alexa fluro 680; Molecular Probes, Invitrogen

4.2.10 Analysis of RNA cargo extracted from exosomes

RNA was isolated from exosomes to profile for expressed miRNAs, this allowed comparison of exosome profiles against those from other sample types.

4.2.10.1 Extraction, quantification and quality analysis of exosomal RNA

QIAzol eluate was collected from the exoEasy collection tube, as described in Section 0, and transferred into a 1.5ml RNase free eppendorf. RNA was extracted using the miRNeasy mini kit as described in Section 3.2.1.1.1. The concentration of RNA was assessed using the Nanodrop as described in Section 3.2.1.1.2. Paired cells were harvested and RNA extracted using the miRNeasy mini kit as described in Section 3.2.1.1.1. RNA from the cells was diluted to 5ng/µl, then along with exosomal RNA (5µl, undiluted) were heated for 2 min at 70°C. The RNA was analysed using the pico and small RNA chips using the agilent bioanalyser 2100 as described in Section 3.2.1.1.2.

4.2.10.2 Profiling of miRNA cargo in isolated exosomes using TLDAs

Due to low detectable RNA yield it was not possible to load miRNA TLDA with 400ng of exosomal total RNA. A total volume of 3.2µl of RNA was instead used in the RT and loaded onto the miRNA TLDA, both as described in Sections 3.2.1.2 and 3.2.1.3.

miRNA TLDA data were not normalised to the global mean due to a low number of miRNAs expressed. Instead raw Ct values were used to inform biological knowledge.

4.2.11 Isolation and characterisation of exosomes from 8 primary NB BM cultures

To assess the signature of miRNAs in exosomal cargo, 8 primary cultures with matched samples of BM and PB at diagnosis were selected to isolate exosomes from. For every sample exosomes were isolated using the affinity column method described in Section 0 and characterised as described above using nanoparticle tracking analysis, flow cytometry, western blotting and ultimately RNA was profiled for miRNA expression. Briefly, 1 T75 flask was used to isolate exosomes for quantification and size profiling using the ZetaView®. For analysis using western blotting, exosomes were isolated from 2 T75 flasks and protein was extracted as described in Section 4.2.9.2.1, immunodetection for exosomal markers CD63, CD81 and TSG-101 and cellular markers early endosome antigen 1 (EEA1), Pan cadherin, lysosomal-associated membrane protein 1 (LAMP-1), stress-70 protein (Grp75) and TATA-box-binding protein (TATA-TBP) was performed alongside paired cell controls (a reduced panel of markers was used due to limited exosomal protein available compared with SH-SH5Y exosomes). Flow cytometry analysis was performed on exosomes secreted from the equivalent of 2 T75 flasks as described in Section 4.2.9.1. RNA for miRNA profiling was extracted from exosomes produced by 2 T75 flasks of cells, a quarter of these exosomes were processed for quantification using nanoparticle tracking analysis to inform number of exosomes profiled. For all exosome experiments, cells were imaged prior to harvesting and after live and dead cells were counted using the trypan blue exclusion assay.

4.2.12 Isolation and characterisation of exosomes from whole BM

BM aspirates in LAM, as described in Section 2.2.3, were centrifuged at 405g for 5 min upon arrival to pellet cells for NB cell isolation. The supernatant (media containing exosomes) was transferred to a falcon and centrifuged for a further 15 min at 3,000g to remove cellular debris. Exosomes were then isolated from this media as described in Section 0. Each sample was then processed for either NTA, RNA isolation, immunodetection or flow cytometry.

4.2.13 Statistical analysis of miRNA profiles

4.2.13.1 Identification of miRNAs predictive of EFS in BM and PB samples

The initial cohort of PB (n=110) and BM (n=124) miRNA profiles were analysed using a previously developed multivariate mathematical model (Gregory *et al.*, 2016). This model assumes that the pattern of OS and EFS event times are related to the amount of residual disease remaining after treatment, and to its subsequent doubling time. Factors can be seen to be related to either or both of these variables. The component that quantifies the remaining residual disease relates to the proportion of patients cured, or with long survival, following treatment. Because of this, variables that are related to the amount of residual disease remaining after treatment have greater relevance for subsequent outcome than those related only to doubling time. The model produces a chi-square for each variable for its effect on both residual disease and on doubling times. The chi-square values for each miRNA calculated from each model component were noted. Averages of the 2 chi-square values were also calculated to enable an overall significance effect to be determined, although the main focus was on factors which predicted for residual disease after treatment. The significant miRNAs identified in the analysis of the initial cohort were assessed for prediction of survival in the validation cohort of PB (n=100) and BM (n=100) using Kaplan-Meier survival analysis for both OS and EFS with optimised cut points.

4.2.13.2 Comparison of RNA isolation methodology and scientist bias on miRNA profiles

Studies have shown that differential methodologies of RNA isolation can lead to changes in the RNA species enriched (Kim *et al.*, 2012). The BM and PB samples were used to assess two hypotheses; that there would be no bias in sample profiles correlating to the scientist and that the methodology used to isolate miRNA would not influence the profiles. PCA plots (as described in Section 3.2.2.2) were used to visualise the data annotated with isolation methodology and cohort. For each comparison the global mean, number of miRNAs expressed and ΔCt values of the snoRNAs U6, U44 and U48 were compared across groups using a t-test.

4.2.13.3   Literature search to identify miRNAs reported to predict EFS in circulating samples

miRNAs predictive of EFS in circulating biomarkers were identified by a systematic review (unpublished data received from Sue Burchill). The presence of these miRNAs was cross-referenced with those present on the miRNA TLDA A. miRNAs present were interrogated for predicting outcome using Kaplan-Meier survival analysis with cut points determined using cox regression analysis.

4.2.13.4   Survival analysis to interrogate if selected miRNAs predict survival

miRNAs identified from the previous analysis and literature to be predictive of survival were assessed in the PB and BM profiles using Kaplan-Meier survival analysis with optimised cut points.

4.2.13.5   Expression of exosomal miRNAs across matched samples

miRNA profiles from exosomes, cells, PB and BM of 4 patients were visualised for expression patterns using heatmaps and PCA plots as described in Section 3.2.2.2. The expression of miRNAs detected in exosomal cargo were assessed in other sample types.

4.2.13.6   Changes in miRNA profiles when cells were placed in depleted serum conditions

Changes in miRNA profiles between cells routinely cultured and cells cultured in medium containing serum depleted of exosomes were assessed. To interrogate differences, ΔCt (normalised to the global mean) values from the routinely cultured cells (RCells) analysis were deducted from the exosome producing cells (ECells) analysis (ECells-RCells=change in ΔCt), miRNAs only expressed (Ct <35) in either sample were also noted.

4.2.13.7   Pathway analysis using selected miRNAs

Significant or interesting miRNAs were further interrogated for pathway analysis, using miRPath as described in Section 3.2.3.1.

4.3 Results

4.3.1 Extraction of RNA from PB and BM

RNA was successfully extracted from 224 diagnostic NB BM, 210 diagnostic NB PB and 36 diagnostic NB plasma. From these samples 100 BM and 100 PB were extracted as a second cohort to validate miRNA profiles identified as significant in the initial cohort.

All RNAs from the PB validation cohort had a RIN greater than 7.5 (n= 38 (62 extracted from FT with no total RNA to generate RIN), median 8.6, maximum 9.4). The mean small RNA concentration was 243±307pg/µl (n=100, range 2-1,779). The BM samples had a median RIN of 7.8 (n=60 (40 extracted from FT with no total RNA to generate RIN), range 2.6-9.5) and a mean small RNA concentration of 884.3±1,300 (n=100, range 16-9,201). Comparisons between cohorts for RIN could not be made as all samples in the initial cohort were extracted using the FT method and therefore did not have total RNA to generate a RIN.

4.3.2 Cohort and RNA isolation effects on miRNA profile

Of the BM samples (n=224) 100 were reverse transcribed, analysed using the miRNA TLDA and data processed by me, the other 114 by Ms Samantha Brownhill. For the PB samples (n=210), 100 were processed by me and the remaining 110 by Ms Samantha Brownhill. All miRNA from the initial samples were isolated using the FT method. Of the validation samples 40 BM and 62 PB were isolated by the FT method and the remainder using complete isolation of total RNA. The data was visualised using PCA plots, shown in Figure 4.3. For both PB and BM there was overlap between the initial and validation sets showing no complete distinction between either data set, the PCA showed around 15% variance in PC1 and 10% variance for PC2 for both sample types.

The global mean, number of expressed miRNAs and snoRNA ΔCt values (normalised to the global mean) between initial and validation cohorts in both BM and PB were assessed using a student's t-test and plotted as box plots, Figure 4.4. No significant differences were seen between the ΔCt values for snoRNAs U6 or U48 between either cohorts. U44 showed significant differences in the BM cohorts (p= 0.04) but

not the PB (p= 0.9). For both cohorts significant differences were seen between global mean values (p= 4×10^5 in BM and p=3×10^{-13} in PB) and the number of miRNA expressed (p= 1×10^{-15} in BM and 2×10^{-17} in PB), in both cases the median global mean was lower in the initial cohorts and the number of miRNA expressed was increased in both initial data sets.
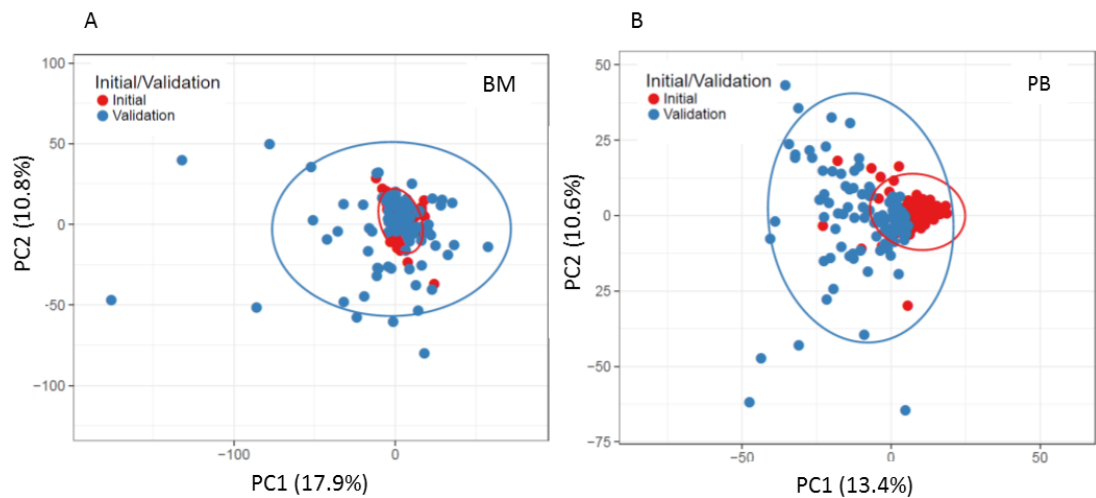
Figure 4.3 PCA plots of initial and validation miRNA profiles.

> Each point represents a sample, prediction ellipses are such that with probability 0.95 a new observation from the same group will fall inside the ellipse. X and Y axis show principal component (PC) 1 and PC2 and the percent of total variance each explains. A, BM initial (red, n=114) and validation (blue, n=100) miRNA profiles. B, PB initial (red, n=110) and validation (blue, n=100) miRNA profiles
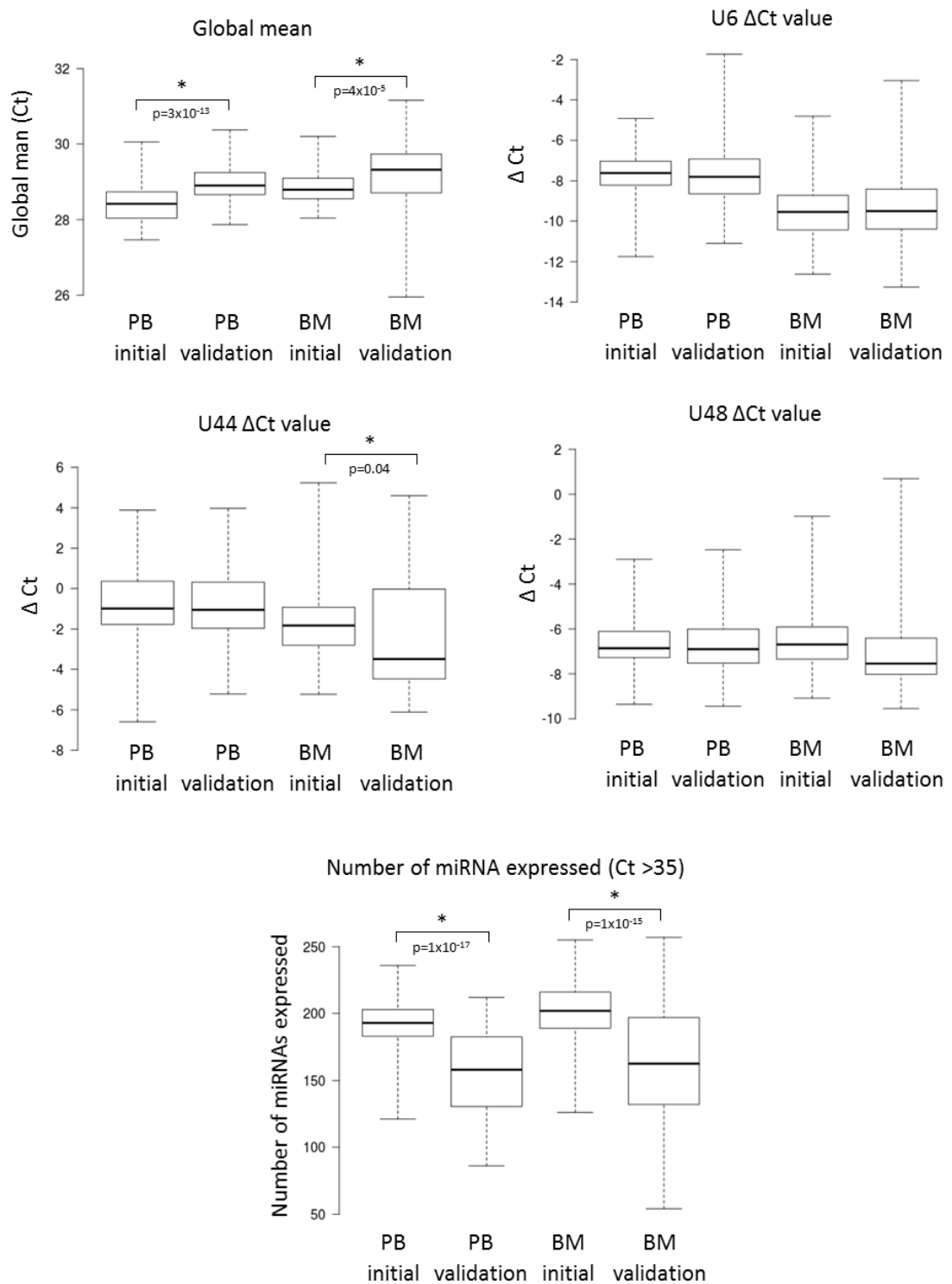
Figure 4.4 Box plots depicting initial vs validation comparison in PB and BM.

Box plots show median, upper and lower quartiles and range of global mean, number of miRNAs expressed (Ct value <35) and ΔCt values of snoRNAs U6, U44 and U48. * depicts significance (student's t-test p-value <0.05). p-values are stated.

A difference between initial and validation cohorts is that the validation cohort contains samples where miRNA was isolated using differing methodologies; the

PAXgene Blood RNA FT or isolation of total RNA using the PAXgene Blood miRNA kit (total). To assess the impact of this both PB and BM profiles were split into groups based on miRNA isolation methodology. The data was visualised using PCA plots, shown in Figure 4.5. For both cohorts there was overlap between the initial and validation sets showing no complete distinction between either cohort.

The mean ΔCt values of U44 (p= 1.3×10^{-6} in PB and 1×10^{-19} in BM, Figure 4.6) and U48 (p = 0.001 in PB and 1×10^{-15} in BM) were significantly lower in the FT cohorts of both sample types, U6 remained not significant. The miRNA TLDA manual states the method to isolate the total RNA must preserve the small RNA fraction, commenting that if the small RNA is later enriched the longer snoRNA transcripts may be lost, suggesting a cause for the lower expression of snoRNAs U44 and U48 in the FT cohorts. There was a significantly higher number of miRNAs expressed in the PB FT cohort, no difference was seen in the BM cohort. The level of miRNA enrichment is known to be effected by sample preparation, small RNAs with a low GC content have a lower isolation when long cellular RNAs are not present to act as carriers for precipitation (Kim *et al.*, 2012). In total there were more statistical differences seen when comparing isolation methodologies, a possible cause for differences present between initial and validation cohorts.
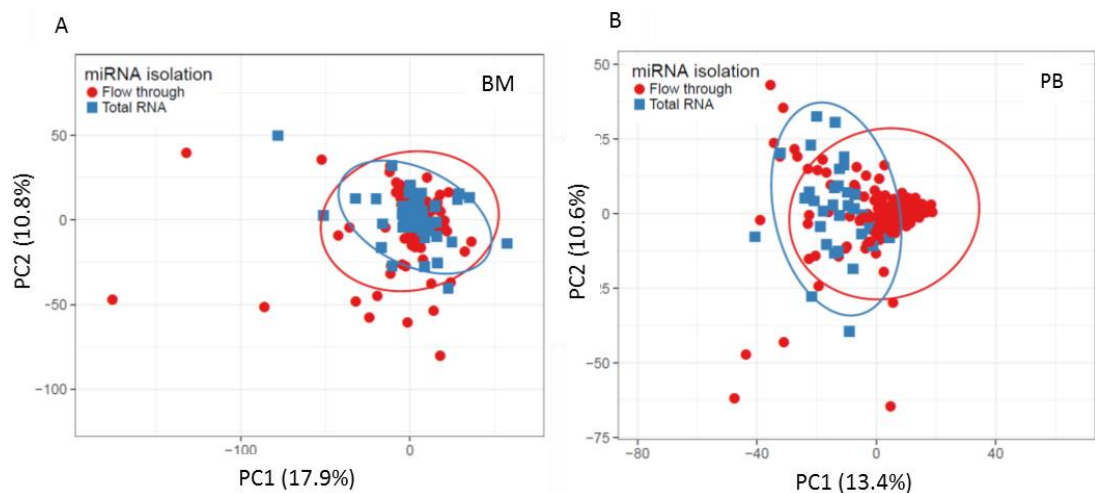
Figure 4.5 PCA plots of FT and total RNA extraction miRNA profiles.

Each point represents a sample, prediction ellipses are such that with probability 0.95 a new observation from the same group will fall inside the ellipse. X and Y axis show PC1 PC2 and the percent of total variance each explains. A, BM FT (red, n=154) and total (blue, n=60) miRNA profiles. B, PB FT (red, n=172) and total (blue, n=38) miRNA profiles.
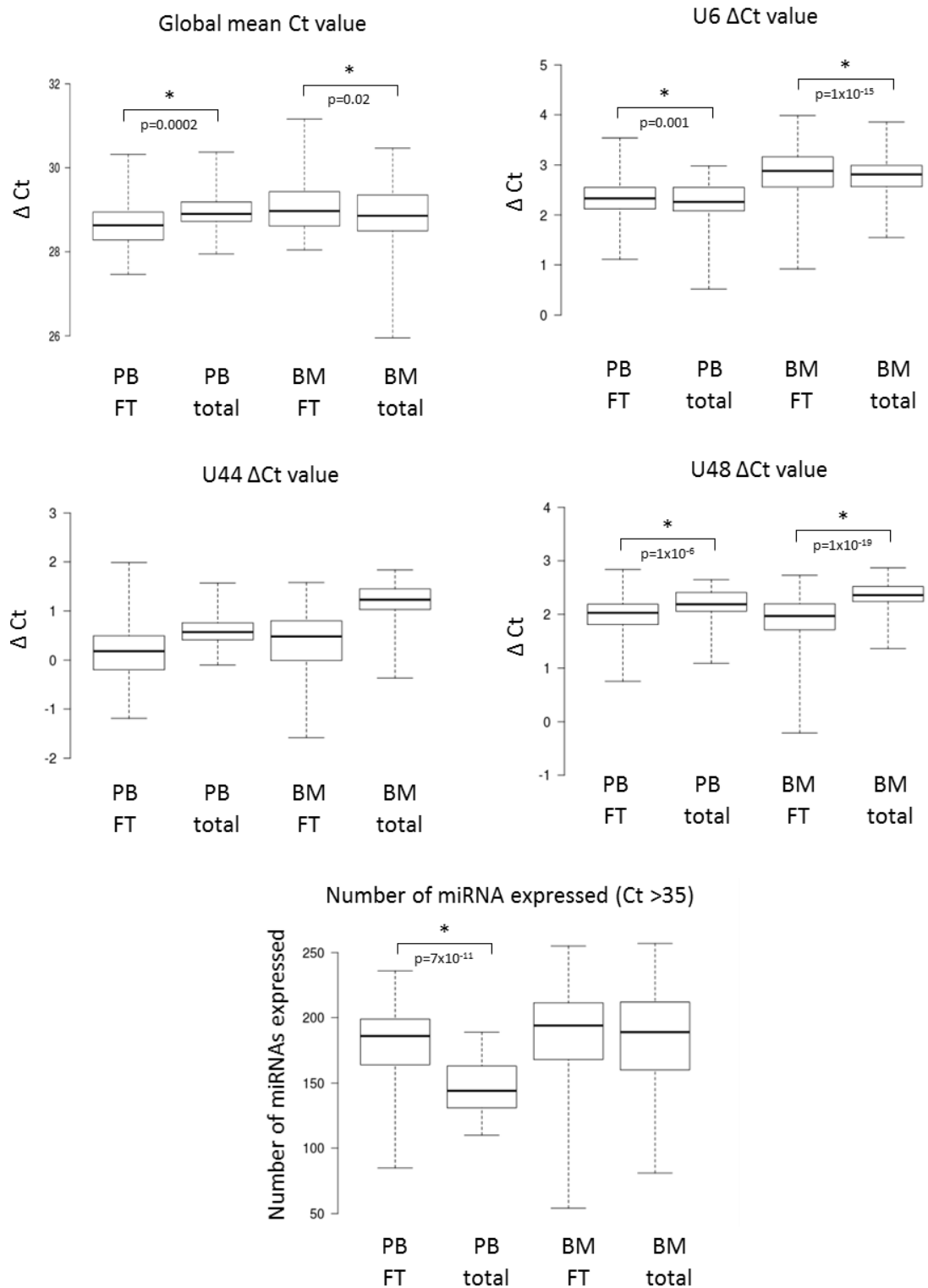
Figure 4.6 Box plots depicting FT vs total RNA extraction comparison in PB and BM.

Box plots show median, upper and lower quartiles and range of global mean, number of miRNAs expressed (Ct value <35) and ΔCt values of snoRNAs U6, U44 and U48. * depicts significance (student's t-test p-value <0.05). p-values are stated.

4.3.3 Initial cohort of PB and BM identified 9 miRNAs as predictive of outcome

Statistical analysis identified hsa-miR-450a, hsa-miR-200c, U6, hsa-miR-23b, hsa-miR-129-3p, hsa-miR-218-5p, hsa-miR-362-3p, hsa-miR-885-5 and hsa-miR-95-3p as having a significant correlation to survival. The analysis modelled both residual disease and doubling time for both EFS and OS, as discussed. The cumulative chi-square scores were calculated for several combinations of groupings, all shown in Table 4.5. Chi-square values greater than 10.8 indicate a p-value of <0.001 and this value was therefore chosen as a cut off to identify significant miRNAs, to allow for the multiple testing nature of the model used. Table 4.5 shows the significant miRNAs identified. The predictive significance of U6 highlights conclusions drawn in Chapter 3 about the unsuitability as a recommended control gene.

Table 4.5 miRNAs expressed in BM or PB significantly predictive of survival.

These miRNAs had a significant chi-square of greater than 10.8, representative of a p-value of 0.001. These miRNAs are predictive of EFS or OS when expressed in the PB or BM. Italics indicate miRNAs identified using the residual disease model and bold those using the doubling time model. There were no significant miRNAs identified in PB OS, PB & BM OS, or PB OS & EFS analyses.

PB EFS	BM OS	BM EFS	PB & BM EFS	BM OS & EFS	All Samples
miR-450a	**miR-200c**	*miR-129-3p*	**miR-200c**	**miR-200c**	**miR-200c**
U6	*miR-23b*	**miR-200c**	*miR-129-3p*	*miR-218-5p*	
miR-200c	*miR-200c*	*miR-218-5p*	**miR-362-3p**	*miR-129-3p*	
		miR-23b		*miR-23b*	
		miR-362-3p		*miR-200c*	
		miR-885-5p			
		miR-95			

Interestingly both miR-362-3p and miR-885-5p are linked to MCM5. In NB miR-885-5p is described to increase p53 via CDK2 and MCM5 resulting in reduced proliferation and cell survival, miR-362-3p has not been studied in NB but in cervical adenocarcinoma shows the same effects on outcome (Wang *et al.*, 2018). miR-218-

5p has also been reported in NB, not in relation to survival but an increase in expression was seen when comparing NB tumour to dorsal root ganglion (Megiorni *et al.*, 2017). miR-129-3p has not been reported within NB but in other cancers is reported to increase drug resistance and promote metastasis (Zhang *et al.*, 2015, Bijnsdorp *et al.*, 2016).

4.3.4   Validation of miR-218-5p

miR-218-5p, one of the identified 9 miRNAs from the initial analysis was validated in the second cohorts using survival analysis. For all other miRNAs p-values were greater than 0.05, showing no significance, Table 4.6. These non-significant results could therefore, have been purely chance findings, or alternatively the variability in outcomes was sufficiently large that sample sizes were insufficient to allow validation. In the initial cohort miR-218-5p was predictive of EFS in the BM, in the validation analysis it was not significant (p=0.4), however it was significant for EFS in the PB (p=0.02, Figure 4.7).

Figure 4.7 Survival vs miR-218-5p expression in PB.

> Kaplan-Meier survival curves of EFS in relation to the expression of miR-218-5p in PB at diagnosis. Red line = ΔCt of miR-218-5p equal to or less than 3, blue line = ΔCt of miR-218-5p greater than 3, n = number of samples analysed.

Table 4.6 Results of validation analyses for miRNA predictive of survival in initial cohort.

For both BM and PB cohorts each miRNA was evaluated against EFS or OS.

BM validation		
miRNA	EFS chi-square (p-value)	OS chi-square (p-value)
miR-450a	0.6 (0.4)	0.5 (0.5)
miR-200c	0.7 (0.4)	0.7 (0.4)
U6	0.7 (0.4)	1.6 (0.2)
miR-23b	0 (1)	0.3 (0.6)
miR-129	2.4 (0.1)	0.2 (0.7)
miR-218	0.9 (0.4)	0.01 (0.9)
miR-362	0.4 (0.5)	0.5 (0.5)
miR-885	0.2 (0.6)	0.4 (0.5)
miR-95	0.04 (0.8)	0.3 (0.6)
PB validation		
miRNA	EFS chi-square (p-value)	OS chi-square (p-value)
miR-450a	0.4 (0.5)	0 (1)
miR-200c	0.4 (0.5)	0.5 (0.5)
U6	0.2 (0.7)	0.5 (0.5)
miR-23b	0.2 (0.7)	0.02 (0.9)
miR-129	2.5 (0.1)	0.6 (0.4)
miR-218	5.2 (0.02)	1.7 (0.2)
miR-362	3.2 (0.07)	0.4 (0.5)
miR-885	0 (1)	0.03 (0.9)
miR-95	3.3 (0.07)	0.5 (0.5)

4.3.5 miR-21-5p, miR-95-3p and miR-376c-3p identified in the literature were predictive of survival in NB

A total of 51 miRNAs were identified from the literature as circulating biomarkers predictive of EFS. Of these 26 were present in the profile of the miRNA TLDA. The expression of these miRNAs were assessed in the validation cohorts of both PB and BM (n=100 in each). There were 3 miRNA identified as predictive of survival. Most significant was miR-21-5p which predicted both EFS and OS in BM (p<0.001 for both, Figure 4.8). miR-95-3p was predictive of EFS in PB (p=0.007, Figure 4.9) and miR-376c-3p was predictive of EFS in the BM (p=0.04, Figure 4.10).
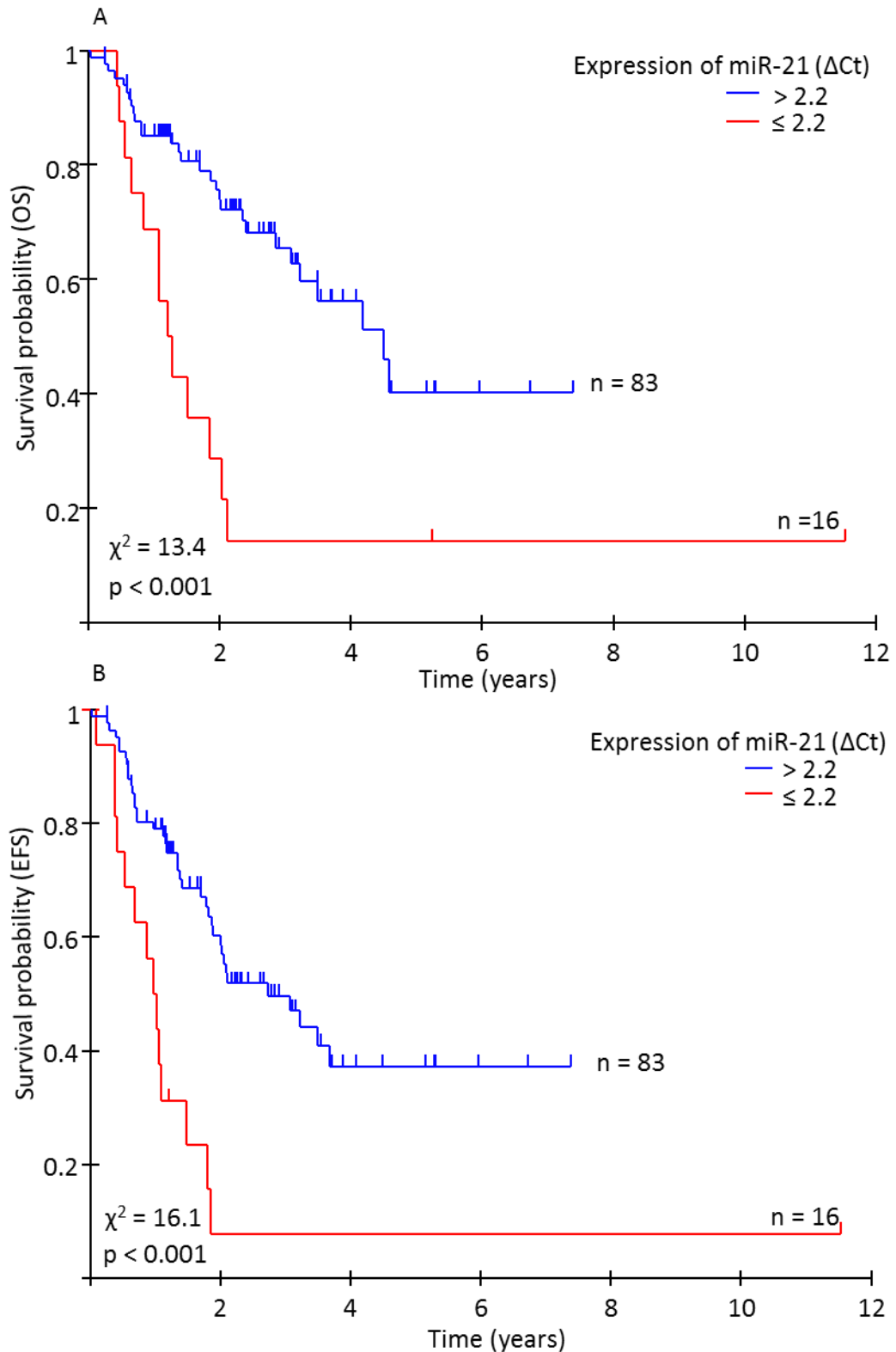
Figure 4.8 Survival vs miR-21-5p expression in BM.

Kaplan-Meier survival curves of OS (A) and EFS (B) in relation to the expression of miR-21-5p in BM at diagnosis. Red line = ΔCt of miR-21-5p equal to or less than 2.2, blue line = ΔCt of miR-21-5p greater than 2.2, n = number of samples analysed.
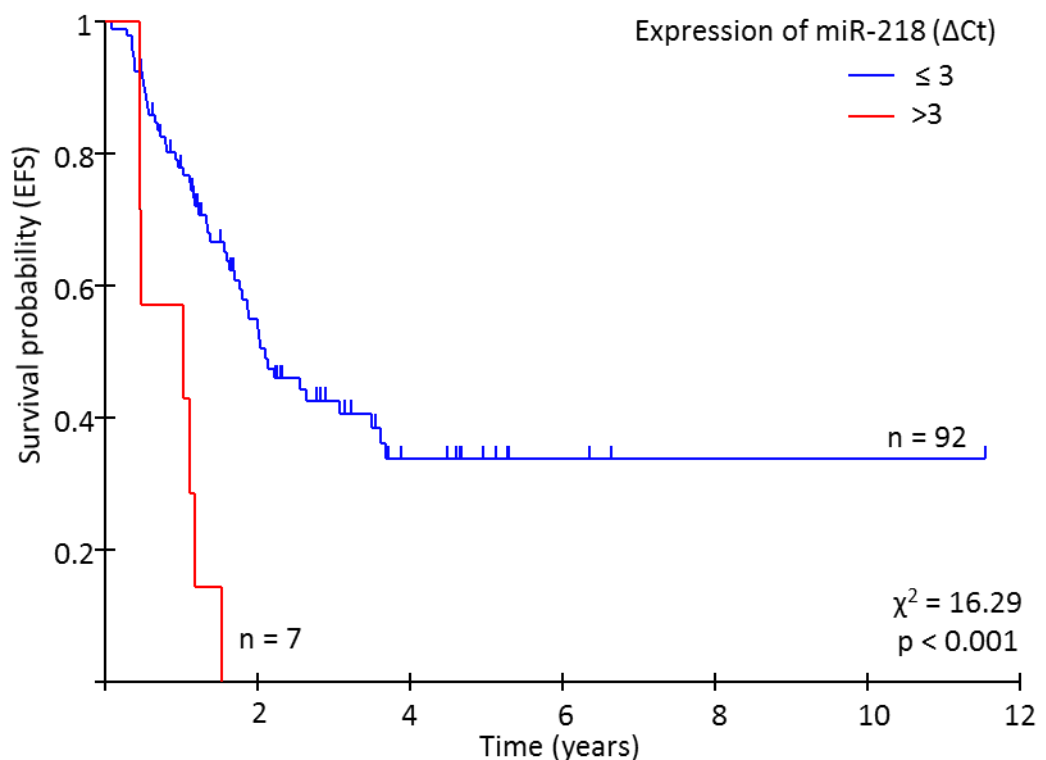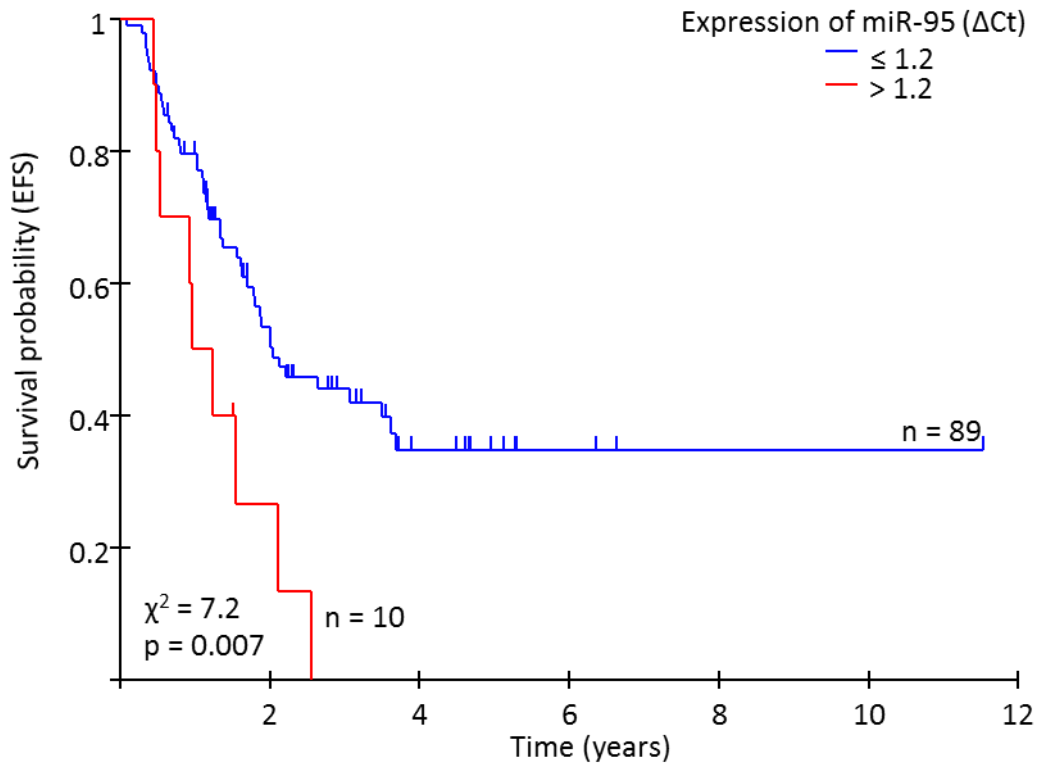
Figure 4.9 Survival vs miR-95-3p expression in PB.

Kaplan-Meier survival curve of EFS in relation to the expression of miR-95-3p in BM at diagnosis. Blue line = ΔCt of miR-95-3p equal to or less than 21, red line = ΔCt of miR-95-3p greater than 2.2, n = number of samples analysed.
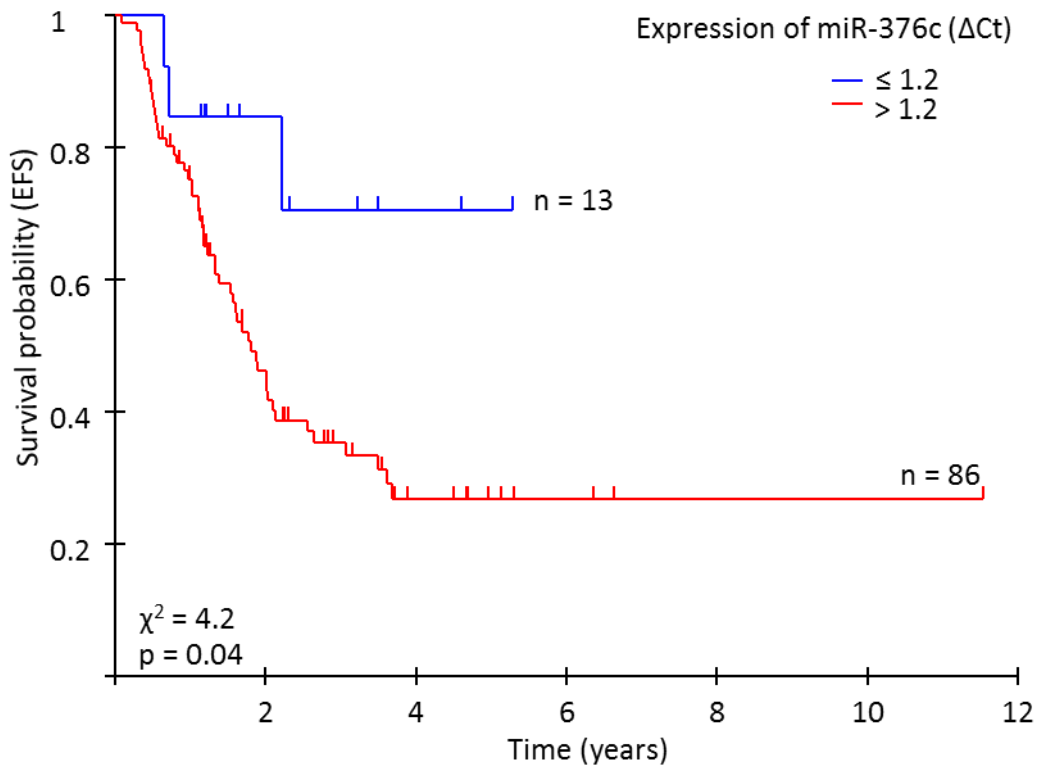
Figure 4.10 Survival vs miR-376c-3p **expression in BM.**

Kaplan-Meier survival curves of OS (A) and EFS (B) in relation to the expression of miR-376c-3p in BM at diagnosis. Blue line = ΔCt of miR-376c-3p equal to or less than 1.2, red line = ΔCt of miR-376c-3p greater than 1.2, n = number of samples analysed.

4.3.6   miRNAs significantly linked to migration detected in PB and BM

The miRNA identified in Chapter 3 as correlating with migration was miR-487a-3p. Within the PB and BM cohort (both initial and validation) there were more samples without expression of miR-487a-3p. In the BM cohort, 132 samples did not express the miRNA but there were 84 samples with detectable expression. In the PB 189 samples did not express whereas 21 did. However, miR-487a-3p was not predictive in the BM or PB.

4.3.7   miRNAs significantly linked to self-renewal detected in PB and BM

Several miRNAs were correlated with a self-renewing phenotype in Chapter 3, miR-885-5p, miR-618-5p, miR-186-5p, miR-744-5p, let-7c-5p and miR-331-5p. The presence of these miRNAs in PB and BM samples is summarised in Table 4.7. The miRNAs with the highest expression are the same for both cohorts, miR-186-5p is expressed in all BM and PB samples, and was also expressing in all NB cells profiled. Next most highly expressed in both cohorts in miR-744-5p then miR-885-5p which had the lowest number of cells expressing at only 11 (Table 3.6). In cells a high level of 885-5p correlated with a high self-renewing phenotype, contrary to the literature where high levels have shown increased p53 activation and a downregulation of proliferation. Within the BM, levels of miR-885-5p predicted EFS in the initial cohort, none of the remaining miRNAs identified as predictive of survival in BM NB cells were predictive in PB or BM.

Table 4.7 Detection of miRNA correlating with a self-renewing phenotype in BM and PB cohorts.

The number of samples expressing (Ct value <35) each of the miRNAs identified as correlated to a self-renewing phenotype. BM total is 216 samples; 116 from initial cohort and 100 from validation cohort. PB total is 210 samples; 110 from initial cohort and 100 from validation cohort.

miRNA	Number BM expressing	Number of PB expressing
miR-885-5p	171/216	186/210
miR-186-5p	216/216	210/210
miR-744-5p	212/216	208/210
let-7c-5p	102/216	68/210
miR-618-5p	114/216	108/210
miR-331-5p	117/216	34/210

4.3.8 Determining optimal methods for exosome isolation from cell culture media using SH-SY5Y

SH-SY5Y cells were used to determine the optimum methods for isolation and characterisation of exosomes from the cell media, once optimised these methods were then used to isolated and characterise exosomes from 8 primary NB cultures isolate from diagnostic BM aspirates.

4.3.8.1 Optimum media for collection of exosomes contained depleted serum

There was no difference in the growth curves between SH-SY5Y cells maintained in complete media and media supplemented with depleted serum, Figure 4.11. The growth curve of cells cultured in media without serum showed a significant decrease compared with both full media (adjusted p-value <0.0001) and depleted media (adjusted p-value <0.0001). All further experiments collected exosomes into depleted media as this did not affect the growth of the cells and would prevent isolation and characterisation of bovine exosomes.
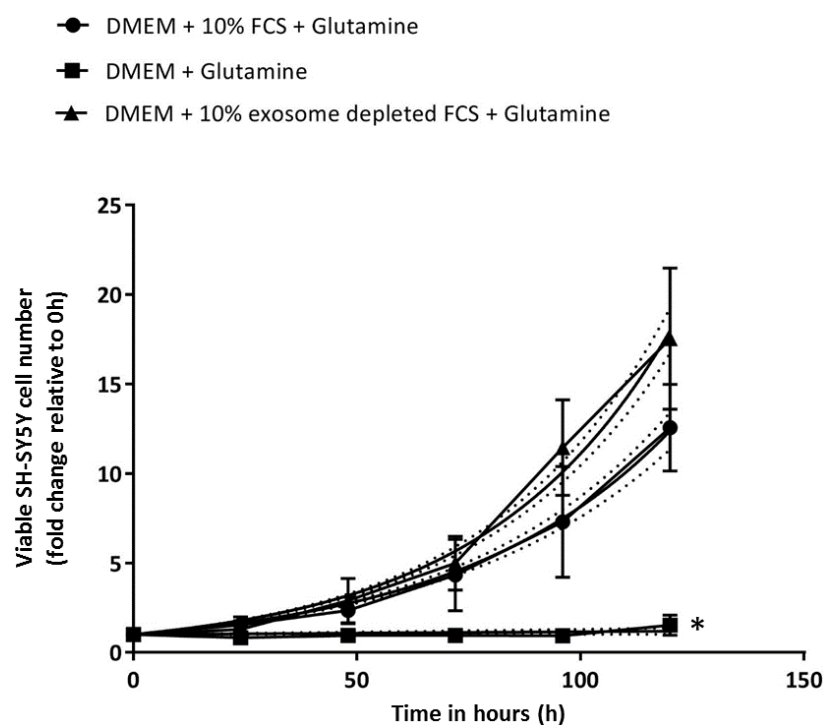
Figure 4.11 Viable SH-SY5Y cell number in different media over 120h.

> Viable cell number is expressed as fold increase to viable cell number at 0h. Cells were counted using the vi-cell after incubation in complete (DMEM + 10% FCS + 2mM glutamine), serum free (DMEM + 2mM glutamine) or depleted (DMEM + 10% depleted FCS + 2mM glutamine) media. * p<0.001.

4.3.8.2 SH-SY5Y reached 90%confluency at 48h after initial seeded at $3x10^6$

Optimal seeding density to achieve 90% confluency at 48h incubation whilst maintaining high viability was $3x10^6$ cells. As shown in Figure 4.12, cells were overly confluent when seeded at $4x10^6$ and when seeded at the lower densities the confluency was under 90% and cell morphology appeared abnormal, the cells were not adherent, rounding and potentially dying. When seeded at $3x10^6$ there was also the highest number of viable cells harvested at 48h, meaning more viable cells to produce exosomes and therefore maximum exosome harvest. All following experiments using SH-SY5Y exosomes were isolated after seeding density of $3x10^6$ cells at 0h replaced with depleted serum media at 24h and incubated for a further 48h.
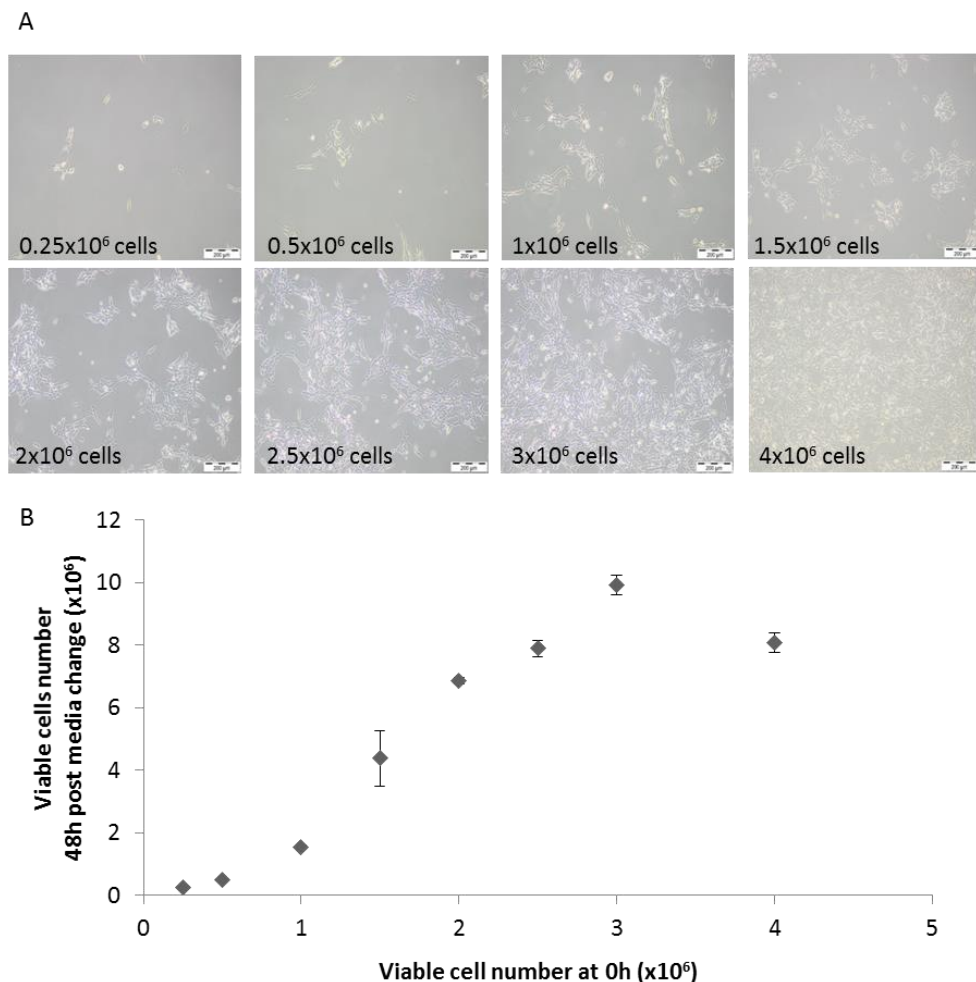
Figure 4.12 Optimisation of seeding density to achieve 90% confluency.

A, photographs of SH-SY5Y cells 48h post media change; all images taken at 10x magnification. B, cells were harvested and counted using the vi-cell, results are shown as mean ± SEM, n=9.

4.3.9 Optimal methods for sizing and quantifying exosomes isolated from NB cells

4.3.9.1 Nanoparticle tracking analysis reports exosomes isolated from NB cells of expected size

Cell Guidance Systems provide a nanoparticle tracking analysis service using the ZetaView. Results of exosomes isolated from 1 T75 flask of SH-SY5Y showed a mean ± standard deviation particle diameter of 100±41nm and a concentration of 8.75×10^8 particles per ml, resulting in a total of 1.75×10^8 particles. The primary cells showed heterogeneity in number of exosomes produced by each sample, mean value was 4000 exosomes per cell (range from 260-13,000) illustrating the range in secretion activity of different samples. All exosome samples analysed from primaries were within the expected size; range of average vesicle size 89-135nm. These sizes of particles are consistent with the reported size of exosomes. A sample of 0.1µm filtered PBS was analysed and no particles were detected.

4.3.9.2 TEM detects exosomes isolated from NB cells of expected size

Exosomes isolated from SH-SY5Y cells were observed with a reported concave morphology and with a diameter of approximately 100nm, also reported. TEM was not performed on exosomes isolated from primary BM NB cells The optimum methodology to image exosomes using TEM was to stain only with UA. Exosomes that were stained using a ratio of methyl cellulose and uranyl acetate appeared less focused than samples stained with uranyl acetate only as shown in Figure 4.13. Samples fixed in 2% PFA were less clumped, allowing observation of the concave morphology of single exosomes as illustrated in Figure 4.14.

No methyl cellulose   Methyl cellulose
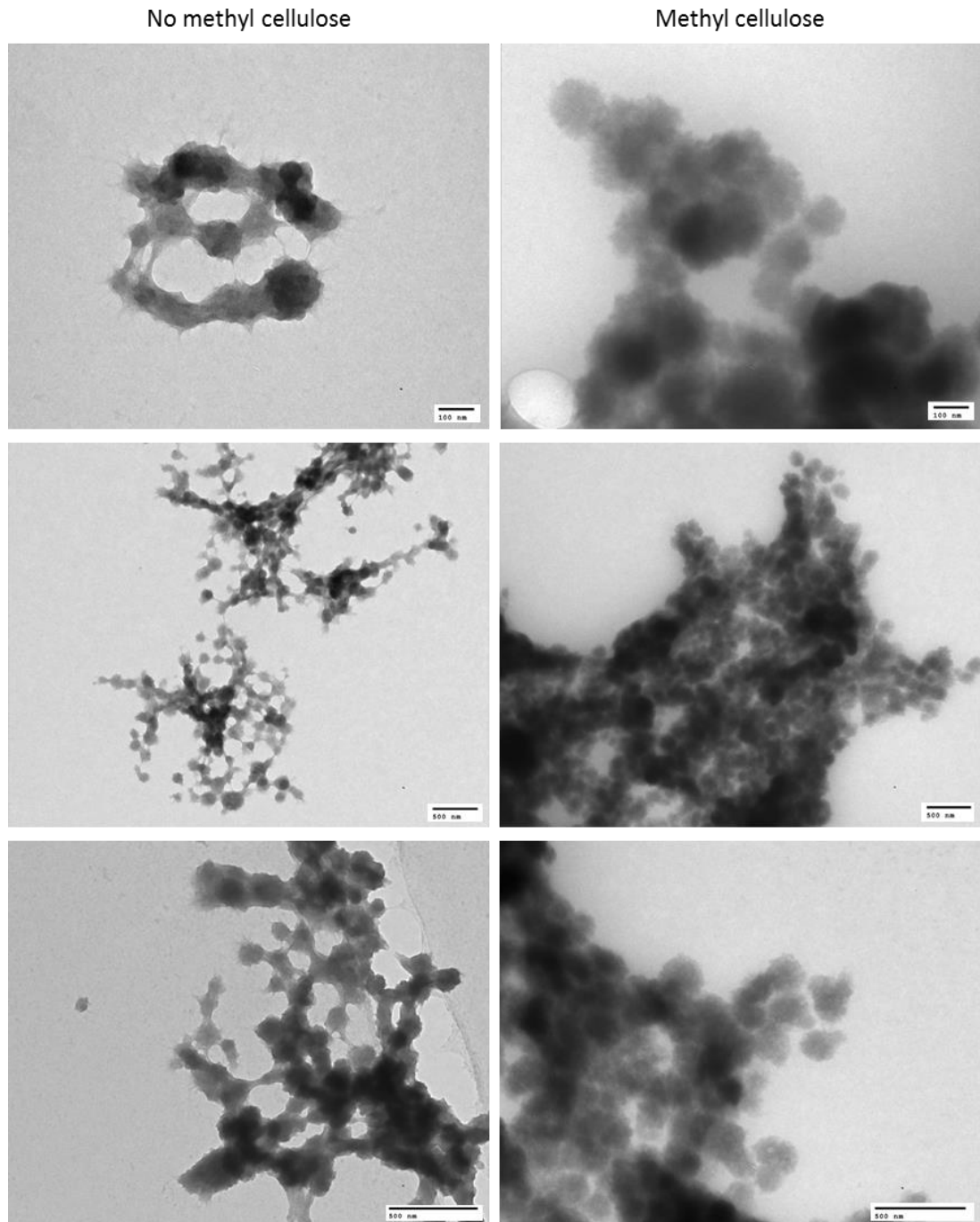
Figure 4.13 TEM images of exosomes stained with or without methyl cellulose.

Exosomes were isolated from SH-SY5Y cells and after processing were imaged using a JEM 1400 transmission electron microscope at 100Kv. Images were captured on AMT 1k CCD running on AMT c602 software. All images are taken from exosomes stained 96h post isolation resuspended in PBS.

Exosomes resuspended in PBS   Exosomes resuspended in 2% PFA
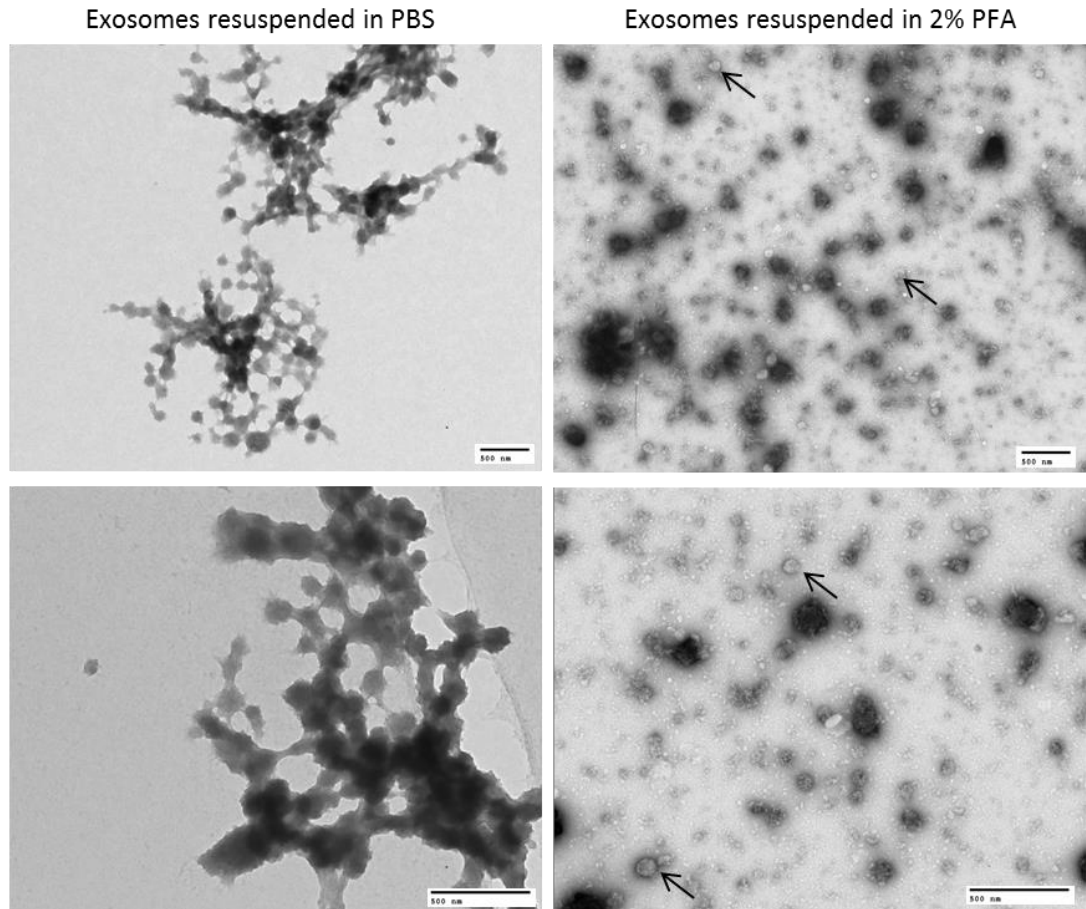
Figure 4.14 TEM images of exosomes fixed in 2% PFA or resuspended in PBS.

> Exosomes were isolated from SH-SY5Y cells and after processing were imaged using a JEM 1400 transmission electron microscope at 100Kv. Images were captured on AMT 1k CCD running on AMT c602 software. All samples were processed 96h after isolation. Single exosomes with concave morphology are highlighted by arrow.

4.3.9.3   Exosomes isolated from NB cells with a size between 100-300nm were detected and quantified using flow cytometry

SH-SY5Y exosomes were used to optimise detection of exosomes using flow cytometry. CellTrace positive vesicles ranging in size from100-900nm were recorded for all primary cultures analysed (n=8). The mean CellTrace positive event number (sizes 100-900nm) was 87,290 (n=8; range 6177-288,773) this reflects the heterogeneity seen when number was analysed using nanoparticle tracking analysis. The mean CellTrace positivity was 31% of events in the 100-900nm gate (n=8; range 11-50). Although exosomes are reported to be around 20-150nm in diameter (Lötvall *et al.*, 2014)CellTrace positive events were visualised in the 300-500nm and 500-900nm gates. These events may be larger vesicles stained with CellTrace, or doublets

and larger aggregations of exosomes. The latter is supported by the linear relationship between size and fluorescence seen in Figure 4.15. To determine if all of these vesicles detected in larger gate sizes were exosomes staining with antibodies against exosomal markers was done, see Section 4.3.10.2.
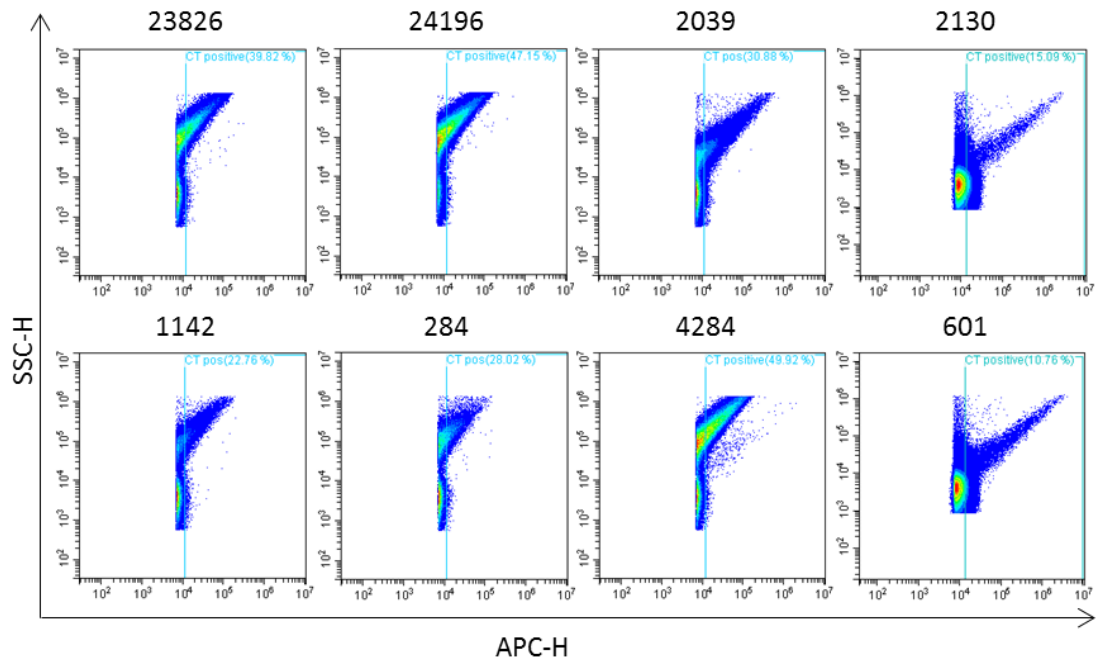
Figure 4.15 CellTrace positive exosomes isolated from BM NB cells.

Exosomes were stained with 1µM CellTrace and analysed for 2 min at a flow rate of 10µl/min. Events within 100-900nm gate are shown. The CellTrace fluorescence was measured on the APC channel. Blue gate shows CellTrace positivity as defined by a CellTrace only sample. n=8 primary exosome samples were analysed. SSC denotes side scatter.

At a concentration of 2µM the CellTrace alone generated a first-in-first-out (FIFO) abort rate of 18%, this dropped to 2% at 1µM and fell even lower for each further drop in concentration, as shown in Figure 4.16. For each concentration exosomes from the equivalent of 1, 0.5 and 0.25 million cells were stained, the optimum number of exosomes to stain was that from 0.5 million cells. At 1µM there is no difference in particle number between 0.5 or 1 million cells equivalent exosomes, as the amount of CellTrace cannot stain anymore particles, as shown in Figure 1.16.
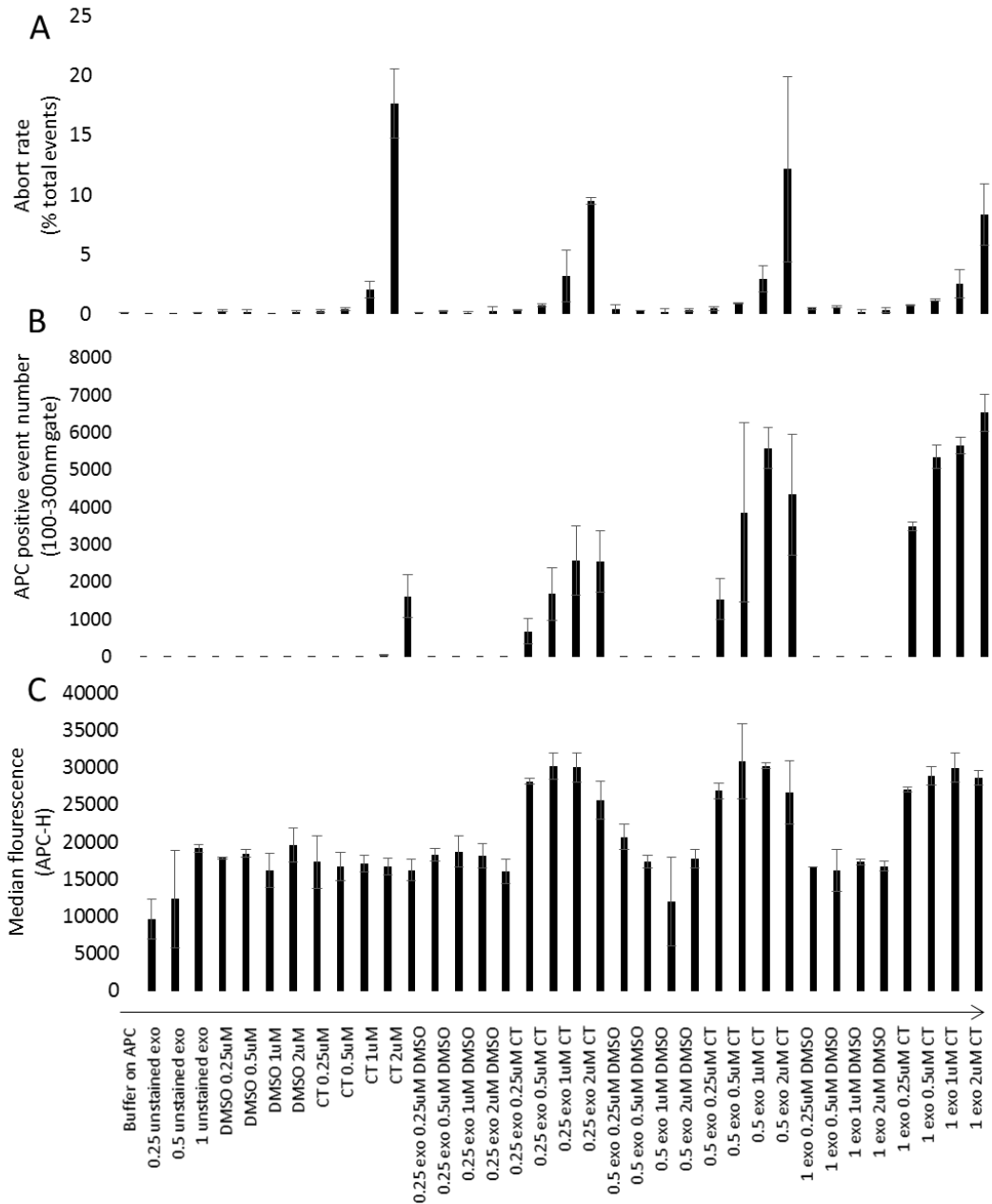
Figure 4.16 Optimisation of exosome number and CellTrace staining concentration.

Buffer (PBS), unstained exosomes and DMSO control tubes are shown. A, abort rate of each sample tube as a percentage of total events. B, APC positive event number; events within the 100-300nm gate. C, median fluorescence of APC height. All samples were run with a fluorescent APC threshold of 7,000. The APC positive gate was set using a sample of 0.1μm filtered PBS and the size gates were set using Megamix Plus FSC beads.

4.3.10 Expression of exosome specific markers

4.3.10.1 Exosome marker CD63 was detected by western blotting

SH-SY5Y exosome protein showed expression of exosomal markers CD63 and TSG-101, however, exosomal markers CD9 and cell division control protein 42 homolog (CDC42) were not detected within the SH-SY5Y exosomes. Literature suggests that exosomes from differing origins will express varying exosomal markers (Yoshioka *et al.*, 2013). The presence of 50% of the tested exosomal markers is good evidence exosomes were isolated. Further confidence comes from no presence of cellular membrane marker pan cadherin, mitochondrial markers heat shock protein (Hsp) 70, Hsp90 or Grp75, endosomal marker EEA1 or nuclear market TATA TBP within the exosomal protein extract suggesting the pellet was free from these cellular contaminants. There was also no detection of Ago2 a protein linked to circulating miRNA, suggesting no cell-free miRNA that was not packaged within exosomes had been isolated alongside the vesicles, this observation is important as circulating miRNAs contaminating the exosomal fraction would make it difficult to draw biological conclusions from the hypothesis that miRNAs profiled have importance due to active packaging. There was a band detected for β-actin within the exosomal fraction, this is widely reported within the literature, sometimes used as a loading control (Bosque *et al.*, 2016). The presence of LAMP-1, a lysosomal marker, and glyceraldehyde 3-phosphate dehydrogenase (GAPDH), a cytosolic marker, suggest impurities within the exosome fraction. Although LAMP-1 is used as a lysosomal marker, results from vesiclepedia (a publicly available database with information on extracellular vesicles www.microvesicles.org) show the detection of this protein within exosomes by mass spectrometry, flow cytometry, western blotting and TEM, suggesting this may be a true marker within exosomes rather than lysosomal impurities. GAPDH is also commonly reported to be present within exosomes isolated from a wide range of cells, including NB (Marimpietri *et al.*, 2013). All cellular markers were present within the matched SH-SY5Y cell protein extract confirming the success of immunodetection (Figure 4.17).
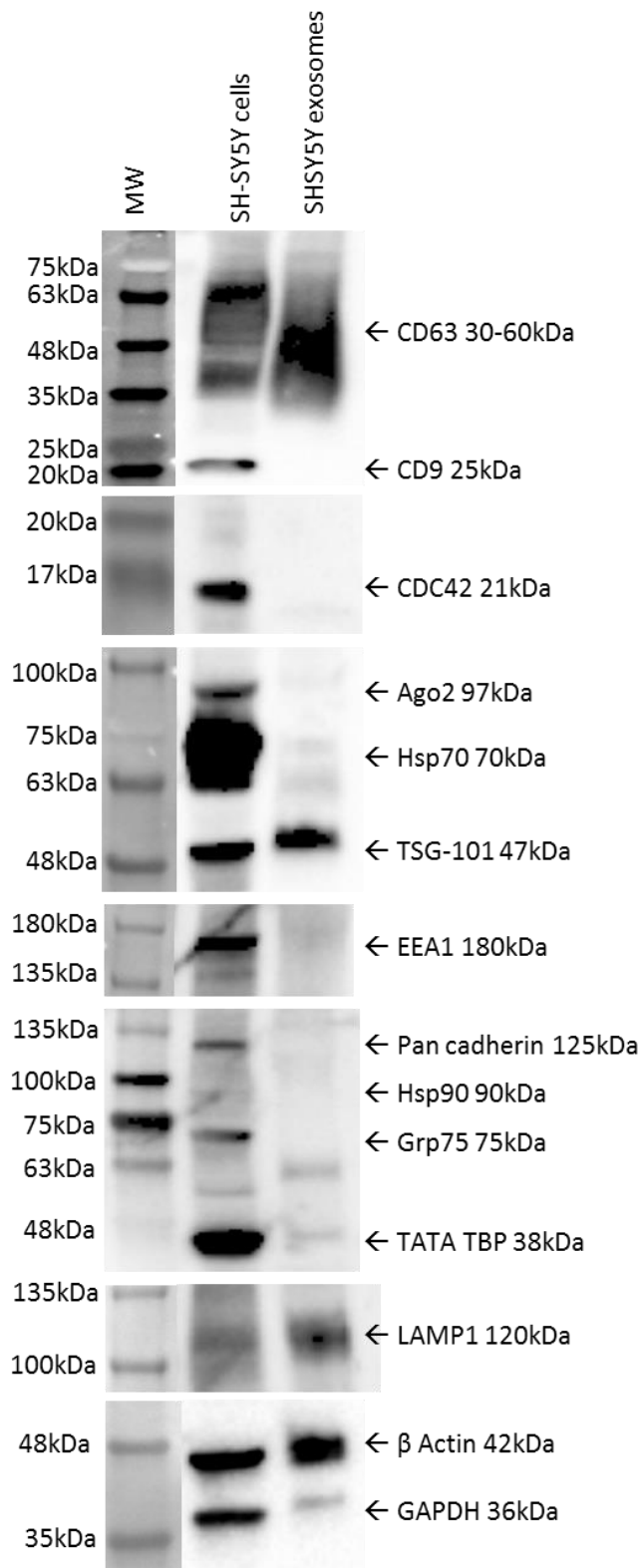
Figure 4.17 Immunodetection of exosome and cellular markers in SH-SY5Y exosome and paired cell protein

20µg of protein was loaded into each well. MW = molecular weight marker. kDa denotes kilodalton.
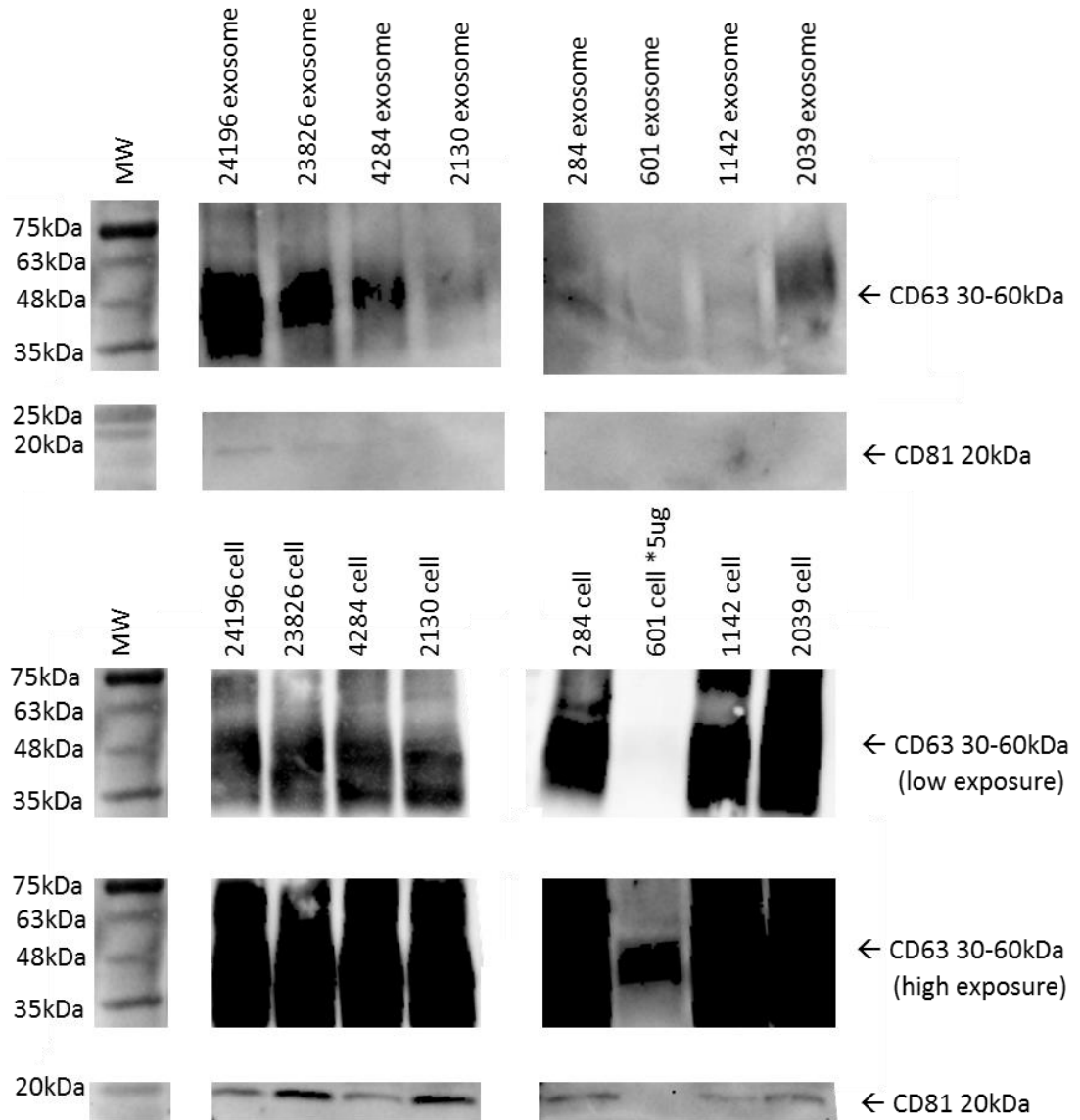
Figure 4.18 Immunodetection of exosomal markers in primary BM NB exosome and paired cell protein.

20µg of cellular protein was loaded for each primary apart from 601, denoted by *, where 5µg was loaded. A volume of 5µl of protein was loaded for each exosomal well. MW = molecular weight marker. When exposed for the time needed to detect exosomal bands (high exposure) cell extracts were over exposed for CD63, therefore a lower exposure image is also included. kDa denotes kilodalton.

Exosomes isolated from all 8 primary cultures showed expression of CD63 (Figure 4.18), with a lower intensity than that of the parent cells, this is due to lower levels of protein loaded into the exosome wells. None of the exosomes showed expression of CD81 (Figure 4.18) or TSG-101 (data not shown) but this could be a result of low level protein. For the SH-SY5Y blot 20µg of protein was needed to detect TSG-101.

There were no cellular markers detected in the exosomal fractions of the 8 primary cultures and all positive controls showed strong bands (data not shown).

4.3.10.2 Exosome markers CD63 and CD81 were detected using flow cytometry

Exosomes from 8 BM NB cells were positive for CD63, CD81 and GD_2 (Figure 4.19). Exosomes were first selected by CellTrace positivity and presence within the 100-900nm gate, see Section 4.3.9.3. This positive population was then analysed for positivity of exosomal or NB marker. Exosomal markers were present on all exosome populations; CD63 mean positivity 81% (n=8; range 50-99), CD81 mean positivity 88% (n=8, range 55-99). These results suggest that most of the vesicles isolated from BM NB cells are exosomes as they expressed exosomal markers. GD_2 expression would infer exosomes are being secreted by GD_2 positive cells, although lower than CD63 and CD81 GD_2 was detected in all exosome populations. Mean GD_2 positivity 23% (n=8; range 3-32). These results confirm I have isolated exosomes from GD_2 positive cells.
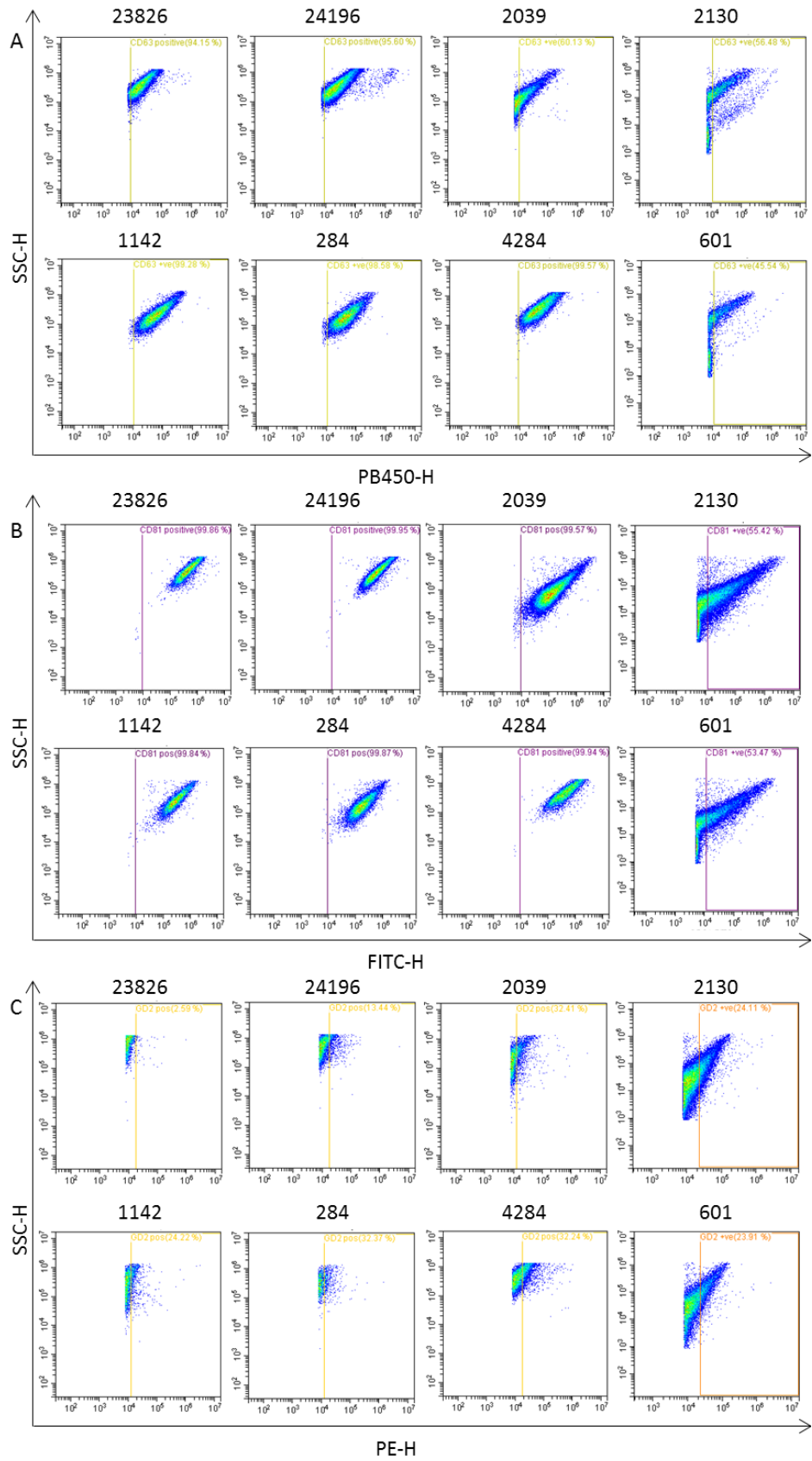
Figure 4.19 CD63, CD81 and GD₂ positive exosomes isolated from BM NB cells.

Exosomes were stained with CellTrace and for either CD63, CD81 or GD_2 then analysed for 2 min at a flow rate of 10μl/min. The CellTrace fluorescence was measured on the APC channel, CD63 on the PB450, CD81 on the FITC and GD_2 on the PE. Events within 100-900nm gate are shown. A shows CellTrace positive cells stained for CD63; B, CellTrace positive cells stained for CD81 and C, CellTrace positive cells stained for GD_2. In each case the shows marker positivity as defined by an antibody only sample. 8 primary exosome samples were analysed. SSC denotes side scatter.

4.3.11 Isolation of exosomes from clinical samples

Exosomes were successfully isolated from whole BM before GD_2 positive cells were isolated. After the initial centrifugation step (Section 2.2.3) the LAM was collected and exosomes were isolated as described in Section 0. A total of 21 exosome populations were isolated this way. These exosomes were of expected size when analysed using nanoparticle tracking analysis, mean diameter of particles was 100nm (n=9; range 58-124nm). Detection of exosomal markers CD63 and CD81 was observed. Western blot analysis detected CD63 in 100% samples (n=4) although TSG-101 was not detected in any. This is similar to the cell derived exosomes in which TST-101 was detected only in SH-SY5Y exosomes when a large amount of protein lysate was analysed. Flow cytometry analysis showed both CD63 and CD81 positive vesicles in all samples analysed (n=3). In addition, the NB marker GD_2 was detected suggesting NB cells secrete exosomes into the BM microenvironment. Small RNAs were detected in the exosomal cargo, the mean small RNA concentration was 5773pg/μl (n=5; range 22-27,845) the large range probably due to the range in cell number in each sample (wcc range 117-15,860x10^4). The cargo of these exosomes was not profiled.

4.3.12 Characterisation of isolated exosomes RNA cargo

4.3.12.1 Enrichment of small RNAs in exosome fraction

Small RNAs including miRNAs are enriched in exosomal cargo. The mean small RNA concentration as measured on the agilent significantly (p=0.03, paired t-test) increased from 68pg/μl (n=8, range 7-185) in cell RNA extract to 223pg/μl (n=8, range 141-274) in exosome RNA extract. Similarly there was a significant increase in the miRNA % of these small RNAs (p=3x10^{-5}, paired t-test). Cell RNA had a mean

miRNA % of 11% (n=8, range 1-24), in exosome RNA this increased to 60% (n=8, range 49-91).

4.3.12.2   miRNA profiles cluster into sample-centric groups

Exosomal cargo was isolated from BM derived NB cells from 4 patients, the miRNA content then profiled using miRNA TLDAs. For each of these patients the paired diagnostic BM, PB and cell profiles were available. There were 2 cell profiles; BM derived NB cells in routine culture (RCells) and BM derived NB cells used to secrete exosomes (ECells). miRNA profiles cluster into sample-centric groups rather than patient-centric, this pattern is observed both in the heat map and the PCA plot, Figure 4.20. This suggests there are more miRNAs shared within each sample type than those shared within the same patient. BM and PB samples cluster together, separated from the cell and exosome profiles Figure 4.20. Both PB and BM have a large haematopoietic component expressing the same miRNAs causing them to group within the plots. Although both cell profiles also cluster together, due to similar miRNAs from cellular processes, the two cell sub groups (ECells and RCells) show some difference in clustering in both plots.

4.3.12.3   Comparison of cellular miRNA profiles

Analysis of RCells and ECells revealed different miRNA profiles. To interrogate differences, ΔCt (normalised to the global mean) values from analysis of the RCells were deducted from the ECells analysis (ECells-RCells=change in ΔCt), miRNAs expressed (Ct <35) in only one sample type were noted. A mean of 24 miRNAs were only present in RCells, significantly higher p=0.008 (paired t-test), than in ECells (mean = 9). A single miRNA was consistently present in all ECells and absent in all RCells, miR-590-5p. This is reported to be downregulated by transforming growth factor beta (TGF-β) and further involved in this signalling pathway by inhibiting mothers against decapentaplegic homolog 3 (SMAD3) (Ekhteraei-Tousi *et al.*, 2015, Jafarzadeh and Soltani, 2016, Ouyang *et al.*, 2016). miRPath shows miR-590-5p has involvement in 3 pathways; panthothenate biosynthesis, calcium reabsorption and lung cancer. Comparing the number of miRNAs that had a greater than 2 ΔCt change in expression did not show significance, mean value of 26 miRNAs were more highly expressed in ECells and 25 had lower expression (data not shown).

The ECells were at a higher passage when pelleted after exosome isolation, 601 was 4 passages higher, 2130, 24196 and 4284 were each 1 passage greater than the RCells. This could explain some of the changes seen between the 2 profiles as changes to miRNA profiles are reported in the literature throughout increased culturing (Bonifacio and Jarstfer, 2010, Kuosmanen *et al.*, 2017). However 601, the culture with the greatest passage change is also the culture where RCells and ECells are most similar suggesting this culture is stable. A further explanation is the difference could be caused by the depleted serum culturing conditions; the ECells were harvested after exosome isolation requiring maintenance in culture media with exosome depleted FCS for 48h.
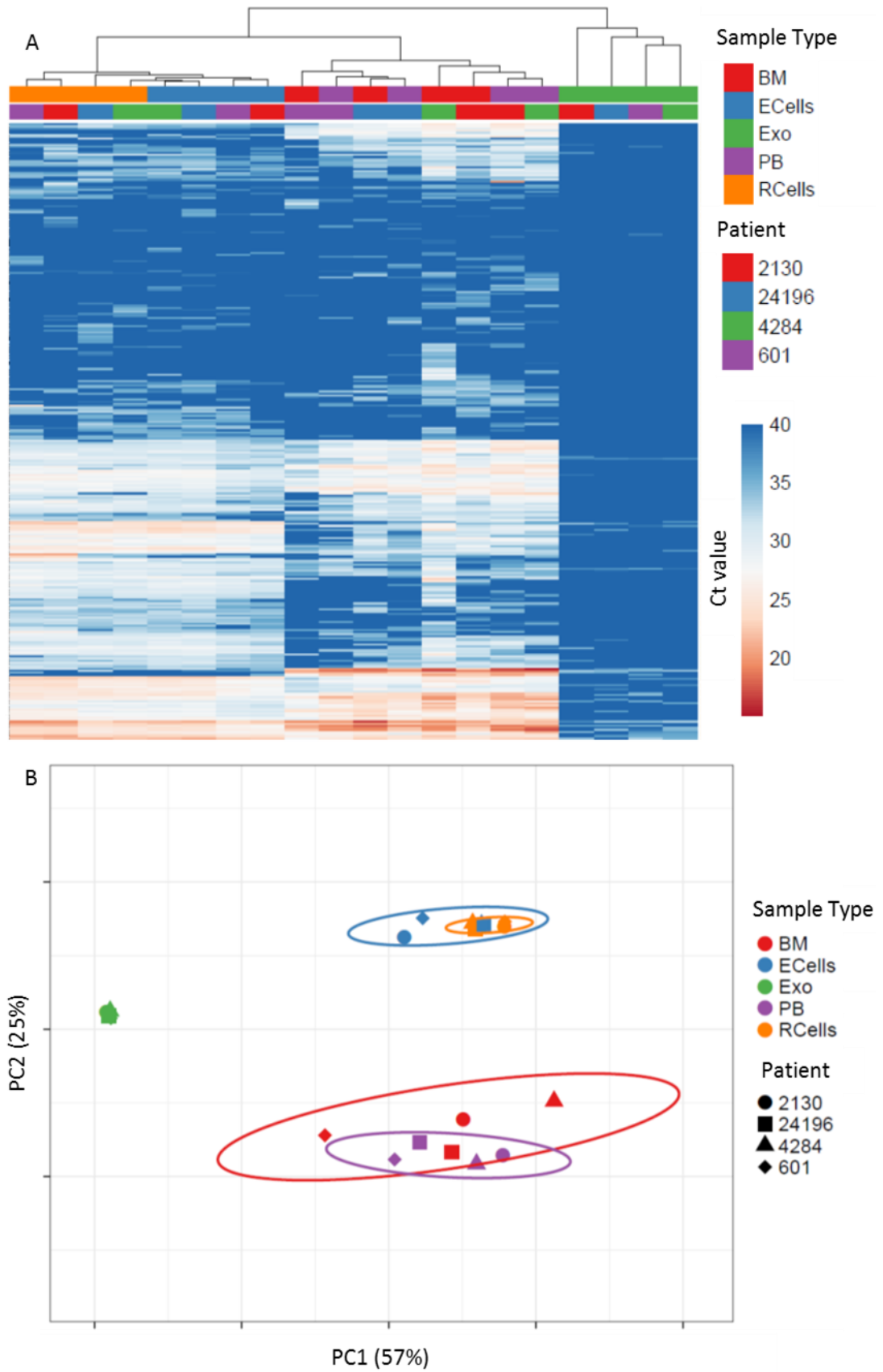
Figure 4.20 Visualisation of miRNA profiles of matched BM, PB, cells and exosomes from 4 patients.

Data was analysed using raw Ct values as insufficient numbers of miRNA are expressed to generate a global mean in the exosome profiles. Data was presented as in ClustVis as A, heatmap using hierarchical clustering for both miRNAs and samples. Similarity metrics used were Euclidean and correlation respectively. The heatmap is annotated with patient and sample type identified as individual colours. B, PCA used SVD imputation with no scaling; colour of markers indicated sample type and shape of marker indicates the patient.

4.3.12.4 Exosomal cargo contained miRNA linked to cancer pathways

The exosomes contained a significantly lower number of miRNAs than expressed in the parent cells (p=0.0003, paired t-test) with a mean expression of 146 in ECells compared with 4 in the exosomal cargo. The reduction in miRNA content of exosomes is reasoned twofold; firstly miRNAs must be actively packaged into exosomes therefore only select miRNAs will be expressed; secondly, the material that the RNA was isolated from was much less than the cells and therefore a lower RNA concentration would yield lower expression levels. There was a single miRNA expressed in all 4 exosome cargo, miR-223-3p which has been reported to be within the cargo of exosomes (Wang *et al.*, 2015b, Moen *et al.*, 2017, Poon *et al.*, 2017, Chen *et al.*, 2018). Within cells miR-223-3p is reported to increase neutrophil infiltrate and apoptosis (Bozec *et al.*, 2017). miRPath identified 15 pathways involving miR-223-3p including mitogen-activated protein kinase (MAPK), a .

4.3.13 Exosome miRNA cargo is detected in circulation

There were 36 diagnostic plasma samples analysed for miRNA expression using the miRNA TLDA. All miRNAs detected in exosomal cargo (Table 4.8) were detected in each of the 36 plasma samples, with the exception of miR-152 (27/36) and U6 (35/36). These miRNAs were also frequently detected in PB and BM samples, Table 4.8. This suggests that exosomes from NB cells isolated from the BM might circulate within the blood or BM of patients to further confirm this hypothesis exosomes from the plasma, BM or PB should be profiled for expression of GD_2.

Table 4.8 miRNAs detected in exosome presence in other sample types.

All miRNAs listed were detected in each of the primary HR NB exosome profiles with a Ct value <35.

miRNA	Number of plasma	Number of BM	Number of PB
miR-106a	36/36	224/224	210/210
miR-138	36/36	189/224	158/210
miR-150	36/36	224/224	210/210
miR-152	27/36	204/224	186/210
miR-16	36/36	224/224	210/210
miR-191	36/36	224/224	210/210
miR-222	36/36	223/224	210/210
miR-223	36/36	224/224	210/210
miR-320	36/36	224/224	210/210
miR-484	36/36	224/224	210/210
U6	35/36	224/224	210/210

4.3.13.1 miRNAs expressed in exosomes not detected in cell profiles

miR-223-3p was detected in all exosome profiles as described above. This miRNA was detected at high levels in the matched BM and PB samples (Ct range 17-22) but at low levels or not detected in the cell profiles (Ct range 31-40). These miRNAs may be produced within the cell then actively packaged within exosomes for microenvironment regulation. All other miRNAs expressed within the exosomes are also detected in paired PB BM and cell profiles.

4.4 Discussion

In this chapter circulating miRNAs were successfully isolated and profiled from BM, PB, plasma and exosomes. These miRNAs have a great potential to act as biomarkers, identifying children who will have poor outcome or highlighting candidate miRNAs for novel treatments. Although biological validation of these miRNAs was not assessed several miRNAs predictive of survival were identified.

Within the PB and BM 3 approaches yielded the identification of predictive miRNAs. When using analyses to model doubling time and residual disease 9 miRNAs were identified and miR-218-5p was validated in a secondary cohort. miR-218-5p is reported in one paper regarding expression in NB, it is observed at higher levels in NB when compared to dorsal root ganglion (Megiorni *et al.*, 2017). In wider literature miR-218-5p is reported as a TSG; in lung it elicits anti-tumour effects, with decreases leading to increased metastasis and in gallbladder cancer it restores sensitivity to gemcitabine (Zhu *et al.*, 2016, Shi *et al.*, 2017, Wang *et al.*, 2017). This agrees with results in this chapter where miR-218-5p low expression is predictive of a worse outcome. Biological validation of this result in NB cells may also identify one of the pathways described in the literature.

In the analyses where candidate miRNAs were identified using published works 3 were validated as predictive miRNAs in NB. For miR-21-5p a lower expression was predictive of good survival, a similar relationship was seen in the literature. In laryngeal squamous cell carcinoma and gastric higher expression was detected in higher levels in cancer compared to normal. In gastric cancer miR-21-5p was also detected as a circulating biomarker, within urine, and proposed as a candidate diagnostic miRNA (Kao *et al.*, 2017). Both miR-95-3p and miR-376c-3p a better survival was correlated to higher expression of the miRNA. In literature this relationship was reported for miR-376c-3p with increased expression in both gastric and human oral squamous cancer reporting over expression leading to decreased growth and other pro tumour phenotypes whilst increasing apoptosis (Tu *et al.*, 2016, Wang *et al.*, 2017b). However, contradictory findings were observed for miR-95-3p in hepatocellular carcinoma where increased expression was representative of increased tumorigenesis (Ye *et al.*, 2016).The final analyses of this kind assessed

the miRNAs correlated to phenotype identified in Chapter 2, although none were validated in the survival analyses, miR-885-5p was identified in the modelling analysis. There are several papers that evaluate circulating miRNAs within serum or plasma from NB patients but none to date that look at isolating and profiling whole PB or BM to profile for miRNA content.

Exosomes were successfully isolated and characterised from both NB cells and BM aspirates, isolated exosomes were within the reported range of 20-150nm in diameter (Lötvall *et al.*, 2014) and expressed markers including CD63, CD81 and TSG-101 (Yoshioka *et al.*, 2013, Sohel, 2016). Interestingly CD9, another reported exosomal marker, was not detected on these isolated exosomes. It may be that NB exosomes do not express CD9, as it is reported that expression of exosomal markers can vary depending on cell type, thus highlighting the importance of multiple marker analysis (Yoshioka *et al.*, 2013). In addition to isolation of exosomes from NB cells successful isolation from whole BM was achieved. Expression of GD_2 on exosome from NB cells suggests these exosomes were secreted by NB cells expressing GD_2, supporting other literature where cancer antigens have been detected on secreted exosomes (Castillo *et al.*, 2018). A subset of exosomes isolated from whole BM aspirates showed expression of GD_2, suggesting NB cells were present within the BM sample and actively secreting exosomes into the microenvironment. If GD_2 positive exosomes were detected within a patient's blood and correlated to the presence of BM cell infiltration it may be hypothesised that these NB exosomes could act as surrogates for BM metastasis or MRD using a less invasive blood test, not requiring BM aspirates to be collected.

Exosomes isolated from NB cells were successfully profiled for miRNA content. There were much fewer miRNAs detected in the exosomal cargo than in the match cells, BM or PB. This could be a reflection of biology, that a much smaller proportion of transcribed miRNAs are packaged into exosomes for secretion. It may also, and more likely, be a result of much lower RNA extraction, a limitation of the experiment, to produce a yield enabling 400ng RNA to be loaded into the RT for exosomes would require an unachievable number of cells. Within the literature miRNAs have also been isolated from NB cells, but cell lines rather than primary cultures. However,

results showed presence of MYCN related miRNAs and successful uptake of NB exosomes by recipient cells (Haug *et al.*, 2015). Similar experiments using exosomes isolated in this chapter would act as good functional validation, informing the biological relevance of the miRNAs packaged within exosomes. The presence of the miRNAs detected within exosomes alone can provide information as packaging miRNAs into exosomes is an active process allowing cells to influence surrounding cells (Bosque *et al.*, 2016). miRNAs within exosomes may therefore have a greater role in understanding biological function.

miR-223-3p was detected in the exosomal cargo of the 4 populations profiled. This miRNA has been described within the literature to inhibit cell proliferation and migration, a hypothesis that could be tested for biological validation as mentioned previously (Ding *et al.*, 2018) In addition to proliferation involvement miR-223-3p is linked to 15 pathways when interrogated using miRPath. One of these pathways is the MAPK signalling pathway, reported to compensate and cross-talk with the PI3K pathway, identified as important in NB BM cells in chapter 3 (Mendoza *et al.*, 2011). It is not surprising that a common pathway to all cells was common to all its secreted exosomes.

Within the literature there are several methodologies for isolating exosomes, the dominant technique utilising ultra-centrifugation (Livshits *et al.*, 2015). Other techniques include precipitation using binding agents such as polyethylene glycol, immunoaffinity techniques including ELIZA, magnetic sorting or size exclusion based techniques including filtration, fractionation and chromatography (Zeringer *et al.*, 2015, Li *et al.*, 2017). In this chapter an exosome affinity binding column methodology was utilised. Although ultra-centrifugation is most popular, exosomal isolations of this manner often contain protein contaminants. This in part may be resolved using additional steps but this is countered by the additional workload and costs on an already time consuming and expensive protocol. Filtration, a common size exclusion technique is limited by clogging filters resulting in trapping of vesicles and a reduced yield (Liga *et al.*, 2015, Li *et al.*, 2017). Size exclusion chromatography yields a more pure population of exosomes with reproducible data, however, it cannot be easily scaled up and requires dedicated equipment (Zeringer *et al.*, 2015).

The simplest methodology is arguably precipitation but co-precipitation of impurities is often reported (Gyorgy *et al.*, 2011). The use of immunoaffinity, including the column based approach in this chapter relied on all exosomes sharing the same biochemical trait. The column affinity exploited in the exoEasy kit is company proprietary, this method did allow isolation of a relatively large quantity of media in a reasonable amount of time. Downstream characterisation showed good evidence that vesicles isolated were indeed exosomes.

The characterisation of exosomes implemented within this chapter included verifying the size using nanoparticle tracking analysis, TEM and to some extent using flow cytometry. In addition to size markers of exosomes were confirmed using western blotting and flow cytometry. All implemented characterisation techniques are described within the literature as approaches to identify exosomes (Lötvall *et al.*, 2014). A recommendation within the literature is to ensure at least 2 different technologies are implemented to characterise vesicles which were exceeded within this chapter.

The implementation of miRNAs as circulating biomarkers for NB within the clinic is feasible, however further validation is still needed. For prognostic or predictive biomarkers larger scale validation of significance is needed and for miRNAs to be implemented as therapy a further understanding of biology and function is required. However, from these studies miRNAs have been repeatedly identified as predictively significant and successfully isolated and profiled in several circulating environments.

Chapter 5   Discussion

Through isolating and characterising self-renewing NB cells from BM aspirates of children with HR NB the aim was to identify miRNA drivers of the BM disease, informing new treatments and biomarkers to develop personalised treatments with the goal of improving outcomes. Analysis of BM NB cell miRNA profiles allowed the identification of miRNAs that were expressed in all samples. These consistently expressed miRNAs were ranked on expression level and the top 10% highest expressed used for analysis. Utilising the annotations of these miRNAs and their links within the KEGG pathway database, miRPath highlighted 10 of these miRNAs to have a role in the PI3K pathway. When primary NB cells were treated with PI3K inhibitors cell death was seen, functionally validating the experimental screening approach and the data analysis techniques used.

Proteins in the PI3K signalling cascade are among the most commonly altered in cancer (Porta *et al.*, 2014). In NB, classic mutations in the signalling genes are not present, instead its involvement was first determined through the association with MYCN (Chesler *et al.*, 2006). In addition the receptor tyrosine kinase ALK, expressed in 90% NB (Lamant *et al.*, 2000) and mutated in 7% (De Brouwer *et al.*, 2010a) is an upstream activator of PI3K signalling, adding further evidence to the importance of this pathway in NB. Increased growth, survival and drug resistance predicting poor outcome are associated with PI3K signalling (Li and Thiele, 2007, Boller *et al.*, 2008, Opel *et al.*, 2008). Enriched PI3K was predicted by miRPath in the BM NB cells isolated and agrees with the increased self-renewal and survival common to metastatic BM disease in NB. When PI3K inhibitors were used in conjunction with doxorubicin no additive effects were seen, literature reports that reduction in proliferation caused by inhibiting the PI3K pathway can reduce the effects of cell cycle chemotherapeutics (Westhoff *et al.*, 2013b) this suggests careful timings of combination therapies would need to be correctly devised to lead to increased cell death.

There have been many inhibitors developed against PI3K, and many clinical trials have utilised each, with both pan and isoform specific inhibitors being tested. Within this thesis it is not apparent which isoforms are important, to address this RNA

analysis could be performed to identify subsets of isoforms within the BM NB samples. Most pan inhibitors have not progressed in clinical development due to severe adverse effects or low pharmacokinetic efficiency. This is particularly true in solid tumours (Megison *et al.*, 2013) the poor results may be linked to high insulin levels and therefore may be overcome by combining PI3K inhibitors with a low-fat diet or inhibition of insulin (Hopkins *et al.*, 2018). More success has been reported within blood cancer with idelalisib, the first PI3K inhibitor to be licensed for the treatment of CLL, acute lymphoblastic leukaemia and follicular B-cell non-Hodgkin's lymphoma. This inhibitor is isoform specific and therefore requires careful patient selection. Specific to NB, several papers report *in vitro* benefits of PI3K inhibitors (Segerström *et al.*, 2011, Westhoff *et al.*, 2013b) and inhibition of growth of NB tumour in mouse models after treatment with PI3K inhibitors are reported (Cage *et al.*, 2015). These results are in agreement with those in this study and showing further evidence of the PI3K involvement which was highlighted within this study through miRNA profiles analysis.

Another approach to identify driver miRNAs was to assess their expression in relation to aggressive phenotypes. Self-renewal is a putative oncogenic phenotype, one that is enriched in aggressive cancer cells. Therefore, by characterising self-renewing cells and identifying miRNAs that drive this phenotype it may be possible to reveal targets for treatment. Through regression analysis 6 miRNAs were linked to self-renewal, miR-618, miR-186-5p, miR-744-5p, let-7c-5p, miR-331-5p and miR-885-5p. In the literature there are many papers which have investigated a similar hypothesis to determine miRNAs that are integral to a self-renewing phenotype, but at present there are no direct investigations between NB self-renewal and miRNAs. Interestingly miR-618 was reported within the literature to correlate negatively with migration and outcome in prostate cancer, leading to a hypothesis that higher miR-618 expression would leave to a reduced self-renewal, the converse relationship to that seen with NB self-renewal and miRNA TLDA expression data.

Isolated NB cells were also characterised for their migratory ability, again as this is a key oncogenic phenotype. In addition, migratory ability is needed for cells to metastasise to the BM and unveiling miRNAs driving this phenotype may help to

prevent recurrent metastases. From the analysis, high levels of a single miRNA, miR-487a-3p, was linked to high levels of migration. In the literature this relationship has been described in breast cancer when migration was quantified using the scratch assay (Ma *et al.*, 2013). As with self-renewal there are no papers examining the link between migration of NB cells to miRNA expression.

In my study miR-618 was the most interesting miRNA identified by association to phenotype as it produced the most significant p-value and there was a clear bimodal distribution of non-expressing and expressing samples. This expression profile made for an exciting candidate as the absence/presence pattern (binary) is beneficial in both quantification of a biomarker and exploiting the expression as a therapeutic target. For these reasons miR-618 expression was further validated. The same RNA extract used for the miRNA TLDA was assessed using A-o-D primers and probes for individual RTqPCR validation for all 50 samples. Experimental validation was essential to ensure the results from the miRNA TLDA were reproducible, as the A-o-D have a higher sensitivity, therefore an ability to detect low level expression that may return a negative result in the miRNA TLDA analysis.

The validation did not indicate correlation of expression between the miRNA TLDA and A-o-D as was expected, showing a poor R square value of 0.2. To confirm the analysis was performed correctly the raw data from both the validation A-o-D RTqPCR and the miRNA TLDA were independently evaluated assessed by Ms Samantha Brownhill. After confirming the data analysis was correct the validation A-o-D RTqPCR experiment was repeated in all 50 samples for miR-618. The correlation between the independent observer and my own A-o-D validation data sets gave R square values of 0.9, demonstrating high concordance. The lower Ct values, indicative of high expression, were not detected within the A-o-D results, leading to the conclusion these Ct values were false positives from the miRNA TLDA analysis. An investigation with Thermo Fisher is ongoing. To date several issues have been explored with Thermo Fisher. The first issue to be addressed was the interpretation of the raw data and other quality control analysis. Thermo Fisher concurred the data analysis was sufficient and correct, confirming the false positive Ct values were not as a result of poor data analysis. Further analysis of miR-618 expression across all

miRNA TLDA data recorded within the CCRG revealed the bi-modal distribution of miR-618 Ct values was not limited to BM NB cell profiles, this expression pattern was apparent in the PB, BM and plasma samples analysed within NB and Ewing's sarcoma samples. These false-positive Ct values correlated to several specific miRNA TLDA lot numbers, overall around 30% of total miRNA TLDAs used.

Thermo Fisher provided information on their lot to lot validation which involved running 2 miRNA TLDAs; one with a no template control (NTC) and another analysing synthetic RNA to assess U6 expression. The NTC tests are extremely robust and any fluorescent signal above the baseline detected will render that lot number failed. Synthetic RNA was profiled on the miRNA TLDA and the U6 Ct values are recorded. U6 is analysed over 4 wells on each miRNA TLDA, the raw Ct values are analysed, and variance of less than 0.5 Ct standard deviation is accepted within and between plates. It is unsurprising that the validation in place to assess lot to lot variation of miRNA TLDAs has been insufficient in preventing the false positive detection of miR-618 as the implementation of a snoRNA as the only quality control check would not highlight issues with any other well on the plate, miR-618 included. In updated recommendations made by Thermo Fisher snoRNAs are no longer a recommended housekeeping method, therefore should not be relied upon for detection of technical issues in lot to lot production. All miRNA performance should be evaluated during lot batch testing. This again highlights the importance of in house validation of any significant results detected using miRNA TLDAs.

In this study I have investigated the role of miRNAs rather than genomic or mRNA expression profiling because of the impact miRNAs are known to have regulating multiple gene expression and in turn the pathways they are involved in. Through these regulatory pathways miRNAs are major drivers of biological effects and function, the large downstream effects of a singular miRNA through multiple mRNA targets can control whole pathways. This allows the potential for miRNA control as a treatable strategy correcting multiple genetic aberrations. Methylation studies also allow insight into large genomic regulation, as DNA methylation interferes with the expression of multiple genes and signalling pathways, also controlling regulatory regions of miRNAs, but prove more complex both experimentally and in data

analysis. Within NB, general increased methylation status of a tumour is predictive of poor outcome. More detailed analysis of methylation status can inform pathways; more differentiated NB tumours show increased retinoic acid pathway gene expression caused by the increased expression of an aberrant splice form of DNA methyltransferase, DNMT3B7 (Ostler *et al.*, 2012). However, miRNAs can be detected in circulation as cell free miRNAs, allowing detection as biomarkers without the shedding of tumour cells.

miRNAs identified throughout this study, either as linked with phenotype or survival should be further assessed within the BM *in situ* and tumour samples. BM trephines could be utilised to look for expression of miRNAs identified or to assess if predicted pathways are amplified *in situ*, removing the chance of results being due to *in vitro* culturing effects. Within tumours, frozen samples could be used to assess expression of enriched pathways using immunohistochemistry. This would allow comparisons between primary tumour and BM metastasis, assessing if adaptations to cells are BM dwelling specific.

A single relapse sample was received and successfully cultured during the study, it is hypothesised that aggressive phenotypes would be increased and that any miRNAs enriched within the relapse could be contributing to a refractory drug resistant phenotype. It is also hypothesised that the relapse cells would have been present in the bulk tumour at diagnosis, as a sub-clone. Analysis of both profiles showed changes in miRNA expression between the diagnostic and relapse sample. A total of 124 miRNAs were expressed at similar levels in both samples (defined as within a 2 Ct range). The large amount of similar miRNAs suggest the presence of the majority of the relapse genotype within the BM disease at diagnosis, more informative would be the miRNAs that have become upregulated or have induced expression after exposure to therapy. Pathway analyses of these differing miRNAs highlighted drug metabolism pathways within the relapse sample suggesting regulation of miRNAs played a role in the drug refractory phenotype of the cells within the relapse sample.

From the diagnostic data there were other pathways identified as enriched in BM isolated NB cells, although not validated during these studies these included the focal adhesion, epidermal growth factor receptor (ErbB), mammalian target of

rapamycin (mTOR), hypoxia-inducible factor (HIF) -1 and TGF-β signalling pathway. Interestingly the mTOR, ErbB and TGF-β signalling pathways are all reported to interlink with the PI3K pathway; the ErbB heterodimer, HER3, acts as a docking site for p85, the regulatory subunit of PI3K (Arteaga and Engelman, 2014); mTOR is a downstream component of PI3K (Laplante and Sabatini, 2012); TGF-β is another upstream activator of PI3K and in turn PI3K activation can convert tumour suppressing into tumour promoting TGF-β (Zhang *et al.*, 2013). HIF-1 is a crucial pathway in survival of BM cells within a hypoxic microenvironment, working with the TGF-β pathway to increase angiogenesis (Shiozawa *et al.*, 2015). This highlights the complexity of BM disease and it can be theorised that each of these pathways would need to be validated to elicit which inhibitors would work best in conjunction to thoroughly eradicate BM disease.

NB is a complex and heterogeneous disease, even within the reduced subset of HR BM disease it can be noted that there are many sub groups based on miRNA expression, highlighted by PCA and heatmaps in Chapter 3. The above analysis has been informed by the consistencies of the miRNA profiles inferring the similarities across all BM NB samples. However, there is a great need to understand this heterogeneity to allow identification of drug resistance and other drivers of relapse and to allow optimal therapy selection, for example treating with an inhibitors when pathway enrichment is not present would not be beneficial. Expanding individual clones of these cultures would allow a more in depth analysis; through generating single cell clones the genetic heterogeneity within one patients' cell population could be interrogated more deeply.

The cells isolated from the bone marrow differ from those of the bulk tumour, although there no paired expression profiles to compare, it is clear from dendograms the tumour to BM divide is greater than the patient to patient miRNA signature. This is most likely due to the commonalities of cells thriving within the BM, such as the enrichment of the aforementioned pathways. This site signature had been described within colorectal and breast cancer (D'Amico *et al.*, 2013, Hur *et al.*, 2015). Unveiling this signature of the BM in NB may give rise to better detection or prediction of BM

metastases and ultimately lead to identification of the genetic adaptations of these cells that allows them to thrive as metastasis.

Excitingly, miRNAs may serve as good biomarkers both for diagnosis and staging of NB (Bienertova-Vasku *et al.*, 2013), many studies have identified miRNA panels that are differentially expressed in different subtypes, such as MYCN amplified and between risk groups (Chen and Stallings, 2007c, Bray *et al.*, 2009, Bienertova-Vasku *et al.*, 2013). However, the staging system within NB and allocation of risk is currently viable and miRNA biomarkers informing established stratifications do not benefit clinical practice. A miRNA would need to be of additional clinical benefit over and above current practice from the presently described and utilised tumour biology, clinical characteristics and circulating DNA or mRNA profiles that currently validated to stage or inform prognosis. Then these miRNAs may show added clinical benefit for the patients, either by detecting earlier relapse or a predicting poor response to treatment. One area that miRNA biomarkers could prove beneficial is in detection of BM metastasis which are rarely identified by mIBG scans and could be more sensitive than cytology; giving rise to earlier detection. As this project focused on these BM derived NB cells, perhaps with comparisons to matched tumour data it may be possible to derive a NB BM signature that could be screened for within children, as mentioned previously. The potential for circulating biomarkers to identify highly aggressive disease is exciting as survival rates within children with HR disease are still too low, around 40% (Cheung and Dyer, 2013). This approach of a screening test has been shown to predict clinical outcome, a subset of 'ultra' HR children can be significantly identified by mRNA levels of PHOX2B and TH mRNA in blood and identified to some extent in BM (Viprey *et al.*, 2014). miRNAs have the advantage over mRNAs of being much more stable biomarkers. Frustratingly, NB is an incredibly heterogeneous disease, this is a major obstacle for any biomarker, a true biomarker should be able to account for the heterogeneity within samples and be specific, sensitive and preferable non-invasive. Most excitingly, is the ability of miRNAs to reveal targets for therapy leading to a more personalised treatment approach.

For all these benefits to be realised robust validation must be implemented. Results from this thesis require validation in larger sample cohorts and confirming using

preclinical models to functionally validate findings. Then to test if the biomarker changes outcome if it is acted upon within a qualification study, eventually leading into clinical trials. It is also important to note that after positive validation the transfer from science to clinic is a bottleneck of progress as there are currently a wealth of papers within NB describing predictive and prognostic biomarkers, from NB specific mRNAs (Viprey *et al.*, 2014, Corrias *et al.*, 2018) to miRNA profiles (Guo *et al.*, 2010, Lin *et al.*, 2010, Schulte *et al.*, 2010b, De Preter *et al.*, 2011), currently MYCN is the only tumour biology utilised within the clinic. Is it worth remembering that many miRNAs described do not add to the stratification power of MYCN and therefore additional money and time would not be well spent introducing these miRNA into the clinic, as they do not add to the predictive power of MYCN amplification. However, MYCN amplification accounts for 25-30% of tumours, miRNAs may be informative in the remaining 70-75% of children.

Further difficulty in validation lies with low sample numbers yielding low statistical power and increasing the difficulty for testing within validation cohorts, highlighting the benefits of international group collaboration on sample collection. One of the challenges of implementing miRNAs into clinical practice is the lack of standardisation, as demonstrated within this study there is a lack of standards for miRNA reporting and normalisation within the field. Furthermore, upon implementation within the clinic, a biomarker to predict for children who will not respond to current therapies is only beneficial if alternate therapies are available to give a chance at improved outcome. Perhaps miRNA may provide further answers, not only highlighting these children predicted to have poor outcome but to highlight the pathways in which are causing their lack of response.

Tumour biopsy samples or more excitingly circulating cells or cell free miRNAs can be profiled, with potential for a range of clinical applications. Currently most biomarker studies have been retrospective and not further validated within independent cohorts; prospective studies are needed to evaluate miRNA biomarker signatures in a clinical setting. Exploiting miRNAs for therapeutic strategies is a large research area, using mimetics to reinstate tumour suppressing miRNAs and the associated pathways or knockdown strategies to target oncogenic miRNAs both offer

therapeutic benefits. To move a biomarker test into routine clinical testing blood is an attractive sample type as the sampling is minimally invasive. To implement this, or any circulating biomarker as an approach the natural variation of these miRNAs would need to be evaluated, including their presentation in healthy individuals and responses to natural influences such as time, exercise and diet. There are papers reporting changes in miRNA expression to these factors and others including circadian rhythm (Hansen *et al.*, 2011, Polakovičová *et al.*, 2016, Quintanilha *et al.*, 2017). A more thorough understanding of the biology of the biomarker miRNA would be needed to determine their true importance, for example whether they are a marker of bulk disease and are better utilised in predicting early relapse or they may be indicative of immune response or drug resistance and would be useful as a surrogate marker of response. A candidate miRNA may be the biological driver of an aggressive phenotype, whilst still predictive of outcome, proving helpful in developing therapies to treat NB. It is also useful to remember other biological samples in which biomarkers may present such as urine or saliva, presence of miRNAs has been detected in both sample types and be utilised within NB (Gallo and Alevizos, 2013, Mall *et al.*, 2013).

Within the field of NB miRNAs can serve as good biomarkers both for diagnosis and staging of NB (Bienertova-Vasku *et al.*, 2013). As mentioned above, many studies have identified miRNA panels that are differentially expressed in different subtypes, such as *MYCN* amplified and between risk groups (Chen and Stallings, 2007c, Bray *et al.*, 2009, Bienertova-Vasku *et al.*, 2013). However the staging system within NB and allocation of risk is currently viable and miRNA biomarkers informing established stratifications do not benefit clinical practice. To overcome the invasiveness of BM biopsies it would perhaps be more beneficial to be able to detect a NB BM signature within the blood of children, a possibility explored in more detail in Chapter 5. This strategy would exploit the ability of NB cells to secrete miRNAs into the microenvironment in vesicles such as exosomes. There is only one published study investigating the BM infiltrating NB cell miRNA profile. The results suggest differential expression of 160 miRNAs in the metastatic cells compared with the tumour (Stigliani *et al.*, 2015).

Exploitation of miRNAs to treat NB can be achieved by one of two strategies, miRNAs can be targeted for degradation to prevent them from aiding the cancer growth or mimetics can be administered to return depleted miRNA levels to normal for a therapeutic benefit. A combination of miRNA and siRNA therapy has been used *in vivo* to treat ovarian cancer cell lines. Reduction in tumour growth was seen after siRNA-mediated silencing of the oncogene EphA2, this was further enhanced when a miRNA targeting EphA2 was also administered (Nishimura *et al.*, 2013). This study shows the potential benefit of miRNA therapy for inclusion in a multi model strategy, by boosting existing drugs anti-tumour effects.

Upon identification of a miRNA target to be targeted using a knock-down approach it needs to be kept in mind that miRNAs have many downstream targets and that this carries a potential of severe adverse side effects, conversely it may enhance the potency of miRNA drugs, as many downstream targets may reside within the same oncogenic pathway. It could also limit the number of drugs needed as several targets could be affected with targeted by one drug potentially reducing toxicity.

There are many miRNAs identified as oncogenic, potential targets for inhibition, and tumour suppressor, ideal for replacement or mimetic therapies. One example of a putative tumour suppressive miRNA is miR-34a; a downstream target of p53 whose targets include MYCN, Bcl2, AXL, cyclins and cyclin dependant kinases, initiating G1 arrest, apoptosis and inhibiting metastasis and cell proliferation. miR-34a maps to chromosome 1p36, an area in NB commonly deleted, both *in vitro* and *in vivo* studies have shown the potential of miR-34a in the treatment of NB (Welch *et al.*, 2007, Tivnan *et al.*, 2011, Tivnan *et al.*, 2012). Replacement or mimic therapies using miR-34a have an added advantage in MYCN amplified NB as the gene is silenced by miR-34a. miR-34a has been identified in several papers for its tumour suppressing ability (Welch *et al.*, 2007, Tivnan *et al.*, 2011, De Antonellis *et al.*, 2014), an increase is seen upon p53 activation and in turn miR-34a inhibits CCNF2 and CCND1, inhibiting cell transition into S phase, preventing self-renewal. This miRNA has also been used in a therapeutic environment in mice (Tivnan *et al.*, 2012). Nanoparticles exploited NBs expression of GD_2 to accomplish targeted delivery of pre-miR-34a to tumours in the mice. Results promisingly showed reduced tumour burden and decreased

vascularisation of the mice treated with the pre-miR. Upon further investigation the reduction in vascularisation was attributed to decreased levels of TIMP2, another downstream target of miR-34a. A further benefit of treatment using miR-34a, as reported in other literature, is its inhibitory effects on *MYCN*, which in turn further reduce aggressive characteristics of tumour(Wei *et al.*, 2008). The example of miR-34a highlights the potential for targeting multiple pathways with one miRNA drug.

Currently one miRNA drug has entered clinical trial, MRX34, a mimic of the tumour suppressor miR-34 which effects multiple oncogenic pathways (Bader, 2012). As discussed in the introduction this trial was halted due to multiple immune-related serious adverse events resulting in death. However, some positive results were recorded within the trial. Within NB miR-34 has been identified as a potent tumour suppressor, with upregulation decreasing tumour growth (Welch *et al.*, 2007b, Tivnan *et al.*, 2011, De Antonellis *et al.*, 2014).

To get a functioning miRNA mimetic into cancer cells poses several challenges. The first is to create a drug that will be active as a miRNA in the cell mimicking the pre-miRNA molecule. One strategy, as above, is to create a double-stranded RNA mimic of the chosen miRNA. One strand contains the sequence identical to the miRNA and the other is a passenger strand coded to facilitate correct loading of the active strand into the RISC complex. A further obstacle is to ensure incorporation into the target cell, as miRNAs are abundant in human cells delivery to non-cancer cells should not cause any aggressive side effects, however specialised delivery could be achieved through conjugation of nanoparticles to antibodies, such as GD_2 which is a putative surface marker for NB. This has been achieved in preclinical studies of NB, targeted delivery of miRNA-34a in nanoparticles coated with GD_2 to SK-N-AS cells resulted in inhibition of growth, increased apoptosis and reduced vascularisation of tumour in mice (Tivnan *et al.*, 2012). GD_2 is uniformly expressed on NB cancer cells and is currently being exploited with antibodies (ch14.18) in NB trials and has shown improvement in patient outcome (Navid *et al.*, 2010, Fisher *et al.*, 2016). Unfortunately, there are signs of high toxicity and adverse side effects such as pain, potentially due to expression of GD_2 in peripheral nerve tissue. The possibility to use GD_2 as a beacon for targeted delivery of a miRNA mimic could prevent these side

effects and correct delivery of therapeutic miRNAs into cancer cells could allow inhibition of multiple oncogenic pathways, a unique aspect of miRNA therapy which can be used to combat the complex processes in NB.

Knockdown of miRNAs has not been used as a therapeutic strategy in clinical trial. However, it has been shown to elicit anti-tumour effects *in vivo*, SK-N-SH cells entered cell cycle arrest and apoptosis increased when treated with miR-124 inhibitor (Huang *et al.*, 2011, Murray *et al.*, 2015). Delivery of miRNA inhibitors could use the same mechanisms as currently exploited for mimetic delivery. CRISPR gene editing offers a novel therapeutic approach and has been successful in miRNA silencing (Zhao *et al.*, 2014). There are several miRNAs identified that are up-regulated in NB including miR-21, -155, -9-3p, -124-3p, -218-5p, -490-5p, -1538 that could all be potential targets for silencing using these methods(Murray *et al.*, 2015). More experimental validation is needed for the pathways and genes downstream of the dysregulated miRNA to ensure the best and most promising miRNAs are taken forward into pre-clinical studies. Some miRNAs important in NB are also relevant in other cancers and cancer in general such as miR-21, making them ideal development choices (Wang *et al.*, 2015).

The miRNA TLDA is a suitable medium throughput screening platform with high sensitivity, specificity and a large dynamic range, however, this study has highlighted the importance of validating the results of these miRNA TLDA using single target RTqPCR. Retrospectively, the choice to create a customised array with a megaplex validated against single tube expression would have given more reliable expression data. In this approach miRNAs currently annotated could still have been chosen, still allowing for current biological information to be used when relating expression profiles to pathogenesis. Other limitations arise from using an array based method including restricted well number limiting the number of miRNAs that can be profiled. This limitation does not apply when using RNA sequencing to profile miRNA expression.

RNA sequencing is highly sensitive and allows detection of novel miRNAs from little starting material. Unfortunately, sequencing is costly and is less user friendly as analysis requires specialist training. Microarrays allow screening of many miRNAs but

lack sensitivity and specificity. The aims of this study were to identify miRNAs that are linked to aggressive oncogenic phenotypes, to allow downstream identification of pathways these miRNAs are integral in or inhibitors to target these miRNAs. For this purpose, it was beneficial to identify the expression levels of miRNAs with annotated functions and target mRNAs, allowing streamlining of biological analysis and generation of validation experiments. Another contributing factor towards miRNA TLDAs is the use of this platform in the SIOPEN HR NBL 1.0, 1.5 and 1.7 study where bloods and bone marrows, some from matched patients where BM NB cultures were obtained, were profiled on the same platform. This allows analysis across sample types which is explored in Chapter 5. The miRNA TLDA can be performed with starting material of 100ng RNA, lesser starting amounts require a pre-amp step which adds further variation, increasing the number of miRNA probes highlighted to perform less well (Thermo Fisher correspondence) and the potential introduce amplification bias (Chen *et al.*, 2009).

As the platform was already in use on the SIOPEN clinical trial it was important to keep the experimental procedure standardised to allow analysis across groups. As is most common in current practice, the standard operating procedure (SOP) for the trial loaded a fixed amount of RNA (400ng) of each sample to assess miRNA expression. To assess how suitable this method is, a small cohort of samples were run in repeat, one miRNA TLDA with 400ng RNA loaded, another with 21pg miRNA loaded. This amount of miRNA was chosen as it was the maximum that could be loaded (in 3.2µl) from the sample with the lowest miRNA content. As there is no relationship between the concentration of miRNA and RNA it would be hypothesised that loading a set amount of miRNA would be more informative. However, it is important to keep in mind that loading with miRNA presents challenges, as measuring miRNA concentrations proves difficult and costly being imprecise and more variable.

Another challenge faced using the miRNA TLDAs is upon reporting the data. Across published datasets there is no standard to which data is analysed, normalised or reported. In these data we used an automatic baseline which is calculated across the cycles where only noise is detected, normally cycles 3-15. A manually set threshold

of 0.2, was chosen for its position as all curves were in exponential phase and parallel to one another. The normalisation methodology was tested and the global mean determined as optimal in both the NB cells, PB, BM and in a small amount of tumour data received. When U6, a small nucleolar RNA was evaluated as a reference gene a large amount of experimental noise was added to the data. The use of U6 as a reference is common in published data sets as it was recommended endogenous gene by Thermo Fisher. A final obstacle in reporting the miRNA TLDA results was those at which the Ct value was determined to be 35 or above. Higher variation occurs when Ct values reach 35-40 and are not reproducibly detected, therefore, no different to a value of 'undetermined', for this reason any miRNA with a Ct value of 35 or above was denoted as not expressed.

When isolating the NB cells from BM aspirates it is important to remain aware of the changes acquired when removing these cells from the BM microenvironment and propagating the cells on plastic. The changes to miRNA profile upon culturing are apparent when clustering was used to assess profiles derived NB cells isolated from BM aspirates in the Giannina Gaslini Institute, where the cells were not further cultured but RNA was extracted upon isolation to those profiled from cells cultured in this study; both groups clustered on different arms of the dendograms. Propagation of the BM derived NB cells was necessary to allow full characterisation including self-renewing and migratory phenotypes. It may be hypothesised that by co-culturing the tumour cells with BM cells through an *in vitro* model a truer image could be recapitulated. This method has been explored using spheroids of NB cell lines with promising results as cells showed rosette like morphology, concordant with NB tumour structure (Yeung *et al.*, 2015). However, more development is needed in such models to incorporate other parameters of cancer such as vasculature. Also this model has not been validated using primary cultures which are more informative than cell lines that have been cultured for many years. Over this time cell lines adapt, changing their miRNA profiles as can be seen when cluster analysis between primary and cell lines was performed. Subcutaneous injection of primary cells into mice did not yield tumour growth however they are yet to be tested for growth when implanted into the adrenal orthotopic site or within the BM

environment, it could be hypothesised that the BM injections would yield the best results for growth as the isolated cells have adapted to best thrive in the BM niche.

A second limitation in isolating NB cells from BM aspirates is the methodology used to do so, through selecting GD_2 positive cells only, any NB cells not expressing this marker would be lost. Within the diagnostic samples no expansion was seen in the negative population, however if more relapse samples were collected this may pose a greater risk as there is some evidence GD_2 is decreased in NB cells after treatment (Schumacher-Kuckelkorn *et al.*, 2017).In my study, the eventuality of GD_2 negative cells is covered through collection and culture of negative cells, therefore any NB cells without GD_2 expression would still propagate.

Packaging into exosomes, high-density lipoproteins or association with Ago proteins, protects miRNAs against processing by ribonucleases. After extraction it has been shown that miRNAs remain stable for up to 12 months when stored at -70°C (Sourvinou *et al.*, 2013), thus making exosomes an good candidate to profile for miRNA biomarkers. The exosome work within this study was limited due to time, in further studies the miRNA cargo could be further explored to better understand the biology of these biomarkers. The packaging and secretion of exosomes and their miRNA cargo is an active cellular process, suggesting the contents are of great importance to cellular process, and in turn may inform novel therapeutics. The biology of exosomes can be further exploited as a novel targeted delivery system of chemotherapeutics, with the ability to evade the host immune system and have a long circulatory capability. By labelling exosomes with GD_2 it is possible to deliver higher concentrations of drug to only NB cells, minimising side effects. This approach has been utilised in clinical trials for patients with advanced pancreatic cancer (Dhillon *et al.*, 2008). More relevant to NB is the packaging of doxorubicin, a drug used to treat NB, which showed promising uptake in zebrafish and mice models (Tian *et al.*, 2014, Yang *et al.*, 2015) and further benefits with suppression of tumour growth confirming the ability for exosomes to deliver the doxorubicin efficiently.

In this study I have shown the importance of miRNA expression validation and the promise in the approach of identifying both biomarkers and potential therapeutic pathways in NB cells within the BM. Further studies would include functional

validation of biomarkers; for miRNAs significantly related to outcome what happens if these miRNAs are knocked down within cells, it could be hypothesised they die or reduce in self-renewing ability.

To further recapitulate the *in vivo* attributes of BM NB cells, co-culturing the primary cells with factors constituting the BM microenvironment in 3D models including mesenchymal stem cells or immune cells. The BM microenvironment could be more easily mirrored through culturing primary cells under hypoxic conditions. Using the isolated cells to screen for drugs or drug combinations could identify candidate strategies to eradicate BM disease.

A further biomarker analysis would move to incorporate later time point BM and PB samples to identify if changes in miRNA profiles could be used as surrogates for predicting toxicity or response in children.

In conclusion, there is great value in the NB cells isolated from BM aspirates and their potential to unveil miRNAs integral in the disease can lead to the design of personalised adaptive therapies, driven by biology, ultimately improving the outcome of children with HR NB.

Commercial Suppliers

Abcam
330 Cambridge Science Park,

Cambridge,

CB4 0FL, UK

www.abcam.com

Addgene
75 Sidney Street, Suite 550A,

Cambridge

Massachusetts,

02139, USA

www.addgene.org

AGAR Scientific
Unit 7, M11 Business Link,

Parsonage Lane,

Stansted,

Essex,

CM24 8GF, UK

www.agarscientific.com

Agilent
5301 Stevens Creek Blvd,

Santa Clara,

California,

95051, USA

www.agilent.com

Amity International
Libra House, West Street,

Worsborough Dale,

Barnsley,

S70 5PG, UK

www.amityinternational.com

BD Biosciences
Edmund Halley Road,

Oxford Science Park,

Oxford,

OX4 4DQ, UK

www.bdbioscience.com

Beckman Coulter
Oakley Court,

Kingsmead Business Park, London Road
Buckinghamshire,

HP11 1JU, UK

www.beckman.com

Bibby Scientific Ltd
Beacon Road,

Stone,

Staffordshire,

ST15 0SA, UK

ww.techne.com

Bio-Rad Laboratories
Bio-Rad House,

Maxted Road,

Hemel Hempstead,

Hertfordshire, HP2 7DX, UK

www.bio-rad.com

Biocytex   140 Chemin de l'Armée d'Afrique,

13010 Marseille,

France

www.biocytex.com

Cambridge Bioscience   Munro House,

Trafalgar way,

Cambridge,

CB23 8SQ, UK

www.bioscience.co.uk

Cell Signalling Technology 3 Trask Lane,

Danvers,

Massachusetts, 01923, USA

www.cellsignal.com

GE Healthcare   Amersham Place,

Little Chalfont,

Buckinghamshire,

UK, HP7 9NA

www.amershambiosciences.com

Geneflow Ltd

Paul Fisher House,

 1 The Sycamore Tree,

Elmhurst Business Park,

Elmhurst, Lichfield, Staffordshire,

WS13 8EX, UK

www.geneflow.co.uk

Gilson

3000 Parmenter Street

PO Box 620027

Middleton,

WI 53562-0027, USA

www.gilson.com

GraphPad Software

7825 Fay Avenue, Suite 230,

La Jolla

California,

92037, USA

www.graphpad.com

IBM Ltd

PO Box 41,

North Harbour,

Portsmouth, Hampshire,

PO6 3AU, UK

www.ibm.com

IKA England Ltd

Pure Offices

Suite 1 Fountain House

John Smith Drive

Oxford Business Park, Oxford

OX4 2JY, UK

www.ika.com

Interactive Software Ltd

Ashted Lock,

Birmingham Science Park Aston,

Birmingham,

B7 4AZ , UK

ww.achievermedical.com

JEOL

11 Dearborn Road,

Peabody, Massachusetts,

USA, 01960

www.jeolusa.com

Labtech International Ltd

2 Birch House,

Brambleside,

Bellbrook Industrial Estate,

Uckfield, East Sussex,

TN22 1QQ , UK

ww.labtech.com

Merck

Croxley Green Business Park,

Watford,

Hertfordshire,

WD18 8YH, UK

www.merkmillipore.com

Miltenyi Biotech

Almac House,

Church Lane,

Bisley, Surrey,

GU24 9DR, UK

ww.miltenyibiotec.com

Mirus Bio

545 Science Drive,

Madison, Wisconsin,

USA, 53711

www.mirusbio.com

New England Biolabs

75-77 Knowl Piece,

Wilbury Way,

Hitchin,

Hertfordshire,

SG4 0TY, UK

www.neb.uk.com

Nikon

380 Richmond Road,

Kingston Upon Thames,

Surrey,

KT2 5PR, UK

www.nikoninstruments.com

Olympus

KeyMed House,

Stock Road,

Southend-on-Sea,

Essex,

SS2 5QH, UK

www.olympus.co.uk

Oxoid Limited

Wade Road,

Basingstoke,

Hampshire,

RG24 8PW, UK

www.oxoid.com

Particle Metrix

Wildmoos 4,

82266 Inning am Ammersee

Germany

www.particle-metrix.de

Promega

Delta House,

Southampton Science Park,

Southampton,

SO16 7NS, UK

www.promega.co.uk

Qiagen

Skelton house,

Lloyd Street,

North Manchester,

M15 6SH, UK

ww.qiagen.com

Santa Cruz

10410 Finnell Street,

Dallas,

Texas,

75220, USA

www.scbt.com

Sanyo Gallenkamp Plc

The Office Village,

Loughborough,

Leicestershire,

LE11 1QJ, UK

www.sanyo-biomedical.co.uk

Sarstedt Ltd

Sarstedtstaße 1

51588 Nümbrecht,

Germany

www.sarstedt.com

Sigma

3050 Spruce St.,

St. Louis, MO,

63103, USA

www.sigmaaldrich.com

SLS

Wilford Industrial Estate,

Ruddington Lane,

Wilford,

Nottingham,

NG11 7EP, UK

ww.scientificlabs.co.uk

Thermo Fisher

Inchinnan Business Park,

3 Fountain Drive,

Paisley,

PA4 9RF, UK

www.thermofisher.com

Tristel

Lynx Business Park,

Fordham Road,

Snailwell,

Cambridgeshire,

CB8 7NY, UK

ww.tristel.com

VWR   Hunter Boulevard, Magna Park

Lutterworth, Leicestershire,

LE17 4XN, UK

www.uk.vwr.com

Appendix A

miRNA TLDA human A card contents

The miRNA TLDA human A card was used throughout this thesis to profile the expression of 377 miRNAs, 3 snoRNAs and 1 *Arabidopsis thaliana* miRNA. Details of each well are shown below. Highlighted in green are the 6 wells to analyse snoRNAs; 1 repeat of U44 and U48 and 3 repeats of U6. In red is the well for analysis of the *Arabidopsis thaliana* miRNA

List of References

A. KESROUANI, F. D., M. SEILANIAN, J. M. MURAY 1999. Prenatal diagnosis of adrenal neuroblastoma by ultrasound: a report of two cases and review of the literature. *Ultrasound Obstet Gynecol,* 13**,** 446-449.

ABBASI, M. R., RIFATBEGOVIC, F., BRUNNER, C., LADENSTEIN, R., AMBROS, I. M. & AMBROS, P. F. 2015. Bone marrows from neuroblastoma patients: an excellent source for tumor genome analyses. *Mol Oncol,* 9**,** 545-54.

ABEL, F., DALEVI, D., NETHANDER, M., JORNSTEN, R., DE PRETER, K., VERMEULEN, J., STALLINGS, R. L., KOGNER, P., MARIS, J. & NILSSON, S. 2011. A 6-gene signature identifies four molecular subgroups of neuroblastoma. *Cancer Cell International,* 11**,** 1-15.

ALAN D. SMITH, D. R., TIMOTHY A. YAP 2014. Strategies for modern biomarker and drug development in oncology. *Jounal of Hematology & Oncology,* 7**,** 1-16.

ALTHOFF, K., LINDNER, S., ODERSKY, A., MESTDAGH, P., BECKERS, A., KARCZEWSKI, S., MOLENAAR, J. J., BOHRER, A., KNAUER, S., SPELEMAN, F., EPPLE, M., KOZLOVA, D., YOON, S., BAEK, K., VANDESOMPELE, J., EGGERT, A., SCHRAMM, A. & SCHULTE, J. H. 2015. miR-542-3p exerts tumor suppressive functions in neuroblastoma by downregulating Survivin. *Int J Cancer,* 136**,** 1308-20.

AMBROS, P. F., AMBROS, I. M., BRODEUR, G. M., HABER, M., KHAN, J., NAKAGAWARA, A., SCHLEIERMACHER, G., SPELEMAN, F., SPITZ, R., LONDON, W. B., COHN, S. L., PEARSON, A. D. & MARIS, J. M. 2009. International consensus for neuroblastoma molecular diagnostics: report from the International Neuroblastoma Risk Group (INRG) Biology Committee. *Br J Cancer,* 100**,** 1471-82.

AMBROS, V., BARTEL, B., BARTEL, D. P., BURGE, C. B., CARRINGTON, J. C., CHEN, X. M., DREYFUSS, G., EDDY, S. R., GRIFFITHS-JONES, S., MARSHALL, M., MATZE, M., RUVKUN, G. & TUSCHL, T. 2003. A uniform system for microRNA annotation. *RNA,* 9**,** 277-279.

ANDERSEN, C. L., JENSEN, J. L. & ORNTOFT, T. F. 2004. Normalization of real-time quantitative reverse transcription-PCR data: a model-based variance estimation approach to identify genes suited for normalization, applied to bladder and colon cancer data sets. *Cancer Res,* 64.

ARA, T., SONG, L., SHIMADA, H., KESHELAVA, N., RUSSELL, H. V., METELITSA, L. S., GROSHEN, S. G., SEEGER, R. C. & DECLERCK, Y. A. 2009. Interleukin-6 in the bone marrow microenvironment promotes the growth and survival of neuroblastoma cells. *Cancer research,* 69**,** 329-337.

ARTEAGA, CARLOS L. & ENGELMAN, JEFFREY A. 2014. ERBB Receptors: From Oncogene Discovery to Basic Science to Mechanism-Based Cancer Therapeutics. *Cancer Cell,* 25**,** 282-303.

ASADI, J., FERGUSON, S., RAJA, H., HACKER, C., MARIUS, P., WARD, R., PLIOTAS, C., NAISMITH, J. & LUCOCQ, J. 2017. Enhanced imaging of lipid rich nanoparticles embedded in methylcellulose films for transmission electron microscopy using mixtures of heavy metals. *Micron,* 99**,** 40-48.

ASGHARZADEH, S., PIQUE-REGI, R., SPOSTO, R., WANG, H., YANG, Y., SHIMADA, H., MATTHAY, K. K., BUCKLEY, J., ORTEGA, A. & SEEGER, R. C. 2006. Prognostic

significance of gene expression profiles of metastatic neuroblastomas lacking MYCN gene amplification. *Journal of the National Cancer Institute,* 98**,** 1193-1203.

BADER, A. G. 2012. miR-34 - a microRNA replacement therapy is headed to the clinic. *Front Genet,* 3**,** 120.

BARCO, S., GENNAI, I., REGGIARDO, G., GALLENI, B., BARBAGALLO, L., MAFFIA, A., VISCARDI, E., DE LEONARDIS, F., CECINATI, V., SORRENTINO, S., GARAVENTA, A., CONTE, M. & CANGEMI, G. 2014. Urinary homovanillic and vanillylmandelic acid in the diagnosis of neuroblastoma: report from the Italian Cooperative Group for Neuroblastoma. *Clin Biochem,* 47**,** 848-52.

BATE-EYA, L. T., EBUS, M. E., KOSTER, J., DEN HARTOG, I. J., ZWIJNENBURG, D. A., SCHILD, L., VAN DER PLOEG, I., DOLMAN, M. E., CARON, H. N., VERSTEEG, R. & MOLENAAR, J. J. 2014. Newly-derived neuroblastoma cell lines propagated in serum-free media recapitulate the genotype and phenotype of primary neuroblastoma tumours. *Eur J Cancer,* 50**,** 628-37.

BECKERS, A., VAN PEER, G., CARTER, D. R., METS, E., ALTHOFF, K., CHEUNG, B. B., SCHULTE, J. H., MESTDAGH, P., VANDESOMPELE, J., MARSHALL, G. M., DE PRETER, K. & SPELEMAN, F. 2015. MYCN-targeting miRNAs are predominantly downregulated during MYCNdriven neuroblastoma tumor formation. *Oncotarget,* 6**,** 5204-16.

BEG, M. S., BRENNER, A. J., SACHDEV, J., BORAD, M., KANG, Y. K., STOUDEMIRE, J., SMITH, S., BADER, A. G., KIM, S. & HONG, D. S. 2017. Phase I study of MRX34, a liposomal miR-34a mimic, administered twice weekly in patients with advanced solid tumors. *Invest New Drugs,* 35**,** 180-188.

BEISKE, K., BURCHILL, S. A., CHEUNG, I. Y., HIYAMA, E., SEEGER, R. C., COHN, S. L., PEARSON, A. D. & MATTHAY, K. K. 2009. Consensus criteria for sensitive detection of minimal neuroblastoma cells in bone marrow, blood and stem cell preparations by immunocytology and QRT-PCR: recommendations by the International Neuroblastoma Risk Group Task Force. *Br J Cancer,* 100**,** 1627-37.

BIENERTOVA-VASKU, J., MAZANEK, P., HEZOVA, R., CURDOVA, A., NEKVINDOVA, J., KREN, L., STERBA, J. & SLABY, O. 2013. Extension of microRNA expression pattern associated with high-risk neuroblastoma. *Tumour Biol,* 34**,** 2315-9.

BIJNSDORP, I. V., HODZIC, J., LAGERWEIJ, T., WESTERMAN, B., KRIJGSMAN, O., BROEKE, J., VERWEIJ, F., NILSSON, R. J. A., ROZENDAAL, L., VAN BEUSECHEM, V. W., VAN MOORSELAAR, J. A., WURDINGER, T. & GELDOF, A. A. 2016. miR-129-3p controls centrosome number in metastatic prostate cancer cells by repressing CP110. *Oncotarget,* 7**,** 16676-16687.

BOCKMEYER, C. L., SÄUBERLICH, K., WITTIG, J., EßER, M., ROEDER, S. S., VESTER, U., HOYER, P. F., AGUSTIAN, P. A., ZEUSCHNER, P., AMANN, K., DANIEL, C. & BECKER, J. U. 2016. Comparison of different normalization strategies for the analysis of glomerular microRNAs in IgA nephropathy. *Scientific Reports,* 6**,** 31992.

BOLLER, D., SCHRAMM, A., DOEPFNER, K. T., SHALABY, T., VON BUEREN, A. O., EGGERT, A., GROTZER, M. A. & ARCARO, A. 2008. Targeting the phosphoinositide 3-kinase isoform p110delta impairs growth and survival in neuroblastoma cells. *Clin Cancer Res,* 14.

BOMKEN, S. N., REDFERN, K., WOOD, K. M., REID, M. M. & TWEDDLE, D. A. 2006. Limitations in the ability of NB84 to detect metastatic neuroblastoma cells in bone marrow. *Journal of Clinical Pathology,* 59**,** 927-929.

BONIFACIO, L. N. & JARSTFER, M. B. 2010. MiRNA Profile Associated with Replicative Senescence, Extended Cell Culture, and Ectopic Telomerase Expression in Human Foreskin Fibroblasts. *PLoS ONE,* 5**,** e12519.

BOSQUE, A., DIETZ, L., GALLEGO-LLEYDA, A., SANCLEMENTE, M., ITURRALDE, M., NAVAL, J., ALAVA, M. A., MARTÍNEZ-LOSTAO, L., THIERSE, H.-J. & ANEL, A. 2016. Comparative proteomics of exosomes secreted by tumoral Jurkat T cells and normal human T cell blasts unravels a potential tumorigenic role for valosin-containing protein. *Oncotarget,* 7**,** 29287-29305.

BOZEC, A., ZANGARI, J., BUTORI-PEPINO, M., ILIE, M., LALVEE, S., JUHEL, T., BUTORI, C., BREST, P., HOFMAN, P. & VOURET-CRAVIARI, V. 2017. MiR-223-3p inhibits angiogenesis and promotes resistance to cetuximab in head and neck squamous cell carcinoma. *Oncotarget,* 8**,** 57174-57186.

BRAY, I., BRYAN, K., PRENTER, S., BUCKLEY, P. G., FOLEY, N. H., MURPHY, D. M., ALCOCK, L., MESTDAGH, P., VANDESOMPELE, J., SPELEMAN, F., LONDON, W. B., MCGRADY, P. W., HIGGINS, D. G., O'MEARA, A., O'SULLIVAN, M. & STALLINGS, R. L. 2009. Widespread dysregulation of MiRNAs by MYCN amplification and chromosomal imbalances in neuroblastoma: association of miRNA expression with survival. *PLoS One,* 4**,** e7850.

BRODEUR, G., PRITCHARD, J., BERTHOLD, F., CARLSEN, N., CASTEL, V., CASTLEBERRY, R. P., DE BERNARDI, B., EVANS, A., FAVROT, M., HEDBORG, F., KANEKO, M., KEMSHEAD, J., LAMPERT, F., LEE, R., COOK, T., PEARSON, A. D. J., PHILIP, T., ROALD, B., SAWADA, T., SEEGER, R. C., TSUCHIDA, Y. & VOUTE, P. A. 1993. Revisions of the international criteria for neuroblastoma diagnosis, staging and response to treatment. *Journal of Clinical Oncology,* 11**,** 1466-1477.

BRODEUR, G. M. & BAGATELL, R. 2014. Mechanisms of neuroblastoma regression. *Nature Reviews Clinical Oncology,* 11**,** 704-713.

BRODEUR, G. M., ILYER, R., CROUCHER, J. L., ZHUANG, T., HIGASHI, M. & KOLLA, V. 2014. Therapeutic targets for neuroblastomas. *Expert Opinion Therapeutic Targets,* 18**,** 277-292.

BURCHILL, S. A. 2003. Ewing's sarcoma: diagnostic, prognostic, and therapeutic implications of molecular abnormalities. *Journal of Clinical Pathology,* 56**,** 96-102.

BURCHILL, S. A., BEISKE, K., SHIMADA, H., AMBROS, P. F., SEEGER, R., TYTGAT, G. A., BROCK, P. R., HABER, M., PARK, J. R. & BERTHOLD, F. 2017. Recommendations for the standardization of bone marrow disease assessment and reporting in children with neuroblastoma on behalf of the International Neuroblastoma Response Criteria Bone Marrow Working Group. *Cancer,* 123**,** 1095-1105.

BURCHILL, S. A., BRADBURY, F. M., SMITH, B., LEWIS, I. J. & SELBY, P. 1994. Neuroblastoma cell detection by reverse transcriptase-polymerase chain reaction (RT-PCR) for tyrosine hydroxylase mRNA. *Int J Cancer,* 57**,** 671-5.

CAGE, T. A., CHANTHERY, Y., CHESLER, L., GRIMMER, M., KNIGHT, Z., SHOKAT, K., WEISS, W. A. & GUSTAFSON, W. C. 2015. Downregulation of MYCN through PI3K Inhibition in Mouse Models of Pediatric Neural Cancer. *Frontiers in Oncology,* 5**,** 111.

CASTILLO, J., BERNARD, V., SAN LUCAS, F. A., ALLENSON, K., CAPELLO, M., KIM, D. U., GASCOYNE, P., MULU, F. C., STEPHENS, B. M., HUANG, J., WANG, H., MOMIN, A. A., JACAMO, R. O., KATZ, M., WOLFF, R., JAVLE, M., VARADHACHARY, G., WISTUBA, II, HANASH, S., MAITRA, A. & ALVAREZ, H. 2018. Surfaceome profiling enables isolation of cancer-specific exosomal cargo in liquid biopsies from pancreatic cancer patients. *Ann Oncol,* 29**,** 223-229.

CHEN, L., LU, F. B., CHEN, D. Z., WU, J. L., HU, E. D., XU, L. M., ZHENG, M. H., LI, H., HUANG, Y., JIN, X. Y., GONG, Y. W., LIN, Z., WANG, X. D. & CHEN, Y. P. 2018. BMSCs-derived miR-223-containing exosomes contribute to liver protection in experimental autoimmune hepatitis. *Mol Immunol,* 93**,** 38-46.

CHEN, Y., GELFOND, J. A., MCMANUS, L. M. & SHIREMAN, P. K. 2009. Reproducibility of quantitative RT-PCR array in miRNA expression profiling and comparison with microarray analysis. *BMC Genomics,* 10**,** 1-10.

CHEN, Y. & STALLINGS, R. L. 2007. Differential patterns of microRNA expression in neuroblastoma are correlated with prognosis, differentiation, and apoptosis. *Cancer Res,* 67**,** 976-83.

CHEN, Y. & STALLINGS, R. L. 2007b. Differential patterns of microRNA expression in neuroblastoma are correlated with prognosis, differentiation, and apoptosis. *Cancer Res,* 67.

CHEN, Y. & STALLINGS, R. L. 2007c. Differential patterns of miRNA expression in neuroblastoma are correlated with prognosis, differentiation and apoptosis. *Cancer Research,* 67**,** 976-983.

CHENG, Q., ZHANG, X., XU, X. & LU, X. 2014. MiR-618 inhibits anaplastic thyroid cancer by repressing XIAP in one ATC cell line. *Ann Endocrinol (Paris),* 75**,** 187-93.

CHESLER, L., SCHLIEVE, C., GOLDENBERG, D. D., KENNEY, A., KIM, G., MCMILLAN, A., MATTHAY, K. K., ROWITCH, D. & WEISS, W. A. 2006. Inhibition of phosphatidylinositol 3-kinase destabilizes Mycn protein and blocks malignant progression in neuroblastoma. *Cancer Res,* 66.

CHEUNG, N.-K. V., ZHANG, J., LU, C., PARKER, M., BAHRAMI, A., TICKOO, S. K., HEGUY, A., PAPPO, A. S., FEDERICO, S., DALTON, J., CHEUNG, I. Y., DING, L., FULTON, B., WANG, J., CHEN, X., BECKSFORT, J., WU, J., BILLUPS, C. A., ELLISON, D., MARDIS, E. R., WILSON, R. K., DOWNING, J. R. & DYER, M. A. 2012. Association of Age at Diagnosis and Genetic Mutations in Patients with Neuroblastoma. *JAMA : the journal of the American Medical Association,* 307**,** 1062-1071.

CHEUNG, N. K., HELLER, G., KUSHNER, B. H., LIU, C. & CHEUNG, I. Y. 1997. Detection of metastatic neuroblastoma in bone marrow: when is routine marrow histology insensitive? *J Clin Oncol,* 15**,** 2807-17.

CHEUNG, N. V. & DYER, M. A. 2013. Neuroblastoma: developmental biology, cancer genomics and immunotherapy. *Nature Reviews Cancer,* 13**,** 397-411.

CHU, C. M., RASALKAR, D. D., HU, Y. J., CHENG, F. W. T., LI, C. K. & CHU, W. C. W. 2011. Clinical presentations and imaging findings of neuroblastoma beyond abdominal mass and a review of imaging algorithm. *The British Journal of Radiology,* 84**,** 81-91.

CICHOCKI, B., EKIEL-JEZEWSKA, M. L. & WAJNRYB, E. 2015. Brownian motion of a particle with arbitrary shape. *J Chem Phys,* 142**,** 214902.

COOPER, G. 2000. *The Cell: A Molecular Approach 2nd Edition,* Sunderland (MA), Sinauer Associates.

CORRIAS, M. V., PARODI, S., HAUPT, R., LACITIGNOLA, L., NEGRI, F., SEMENTA, A. R., DAU, D., SCUDERI, F., CARLINI, B., BIANCHI, M., CASALE, F., FAULKNER, L. & GARAVENTA, A. 2008. Detection of GD2-positive cells in bone marrow samples and survival of patients with localised neuroblastoma. *British Journal Of Cancer,* 98**,** 263.

CORRIAS, M. V., PARODI, S., TCHIRKOV, A., LAMMENS, T., VICHA, A., PASQUALINI, C., TRAGER, C., YANEZ, Y., DALLORSO, S., VARESIO, L., LUKSCH, R., LAUREYS, G., VALTEAU-COUANET, D., CANETE, A., POETSCHGER, U., LADENSTEIN, R. & BURCHILL, S. A. 2018. Event-free survival of infants and toddlers enrolled in the HR-NBL-1/SIOPEN trial is associated with the level of neuroblastoma mRNAs at diagnosis. *Pediatr Blood Cancer***,** e27052.

CULLINANE, C. J., BURCHILL, S. A., SQUIRE, J. A., O'LEARY, J. J. & LEWIS, I. 2003. *Molecular biology and pathology of paediatric cancer,* Oxford, Oxford University Press.

D'AMICO, L., PATANÈ, S., GRANGE, C., BUSSOLATI, B., ISELLA, C., FONTANI, L., GODIO, L., CILLI, M., D'AMELIO, P., ISAIA, G., MEDICO, E., FERRACINI, R. & ROATO, I. 2013. Primary breast cancer stem-like cells metastasise to bone, switch phenotype and acquire a bone tropism signature. *British Journal Of Cancer,* 108**,** 2525.

DAUBNER, S. C., LE, T. & WANG, S. 2011. Tyrosine Hydroxylase and Regulation of Dopamine Synthesis. *Archives of biochemistry and biophysics,* 508**,** 1-12.

DAVIS, H. E., MORGAN, J. R. & YARMUSH, M. L. 2002. Polybrene increases retrovirus gene transfer efficiency by enhancing receptor-independent virus adsorption on target cell membranes. *Biophys Chem,* 97**,** 159-72.

DE ANTONELLIS, P., CAROTENUTO, M., VANDENBUSSCHE, J., DE VITA, G., FERRUCCI, V., MEDAGLIA, C., BOFFA, I., GALIERO, A., DI SOMMA, S., MAGLIULO, D., AIESE, N., ALONZI, A., SPANO, D., LIGUORI, L., CHIAROLLA, C., VERRICO, A., SCHULTE, J. H., MESTDAGH, P., VANDESOMPELE, J., GEVAERT, K. & ZOLLO, M. 2014. Early targets of miR-34a in neuroblastoma. *Mol Cell Proteomics,* 13**,** 2114-31.

DE BROUWER, S., DE PRETER, K., KUMPS, C., ZABROCKI, P., PORCU, M., WESTERHOUT, E. M., LAKEMAN, A., VANDESOMPELE, J., HOEBEECK, J., VAN MAERKEN, T., DE PAEPE, A., LAUREYS, G., SCHULTE, J. H., SCHRAMM, A., VAN DEN BROECKE, C., VERMEULEN, J., VAN ROY, N., BEISKE, K., RENARD, M., NOGUERA, R., DELATTRE, O., JANOUEIX-LEROSEY, I., KOGNER, P., MARTINSSON, T., NAKAGAWARA, A., OHIRA, M., CARON, H., EGGERT, A., COOLS, J. & VERSTEEG, R. 2010. Meta-analysis of neuroblastomas reveals a skewed ALK mutation spectrum in tumors with MYCN amplification. *Clin Cancer Res,* 16.

DE GIORGI, U., COHEN, E. N., GAO, H., MEGO, M., LEE, B. N., LODHI, A., CRISTOFANILLI, M., LUCCI, A. & REUBEN, J. M. 2011. Mesenchymal stem cells expressing GD2 and CD271 correlate with breast cancer-initiating cells in bone marrow. *Cancer Biol Ther,* 11**,** 812-5.

DE PRETER, K., MESTDAGH, P., VERMEULEN, J., ZEKA, F., NARANJO, A., BRAY, I., CASTEL, V., CHEN, C., DROZYNSKA, E., EGGERT, A., HOGARTY, M. D., IŻYCKA-SWIESZEWSKA, E., LONDON, W. B., NOGUERA, R., PIQUERAS, M., BRYAN, K., SCHOWE, B., VAN SLUIS, P., MOLENAAR, J. J., SCHRAMM, A., SCHULTE, J. H., STALLINGS, R. L., VERSTEEG, R., LAUREYS, G., VAN ROY, N., SPELEMAN, F. &

VANDESOMPELE, J. 2011. miRNA Expression Profiling Enables Risk Stratification in Archived and Fresh Neuroblastoma Tumor Samples. *Clinical cancer research : an official journal of the American Association for Cancer Research,* 17**,** 7684-7692.

DE PRETER, K., VERMEULEN, J., BRORS, B., DELATTRE, O., EGGERT, A., FISCHER, M., JANOUEIX-LEROSEY, I., LAVARINO, C., MARIS, J., MORA, J., NAKAGAWARA, A., OBERTHUER, A., OHIRA, M., SCHLEIERMACHER, G., SCHRAMM, A., SCHULTE, J. H., WANG, Q., WESTERMANN, F., SPELEMAN, F. & VANDESOMPELE, J. 2010. Accurate outcome prediction in neuroblastoma across independant data sets using a multigene signature. *Clinical Cancer Research,* 16**,** 1532-1541.

DH'HAESELEER, P. 2005. How does gene expression clustering work? *Nature Biotechnology,* 23**,** 1499-1501.

DHILLON, N., AGGARWAL, B. B., NEWMAN, R. A., WOLFF, R. A., KUNNUMAKKARA, A. B., ABBRUZZESE, J. L., NG, C. S., BADMAEV, V. & KURZROCK, R. 2008. Phase II trial of curcumin in patients with advanced pancreatic cancer. *Clin Cancer Res,* 14**,** 4491-9.

DI LEVA, G., GAROFALO, M. & CROCE, C. M. 2014. microRNAs in cancer. *Annual review of pathology,* 9**,** 287-314.

DING, Q., SHEN, L., NIE, X., LU, B., PAN, X., SU, Z., YAN, A., YAN, R., ZHOU, Y., LI, L. & XU, J. 2018. MiR-223-3p overexpression inhibits cell proliferation and migration by regulating inflammation-associated cytokines in glioblastomas. *Pathology - Research and Practice,* 214**,** 1330-1339.

DOMINGO-FERNANDEZ, R., WATTERS, K., PISKAREVA, O., STALLINGS, R. L. & BRAY, I. 2013. The role of genetic and epigenetic alterations in neuroblastoma disease pathogenesis. *Pediatric Surgery International,* 29**,** 101-119.

DRAGOMIR, M., MAFRA, A. C. P., DIAS, S. M. G., VASILESCU, C. & CALIN, G. A. 2018. Using microRNA Networks to Understand Cancer. *Int J Mol Sci,* 19.

DUBOIS, S. G., KALIKA, Y., LUKENS, J. N., BRODEUR, G. M., SEEGER, R. C., ATKINSON, J. B., HAASE, G. M., BLACK, C. T., PEREZ, C., SHIMADA, H., GERBING, R., STRAM, D. O. & MATTHAY, K. K. 1999. Metastatic sites in stage IV and IVS neuroblastoma correlate with age, tumor biology, and survival. *J Pediatr Hematol Oncol,* 21**,** 181-9.

EKHTERAEI-TOUSI, S., MOHAMMAD-SOLTANI, B., SADEGHIZADEH, M., MOWLA, S. J., PARSI, S. & SOLEIMANI, M. 2015. Inhibitory effect of hsa-miR-590-5p on cardiosphere-derived stem cells differentiation through downregulation of TGFB signaling. *J Cell Biochem,* 116**,** 179-91.

EKLÖF, O. & GOODING, C. A. 1967. Paravertebral widening in cases of neuroblastoma. *British Journal Radiology,* 40**,** 358-365.

ESSER, R., GLIENKE, W., BOCHENNEK, K., ERBEN, S., QUAISER, A., PIEPER, C., EGGERT, A., SCHRAMM, A., ASTRAHANTSEFF, K., HANSMANN, M. L., SCHWABE, D., KLINGEBIEL, T. & KOEHL, U. 2011. Detection of neuroblastoma cells during clinical follow up: advanced flow cytometry and rt-PCR for tyrosine hydroxylase using both conventional and real-time PCR. *Klin Padiatr,* 223**,** 326-31.

ESTELLER, M. 2011. Non-coding RNAs in human disease. *Nat Rev Genet,* 12**,** 861-74.

ETHERIDGE, A., LEE, I., HOOD, L., GALAS, D. & WANG, K. 2011. Extracellular microRNA: a new source of biomarkers. *Mutation research,* 717**,** 85-90.

EULALIO, A., HUNTZINGER, E., NISHIHARA, T., REHWINKEL, J., FAUSER, M. & IZAURRALDE, E. 2009. Deadenylation is a widespread effect of miRNA regulation. *RNA,* 15**,** 21-32.

FARID, M., DEMICCO, E. G., GARCIA, R., AHN, L., MEROLA, P. R., CIOFFI, A. & MAKI, R. G. 2014. Malignant Peripheral Nerve Sheath Tumors. *The Oncologist,* 19**,** 193-201.

FENG, D. D., ZHANG, H., ZHANG, P., ZHENG, Y. S., ZHANG, X. J., HAN, B. W., LUO, X. Q., XU, L., ZHOU, H., QU, L. H. & CHEN, Y. Q. 2011. Down-regulated miR-331-5p and miR-27a are associated with chemotherapy resistance and relapse in leukaemia. *J Cell Mol Med,* 15**,** 2164-75.

FISCHER, M., BAUER, T., OBERTHUER, A., HERO, B., THEISSEN, J., EHRICH, M., SPITZ, R., EILS, R., WESTERMANN, F., BRORS, B., KOING, R. & BERTHOLD, F. 2010. Integrated genomic profiling identifies two distinct molecular subtypes with divergent outcome in neuroblastoma with loss of chromosome 11q. *Oncogene,* 29**,** 865-875.

FISHER, J. P., FLUTTER, B., WESEMANN, F., FROSCH, J., ROSSIG, C., GUSTAFSSON, K. & ANDERSON, J. 2016. Effective combination treatment of GD2-expressing neuroblastoma and Ewing's sarcoma using anti-GD2 ch14.18/CHO antibody with Vgamma9Vdelta2+ gammadeltaT cells. *Oncoimmunology,* 5**,** e1025194.

FOLEY, N. H., BRAY, I. M., TIVNAN, A., BRYAN, K., MURPHY, D. M., BUCKLEY, P. G., RYAN, J., O'MEARA, A., O'SULLIVAN, M. & STALLINGS, R. L. 2010. MicroRNA-184 inhibits neuroblastoma cell survival through targeting the serine/threonine kinase AKT2. *Mol Cancer,* 9**,** 83.

FOYE, C., YAN, I. K., DAVID, W., SHUKLA, N., HABBOUSH, Y., CHASE, L., RYLAND, K., KESARI, V. & PATEL, T. 2017. Comparison of miRNA quantitation by Nanostring in serum and plasma samples. *PLoS ONE,* 12**,** e0189165.

FU, A., HOFFMAN, A. E., LIU, R., JACOBS, D. I., ZHENG, T. & ZHU, Y. 2014. Targetome profiling and functional genetics implicate miR-618 in lymphomagenesis. *Epigenetics,* 9**,** 730-7.

FU, X., MAO, X., WANG, Y., DING, X. & LI, Y. 2017. Let-7c-5p inhibits cell proliferation and induces cell apoptosis by targeting ERCC6 in breast cancer. *Oncol Rep,* 38**,** 1851-1856.

FUJITA, T., IGARASHI, J., OKAWA, E. R., GOTOH, T., MANNE, J., KOLLA, V., KIM, J., ZHAO, H., PAWEL, B. R., LONDON, W. B., MARIS, J. M., WHITE, P. S. & BRODEUR, G. M. 2008. CHD5, a Tumor Suppressor Gene Deleted From 1p36.31 in Neuroblastomas. *JNCI Journal of the National Cancer Institute,* 100**,** 940-949.

FULDA, S. 2009. The PI3K/Akt/mTOR pathway as therapeutic target in neuroblastoma. *Curr Cancer Drug Targets,* 9**,** 729-37.

GAJRIA, D. & CHANDARLAPATY, S. 2011. HER2-amplified breast cancer: mechanisms of trastuzumab resistance and novel targeted therapies. *Expert Review of Anticancer Therapy,* 11**,** 263-275.

GALLO, A. & ALEVIZOS, I. 2013. Isolation of circulating microRNA in saliva. *Methods Mol Biol,* 1024**,** 183-90.

GAMBLE, L. D., HOGARTY, M. D., LIU, X., ZIEGLER, D. S., MARSHALL, G., NORRIS, M. D. & HABER, M. 2012. Polyamine pathway inhibition as a novel therapeutic approach to treating neuroblastoma. *Frontiers in Oncology,* 2**,** 162.

GANGODA, L., KEERTHIKUMAR, S., FONSEKA, P., EDGINGTON, L. E., ANG, C. S., OZCITTI, C., BOGYO, M., PARKER, B. S. & MATHIVANAN, S. 2015. Inhibition of cathepsin proteases attenuates migration and sensitizes aggressive N-Myc amplified human neuroblastoma cells to doxorubicin. *Oncotarget,* 6**,** 11175-90.

GEMINDER, H., SAGI-ASSIF, O., GOLDBERG, L., MESHEL, T., RECHAVI, G., WITZ, I. P. & BEN-BARUCH, A. 2001. A possible role for CXCR4 and its ligand, the CXC chemokine stromal cell-derived factor-1, in the development of bone marrow metastases in neuroblastoma. *J Immunol,* 167**,** 4747-57.

GERALD, W. L. & HABER, D. A. 2005. The EWS-WT1 gene fusion in desmoplastic small round cell tumor. *Semin Cancer Biol,* 15**,** 197-205.

GIT, A., DVINGE, H., SALMON-DIVON, M., OSBORNE, M., KUTTER, C., HADFIELD, J., BERTONE, P. & CALDAS, C. 2010. Systematic comparison of microarray profiling, real-time PCR, and next-generation sequencing technologies for measuring differential microRNA expression. *RNA,* 16**,** 991-1006.

GREGORY, W. M., TWELVES, C. J., BELL, R., SMYE, S. W., HOWARD, D. R., COLEMAN, R. E. & CAMERON, D. A. 2016. Characterizing and quantifying the effects of breast cancer therapy using mathematical modeling. *Breast Cancer Res Treat,* 155**,** 303-11.

GUO, J., DONG, Q., FANG, Z., CHEN, X., LU, H., WANG, K., YIN, Y., CAI, X., ZHAO, N., CHEN, J., ZEN, K., ZHANG, J. & ZHANG, C. Y. 2010. Identification of miRNAs that are associated with tumor metastasis in neuroblastoma. *Cancer Biol Ther,* 9**,** 446-52.

GUTHRIE, J. L., SEAH, C., BROWN, S., TANG, P., JAMIESON, F. & DREWS, S. J. 2008. Use of Bordetella pertussis BP3385 to establish a cutoff value for an IS481-targeted real-time PCR assay. *J Clin Microbiol,* 46.

GYORGY, B., MODOS, K., PALLINGER, E., PALOCZI, K., PASZTOI, M., MISJAK, P., DELI, M. A., SIPOS, A., SZALAI, A., VOSZKA, I., POLGAR, A., TOTH, K., CSETE, M., NAGY, G., GAY, S., FALUS, A., KITTEL, A. & BUZAS, E. I. 2011. Detection and isolation of cell-derived microparticles are compromised by protein complexes resulting from shared biophysical parameters. *Blood,* 117**,** e39-48.

HADUONG, J. H., BLAVIER, L., BANIWAL, S. K., FRENKEL, B., MALVAR, J., PUNJ, V., SPOSTO, R. & DECLERCK, Y. A. 2015. Interaction between bone marrow stromal cells and neuroblastoma cells leads to a VEGFA-mediated osteoblastogenesis. *International journal of cancer,* 137**,** 797-809.

HAN, L., WITMER, P. D., CASEY, E., VALLE, D. & SUKUMAR, S. 2007. DNA methylation regulates MicroRNA expression. *Cancer Biol Ther,* 6**,** 1284-8.

HANSEN, K. F., SAKAMOTO, K. & OBRIETAN, K. 2011. MicroRNAs: a potential interface between the circadian clock and human health. *Genome Medicine,* 3**,** 10-10.

HANSFORD, L. M., MCKEE, A. E., ZHANG, L., GEORGE, R. E., GERSTLE, J. T., THORNER, P. S., SMITH, K. M., LOOK, A. T., YEGER, H., MILLER, F. D., IRWIN, M. S., THIELE, C. J. & KAPLAN, D. R. 2007. Neuroblastoma Cells Isolated from Bone Marrow Metastases Contain a Naturally Enriched Tumor-Initiating Cell. *Cancer Research,* 67**,** 11234.

HANSFORD, L. M., MCKEE, A. E., ZHANG, L., GERORGE, R. E., GERSTLE, J. T., THORNER, P. S., SMITH, K. M., LOOK, A. T., YEGER, H., MILLER, F. D., IRWIN, M. S., THIELE, C. J. & KAPLAN, D. R. 2007b. Neuroblastoma cells isolated from bone marrow

metastases contain a naturally enriched tumour-initiating cell. *Cancer Research,* 67**,** 11234-11243.

HASAN, K., NAFADY, A., TAKATORI, A., KISHIDA, S., OHIRA, M., SUENAGA, Y., HOSSAIN, S., AKTER, J., OGURA, A., NAKAMURA, Y., KADOMATSU, K. & NAKAGAWARA, A. 2013. *ALK* is a MYCN target gene and regulates cell migration and invasion in neuroblastoma. *Nature Scientific Reports,* 3.

HAUG, B. H., HALD, O. H., UTNES, P., ROTH, S. A., LOKKE, C., FLAEGSTAD, T. & EINVIK, C. 2015. Exosome-like Extracellular Vesicles from MYCN-amplified Neuroblastoma Cells Contain Oncogenic miRNAs. *Anticancer Res,* 35**,** 2521-30.

HENRY, N. L. & HAYES, D. F. 2012. Cancer biomarkers. *Molecular Oncology,* 6**,** 140-146.

HERNANDEZ, J. E., LLACUACHAQUI, M., PALACIO, G. V., FIGUEROA, J. D., MADRID, J., LEMA, M., ROYER, R., LI, S., LARSON, G., WEITZEL, J. N. & NAROD, S. A. 2014. Prevalence of BRCA1 and BRCA2 mutations in unselected breast cancer patients from medellin, Colombia. *Hered Cancer Clin Pract,* 12**,** 11.

HIYAMA, E. 2014. Pediatric hepatoblastoma: diagnosis and treatment. *Translational Pediatrics,* 3**,** 293-299.

HO, R., EGGERT, A., HISHIKI, T., MINTURN, J. E., IKEGAKI, N., FOSTER, P., CAMORATTO, A. M., EVANS, A. E. & BRODEUR, G. M. 2002. Resistance to chemotherapy mediated by TrkB in neuroblastomas. *Cancer Res,* 62**,** 6462-6.

HOGARTY, M. D., NORRIS, M. D., DAVIS, K., LIU, X., EVAGELIOU, N. F., HAYES, C. S., PAWEL, B., GUO, R., ZHAO, H., SEKYERE, E., KEATING, J., THOMAS, W., CHENG, N. C., MURRAY, J., SMITH, J., SUTTON, R., VENN, N., LONDON, W. B., BUXTON, A., GILMOUR, S. K., MARSHALL, G. M. & HABER, M. 2008. ODC1 is a critical determinant of MYCN oncogenesis and a therapeutic target in neuroblastoma. *Cancer research,* 68**,** 9735-9745.

HOPKINS, B. D., PAULI, C., DU, X., WANG, D. G., LI, X., WU, D., AMADIUME, S. C., GONCALVES, M. D., HODAKOSKI, C., LUNDQUIST, M. R., BAREJA, R., MA, Y., HARRIS, E. M., SBONER, A., BELTRAN, H., RUBIN, M. A., MUKHERJEE, S. & CANTLEY, L. C. 2018. Suppression of insulin feedback enhances the efficacy of PI3K inhibitors. *Nature,* 560**,** 499-503.

HSU, C. Y., HSIEH, T. H., TSAI, C. F., TSAI, H. P., CHEN, H. S., CHANG, Y., CHUANG, H. Y., LEE, J. N., HSU, Y. L. & TSAI, E. M. 2014. miRNA-199a-5p regulates VEGFA in endometrial mesenchymal stem cells and contributes to the pathogenesis of endometriosis. *J Pathol,* 232**,** 330-43.

HUANG, T. C., CHANG, H. Y., CHEN, C. Y., WU, P. Y., LEE, H., LIAO, Y. F., HSU, W. M., HUANG, H. C. & JUAN, H. F. 2011. Silencing of miR-124 induces neuroblastoma SK-N-SH cell differentiation, cell cycle arrest and apoptosis through promoting AHR. *FEBS Lett,* 585**,** 3582-6.

HUNTZINGER, E. & IZAURRALDE, E. 2011. Gene silencing by microRNAs: contributions of translational repression and mRNA decay. *Nat Rev Genet,* 12**,** 99-110.

HUR, K., TOIYAMA, Y., SCHETTER, A. J., OKUGAWA, Y., HARRIS, C. C., BOLAND, C. R. & GOEL, A. 2015. Identification of a Metastasis-Specific MicroRNA Signature in Human Colorectal Cancer. *JNCI Journal of the National Cancer Institute,* 107**,** dju492.

IEHARA, T., HIYAMA, E., TAJIRI, T., YONEDA, A., HAMAZAKI, M., FUKUZAWA, M., HOSOI, H., SUGIMOTO, T. & SAWADA, T. 2012. Is the prognosis of stage 4s neuroblastoma in patients 12 months of age and older really excellent? *European Journal of Cancer,* 48**,** 1707-1712.

ISLAM, F., GOPALAN, V., VIDER, J., WAHAB, R., EBRAHIMI, F., LU, C. T., KASEM, K. & LAM, A. K. Y. 2017. MicroRNA-186-5p overexpression modulates colon cancer growth by repressing the expression of the FAM134B tumour inhibitor. *Exp Cell Res,* 357**,** 260-270.

JAFARZADEH, M. & SOLTANI, B. M. 2016. Hsa-miR-590-5p Interaction with SMAD3 Transcript Supports Its Regulatory Effect on The TGFβ Signaling Pathway. *Cell Journal (Yakhteh),* 18**,** 7-12.

JANUSZYK, M., RENNERT, R. C., SORKIN, M., MAAN, Z. N., WONG, L. K., WHITTAM, A. J., WHITMORE, A., DUSCHER, D. & GURTNER, G. C. 2015. Evaluating the Effect of Cell Culture on Gene Expression in Primary Tissue Samples Using Microfluidic-Based Single Cell Transcriptional Analysis. *Microarrays,* 4**,** 540-550.

JIN, B., WANG, W., MENG, X. X., DU, G., LI, J., ZHANG, S. Z., ZHOU, B. H. & FU, Z. H. 2016. Let-7 inhibits self-renewal of hepatocellular cancer stem-like cells through regulating the epithelial-mesenchymal transition and the Wnt signaling pathway. *BMC Cancer,* 16**,** 863.

JODELE, S., CHANTRAIN, C. F., BLAVIER, L., LUTZKO, C., CROOKS, G. M., SHIMADA, H., COUSSENS, L. M. & DECLERCK, Y. A. 2005. The contribution of bone marrow-derived cells to the tumor vasculature in neuroblastoma is matrix metalloproteinase-9 dependent. *Cancer Res,* 65**,** 3200-8.

JOHNSEN, J. I., SEGERSTRÖM, L., ORREGO, A., ELFMAN, L., HENRIKSSON, M., KÅGEDAL, B., EKSBORG, S., SVEINBJÖRNSSON, B. & KOGNER, P. 2007. Inhibitors of mammalian target of rapamycin downregulate MYCN protein expression and inhibit neuroblastoma growth in vitro and in vivo. *Oncogene,* 27**,** 2910.

JONES, D. Z., SCHMIDT, M. L., SUMAN, S., HOBBING, K. R., BARVE, S. S., GOBEJISHVILI, L., BROCK, G., KLINGE, C. M., RAI, S. N., PARK, J., CLARK, G. J., AGARWAL, R. & KIDD, L. R. 2018. Micro-RNA-186-5p inhibition attenuates proliferation, anchorage independent growth and invasion in metastatic prostate cancer cells. *BMC Cancer,* 18**,** 421.

JORGE, K., SOUZA, R. P., ASSIS, M. T. A., ARAUJO, M. G., LOCATI, M., JESUS, A. M. R., DIAS BAPTISTA, I. M. F., LIMA, C. X., TEIXEIRA, A. L., TEIXEIRA, M. M. & SORIANI, F. M. 2017. Characterization of MicroRNA Expression Profiles and Identification of Potential Biomarkers in Leprosy. *J Clin Microbiol,* 55**,** 1516-1525.

KANEKO, Y. & KNUDSON, A. G. 2000. Mechanism and relevance of ploidy in neuroblastoma. *Genes, Chromosomes & Cancer,* 29**,** 89-95.

KAO, H. W., PAN, C. Y., LAI, C. H., WU, C. W., FANG, W. L., HUANG, K. H. & LIN, W. C. 2017. Urine miR-21-5p as a potential non-invasive biomarker for gastric cancer. *Oncotarget,* 8**,** 56389-56397.

KATZ, R. L. & KRISHNAMURTHY, S. 2008. CHAPTER 27 - Kidneys, Adrenals, and Retroperitoneum. *In:* BIBBO, M. & WILBUR, D. (eds.) *Comprehensive Cytopathology (Third Edition).* Edinburgh: W.B. Saunders.

KHVOROVA, A., REYNOLDS, A. & JAYASENA, S. D. 2003. Functional siRNAs and miRNAs exhibit strand bias. *Cell,* 115**,** 209-16.

KIM, Y.-K., YEO, J., KIM, B., HA, M. & KIM, V. N. 2012. Short Structured RNAs with Low GC Content Are Selectively Lost during Extraction from a Small Number of Cells. *Molecular Cell,* 46**,** 893-895.

KLEEMANN, M., SCHNEIDER, H., UNGER, K., SANDER, P., SCHNEIDER, E. M., FISCHER-POSOVSZKY, P., HANDRICK, R. & OTTE, K. 2018. MiR-744-5p inducing cell death by directly targeting HNRNPC and NFIX in ovarian cancer cells. *Scientific Reports,* 8**,** 9020.

KOMADA, Y., ZHANG, X. L., ZHOU, Y. W., INABA, H., DEGUCHI, T., AZUMA, E. & SAKURAI, M. 1998. Flow cytometric analysis of peripheral blood and bone marrow for tumor cells in patients with neuroblastoma. *Cancer,* 82**,** 591-9.

KOSCIANSKA, E., STAREGA-ROSLAN, J. & KRZYZOSIAK, W. J. 2011. The Role of Dicer Protein Partners in the Processing of MicroRNA Precursors. *PLoS ONE,* 6**,** e28548.

KUOSMANEN, S. M., KANSANEN, E., SIHVOLA, V. & LEVONEN, A.-L. 2017. MicroRNA Profiling Reveals Distinct Profiles for Tissue-Derived and Cultured Endothelial Cells. *Scientific Reports,* 7**,** 10943.

LADENSTEIN, R., VALTEAU-COUANET, D., BROCK, P., YANIV, I., CASTEL, V., LAUREYS, G., MALIS, J., PAPADAKIS, V., LACERDA, A., RUUD, E., KOGNER, P., GARAMI, M., BALWIERZ, W., SCHROEDER, H., BECK-POPOVIC, M., SCHREIER, G., MACHIN, D., POTSCHGER, U. & PEARSON, A. 2010. Randomized Trial of prophylactic granulocyte colony-stimulating factor during rapid COJEC induction in pediatric patients with high-risk neuroblastoma: the European HR-NBL1/SIOPEN study. *J Clin Oncol,* 28**,** 3516-24.

LAGOS-QUINTANA, M., RAUHUT, R., LENDECKEL, W. & TUSCHL, T. 2001. Identification of novel genes coding for small expressed RNAs. *Science,* 294**,** 853-8.

LAMANT, L., PULFORD, K., BISCHOF, D., MORRIS, S. W., MASON, D. Y., DELSOL, G. & MARIAME, B. 2000. Expression of the ALK tyrosine kinase gene in neuroblastoma. *Am J Pathol,* 156.

LAMMIE, G., CHEUNG, N., GERALD, W., ROSENBLUM, M. & CORDONCARDO, C. 1993. Ganglioside gd(2) expression in the human nervous-system and in neuroblastomas - an immunohistochemical study. *Int J Oncol,* 3**,** 909-15.

LAPLANTE, M. & SABATINI, D. M. 2012. mTOR signaling in growth control and disease. *Cell,* 149.

LAUG, W. E., SIEGEL, S. E., SHAW, K. N., LANDING, B., BAPTISTA, J. & GUTENSTEIN, M. 1978. Initial urinary catecholamine metabolite concentrations and prognosis in neuroblastoma. *Pediatrics,* 62**,** 77-83.

LEE, R. C., FEINBAUM, R. L. & AMBROS, V. 1993. The C. elegans heterochronic gene lin-4 encodes small RNAs with antisense complementarity to lin-14. *Cell,* 75**,** 843-54.

LESSIG, M. K. 2009. The role of 131 I-MIBG in high-risk neuroblastoma treatment. *Pediatric Oncology Nursing,* 26**,** 208-216.

LI, J., XIA, L., ZHOU, Z., ZUO, Z., XU, C., SONG, H. & CAI, J. 2018. MiR-186-5p upregulation inhibits proliferation, metastasis and epithelial-to-mesenchymal transition of colorectal cancer cell by targeting ZEB1. *Arch Biochem Biophys,* 640**,** 53-60.

LI, P., KASLAN, M., LEE, S. H., YAO, J. & GAO, Z. 2017. Progress in Exosome Isolation Techniques. *Theranostics,* 7**,** 789-804.

LI, Z. & THIELE, C. J. 2007. Targeting Akt to increase the sensitivity of neuroblastoma to chemotherapy: lessons learned from the brain-derived neurotrophic factor/TrkB signal transduction pathway. *Expert Opin Ther Targets,* 11.

LIGA, A., VLIEGENTHART, A. D., OOSTHUYZEN, W., DEAR, J. W. & KERSAUDY-KERHOAS, M. 2015. Exosome isolation: a microfluidic road-map. *Lab Chip,* 15**,** 2388-94.

LIN, R. J., LIN, Y. C., CHEN, J., KUO, H. H., CHEN, Y. Y., DICCIANNI, M. B., LONDON, W. B., CHANG, C. H. & YU, A. L. 2010. microRNA signature and expression of Dicer and Drosha can predict prognosis and delineate risk groups in neuroblastoma. *Cancer Res,* 70**,** 7841-50.

LINDER, S., HENSSEN, A., ASTRAHANTSEFF, K. & SCHULTE, J. H. 2014. ALK pERKs up MYCN in neuroblastoma. *Science Signalling,* 7**,** 27.

LIU, N., ZHANG, L., WANG, Z., CHENG, Y., ZHANG, P., WANG, X., WEN, W., YANG, H., LIU, H., JIN, W., ZHANG, Y. & TU, Y. 2017. MicroRNA-101 inhibits proliferation, migration and invasion of human glioblastoma by targeting SOX9. *Oncotarget,* 8**,** 19244-19254.

LIU, Z., YANG, X., LI, Z., MCMAHON, C., SIZER, C., BARENBOIM-STAPLETON, L., BLISKOVSKY, V., MOCK, B., RIED, T., LONDON, W. B., MARIS, J., KHAN, J. & THIELE, C. J. 2011. CASZ1, a candidate tumor-suppressor gene, suppresses neuroblastoma tumor growth through reprogramming gene expression. *Cell Death Differ,* 18**,** 1174-83.

LIVSHITS, M. A., KHOMYAKOVA, E., EVTUSHENKO, E. G., LAZAREV, V. N., KULEMIN, N. A., SEMINA, S. E., GENEROZOV, E. V. & GOVORUN, V. M. 2015. Isolation of exosomes by differential centrifugation: Theoretical analysis of a commonly used protocol. *Scientific Reports,* 5**,** 17319.

LONERGAN, G. J., SCHWAB, C. M., SUAREZ, E. S. & CARLSON, C. L. 2002. Neuroblastoma, ganglioneuroblastoma, and ganglioneuroma: radiologic-pathologic correlation. *Radiographics,* 22**,** 911-34.

LÖTVALL, J., HILL, A. F., HOCHBERG, F., BUZÁS, E. I., DI VIZIO, D., GARDINER, C., GHO, Y. S., KUROCHKIN, I. V., MATHIVANAN, S., QUESENBERRY, P., SAHOO, S., TAHARA, H., WAUBEN, M. H., WITWER, K. W. & THÉRY, C. 2014. Minimal experimental requirements for definition of extracellular vesicles and their functions: a position statement from the International Society for Extracellular Vesicles. *Journal of Extracellular Vesicles,* 3**,** 10.3402/jev.v3.26913.

LOUIS, C. U. & SHOHET, J. M. 2014. Neuroblastoma: molecular pathogenesis and therapy. *The Annual Review of Medicine,* 66**,** 1-23.

LOWRY, O. H., ROSEBROUGH, N. J., FARR, A. L. & RANDALL, R. J. 1951. Protein measurement with the Folin phenol reagent. *J Biol Chem,* 193**,** 265-75.

LUND, E., GUTTINGER, S., CALADO, A., DAHLBERG, J. E. & KUTAY, U. 2004. Nuclear export of microRNA precursors. *Science,* 303**,** 95-8.

LUO, H., YANG, R., LI, C., TONG, Y., FAN, L., LIU, X. & XU, C. 2017. MicroRNA-139-5p inhibits bladder cancer proliferation and self-renewal by targeting the Bmi1 oncogene. *Tumour Biol,* 39**,** 1010428317718414.

LYNCH, J., FAY, J., MEEHAN, M., BRYAN, K., WATTERS, K. M., MURPHY, D. M. & STALLINGS, R. L. 2012. MiRNA-335 suppresses neuroblastoma cell

invasiveness by direct targeting of multiple genes from the non-canonical TGF-beta signalling pathway. *Carcinogenesis,* 33**,** 976-85.

MA, J., SUN, F., LI, C., ZHANG, Y., XIAO, W., LI, Z., PAN, Q., ZENG, H., XIAO, G., YAO, K., HONG, A. & AN, J. 2014. Depletion of intermediate filament protein Nestin, a target of microRNA-940, suppresses tumorigenesis by inducing spontaneous DNA damage accumulation in human nasopharyngeal carcinoma. *Cell Death &Amp; Disease,* 5**,** e1377.

MA, M. T., HE, M., WANG, Y., JIAO, X. Y., ZHAO, L., BAI, X. F., YU, Z. J., WU, H. Z., SUN, M. L., SONG, Z. G. & WEI, M. J. 2013. MiR-487a resensitizes mitoxantrone (MX)-resistant breast cancer cells (MCF-7/MX) to MX by targeting breast cancer resistance protein (BCRP/ABCG2). *Cancer Lett,* 339**,** 107-15.

MACFARLANE, L.-A. & MURPHY, P. R. 2010. MicroRNA: Biogenesis, Function and Role in Cancer. *Current Genomics,* 11**,** 537-561.

MAKAROV, D. V., LOEB, S., GETZENBERG, R. H. & PARTIN, A. W. 2009. Biomarkers for prostate cancer. *Annu Rev Med,* 60**,** 139-51.

MALL, C., ROCKE, D. M., DURBIN-JOHNSON, B. & WEISS, R. H. 2013. Stability of miRNA in human urine supports its biomarker potential. *Biomarkers in medicine,* 7**,** 10.2217/bmm.13.44.

MARIMPIETRI, D., PETRETTO, A., RAFFAGHELLO, L., PEZZOLO, A., GAGLIANI, C., TACCHETTI, C., MAURI, P., MELIOLI, G. & PISTOIA, V. 2013. Proteome Profiling of Neuroblastoma-Derived Exosomes Reveal the Expression of Proteins Potentially Involved in Tumor Progression. *PLoS ONE,* 8**,** e75054.

MARTÍN-GUERRERO, I., DÍAZ-NAVARRO, A., GUTIERREZ-CAMINO, A. & GARCIA-ORAD, A. 2016. Genetic variant in miR-618 in the risk of chronic lymphocytic leukemia. *European Journal of Cancer,* 61**,** S29.

MARTINEZ, C., HOFMANN, T. J., MARINO, R., DOMINICI, M. & HORWITZ, E. M. 2007. Human bone marrow mesenchymal stromal cells express the neural ganglioside GD2: a novel surface marker for the identification of MSCs. *Blood,* 109**,** 4245-4248.

MARTUCCI, V. L. & PACAK, K. 2014. Pheochromocytoma and Paraganglioma: Diagnosis, Genetics, Management, and Treatment. *Current problems in cancer,* 38**,** 7-41.

MATSUMOTO, K., WADA, R. K., YAMASHIRO, J. M., KAPLAN, D. R. & THIELE, C. J. 1995. Expression of brain-derived neurotrophic factor and p145TrkB affects survival, differentiation, and invasiveness of human neuroblastoma cells. *Cancer Res,* 55**,** 1798-806.

MATTHAY, K. K., ATKINSON, J. B., STRAM, D. O., SELCH, M., REYNOLDS, C. P. & SEEGER, R. C. 1993. Patterns of relapse after autologous purged bone marrow transplantation for neuroblastoma: a Childrens Cancer Group pilot study. *J Clin Oncol,* 11**,** 2226-33.

MATTHAY, K. K., SHULKIN, B., LADENSTEIN, R., MICHON, J., GIAMMARILE, F., LEWINGTON, V., PEARSON, A. D. & COHN, S. L. 2010. Criteria for evaluation of disease extent by (123)I-metaiodobenzylguanidine scans in neuroblastoma: a report for the International Neuroblastoma Risk Group (INRG) Task Force. *Br J Cancer,* 102**,** 1319-26.

MEADS, M. B., HAZLEHURST, L. A. & DALTON, W. S. 2008. The Bone Marrow Microenvironment as a Tumor Sanctuary and Contributor to Drug Resistance. *Clinical Cancer Research,* 14**,** 2519-2526.

MEGIORNI, F., COLAIACOVO, M., CIALFI, S., MCDOWELL, H. P., GUFFANTI, A., CAMERO, S., FELSANI, A., LOSTY, P. D., PIZER, B., SHUKLA, R., CAPPELLI, C., FERRARA, E., PIZZUTI, A., MOLES, A. & DOMINICI, C. 2017. A sketch of known and novel MYCN-associated miRNA networks in neuroblastoma. *Oncology Reports,* 38**,** 3-20.

MEGISON, M. L., GILLORY, L. A. & BEIERLE, E. A. 2013. Cell survival signaling in neuroblastoma. *Anticancer Agents Med Chem,* 13.

MEHES, G., LUEGMAYR, A., AMBROS, I. M., LADENSTEIN, R. & AMBROS, P. F. 2001. Combined automatic immunological and molecular cytogenetic analysis allows exact identification and quantification of tumor cells in the bone marrow. *Clin Cancer Res,* 7**,** 1969-75.

MENDOZA, M. C., ER, E. E. & BLENIS, J. 2011. The Ras-ERK and PI3K-mTOR Pathways: Cross-talk and Compensation. *Trends in biochemical sciences,* 36**,** 320-328.

MERUGU, S. & TWEDDLE, D. 2017. Abstract 1711: Detection of circulating tumor cells for use as prognostic, predictive and pharmacodynamic biomarkers in neuroblastoma. *Cancer Research,* 77**,** 1711.

MESTDAGH, P., VAN VLIERBERGHE, P., DE WEER, A., MUTH, D., WESTERMANN, F., SPELEMAN, F. & VANDESOMPELE, J. 2009. A novel and universal method for microRNA RT-qPCR data normalization. *Genome Biology,* 10**,** R64.

METSALU, T. & VILO, J. 2015. ClustVis: a web tool for visualizing clustering of multivariate data using Principal Component Analysis and heatmap. *Nucleic Acids Res,* 43**,** W566-70.

MINTURN, J. E., EVANS, A. E., VILLABLANCA, J. G., YANIK, G. A., PARK, J. R., SHUSTERMAN, S., GROSHEN, S., HELLRIEGEL, E. T., BENSEN-KENNEDY, D., MATTHAY, K. K., BRODEUR, G. M. & MARIS, J. M. 2011. Phase I trial of lestaurtinib for children with refractory neuroblastoma: a new approaches to neuroblastoma therapy consortium study. *Cancer Chemother Pharmacol,* 68**,** 1057-65.

MIYAMAE, M., KOMATSU, S., ICHIKAWA, D., KAWAGUCHI, T., HIRAJIMA, S., OKAJIMA, W., OHASHI, T., IMAMURA, T., KONISHI, H., SHIOZAKI, A., MORIMURA, R., IKOMA, H., OCHIAI, T., OKAMOTO, K., TANIGUCHI, H. & OTSUJI, E. 2015. Plasma microRNA profiles: identification of miR-744 as a novel diagnostic and prognostic biomarker in pancreatic cancer. *Br J Cancer,* 113**,** 1467-76.

MOEN, A., JACOBSEN, D., PHUYAL, S., LEGFELDT, A., HAUGEN, F., RØE, C. & GJERSTAD, J. 2017. MicroRNA-223 demonstrated experimentally in exosome-like vesicles is associated with decreased risk of persistent pain after lumbar disc herniation. *Journal of Translational Medicine,* 15**,** 89.

MOLENAAR, J. J., DOMINGO-FERNANDEZ, R., EBUS, M. E., LINDNER, S., KOSTER, J., DRABEK, K., MESTDAGH, P., VAN SLUIS, P., VALENTIJN, L. J., VAN NES, J., BROEKMANS, M., HANEVELD, F., VOLCKMANN, R., BRAY, I., HEUKAMP, L., SPRUSSEL, A., THOR, T., KIECKBUSCH, K., KLEIN-HITPASS, L., FISCHER, M., VANDESOMPELE, J., SCHRAMM, A., VAN NOESEL, M. M., VARESIO, L., SPELEMAN, F., EGGERT, A., STALLINGS, R. L., CARON, H. N., VERSTEEG, R. & SCHULTE, J. H. 2012. LIN28B induces neuroblastoma and enhances MYCN levels via let-7 suppression. *Nat Genet,* 44**,** 1199-206.

MONCLAIR, T., BRODEUR, G. M., AMBROS, P. F., BRISSE, H. J., CECCHETTO, G., HOLMES, K., KANEKO, M., LONDON, W. B., MATTHAY, K. K., NUCHTERN, J. G.,

VON SCHWEINITZ, D., SIMON, T., COHN, S. L. & PEARSON, A. D. 2009. The International Neuroblastoma Risk Group (INRG) staging system: an INRG Task Force report. *J Clin Oncol,* 27**,** 298-303.

MONTEYS, A. M., SPENGLER, R. M., WAN, J., TECEDOR, L., LENNOX, K. A., XING, Y. & DAVIDSON, B. L. 2010. Structure and activity of putative intronic miRNA promoters. *RNA,* 16**,** 495-505.

MORANDI, F., SCARUFFI, P., GALLO, F., STIGLIANI, S., MORETTI, S., BONASSI, S., GAMBINI, C., MAZZOCCO, K., FARDIN, P., HAUPT, R., ARCAMONE, G., PISTOIA, V., TONINI, G. P. & CORRIAS, M. V. 2012. Bone marrow-infiltrating human neuroblastoma cells express high levels of calprotectin and HLA-G proteins. *PLoS One,* 7**,** e29922.

MORENO, L., MARSHALL, L. V. & PEARSON, A. 2013. At the frontier of progress for paediatric oncology: the neuroblastoma paradigm. *British Medical Bulletin,* 108**,** 173-188.

MOSS, T. J., REYNOLDS, C. P., SATHER, H. N., ROMANSKY, S. G., HAMMOND, G. D. & SEEGER, R. C. 1991. Prognostic value of immunocytologic detection of bone marrow metastases in neuroblastoma. *The New England Journal of Medicine,* 324**,** 219-226.

MOSSE, Y. P., LIM, M. S., VOSS, S. D., WILNER, K., RUFFNER, K., LALIBERTE, J., ROLLAND, D., BALIS, F. M., MARIS, J. M., WEIGEL, B. J., INGLE, A. M., AHERN, C., ADAMSON, P. C. & BLANEY, S. M. 2013. Safety and activity of crizotinib for paediatric patients with refractory solid tumours or anaplastic large-cell lymphoma: a Children's Oncology Group phase 1 consortium study. *Lancet Oncol,* 14**,** 472-80.

MUJOO, K., CHERESH, D. A., YANG, H. M. & REISFELD, R. A. 1987. Disialoganglioside GD2 on human neuroblastoma cells: target antigen for monoclonal antibody-mediated cytolysis and suppression of tumor growth. *Cancer Res,* 47**,** 1098-104.

MURRAY, M. J., RABY, K. L., SAINI, H. K., BAILEY, S., WOOL, S. V., TUNNACLIFFE, J. M., ENRIGHT, A. J., NICHOLSON, J. C. & COLEMAN, N. 2015. Solid tumors of childhood display specific serum microRNA profiles. *Cancer Epidemiol Biomarkers Prev,* 24**,** 350-60.

NAKANISHI, H., OZAKI, T., NAKAMURA, Y., HASHIZUME, K., IWANAKA, T. & NAKAGAWARA, A. 2007. Purification of human primary neuroblastomas by magnetic beads and their in vitro culture. *Oncol Rep,* 17**,** 1315-20.

NAVID, F., SANTANA, V. M. & BARFIELD, R. C. 2010. Anti-GD2 Antibody Therapy for GD2-expressing Tumors. *Current cancer drug targets,* 10**,** 200-209.

NERADIL, J. & VESELSKA, R. 2015. Nestin as a marker of cancer stem cells. *Cancer Science,* 106**,** 803-811.

NISHIMURA, M., JUNG, E.-J., SHAH, M. Y., LU, C., SPIZZO, R., SHIMIZU, M., HAN, H. D., IVAN, C., ROSSI, S., ZHANG, X., NICOLOSO, M. S., WU, S. Y., ALMEIDA, M. I., BOTTSFORD-MILLER, J., PECOT, C. V., ZAND, B., MATSUO, K., SHAHZAD, M. M., JENNINGS, N. B., RODRIGUEZ-AGUAYO, C., LOPEZ-BERESTEIN, G., SOOD, A. K. & CALIN, G. A. 2013. Therapeutic synergy between microRNA and siRNA in ovarian cancer treatment. *Cancer discovery,* 3**,** 10.1158/2159-8290.CD-13-0159.

OPEL, D., POREMBA, C., SIMON, T., DEBATIN, K. M. & FULDA, S. 2007. Activation of Akt predicts poor outcome in neuroblastoma. *Cancer Res,* 67.

OPEL, D., WESTHOFF, M. A., BENDER, A., BRAUN, V., DEBATIN, K. M. & FULDA, S. 2008. Phosphatidylinositol 3-kinase inhibition broadly sensitizes glioblastoma cells to death receptor- and drug-induced apoptosis. *Cancer Res,* 68.

ORA, I. & EGGERT, A. 2011. Progress in treatment and risk stratification of neuroblastoma: impact on future clinical and basic research. *Semin Cancer Biol,* 21**,** 217-28.

OSTLER, K. R., YANG, Q., LOONEY, T. J., ZHANG, L., VASANTHAKUMAR, A., TIAN, Y., KOCHERGINSKY, M., RAIMONDI, S. L., DEMAIO, J. G., SALWEN, H. R., GU, S., CHLENSKI, A., NARANJO, A., GILL, A., PEDDINTI, R., LAHN, B. T., COHN, S. L. & GODLEY, L. A. 2012. Truncated DNMT3B isoform DNMT3B7 suppresses growth, induces differentiation, and alters DNA methylation in human neuroblastoma. *Cancer Res,* 72**,** 4714-23.

OUYANG, X., JIANG, X., GU, D., ZHANG, Y., KONG, S. K., JIANG, C. & XIE, W. 2016. Dysregulated Serum MiRNA Profile and Promising Biomarkers in Dengue-infected Patients. *International Journal of Medical Sciences,* 13**,** 195-205.

PAGE, S., BIRERDINC, A., ESTEP, M., STEPANOVA, M., AFENDY, A., PETRICOIN, E., YOUNOSSI, Z., CHANDHOKE, V. & BARANOVA, A. 2013. Knowledge-based identification of soluble biomarkers: hepatic fibrosis in NAFLD as an example. *PLoS One,* 8**,** e56009.

PAN, C., KUMAR, C., BOHL, S., KLINGMUELLER, U. & MANN, M. 2009. Comparative proteomic phenotyping of cell lines and primary cells to assess preservation of cell type-specific functions. *Mol Cell Proteomics,* 8**,** 443-50.

PANDA, S. P., CHINNASWAMY, G., VORA, T., PRASAD, M., BANSAL, D., KAPOOR, G., RADHAKRISHNAN, V., AGARWALA, S., LASKAR, S., ARORA, B., KAUR, T., RATH, G. K. & BAKHSHI, S. 2017. Diagnosis and Management of Rhabdomyosarcoma in Children and Adolescents: ICMR Consensus Document. *Indian J Pediatr,* 84**,** 393-402.

PARK, J. R., EGGERT, A. & CARON, H. 2010. Neuroblastoma: biology, prognosis, and treatment. *Hematol Oncol Clin North Am,* 24**,** 65-86.

PATTYN, A., MORIN, X., CREMER, H., GORIDIS, C. & BRUNET, J.-F. 1999. The homeobox gene Phox2b is essential for the development of autonomic neural crest derivatives. *Nature,* 399**,** 366.

PETERSEN, C. P., BORDELEAU, M. E., PELLETIER, J. & SHARP, P. A. 2006. Short RNAs repress translation after initiation in mammalian cells. *Mol Cell,* 21**,** 533-42.

POLAKOVIČOVÁ, M., MUSIL, P., LACZO, E., HAMAR, D. & KYSELOVIČ, J. 2016. Circulating MicroRNAs as Potential Biomarkers of Exercise Response. *International Journal of Molecular Sciences,* 17**,** 1553.

POON, K.-S., PALANISAMY, K., CHANG, S.-S., SUN, K.-T., CHEN, K.-B., LI, P.-C., LIN, T.-C. & LI, C.-Y. 2017. Plasma exosomal miR-223 expression regulates inflammatory responses during cardiac surgery with cardiopulmonary bypass. *Scientific Reports,* 7**,** 10807.

PORTA, C., PAGLINO, C. & MOSCA, A. 2014. Targeting PI3K/Akt/mTOR Signaling in Cancer. *Front Oncol,* 4.

PRITCHARD, J., BARNES, J., GERMOND, S., HARTMAN, O., DE KRAKER, J., LEWIS, I., LOCKWOOD, L. & WALLENDSZUS, K. 1989. Stage and urinary catecholamine metabolite excretion in neuroblastoma. European Neuroblastoma Study Group. *Lancet,* 2**,** 514-5.

PUGH, T. J., MOROZOVA, O., ATTIYEH, E. F., ASGHARZADEH, S., WEI, J. S., AUCLAIR, D., CARTER, S. L., CIBULSKIS, K., HANNA, M., KIEZUN, A., KIM, J., LAWRENCE, M. S., LICHENSTEIN, L., MCKENNA, A., PEDAMALLU, C. S., RAMOS, A. H., SHEFLER, E., SIVACHENKO, A., SOUGNEZ, C., STEWART, C., ALLY, A., BIROL, I., CHIU, R., CORBETT, R. D., HIRST, M., JACKMAN, S. D., KAMOH, B., KHODABAKSHI, A. H., KRZYWINSKI, M., LO, A., MOORE, R. A., MUNGALL, K. L., QIAN, J., TAM, A., THIESSEN, N., ZHAO, Y., COLE, K. A., DIAMOND, M., DISKIN, S. J., MOSSE, Y. P., WOOD, A. C., JI, L., SPOSTO, R., BADGETT, T., LONDON, W. B., MOYER, Y., GASTIER-FOSTER, J. M., SMITH, M. A., GUIDRY AUVIL, J. M., GERHARD, D. S., HOGARTY, M. D., JONES, S. J., LANDER, E. S., GABRIEL, S. B., GETZ, G., SEEGER, R. C., KHAN, J., MARRA, M. A., MEYERSON, M. & MARIS, J. M. 2013. The genetic landscape of high-risk neuroblastoma. *Nat Genet,* 45**,** 279-84.

QUINTANILHA, B. J., REIS, B. Z., DUARTE, G. B. S., COZZOLINO, S. M. F. & ROGERO, M. M. 2017. Nutrimiromics: Role of microRNAs and Nutrition in Modulating Inflammation and Chronic Diseases. *Nutrients,* 9**,** 1168.

RAMALINGAM, P., PALANICHAMY, J. K., SINGH, A., DAS, P., BHAGAT, M., KASSAB, M. A., SINHA, S. & CHATTOPADHYAY, P. 2014. Biogenesis of intronic miRNAs located in clusters by independent transcription and alternative splicing. *RNA,* 20**,** 76-87.

RASTOGI, P., NASEEM, S., VARMA, N., DAS, R., AHLUWALIA, J., SACHDEVA, M. U. S., SHARMA, P., KUMAR, N. & MARWAHA, R. K. 2015. Bone Marrow Involvement in Neuroblastoma: A Study of Hemato-morphological Features. *Indian Journal of Hematology & Blood Transfusion,* 31**,** 57-60.

REINHART, B. J., SLACK, F. J., BASSON, M., PASQUINELLI, A. E., BETTINGER, J. C., ROUGVIE, A. E., HORVITZ, H. R. & RUVKUN, G. 2000. The 21-nucleotide let-7 RNA regulates developmental timing in Caenorhabditis elegans. *Nature,* 403**,** 901-6.

RODGER, A. 2013. Concentration Determination Using Beer-Lambert Law. *In:* ROBERTS, G. C. K. (ed.) *Encyclopedia of Biophysics.* Berlin, Heidelberg: Springer Berlin Heidelberg.

SALETTA, F., WADHAM, C., ZIELGER, D. S., MARSHALL, G. M., HABER, M., MCCOWAGE, G., NORRIS, M. D. & BYRNE, J. A. 2014. Molecular profiling of childhood cancer: Biomarkers and novel therapies. *BBA Clinical,* 1.

SAUSEN, M., LEARY, R. J., JONES, S., WU, J., REYNOLDS, C. P., LIU, X., BLACKFORD, A., PARMIGIANI, G., DIAZ, L. A., PAPADOPOULOS, N., VOGELSTEIN, B., KINZLER, K. W., VELCULESCU, V. E. & HOGARTY, M. D. 2013. Integrated genomic analyses identify ARID1A and ARID1B alterations in the childhood cancer neuroblastoma. *Nature genetics,* 45**,** 12-17.

SCARUFFI, P., MORANDI, F., GALLO, F., STIGLIANI, S., PARODI, S., MORETTI, S., BONASSI, S., FARDIN, P., GARAVENTA, A., ZANAZZO, G., PISTOIA, V., TONINI, G. P. & CORRIAS, M. V. 2012. Bone marrow of neuroblastoma patients shows downregulation of CXCL12 expression and presence of IFN signature. *Pediatr Blood Cancer,* 59**,** 44-51.

SCARUFFI, P., STIGLIANI, S., MORETTI, S., COCO, S., DE VECCHI, C., VALDORA, F., GARAVENTA, A., BONASSI, S. & TONINI, G. P. 2009. Transcribed-Ultra Conserved Region expression is associated with outcome in high-risk neuroblastoma. *BMC Cancer,* 9**,** 441.

SCHMIDT, M., DECAROLIS, B., SCHNEIDER, C., HERO, B., SIMON, T., ROELS, F., DIETLEIN, M., DRZEZGA, A. & BERTHOLD, F. 2013. Curie and SIOPEN mIBG-scoring systems predict outcome in patients with stage 4 neuroblastoma. *J NUCL MED MEETING ABSTRACTS,* 54**,** 532-.

SCHOOT, R., BLEEKER, G., CARON, H., VAN ECK, B., HEIJ, H., DE KRAKER, J. & TYTGAT, G. 2013. The role of 131I-metaiodobenzylguanidine (MIBG) therapy in unresectable and compromising localised neuroblastoma. *European Journal of Nuclear Medicine and Molecular Imaging,* 40**,** 1516-1522.

SCHROEDER, A., MUELLER, O., STOCKER, S., SALOWSKY, R., LEIBER, M., GASSMANN, M., LIGHTFOOT, S., MENZEL, W., GRANZOW, M. & RAGG, T. 2006. The RIN: an RNA integrity number for assigning integrity values to RNA measurements. *BMC Molecular Biology,* 7**,** 3-3.

SCHULTE, J. H., HORN, S., OTTO, T., SAMANS, B., HEUKAMP, L. C., EILERS, U.-C., KRAUSE, M., ASTRAHANTSEFF, K., KLEIN-HITPASS, L., BUETTNER, R., SCHRAMM, A., CHRISTIANSEN, H., EILERS, M., EGGERT, A. & BERWANGER, B. 2008. MYCN regulates oncogenic MicroRNAs in neuroblastoma. *International Journal of Cancer,* 122**,** 699-704.

SCHULTE, J. H., MARSCHALL, T., MARTIN, M., ROSENSTIEL, P., MESTDAGH, P., SCHLIERF, S., THOR, T., VANDESOMPELE, J., EGGERT, A., SCHREIBER, S., RAHMANN, S. & SCHRAMM, A. 2010. Deep sequencing reveals differential expression of microRNAs in favorable versus unfavorable neuroblastoma. *Nucleic Acids Research,* 38**,** 5919-5928.

SCHULTE, J. H., SCHOWE, B., MESTDAGH, P., KADERALI, L., KALAGHATGI, P., SCHLIERF, S., VERMEULEN, J., BROCKMEYER, B., PAJTLER, K., THOR, T., DE PRETER, K., SPELEMAN, F., MORIK, K., EGGERT, A., VANDESOMPELE, J. & SCHRAMM, A. 2010. Accurate prediction of neuroblastoma outcome based on miRNA expression profiles. *International Journal of Cancer,* 127**,** 2374-2385.

SCHUMACHER-KUCKELKORN, R., VOLLAND, R., GRADEHANDT, A., HERO, B., SIMON, T. & BERTHOLD, F. 2017. Lack of immunocytological GD2 expression on neuroblastoma cells in bone marrow at diagnosis, during treatment, and at recurrence. *Pediatr Blood Cancer,* 64**,** 46-56.

SEEGER, R. C., REYNOLDS, C. P., GALLEGO, R., STRAM, D. O., GERBING, R. B. & MATTHAY, K. K. 2000. Quantitative tumour cell content of bone marrow and blood as a predictor of outcome in stage IV neuroblastoma: A children's cancer group study. *Journal of Clinical Oncology,* 18**,** 4067-4076.

SEGERSTRÖM, L., BARYAWNO, N., SVEINBJÖRNSSON, B., WICKSTRÖM, M., ELFMAN, L., KOGNER, P. & JOHNSEN, J. I. 2011. Effects of small molecule inhibitors of PI3K/Akt/mTOR signaling on neuroblastoma growth in vitro and in vivo. *International Journal of Cancer,* 129**,** 2958-2965.

SHI, Z. M., WANG, L., SHEN, H., JIANG, C. F., GE, X., LI, D. M., WEN, Y. Y., SUN, H. R., PAN, M. H., LI, W., SHU, Y. Q., LIU, L. Z., PEIPER, S. C., HE, J. & JIANG, B. H. 2017. Downregulation of miR-218 contributes to epithelial–mesenchymal transition and tumor metastasis in lung cancer by targeting Slug/ZEB2 signaling. *Oncogene,* 36**,** 2577.

SHIMADA, H., AMBROS, I. M., DEHNER, L. P., HATA, J.-I., JOSHI, V. V., ROALD, B., STRAM, D. O., GERBING, R. B., LUKENS, J. N., MATTHAY, K. K. & CASTLEBERRY,

R. P. 1999. The International Neuroblastoma Pathology Classification (the Shimada system). *Cancer,* 86**,** 364-372.

SHIMADA, H., CHATTEN, J., NEWTON, W. A., SACHS, N., HAMOUDI, A. B., CHIBA, T., MARSDEN, H. B. & MISUGI, K. 1984. Histopathologic prognostic factors in neuroblastic tumors: definition of subtypes of ganglioneuroblastoma and an age-linked classification of neuroblastomas. *Journal of the National Cancer Institute,* 73**,** 405-416.

SHIOZAWA, Y., EBER, M. R., BERRY, J. E. & TAICHMAN, R. S. 2015. Bone marrow as a metastatic niche for disseminated tumor cells from solid tumors. *BoneKEy Rep,* 4.

SMITH, A. D., RODA, D. & YAP, T. A. 2014. Strategies for modern biomarker and drug development in oncology. *Jounal of Hematology & Oncology,* 7**,** 1-16.

SMITH, S. J., DIEHL, N. N., SMITH, B. D. & MOHNEY, B. G. 2010. Urine catecholamine levels as diagnostic markers for neuroblastoma in a defined population: implications for ophthalmic practice. *Eye (Lond),* 24**,** 1792-1796.

SOHARA, Y., SHIMADA, H. & DECLERCK, Y. A. 2005. Mechanisms of bone invasion and metastasis in human neuroblastoma. *Cancer Lett,* 228**,** 203-9.

SOHEL, M. H. 2016. Extracellular/Circulating MicroRNAs: Release Mechanisms, Functions and Challenges. *Achievements in the Life Sciences,* 10**,** 175-186.

SONG, X. L., TANG, Y., LEI, X. H., ZHAO, S. C. & WU, Z. Q. 2017. miR-618 Inhibits Prostate Cancer Migration and Invasion by Targeting FOXP2. *J Cancer,* 8**,** 2501-2510.

SOURVINOU, I. S., MARKOU, A. & LIANIDOU, E. S. 2013. Quantification of Circulating miRNAs in Plasma: Effect of Preanalytical and Analytical Parameters on Their Isolation and Stability. *The Journal of Molecular Diagnostics,* 15**,** 827-834.

STIGLIANI, S., SCARUFFI, P., LAGAZIO, C., PERSICO, L., CARLINI, B., VARESIO, L., MORANDI, F., MORINI, M., GIGLIOTTI, A. R., ESPOSITO, M. R., VISCARDI, E., CECINATI, V., CONTE, M. & CORRIAS, M. V. 2015. Deregulation of focal adhesion pathway mediated by miR-659-3p is implicated in bone marrow infiltration of stage M neuroblastoma patients. *Oncotarget,* 6**,** 13295-308.

STREBY, K. A., SHAHA, N., RANALLI, M. A., KUNKLER, A. & P., C. T. 2014. Nothing but NET: a review of norepinephrine transporter expression and efficacy of ^{131}I-mIBG therapy. *Pediatric Blood Cancer,* 62**,** 5-11.

STRIMBU, K. & TAVEL, J. A. 2010. What are biomarkers? *Curr Opin HIV AIDS,* 5**,** 463-466.

STUTTERHEIM, J., GERRITSEN, A., ZAPPEIJ-KANNEGIETER, L., KLEIJN, I., DEE, R., HOOFT, L., VAN NOESEL, M. M., BIERINGS, M., BERTHOLD, F., VERSTEEG, R., CARON, H. N., VAN DER SCHOOT, C. E. & TYTGAT, G. A. 2008. PHOX2B is a novel and specific marker for minimal residual disease testing in neuroblastoma. *J Clin Oncol,* 26**,** 5443-9.

SWERTS, K., AMBROS, P. F., BROUZES, C., NAVARRO, J. M., GROSS, N., RAMPLING, D., SCHUMACHER-KUCKELKORN, R., SEMENTA, A. R., LADENSTEIN, R. & BEISKE, K. 2005. Standardization of the immunocytochemical detection of neuroblastoma cells in bone marrow. *J Histochem Cytochem,* 53**,** 1433-40.

SWERTS, K., DE MOERLOOSE, B., DHOOGE, C., BRICHARD, B., BENOIT, Y., LAUREYS, G. & PHILIPPE, J. 2004. Detection of residual neuroblastoma cells in bone marrow: comparison of flow cytometry with immunocytochemistry. *Cytometry B Clin Cytom,* 61**,** 9-19.

THOMAS, S. K., MESSAM, C. A., SPENGLER, B. A., BIEDLER, J. L. & ROSS, R. A. 2004. Nestin is a potential mediator of malignancy in human neuroblastoma cells. *J Biol Chem,* 279**,** 27994-9.

THORNER, P. S. 2014. The molecular genetic profile of neuroblastoma. *Diagnostic Histopathology,* 20**,** 76-83.

TIAN, Y., LI, S., SONG, J., JI, T., ZHU, M., ANDERSON, G. J., WEI, J. & NIE, G. 2014. A doxorubicin delivery platform using engineered natural membrane vesicle exosomes for targeted tumor therapy. *Biomaterials,* 35**,** 2383-90.

TIVNAN, A., ORR, W. S., GUBALA, V., NOONEY, R., WILLIAMS, D. E., MCDONAGH, C., PRENTER, S., HARVEY, H., DOMINGO-FERNÁNDEZ, R., BRAY, I. M., PISKAREVA, O., NG, C. Y., LODE, H. N., DAVIDOFF, A. M. & STALLINGS, R. L. 2012. Inhibition of Neuroblastoma Tumor Growth by Targeted Delivery of MicroRNA-34a Using Anti-Disialoganglioside GD$_2$ Coated Nanoparticles. *PLoS ONE,* 7**,** e38129.

TIVNAN, A., TRACEY, L., BUCKLEY, P. G., ALCOCK, L. C., DAVIDOFF, A. M. & STALLINGS, R. L. 2011. MicroRNA-34a is a potent tumor suppressor molecule in vivo in neuroblastoma. *BMC Cancer,* 11**,** 33.

TRAGER, C., KOGNER, P., LINDSKOG, M., PONTHAN, F., KULLMAN, A. & KAGEDAL, B. 2003. Quantitative analysis of tyrosine hydroxylase mRNA for sensitive detection of neuroblastoma cells in blood and bone marrow. *Clin Chem,* 49**,** 104-12.

TROCHET, D., O'BRIEN, L. M., GOZAL, D., TRANG, H., NORDENSKJÖLD, A., LAUDIER, B., SVENSSON, P.-J., UHRIG, S., COLE, T., MUNNICH, A., GAULTIER, C., LYONNET, S. & AMIEL, J. 2005. PHOX2B Genotype Allows for Prediction of Tumor Risk in Congenital Central Hypoventilation Syndrome. *The American Journal of Human Genetics,* 76**,** 421-426.

TSANG, K. S., LI, C. K., TSOI, W. C., LEUNG, Y., SHING, M. M., CHIK, K. W., LEE, V., NG, M. H. & YUEN, P. 2003. Detection of micrometastasis of neuroblastoma to bone marrow and tumor dissemination to hematopoietic autografts using flow cytometry and reverse transcriptase-polymerase chain reaction. *Cancer,* 97**,** 2887-97.

TSUCHIDA, T., SAXTON, R. E., MORTON, D. L. & IRIE, R. F. 1987. Gangliosides of human melanoma. *J Natl Cancer Inst,* 78**,** 45-54.

TU, L., ZHAO, E., ZHAO, W., ZHANG, Z., TANG, D., ZHANG, Y., WANG, C., ZHUANG, C. & CAO, H. 2016. hsa-miR-376c-3p Regulates Gastric Tumor Growth Both In Vitro and In Vivo. *BioMed Research International,* 2016**,** 9604257.

UMAPATHY, G., EL WAKIL, A., WITEK, B., CHESLER, L., DANIELSON, L., DENG, X., GRAY, N. S., JOHANSSON, M., KVARNBRINK, S., RUUTH, K., SCHÖNHERR, C., PALMER, R. H. & HALLBERG, B. 2014. *The kinase ALK stimulates the kinase ERK5 to promote the expression of the oncogene MYCN in neuroblastoma*.

VAN 'T VEER, L. J., DAI, H., VAN DE VIJVER, M. J., HE, Y. D., HART, A. A. M., MAO, M., PETERSE, H. L., VAN DER KOOY, K., MARTON, M. J., WITTEVEEN, A. T., SCHREIBER, G. J., KERKHOVEN, R. M., ROBERTS, C., LINSLEY, P. S., BERNARDS, R. & FRIEND, S. H. 2002. Gene expression profiling predicts clinical outcome of breast cancer. *Nature,* 415**,** 530-536.

VANDEWOESTYNE, M., KUMPS, C., SWERTS, K., MENTEN, B., LAMMENS, T., PHILIPPE, J., DE PRETER, K., LAUREYS, G., VAN ROY, N., SPELEMAN, F. & DEFORCE, D. 2012. Isolation of disseminated neuroblastoma cells from bone marrow

aspirates for pretreatment risk assessment by array comparative genomic hybridization. *Int J Cancer,* 130**,** 1098-108.

VASUDEVAN, S., TONG, Y. & STEITZ, J. A. 2007. Switching from repression to activation: microRNAs can up-regulate translation. *Science,* 318**,** 1931-4.

VESTAD, B., LLORENTE, A., NEURAUTER, A., PHUYAL, S., KIERULF, B., KIERULF, P., SKOTLAND, T., SANDVIG, K., HAUG, K. B. F. & ØVSTEBØ, R. 2017. Size and concentration analyses of extracellular vesicles by nanoparticle tracking analysis: a variation study. *Journal of Extracellular Vesicles,* 6**,** 1344087.

VINKLAREK, J., NOVAK, J., BIENERTOVA-VASKU, J., STERBA, J. & SLABY, O. 2014. [The role of MicroRNAs in the pathophysiology of neuroblastoma and their possible use in diagnosis, prognosis and therapy]. *Klin Onkol,* 27**,** 331-9.

VIPREY, V. F., CORRIAS, M. V. & BURCHILL, S. A. 2012. Identification of reference microRNAs and suitability of archived hemopoietic samples for robust microRNA expression profiling. *Anal Biochem,* 421**,** 566-72.

VIPREY, V. F., CORRIAS, M. V., KAGEDAL, B., OLTRA, S., SWERTS, K., VICHA, A., LADENSTEIN, R. & BURCHILL, S. A. 2007. Standardisation of operating procedures for the detection of minimal disease by QRT-PCR in children with neuroblastoma: quality assurance on behalf of SIOPEN-R-NET. *Eur J Cancer,* 43**,** 341-50.

VIPREY, V. F., GREGORY, W. M., CORRIAS, M. V., TCHIRKOV, A., SWERTS, K., VICHA, A., DALLORSO, S., BROCK, P., LUKSH, R., VALTEAU-COUANET, D., PAPADAKIS, V., LAUREYS, G., PEARSON, A. D. J., LADENSTEIN, R. & BURCHILL, S. A. 2014. Neuroblastoma mRNAs predict outcome in children with stage 4 neuroblastoma: a European HR-NBL1/SIOPEN study. *Journal of Clinical Oncology,* 32**,** 1074-1084.

VLACHOS, I. S., ZAGGANAS, K., PARASKEVOPOULOU, M. D., GEORGAKILAS, G., KARAGKOUNI, D., VERGOULIS, T., DALAMAGAS, T. & HATZIGEORGIOU, A. G. 2015. DIANA-miRPath v3.0: deciphering microRNA function with experimental support. *Nucleic Acids Res,* 43**,** W460-6.

VLAHOS, C. J., MATTER, W. F., HUI, K. Y. & BROWN, R. F. 1994. A specific inhibitor of phosphatidylinositol 3-kinase, 2-(4-morpholinyl)-8-phenyl-4H-1-benzopyran-4-one (LY294002). *J Biol Chem,* 269**,** 5241-8.

WAHID, F., SHEHZAD, A., KHAN, T. & YOUNG KIM, Y. 2010. MircroRNAs: Systhesis, mechanism, function and recent clinical trials. *Biochimica er Biophysica Acta,* 1803**,** 1231-1243.

WANG, D., WANG, H., LI, Y. & LI, Q. 2018. MiR-362-3p functions as a tumor suppressor through targeting MCM5 in cervical adenocarcinoma. *Bioscience Reports,* 38**,** BSR20180668.

WANG, G., CAO, X., LAI, S., LUO, X., FENG, Y., WU, J., NING, Q., XIA, X., WANG, J., GONG, J. & HU, J. 2015. Altered p53 regulation of miR-148b and p55PIK contributes to tumor progression in colorectal cancer. *Oncogene,* 34**,** 912-21.

WANG, H., ZHAN, M., XU, S.-W., CHEN, W., LONG, M.-M., SHI, Y.-H., LIU, Q., MOHAN, M. & WANG, J. 2017. miR-218-5p restores sensitivity to gemcitabine through PRKCE/MDR1 axis in gallbladder cancer. *Cell Death &Amp; Disease,* 8**,** e2770.

WANG, K., JIN, J., MA, T. & ZHAI, H. 2017b. MiR-376c-3p regulates the proliferation, invasion, migration, cell cycle and apoptosis of human oral squamous cancer cells by suppressing HOXB7. *Biomed Pharmacother,* 91**,** 517-525.

WANG, M., ZHOU, C., SUN, Q., CAI, R., LI, Y., WANG, D. & GONG, L. 2013. ALK amplification and protein expression predict inferior prognosis in neuroblastomas. *Experimental and Molecular Pathology,* 95**,** 124-130.

WANG, X., GU, H., QIN, D., YANG, L., HUANG, W., ESSANDOH, K., WANG, Y., CALDWELL, C. C., PENG, T., ZINGARELLI, B. & FAN, G.-C. 2015b. Exosomal miR-223 Contributes to Mesenchymal Stem Cell-Elicited Cardioprotection in Polymicrobial Sepsis. *Scientific Reports,* 5**,** 13721.

WEI, J. S., SONG, Y. K., DURINCK, S., CHEN, Q.-R., CHEUK, A. T. C., TSANG, P., ZHANG, Q., THIELE, C. J., SLACK, A., SHOHET, J. & KHAN, J. 2008. The MYCN oncogene is a direct target of miR-34a. *Oncogene,* 27**,** 5204-5213.

WEILBAECHER, K. N., GUISE, T. A. & MCCAULEY, L. K. 2011. Cancer to bone: a fatal attraction. *Nat Rev Cancer,* 11**,** 411-25.

WELCH, C., CHEN, Y. & STALLINGS, R. L. 2007. MicroRNA-34a functions as a potential tumor suppressor by inducing apoptosis in neuroblastoma cells. *Oncogene,* 26.

WELCSH, P. L. & KING, M.-C. 2001. BRCA1 and BRCA2 and the genetics of breast and ovarian cancer. *Human Molecular Genetics,* 10**,** 705-713.

WESTHOFF, M.-A., FAHAM, N., MARX, D., NONNENMACHER, L., JENNEWEIN, C., ENZENMÜLLER, S., GONZALEZ, P., FULDA, S. & DEBATIN, K.-M. 2013. Sequential Dosing in Chemosensitization: Targeting the PI3K/Akt/mTOR Pathway in Neuroblastoma. *PLoS ONE,* 8**,** e83128.

WHITFILL, T. 2014. The Role Of Gene Regulation In Cancer: Studies Of Cancer-Related Phenotypes Mediated By Mex3d And By Microrna-618 Implicate Their Potential Oncogenic Role. *Public Health Theses,* 1322.

WILLMS, E., JOHANSSON, H. J., MÄGER, I., LEE, Y., BLOMBERG, K. E. M., SADIK, M., ALAARG, A., SMITH, C. I. E., LEHTIÖ, J., EL ANDALOUSSI, S., WOOD, M. J. A. & VADER, P. 2016. Cells release subpopulations of exosomes with distinct molecular and biological properties. *Scientific Reports,* 6**,** 22519.

WINTER, C., PAWEL, B., SEISER, E., ZHAO, H., RAABE, E., WANG, Q., JUDKINS, A. R., ATTIYEH, E. & MARIS, J. M. 2008. Neural cell adhesion molecule (NCAM) isoform expression is associated with neuroblastoma differentiation status. *Pediatr Blood Cancer,* 51**,** 10-6.

WINTER, J., JUNG, S., KELLER, S., GREGORY, R. I. & DIEDERICHS, S. 2009. Many roads to maturity: microRNA biogenesis pathways and their regulation. *Nat Cell Biol,* 11**,** 228-234.

WU, K., YANG, L., CHEN, J., ZHAO, H., WANG, J., XU, S. & HUANG, Z. 2015. miR-362-5p inhibits proliferation and migration of neuroblastoma cells by targeting phosphatidylinositol 3-kinase-C2β. *FEBS Letters,* 589**,** 1911-1919.

WU, Z. L., SCHWARTZ, E., SEEGER, R. & LADISCH, S. 1986. Expression of GD2 ganglioside by untreated primary human neuroblastomas. *Cancer Res,* 46**,** 440-3.

XIN, C., BUHE, B., HONGTING, L., CHUANMIN, Y., XIWEI, H., HONG, Z., LULU, H., QIAN, D. & RENJIE, W. 2013. MicroRNA-15a promotes neuroblastoma migration by targeting reversion-inducing cysteine-rich protein with Kazal motifs (RECK) and regulating matrix metalloproteinase-9 expression. *FEBS Journal,* 280**,** 855-866.

YANG, T., MARTIN, P., FOGARTY, B., BROWN, A., SCHURMAN, K., PHIPPS, R., YIN, V. P., LOCKMAN, P. & BAI, S. 2015. Exosome delivered anticancer drugs across

the blood-brain barrier for brain cancer therapy in Danio rerio. *Pharm Res,* 32**,** 2003-14.

YE, J., YAO, Y., SONG, Q., LI, S., HU, Z., YU, Y., HU, C., DA, X., LI, H., CHEN, Q. & WANG, Q. K. 2016. Up-regulation of miR-95-3p in hepatocellular carcinoma promotes tumorigenesis by targeting p21 expression. *Scientific Reports,* 6**,** 34034.

YEUNG, D. T. & HUGHES, T. P. 2012. Therapeutic targeting of BCR-ABL: prognostic markers of response and resistance mechanism in chronic myeloid leukaemia. *Crit Rev Oncog,* 17**,** 17-30.

YEUNG, P., SIN, H. S., CHAN, S., CHAN, G. C. F. & CHAN, B. P. 2015. Microencapsulation of Neuroblastoma Cells and Mesenchymal Stromal Cells in Collagen Microspheres: A 3D Model for Cancer Cell Niche Study. *PLOS ONE,* 10**,** e0144139.

YI, L. & YUAN, Y. 2015. MicroRNA-618 modulates cell growth via targeting PI3K/Akt pathway in human thyroid carcinomas. *Indian J Cancer,* 52 Suppl 3**,** E186-9.

YOSHIOKA, Y., KONISHI, Y., KOSAKA, N., KATSUDA, T., KATO, T. & OCHIYA, T. 2013. Comparative marker analysis of extracellular vesicles in different human cancer types. *Journal of Extracellular Vesicles,* 2**,** 10.3402/jev.v2i0.20424.

ZERINGER, E., BARTA, T., LI, M. & VLASSOV, A. V. 2015. Strategies for isolation of exosomes. *Cold Spring Harb Protoc,* 2015**,** 319-23.

ZHANG, L., ZHOU, F. & TEN DIJKE, P. 2013. Signaling interplay between transforming growth factor-beta receptor and PI3K/AKT pathways in cancer. *Trends Biochem Sci,* 38**,** 612-20.

ZHANG, Y., WANG, Y., WEI, Y., LI, M., YU, S., YE, M., ZHANG, H., CHEN, S., LIU, W. & ZHANG, J. 2015. MiR-129-3p promotes docetaxel resistance of breast cancer cells via CP110 inhibition. *Scientific Reports,* 5**,** 15424.

ZHANG, Z., QIN, Y.-W., BREWER, G. & JING, Q. 2012. MicroRNA degradation and turnover: regulating the regulators. *Wiley interdisciplinary reviews. RNA,* 3**,** 593-600.

ZHAO, Y., DAI, Z., LIANG, Y., YIN, M., MA, K., HE, M., OUYANG, H. & TENG, C.-B. 2014. Sequence-specific inhibition of microRNA via CRISPR/CRISPRi system. *Scientific Reports,* 4**,** 3943.

ZHAO, Z., MA, X., SUNG, D., LI, M., KOSTI, A., LIN, G., CHEN, Y., PERTSEMLIDIS, A., HSIAO, T. H. & DU, L. 2015. microRNA-449a functions as a tumor suppressor in neuroblastoma through inducing cell differentiation and cell cycle arrest. *RNA Biol,* 12**,** 538-54.

ZHI, F., WANG, R., WANG, Q., XUE, L., DENG, D., WANG, S. & YANG, Y. 2014. MicroRNAs in Neuroblastoma: Small-sized players with a large impact. *Neurochemistry Research,* 39**,** 613-623.

ZHU, H., SHAH, S., SHYH-CHANG, N., SHINODA, G., EINHORN, W. S., VISWANATHAN, S. R., TAKEUCHI, A., GRASEMANN, C., RINN, J. L., LOPEZ, M. F., HIRSCHHORN, J. N., PALMERT, M. R. & DALEY, G. Q. 2010. Lin28a transgenic mice manifest size and puberty phenotypes identified in human genetic association studies. *Nat Genet,* 42**,** 626-30.

ZHU, K., DING, H., WANG, W., LIAO, Z., FU, Z., HONG, Y., ZHOU, Y., ZHANG, C. Y. & CHEN, X. 2016. Tumor-suppressive miR-218-5p inhibits cancer cell proliferation and migration via EGFR in non-small cell lung cancer. *Oncotarget,* 7**,** 28075-85.